HILLSLOPE EXPERIMENTS IN THE NORTH EAST CAPE REGION TO MEASURE AND MODEL SUBSURFACE FLOW PROCESSES

by

LUKE JOHN ESPREY

BSc (Hons)

Submitted in partial
fulfilment of the requirements
for the degree of

MASTER OF SCIENCE

Department of Agricultural Engineering
University of Natal
Pietermaritzburg

December 1997

DECLARATION

I hereby certify that this research reported in this dissertation is my own original and unaided work except where specific acknowledgement is made.

L J ESPREY

ACKNOWLEDGEMENTS

The author wishes to express his sincere appreciation for the assistance given by the following scientists and institutions:

- Dr S A Lorentz, Senior Research Fellow, Department of Agricultural Engineering, University of Natal, for supervision of this project and providing invaluable assistance and encouragement;

- Dr M A Johnston, Department of Agronomy, University of Natal, for acting as co-supervisor, providing good advice and assistance;

- Prof. R E Schulze, Professor of Hydrology, Department of Agricultural Engineering, University of Natal, for initiating this research and acting as co-supervisor, providing both assistance and advice;

- Prof. P W L Lyne, Head of Department, Department of Agricultural Engineering, University of Natal, for administrative input and encouragement;

- Professor P J T Roberts, Director of the Institute for Commercial Forestry Research, for support and encouragement which helped me finish this research;

- The Water Research Commission for partially funding this project;

- The Foundation for Research and Development for partially funding this project;

- Mondi Forests for partially funding this project;

- The Computing Centre for Water Research, for provision of computing facilities;

- Dr M C Dent, Computing Centre of Water Research, for some good advice;

- Dr M Hensley and Mr V Roberts of the Institute for Soil, Water and Climate for providing valuable assistance with the soil survey at Weatherly and calibration of the neutron probe;

- Mr C Tredrea, Senior Technician, for building the prototype four channel logger and for his advice and assistance;

- Messers J J Pretorious, G H Bowker and P Goba, technical staff, Department of Agricultural Engineering, University of Natal, for technical assistance and friendly advice;

- Messers N Nundlall and M Horn, Computing Centre of Water Research, for answering my many computer related questions;

- Mr G O Hughes, Department of Agricultural Engineering, University of Natal, for completing a geological survey of Transect 1 on the Weatherly catchment;

- Mr G Mathews, Department of Agricultural Engineering, University of Natal, for his help in the fieldwork component of this research;

- Mr B J Howe, Department of Agricultural Engineering, University of Natal, for his help in setting up TOP*ACRU*;

- Mr M Mulder, for his help in analysing the surveyed hillslope data;

- the staff and my post graduate colleagues, Department of Agricultural Engineering, University of Natal, for their friendly advice and assistance;

- my Parents and family for their guidance, support and love, and finally to

- Robyn, my girlfriend, who gave endless support, guidance and love which helped make the completion of this dissertation possible.

ABSTRACT

Several hydrological studies claim that available water resources in a catchment are affected by large scale afforestation, especially where the regional rainfall is considered marginal for the support of silviculture. Nevertheless, the mechanisms and magnitude of the perturbations to the receiving water resources due to afforestation are still not clearly understood. To improve this understanding an intensive hydrological experiment has been initiated in the small grassed Weatherly catchment of the Mondi, North East Cape Forests. Details of the soil water dynamics on the Molteno formations in the catchment have been be studied.

This research presents a description and first results of the establishment of an experiment which comprises monitoring the water budget of the grassed catchment prior to the afforestation of the catchment to plantations of exotic trees. The studies currently include, monitoring the infiltration and redistribution of soil water on a hillslope as well as monitoring of interflow mechanisms and localised mechanisms of soil water accumulation influenced by the topography and geology of the catchment. In addition to the intensive soil water monitoring, specific experimentation has been conducted at various locations on the hillslope. These comprise macropore flow process studies and 2-dimensional tracer experiments. Details of these experiments as well as the automated soil water and groundwater monitoring instrumentation are presented. An intensive soil survey on a 30 m x 30 m grid as well as a comprehensive measurement strategy of soil physical and hydraulic properties are highlighted. A review of 2-dimensional numerical hillslope soil water process models is also presented.

Results from this research show that on hillslopes underlain by Molteno sandstones localised perched water tables form. These water bodies, upon reaching a critical height above the bedrock cascade downslope as interflow recharging the water bodies downslope. The response to infiltration increases downslope and in the toe region interflow occurs readily in response to rainfall compared to the midslope where substantial rain needs to infiltrate.

TABLE OF CONTENTS

LIST OF FIGURES

LIST OF TABLES

LIST OF APPENDICES

LIST OF ABBREVIATIONS AND SYMBOLS

AMSL	=	Above mean sea level (m)
AMC	=	Antecedent moisture content ($m^3.m^{-3}$)
AWS	=	Automatic weather station
BR	=	Bedrock elevation (m)
CR	=	Count Ratio
C_f	=	Capillary fringe height (m)
DAE	=	Department of Agricultural Engineering
DEM	=	Digital elevation model
DTM	=	Digital terrain model
DUL	=	Drained upper limit ($m^3.m^{-3}$)
e	=	Source or sink term ($m^3.m^{-3}$)
ET	=	Evapotranspiration ($mm.day^{-1}$)
F	=	Accumulated infiltration (mm)
f	=	Infiltration rate ($mm.h^{-1}$)
GI	=	Groundwater in (m^3)
GO	=	Groundwater out (m^3)
GPR	=	Ground penetrating radar
GW	=	Groundwater tube
H	=	Hydraulic head (m)
He	=	Height (mm)
h	=	Soil water pressure head (m)
h_b	=	Brooks and Corey (1964) bubbling pressure head (m)
H_o	=	Head of water (m)
H_z	=	Depth (m)
i	=	Rainfall intensity ($mm.h^{-1}$)
$I_{mac\ act}$	=	Actual rate into macropore system ($mm.h^{-1}$)
$I_{mac\ pot}$	=	Potential rate into macropore system ($mm.h^{-1}$)
$I_{mac\ empty}$	=	Free space of macropores (m^2)
$I_{mic\ act}$	=	Actual rate into micropore system ($mm.h^{-1}$)
ISCW	=	Institute for Soil, Climate and Water
K	=	Hydraulic conductivity ($mm.h^{-1}$)
K_s	=	Saturated hydraulic conductivity ($mm.h^{-1}$)
K_h	=	Horizontal hydraulic conductivity ($mm.h^{-1}$)
$K(\theta)$	=	Unsaturated hydraulic conductivity ($mm.h^{-1}$)
L	=	Lateral flow (m^3)
L_f	=	Saturated zone (m)
LLF	=	Left lateral flow (m^3)
MAP	=	Mean annual precipitation (mm)
MHP	=	Matric head potential (m)
NEC	=	North East Cape
Nest	=	Tensiometer nest
NMM	=	Neutron moisture meter
NP	=	Neutron probe access tube number

P	=	Percolation (m^3)
ρ_b	=	Bulk density ($Mg.m^{-3}$)
ρ_s	=	Particle density ($Mg.m^{-3}$)
PSD	=	Particle size distribution
PWP	=	Permanent wilting point ($m.m^{-1}$)
Q	=	Inflow ($m^3.h^{-1}$)
$Q(x,t)$	=	Horizontal flux per unit width ($mm.h^{-1}$)
q	=	Flow rate per unit cross sectional area ($mm.h^{-1}$)
R	=	Rainfall (m^3)
r	=	Radius (mm)
RDP	=	Reconstruction and Development Programme
RO	=	Runoff (m^3)
RLF	=	Right lateral flow (m^3)
S_e	=	Effective water content ($m^3.m^{-3}$)
S_f	=	Friction slope
S_f	=	Effective suction at wetting front
ΔSG	=	Change in groundwater storage (m^3)
S_o	=	Surface slope
ΔSV	=	Change in vadose zone storage (m^3)
Δt	=	Duration of time step (h)
t	=	Time (h)
WRC	=	Water retention characteristic
WTH	=	Water table height (m)
V	=	Voltage (V)
V_{mak}	=	Effective macroporosity
y	=	Height difference (mm)
Z	=	Distance in direction of flow (mm)
z	=	Elevation above reference (mm)
ϕ	=	Porosity ($m^3.m^{-3}$)
$\theta_{\%}$	=	Water content by percent volume (%)
θ	=	Water content ($m^3.m^{-3}$)
θ_i	=	Initial water content ($m^3.m^{-3}$)
θ_r	=	Brooks and Corey (1964) residual water content ($m^3.m^{-3}$)
θ_s	=	Saturated water content ($m^3.m^{-3}$)
ψ	=	Matric potential (m)
λ	=	Brooks and Corey (1964) pore size distribution index
Υ	=	Soil interface slope (%)

1. INTRODUCTION

Mondi Forests is playing an important role in assisting with the Reconstruction and Development Programme's (RDP) objectives. One main objective of the RDP is to achieve the building of 300 000 new houses per annum. To achieve this objective, a large supply of saw timber and pulpwood is required. In response to these demands Scotcher (1995), cited by Summerton (1995), has estimated that afforestation needs to increase by 500 000 ha over the next 30 years. A second objective of the RDP is to create jobs for the many unemployed people in South Africa. Forestry has been seen to be an important rural developer, requiring a large work force, especially in large scale afforestation, providing many secondary jobs requiring unskilled labour. In a recent survey, the Eastern Cape Province, within which the north East Cape region (NEC) is located was listed as the second poorest province in South Africa (Gardner, 1997). In response to Scotcher's (1995) assertions and the RDP's requirements, an important question needs to be answered: Which areas, in South Africa, which are not afforested can satisfy future large scale afforestation?

The NEC, although climatically and physiographically marginal for the support of silviculture, was seen to be one of the viable locations for large scale expansion in terms of afforestation and job creation. The NEC was identified to be one of the last remaining areas in southern Africa suitable for afforestation, taking into account the current requirements of the forestry permit system. A factor inducing concern, is that the NEC region forms a major part of the Umzimvubu catchment, which has its source regions in the Drakensberg. Concerns regarding the impacts of commercial forestry on the water resources are therefore justified. Afforestation in southern Africa is occurring more frequently on these hillslope headwater regions and DWAF (1995), cited by Summerton (1995) has estimated that commercial forest plantations are reducing the available water of South Africa by 3.5% (which is approximately 7.6% of the country's total current water demand). Bosch and Hewlett (1982) have shown that the tree species *Pinus patula* and *Eucalyptus grandis* cause an average of 40 mm change in water yields for every 10% change of forest cover.

Furthermore, apart from the impact of afforestation on water resources, concerns extend further, namely to the sustainability of forestry in the NEC. The NEC comprises hilly terrain with mostly shallow soils interfaced with fractured semi-permeable bedrock. The extent of commercial sustainability is therefore questionable when compared with the suitability of

afforestation in Zululand, for example, which has deep soils and good rainfall, rendering excellent conditions for commercial forestry.

Hydrological processes which occur on hillslopes are very complex and therefore a need to study them before reaching conclusions on tree water use under these conditions is essential. Infiltrating water tends to move vertically through the soil profile, and upon reaching the soil-bedrock interface, moves laterally downslope as interflow. Upon reaching the toe region, at the base of the hillslope, a build-up of soil water occurs, creating a saturated region. As this soil water build-up continues, exfiltration may occur, with water exiting the soil profile, moving over the soil surface as return flow, which may later re-infiltrate the soil further downslope. Many NEC soils also exhibit a proliferation of macropores and pipes that are hydrologically important, since water entering these conduits moves as preferential flow, bypassing the soil matrix by moving either directly to the bedrock or exiting further down the slope. Furthermore, where fractured bedrock occurs there is a likelihood that localised and perched water tables may develop.

The dominant questions regarding afforestation on these hillslopes are:

a. the viability of planting trees in this climatically marginal region,
b. the effect of saturated and water logging conditions in the toe region of the hillslopes and
c. the impact of afforestation on the soil moisture, water tables and interflow.

To answer these questions, two research phases have been initiated. The first phase will form the focus of this research and has the following objectives:

a. to understand and identify the dominant subsurface processes occurring at the hillslope scale,
b. using an intensive hillslope experiment, where the soil moisture, water table heights and soil water potentials of the soils will be monitored continuously, followed by
c. the development of a hillslope water budget and the use of an appropriate hillslope model, using measured and monitored data, to describe the soil water movement down a hillslope.

This first phase, approximately two years in duration, will enable questions regarding the dominant subsurface processes at the hillslope scale to be answered. The second phase,

which is not dealt with in this initial study, will be to monitor these dominant processes, once forested trials have been established on the catchment which is currently under natural grassland. Data and results from this second phase, *inter alia*, will enable decisions to be made regarding the viability of afforestation in the NEC.

To meet these first phase objectives, a comprehensive literature review (Chapter 2) has been conducted, in which hillslope subsurface processes are outlined and methods used in their measurement discussed.

In Chapter 3 the selection of appropriate hillslope models is presented, with the various approaches used in modelling infiltration and redistribution being described. Three selected hillslope soil water models, used to simulate subsurface processes at the hillslope scale, are reviewed. These models simulate subsurface processes, especially interflow on hillslopes having shallow soils underlain by semi-impermeable bedrock. These models are TOP*ACRU* (Schulze, 1995: Howe, 1997), HILL5D (Hebbert and Smith, 1996) and the HILLFLOW 3-D (Bronstert, 1995).

A catchment has been selected which typifies the NEC region in terms of the soils, vegetation, geology and topography. The catchment, called Weatherly , is situated 5 km east of Maclear in the NEC. The methodology used in this first phase of research comprised two components. First, initial field work consisting of the determination of particle size distribution (PSD), bulk density (ρ_b), porosity (ϕ), hydraulic conductivity (K) and water retention characteristics (WRC) of the soils at Weatherly was undertaken. These measurements were conducted on one hillslope transect, having a 11% slope. It is on this transect, called Transect 1, where research of this first phase is concentrated. Various surveys were conducted to determine the geology, soils, bedrock and topography of Transect 1. Secondly, an intensive hillslope experiment was established, in an attempt to identify and monitor the dominant subsurface processes that occur at this hillslope scale. The experiment comprises neutron moisture meter (NMM) measurements to measure the soil moisture status, piezometer tubes (GW) to monitor groundwater fluctuations and automated tensiometers (Nest) to monitor soil water potentials. Data from each of these instruments give information regarding the redistribution of water within the soil profile from which the extent of interflow can be inferred. Both components of this first stage of research are outlined in Chapter 4. Data from these field measurements and the monitoring of the instruments, with results, are presented in Chapter 5.

In Chapter 6 a simple hillslope water budget model is developed which takes into account additions to and removals out of the hillslope system. The water budget, in a simplified form, accounts for lateral flow (L), additions to the water table (GI), rainfall (R), removals from the water table (GO), evapotranspiration (ET), runoff (RO) and percolation through the bedrock (P). Using data measured and monitored, each variable is calculated and summed according to the following equation:

$$L+GI+R-(GO+ET+RO+P) = \Delta SV+\Delta SG$$

The result of the left-hand side of the equation should be equal to the sum of the change in the soil water in the vadose zone (ΔSV) and the change in the groundwater store (ΔSG). Such a water budget is used to identify the dominant processes occurring within the hillslope. Results from the water budget study were used to define input parameters for the HILL5D model. This model was used to simulate the movement of the perched water table down the hillslope. Results from these HILL5D simulations were hoped to be similar to those determined using the water budget. These model outputs were then compared with actual monitored data. Conclusions have been drawn regarding the redistribution of soil water within the soil profile, with the movement of perched water tables downslope as interflow.

A discussion of these initial results, both measured and simulated, are presented in Chapter 7, together with a concise conclusion. Since this research is one of the first studies of its kind in South Africa a number of recommendations for future research are summarized in Chapter 8. These recommendations include a discussion on how the experiment can be improved allowing for less maintenance of the instrumentation.

2. HILLSLOPE SUBSURFACE PROCESSES

The generation of streamflow is a complex process and an important one, especially at the hillslope scale, since it is in these areas that major rivers have their source. Runoff, baseflow and subsurface flow processes dominate many catchment storm flow hydrographs. At the hillslope scale, especially where soils are shallow, interfaced with semi-permeable bedrock, subsurface flows may contribute significantly to the hillslope storm flow hydrograph. To determine the extent of this subsurface flow contribution, various techniques and methods can be used to measure it. Sophisticated monitoring leads to a better understanding of subsurface flow processes at hillslope scales, which allows the use of models representing an increasingly complex array of processes (Anderson and Brooks, 1996). These models are very useful once calibrated in a test catchment to simulate the extent of different processes in other un-monitored catchments. The sections which follow include the discussion of selected hydrological processes which occur at the hillslope scale. As a matter of definition, subsurface processes refer to all processes occurring within the soil and subsurface flow is the process of interflow or lateral flow.

2.1 Subsurface Processes

Until the 1960s the notion of runoff generation was predominantly based on the Hortonian concept of overland flow (Horton, 1933 cited by Kirkby, 1988). Subsequent studies by Dunne and Black (1970), Harr (1977), Pilgrim, Huff and Doak Steele (1978) and others, have proved that Hortonian overland flow is only one of several mechanisms by which runoff is generated. The other recognised mechanisms of streamflow generation on hillslopes are subsurface flow (Dunne and Black, 1970), saturated overland and deep aquifer flow (Smith and Hebbert, 1983) and macropore flow (Bevan and Germann, 1982). Hillslope hydrology involves primarily flow processes within the soil and over the soil surface (Anderson and Burt, 1990). Understanding the contribution of each to the overall water budget is important (McCarthy, Flewelling and Skaggs, 1991). This section deals with these subsurface processes which are illustrated in Figure 1.

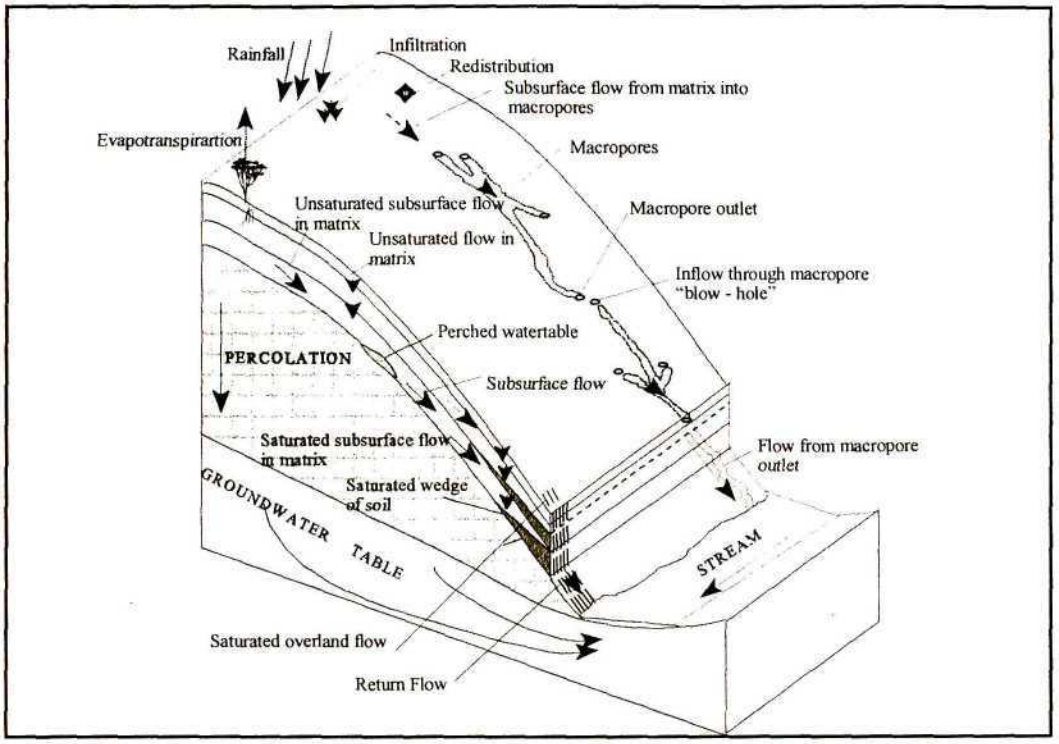

Figure 1. Flow routes of different hillslope processes within the soil (after Anderson and Burt, 1990).

Rainfall is partitioned into overland and subsurface flow processes (Kirkby, 1988) and at any point on a hillslope or within a soil, water moves in response to a potential gradient due to gravity and by a water pressure or tension, also referred to as the soil matric potential. The soil water potential is a key variable in the hillslope hydrological cycle and in the flow mechanisms which operate within the soil. During a rainfall event, infiltration will occur if the rainfall intensity is less than the infiltration rate of the soil. If the rainfall intensity exceeds the infiltration rate, ponding on the soil surface will occur followed by Hortonian overland flow. If ponding is sufficiently high, corresponding to a large head of water, macropore flow may occur, if macropores are present. Infiltration is dependent on the type of soil and its hydraulic conductivity (K). During and after a rainfall event, water redistributes within the soil, following different flow pathways within the saturated and unsaturated zones. Upon reaching a layer of low conductivity, a localised water table may develop followed by downslope subsurface flow in response to hydraulic gradients. This often leads to the possible development of saturated regions inducing return flow (depicted in Figure 1). Each of these processes and their interaction with one another is now reviewed, with reference to Figure 1, beginning with infiltration and redistribution.

2.1.1 Infiltration and Redistribution

Infiltration is defined at the process where water enters the soil from either rainfall, overland flow or irrigation and is determined, according to Morel-Seytoux (1983), by estimating the moisture contents within the soil. The actual infiltration flux is dependent on the antecedent moisture content (AMC) within the soil, which in turn influences the depth of the wetting front. This wetting front moves down the profile, with the area behind it increasing in saturation. Some infiltrated water may finally reach the saturated zone causing a possible rise in the phreatic surface (McCarthy, Skaggs and Farnum, 1991). With prolonged rainfall and depending on the soil depth and the depth to the water table, the phreatic surface could intersect with the soil surface after which saturated overland flow could occur, as shown in Figure 1. Redistribution is the soil water movement from one point to another within the soil (Rawls, Ahuja, Brakensiek and Shirmohammadi, 1992) and is affected by the K of the soil, the WRC, vertical potential gradient across the soil layers and the soil's physical properties. Infiltration, redistribution and position on the hillslope therefore dictates the type of subsurface processes which can occur. These subsurface processes are discussed in the following sections.

2.1.2 Subsurface Flow

Chorley (1978) defines subsurface flow as " that part of streamflow which is derived from the subsurface flow of water in saturated soil zones above water impeding layers, especially in basal hillslope soils, which discharges directly into the stream channel without entering the groundwater zone." It is commonly accepted that subsurface flow is a major runoff generating mechanism (Dunne and Black, 1970) and is a dominant contributor to storm flow (Hewlett, Fortson and Cunningham, 1984). Turton, Haan and Miller (1992) show that subsurface flow contributes to both quickflow and delayed flow. Corbett (1979), cited by Sloan, Moore, Coltharp and Eigel (1983), has estimated subsurface flow to contribute 75-95% of total storm flow volume, causing a rapid contribution to streamflow producing peaks in discharge within one to two hours after a rainfall event (Burt, 1985).

Three mechanisms cause this rapid subsurface discharge, *viz.* pipe flow, macropore flow and flow within the capillary fringe, which can be considered to be slow, but can be increased when the saturated conductivity (K_s) and the phreatic surface are high. The

capillary fringe can be defined as either the unsaturated zone above the water table, but below the point where soil drainage occurs (Burt, 1995), or as the saturated portion between atmospheric and air entry pressure (Lorentz, 1997).

Sklash, Stewart and Pearce (1986) claim that storm flow is dominated by the rapid displacement of old water, which is soil water which resides in the soil before rainfall, and steepened hydraulic gradients resulting from the formation of saturated wedges at seepage faces, which explains a rapid subsurface flow flux. According to Turton, Barnes and de Jesus Navar (1995) streamflow, especially in forested catchments, has varying ratios of old and new water. This ratio gives an indication as to how the water entering the catchment mixes with the soil water and groundwater already present. Conclusions can be drawn from these ratios regarding which processes are dominating the hillslope hydrograph. Both Turton *et al.* (1995) and Wilson, Jardine, Luxmoore, Zelanzny, Lietzke and Todd (1991) have shown that the percentage of old water is initially high with the onset of interflow and then decreases, with the percentage of old water being at its lowest when interflow reaches its peak. In areas which have a proliferation of macropores, new water can bypass the soil matrix to the bedrock, thus contributing to interflow rapidly, after which the mixing of old and new water occurs (Peters, Buttle, Taylor and LaZete, 1995). Factors which affect the ratio of old to new water include the rainfall intensity, duration and AMC. Using the ratio, Wilson *et al.* (1991), have shown that perched water table development is the predominant mechanism of flow through lower layers during moderate to high water fluxes. During higher fluxes, subsurface flow response consists largely of new water which has bypassed the soil matrix via macropore flow, with the percentage of old water increasing during later stages of the event.

Many factors and conditions conducive to subsurface flow have been realised through specific experimentation. A major prerequisite for saturated subsurface flow generation, is shallow permeable soil on steep slopes, with the soil having a relatively high K, but being underlain by a semi-permeable or impermeable layer of lower K (Sloan and Moore, 1984), or bedrock. Factors which influence the timing and amount of subsurface flow include the AMC before the storm (Wilson, Jardine, Luxmoore and Jones, 1990), rainfall amount and intensity, soil depth and the physical properties of the soil such as texture and structure (Whipky and Kirkby, 1978). Lehman and Ahuja (1985) have shown that the water temperature and AMC control subsurface flow. This was substantiated by Turton *et al.*

(1992), who preformed an accurate study of interflow interception on a naturally exposed face at a stream bank where changes as small as 1 litre could be detected. This research showed that as the AMC increased, interflow volumes exiting the soil face increased with time.

Beckedahl (1996) demonstrated that in a coarse textured soil the dominant flow direction is usually vertical, whereas in a fine textured soil the resistance to vertical flow on a slope results in a lateral movement of shallow subsurface flow, which increases with an increase in wetted depth and soil water content (Wallach and Zaslavsky, 1991). It must be made clear that subsurface flow can occur in deep soils, but its response to a storm will be delayed compared with that of a shallow soil. Other factors which influence the timing and amount of subsurface flow are the spatial distribution of the soil water content (Mulholland, Wilson, and Jardine, 1990), slope concavity or convexity, slope length to depth ratio and leakiness of restrictive layers. An entire hillslope does not contribute equally to subsurface flow. Therefore, topography, together with concave regions, is an important controlling factor. Wallach and Zaslasky (1991) have shown that it is only the unsaturated flow component which is proportional to the slope angle and soil anisotropy, with the result that water accumulates in concave regions producing local saturation and exfiltration. These concave regions often occur at the base or toe region of the hillslope. Furthermore, the vegetation, lithology, rainfall duration as well as intensity play important roles in the generation of subsurface flow (Wilson *et al.*, 1990).

Once infiltrated water reaches the interface between layers of differing conductivities, a saturated wedge can form (Weyman, 1973), as shown in Figure 1. If this saturated wedge is on the midslope, subsurface flow moves through the soil laterally as a perched water table as the hydraulic gradient increases. Fernandes, Netto and Lacerda (1994) have shown that interflow depends on the AMC and that the interflow contributing areas expand and contract throughout the rainy season. A saturated wedge at the toe of the hillslope causes possible exfiltration, as discussed in Section 2.1.3 below.

2.1.3 Exfiltration and Return flow

The capillary fringe contributes rapidly to the groundwater response. This zone above the water table, which is diffuse and variable with time (Hillel, 1982), may be saturated under

negative pressures extending to the soil surface. Figure 2 shows the relationship between the WRC of the soil and the capillary fringe. The WRC is defined as the soil's ability to store and release water and is the functional relationship between the soil water content and the soil matric potential of the soil.

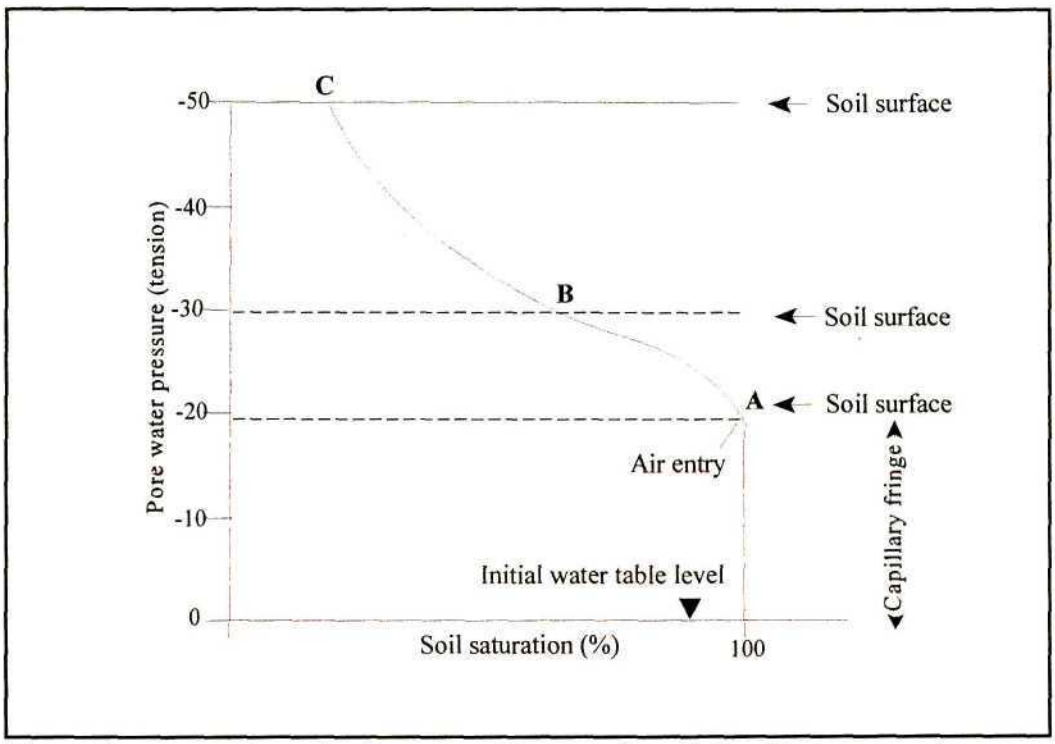

Figure 2. A schematic diagram to illustrate the relationship between the water retention characteristic and the capillary fringe (after Burt, 1985).

Three points: A, B and C represent imaginary soil surfaces. Points A and B represent a near saturated soil with the capillary fringe intersecting the soil surface at B. A low intensity rainfall event will result in most of the rainfall being infiltrated, usually causing an immediate rise of the water table. Flow will then be directed laterally to the toe of the slope, resulting in a region of zero pressure head. On the other hand, at point C, infiltration will occur, with a subsequent delayed subsurface flow response.

Groundwater ridging is another concept which could account for the rapid subsurface flow (Sklash and Farvolden, 1979). Groundwater ridging is limited to the near channel region and is a result of redistribution between the capillary fringe and the phreatic surface after a rainfall event. In this region of the hillslope the phreatic surface could intersect the soil surface and saturated overland flow will occur, as shown in Figure 1.

This process, known as exfiltration, occurs when subsurface flow exits a hillslope through the groundwater body (Wallach and Zaslavsky, 1991) or is diverted by an impermeable layer (in response to increased hydraulic gradients), moving over the soil surface as return flow. It predominates in the lower parts of slopes (Tsukamoto and Ohta, 1988). Exfiltration and return flow depend on topographic convergence, emergence of macropores, thin soils and impermeable layers (Stagnetti and Parlange, 1987) and can occur on flat to moderately steep terrain (Kubota and Sivapalan, 1995). The emergence of macropores in the toe region enhances exfiltration and is discussed in Section 2.1.4 below.

2.1.4 Macropore Flow

Porous media often have a variety of heterogenities such as fractures, cracks, pipes and macropores. These structures affect water movement at the macroscopic scale creating non-uniform flow fields with widely differing velocities (Gerke and van Genuchten, 1993). Soil pores can be described as either macropores, mesopores or micropores. It is often difficult to distinguish between the matrix and macropore flow. Generally, however, laminar flow obeying Darcy's law flows in the matrix, whereas turbulent flow occurs in macropores. Macropores are saturated at pressure potentials near and above zero (Bevan and Germann, 1982), and have been known to be continuous for distances up to a few metres both in the vertical and horizontal direction. They can be large or small, discrete or continuous, relatively straight or tortuous, numerous or scarce, all of which affect the magnitude of possible preferential flow (Ahuja, DeCoursey, Barnes and Rojas, 1991). Pipes are regarded as macropores which have undergone erosion and are enlarged as a result.

There is considerable debate related to water movement in macropores. Shaffer, Fritton, and Baker (1979), cited by Habib, Zartman and Ramsey (1988), claim that in certain soils more than 90% of water can flow along preferential flow pathways. On the other hand Denning, Bouma, Falayi and van Rooyen (1974) report that although macropores make up the highest percentage of total ϕ, they conduct only a small percentage of water. This dichotomy could possibly be explained if one considers the rate of supply of water to the soil. As precipitation begins, water infiltrates the soil matrix through the micropores. As the wetting front moves down the profile, the area behind the front will increase in soil water content. Once the soil is close to saturation, macropore flow could begin if the supply of water is adequate and/or the macropores are open at the surface (Figure 3), with gravity

being the principal driving force for macropore flow (Germann and DiPietro, 1996). This occurs slowly at first with water moving down the walls of the macropores.

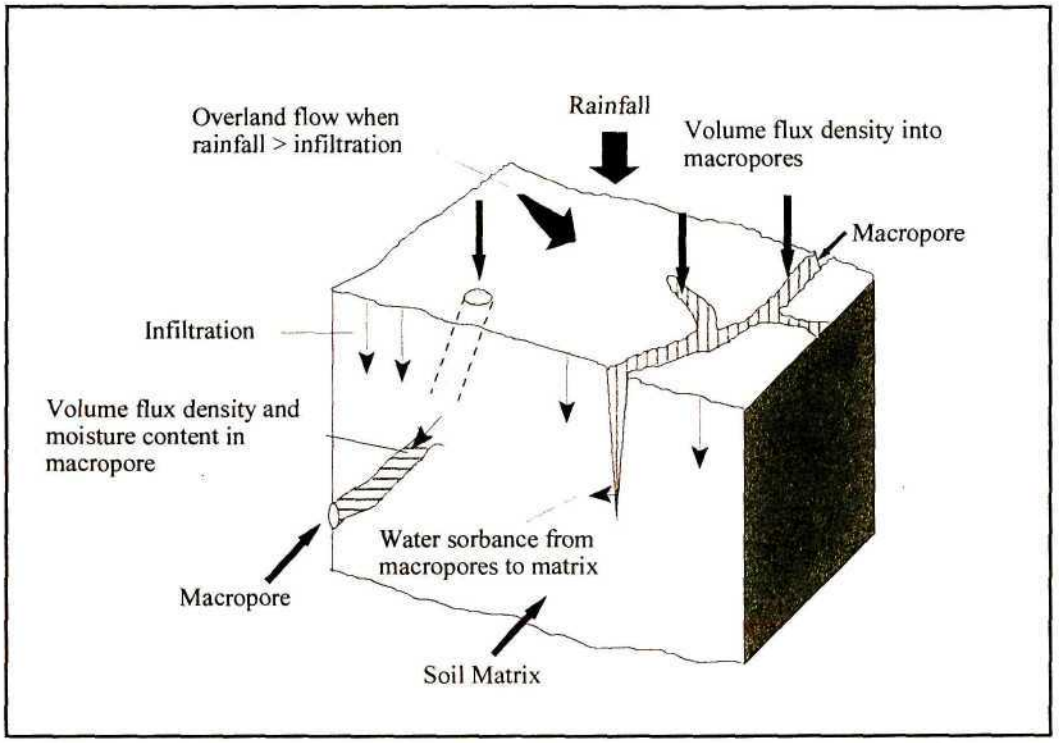

Figure 3. Presentation of the fluxes occurring during infiltration into bimodal soils (after Germann, 1990).

If a hydraulic gradient exists in the surrounding matrix, water sorbance will take place from the macropores to the micropores (Bevan and Germann, 1982), as shown in Figure 3. Flow out of the macropores into the matrix will continue if the matric potential in the matrix remains negative and the gradient from macropore to micropore is positive. As the matrix next to the macropores becomes wetter, the flow into the matrix declines as the hydraulic gradient decreases. When the entire soil profile is saturated, or if the supply rate is sufficiently rapid, ponding will occur on the soil surface with rapid drainage into the macropores (Bevan and Germann, 1982). Macropores can deliver water at greater velocities and lower tensions than the surrounding soil matrix (Bevan and Germann, 1982) and can occur within both unsaturated and saturated zones.

With a clearer understanding of the main subsurface processes which can occur on hillslopes, techniques used in their measurement can be reviewed. Measuring these processes is vital prior to any simulation modelling, as subsurface process contributions can be determined and in addition, the dominant processes can be established under varying

conditions. Some of the more common techniques used to measure these subsurface processes are reviewed next.

2.2 Measurement of Subsurface Processes

In hydrological simulation modelling, more attention and stature are often given to modelling a system rather than to the experiments upon which the modelling should be based (Wagenet, 1988), which leads to a common question: which should come first, the modelling of a system or the understanding of the basic processes operating it? To measure and understand the hydrological processes is important before these processes can be modelled. With a knowledge of these processes and collected data, a sound database can be established by which the model can be tested and verified, which then enables the model to work well for the right reasons (Wagenet, 1988).

To measure the rate or magnitude of any hydrological phenomenon it is necessary to understand what one is trying to measure (Atkinson, 1978). Measuring these processes is a difficult task and can be divided into three categories according to Atkinson (1978), unless otherwise specified.

a. First , methods may be used which involve the interception of flow, where all or part of the flow is intercepted and channelled into measuring devices to determine the volumes of macropore flow, matrix flow and interflow. This includes the addition of tracers, where either radioactive compounds or fluorescent dyes are placed in groundwater piezometers and detected at another point to determine the contributions to the matrix and macropores and the rate of groundwater flow.

b. Secondly, indirect methods may be used where the moisture contents, depth to groundwater and hydraulic potentials are measured over the hillslope. These data are used to calculate and deduce matrix flow, redistribution, movement of localized water tables downslope (interflow) and to calculate the moisture flux in both the unsaturated and saturated zones. These methods include the measurement of old (groundwater) and new (rainfall) water ratios, which are used to determine which processes dominate the streamflow hydrograph (Turton *et al.*, 1995; Anderson and Brooks, 1996).

c. Thirdly, direct methods using specific instruments, such as the sorptivity tube (Clothier and White, 1981), disk permeater (Perroux and White, 1988) or macropore infiltrometer (Wang, Norman and McSweeny 1994) may be applied. These methods are time consuming, give site specific results and cannot determine the geometrical extent of the macropores.

Most of the current experimental research being performed in determining these subsurface processes uses a combination of these three methods. Consequently, common methods used in the literature are reviewed together, omitting the water ratio and direct methods.

2.2.1 Interception of Flow and Indirect Methods

In measuring subsurface and macropore flow, most studies have involved either exposing a vertical face of soil across the base of the hillslope, or the use of an existing natural seepage face. A common experimental setup involves the construction of throughflow troughs and gutters at the base of, or at distinct layers in the exposed face, usually where there is a marked change in ρ_b, to monitor subsurface flow. To determine the extent of macropore flow, tubing is usually placed and sealed within actual macropores and the water is routed to collection vessels. In both cases water flowing from the soil can be measured using flumes or tipping buckets to calculate flow contributions from various horizons, in response to rainfall events. Figure 4 depicts an experiment conducted by Tsuboyama, Sidle, Noguchi and Hosada (1994) where both interflow and macropore flow was intercepted from an exposed vertical face, to identify specific mechanisms and pathways of interflow, with respect to matrix and macropore flow. Macropore continuity, direction and size were determined by probing the macropores with wire and measuring the diameters. Macropores having similar diameters were grouped and channelled into collection containers via tipping buckets as shown in Figure 4.

In this particular experiment (Figure 4) macropores one through seven in the A-horizon were grouped together, with the remainder being grouped according to size. Tensiometers were inserted at different depths upslope of the excavation pit to monitor the redistribution of water in the soil profile. Data collected from the tensiometers enabled the construction of flow lines which were used to correct for distortions in the flow (*cf.* Sections 2.2.1.1 and 2.2.1.2). Results of this experiment showed the variability in contributions from the soil

matrix and macropores. Matrix flow occurred within the surface layers at the onset of rainfall, followed by a rise in the phreatic surface, probably in response to preferential flow (Weyman, 1973).

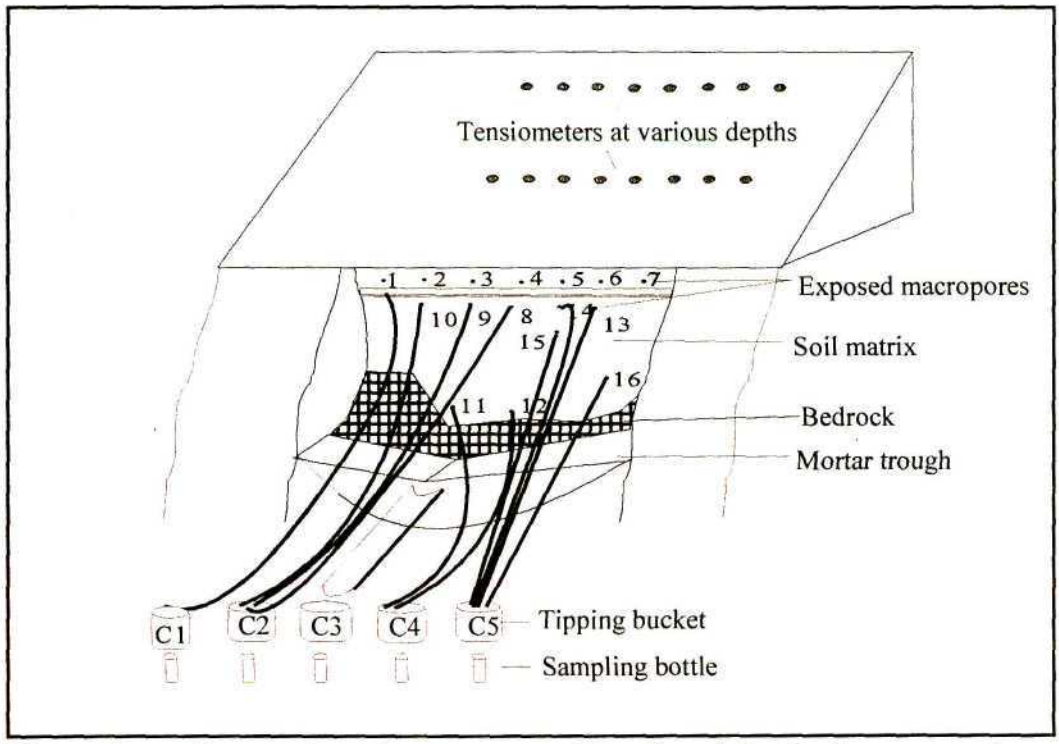

Figure 4. Interception of macropore and interflow (after Tsuboyama *et al.*, 1994).

In a similar experiment Turton *et al.* (1992) showed that macropores can deliver interflow at high velocities and lower tensions than the surrounding matrix, with flow occurring in both saturated and unsaturated conditions (Wilson, Jardine, O'Dell and Collineau 1993). Jeje, Ogunkoya and 'Uyi (1986) showed some unexpected results where much of the measured interflow occurred from the surface horizons only. This occurrence could possibly be explained by a relatively thick litter layer present, having a higher K compared with the physical soil surface.

A common conclusion drawn from interception of flow studies is that interflow occurs predominately in deeper horizons with a large variability of interflow contributions in all the other horizons, dependent on the storm's characteristics (Koide and Wheater, 1992). Hillslopes have different responses and variations can range spatially and temporally (Whipkey and Kirkby, 1978) across a plot and vertically down the soil profile. This is demonstrated by Wilson *et al.* (1991), where a trench was excavated at the base of a hillslope, which had a seepage area running down the centre with converging slopes on

either side of it. Interflow volumes were the greatest from this seepage area as it was surmised that flow converged laterally into this draw region in response to hydraulic gradients. Furthermore Parlange, Steenhuis, Timlin, Stagnitti and Bryant (1989) have shown interflow on hillslopes with fragipan horizons to move vertically through this impermeable layer through cracks exiting beneath it. A fragipan horizon is one which has a high clay content. With the drying of these soils cracks develop, which become filled with smaller soil particles from above. Once a sufficient head of water develops on this layer water is forced through the cracks and water 'leaks' out of the system, exiting as subsurface flow below the impermeable layer.

Using piezometer tubes, installed to either bedrock or within different soil horizons, depth to groundwater can be determined. Piezometer tubes installed within horizons allow the measurement of perched water tables. Depths to groundwater are recorded using either pressure transducers placed at the base of the piezometers, which record pressure changes in response to a changing head of water, or by using styrofoam markers to record maximum water table heights reached (Thompson and Moore, 1996). Groundwater measurements are important, as changes in storage can be calculated together with increases or decreases in the hydraulic gradient, which is the driving force behind the generation of saturated subsurface flow down a hillslope. During low and moderate flows, Tsukamato and Ohtu (1988) observed perched water table development to be small compared with higher flows where there was a substantial growth in the water table, yielding larger subsurface flows.

Although interception of subsurface flow is a commonly used method to determine macropore flow and interflow directly it is not without problems, especially at artificially exposed seepage faces. Artificially excavated seepage faces induce saturated throughflow which almost certainly would not occur in undisturbed profiles. In addition, distortion of flow occurs where water can either converge or diverge away from the seepage face under different conditions as discussed in Sections 2.2.1.1 and 2.2.1.2 below.

2.2.1.1 Saturated Throughflow in Trenches

The technique of collecting water from a seepage face will only collect saturated throughflow (Atkinson, 1978). In order for the water to move out of the face, atmospheric pressure must be reached. Thus, the soil at this exposed face must be saturated and

inevitably a wedge of saturated soil will extend upslope which would not normally be there had an artificial face not been constructed. This anomaly is shown in Figure 5.

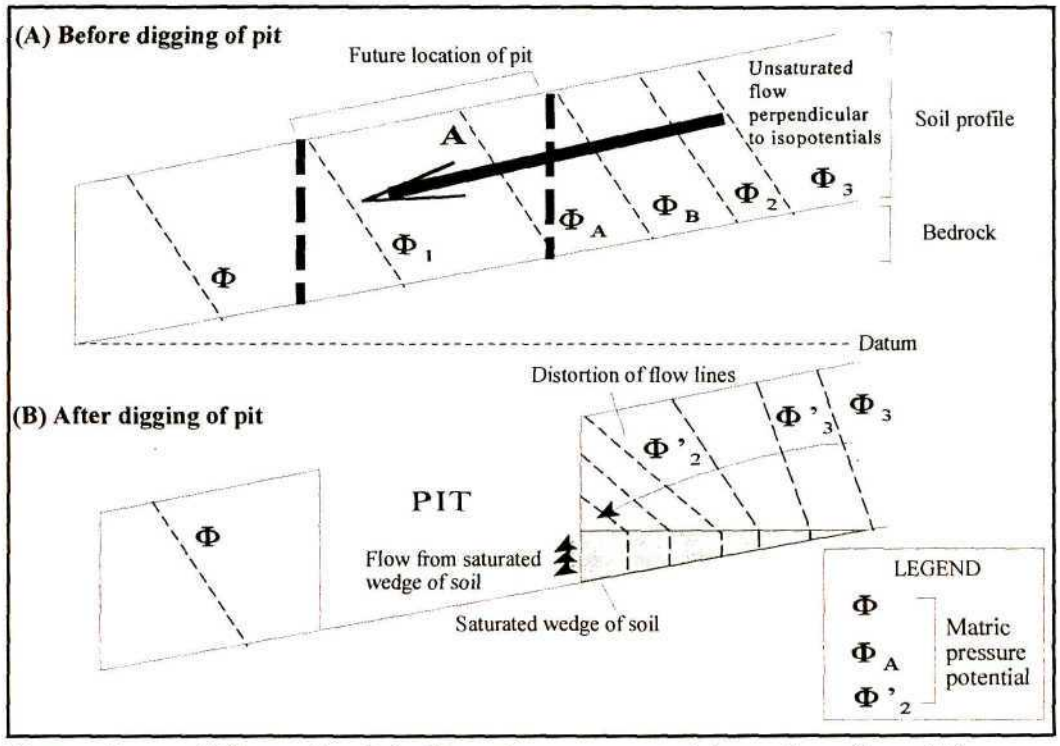

Figure 5. Effects of a pit in distorting unsaturated downslope flow. (A) Profile before the digging of the pit, and (B) the profile after the pit has been dug (after Atkinson, 1978).

If there is a downslope flux of moisture throughout the whole thickness of the soil under unsaturated conditions, point A, shown in Figure 5, will have a pressure potential which varies between ϕ_A to ϕ_B at the base of the soil profile. Unsaturated flow will prevail in the absence of a water table. After a soil face is exposed, water can only leave the free surface once the matric potential at the free face exceeds zero. For this condition to be met the soil needs to be saturated. A saturated wedge forms upslope of the exposed face, giving rise to a hydraulic gradient which results in a subsequent pressure increase, which forces water out of the exposed face as saturated throughflow.

2.2.1.2 Distortion of Flow

Apart from saturated throughflow occurring at artificially exposed seepage faces, the net hydraulic potential on the hillslope is distorted, as depicted in Figure 6. This implies that the exposed face receives drainage from areas which are not directly upslope. The hydraulic potential within the slope is distorted above the exposed face so that downslope drainage

on either side of the pit is channelled towards the free face when the natural interflow is unsaturated (Figure 6a) and outwards around the pit when a wedge of saturated soil (Figure 6b) is formed (Knapp, 1973; cited by Atkinson, 1978).

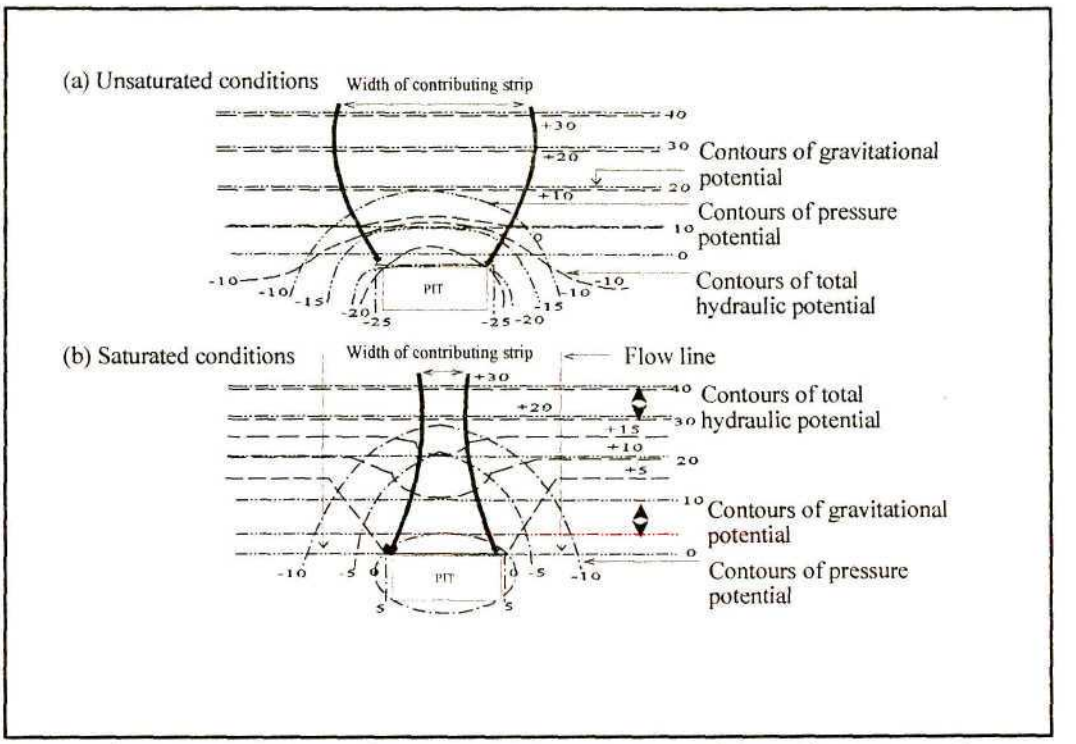

Figure 6. Distortions of flow. (a) Unsaturated conditions. (b) Saturated conditions (after Atkinson, 1978).

Using tensiometers upslope of these exposed faces, these anomalies can be corrected by determining the hydraulic potentials within the soil at different depths. These data were used to construct equi-potential lines and flow lines delimiting the contributing area. A solution to circumvent these effects would be to backfill the trench following the installation of the gutters and troughs. If done correctly, hydraulic continuity can be achieved, thus eliminating these effects.

The hydrology of subsurface flow on a hillslope is essentially a black-box problem (Atkinson, 1978). To measure these processes directly, one is often forced to use methods or instruments which disturb the very things one is trying to measure. This situation can be avoided by using tracers to obtain information on the path, dilution and dispersion of soil water through hillslopes, thus the velocity, direction of soil water movement and flow pathways can be elucidated. Section 2.2.2 outlines briefly some of the more important tracers used to measure hydrological processes.

2.2.2 Tracers

Tracers are unique in investigating hydrological processes on a large temporal and spatial scale, with the most useful tracers being tritium, chloride-36 and meteoric chloride. Dye tracers are useful to trace subsurface flow since they are mobile, distinctly visible and non toxic (Flury and Fluhler, 1995). Two main dye tracers are used in the study of soil water movement. The first are fluorescent dyes, which strongly absorb light of certain wavelengths and reflect radiation of a longer wavelength. These dyes adsorb to clays and organic matter and a compromise proposed by Trudgill, Pickles, Smettem, and Crabtree (1983) is that if the subsurface flow is rapid, the adsorption rate may be slow in comparison. Non fluorescent dyes are classified as acid, basic or dispersive, with the former being most suited to water tracing. Radioactive tracers are an excellent way to monitor subsurface flows since they are easily detectable at low concentrations, but they require sophisticated detection equipment, knowledge of safety measures and skilled personnel to use them (Gupta, Moravcik and Lau, 1994). Tracers have been used often, but they are generally expensive, relatively unstable in the soil, undetectable over a wide range of conditions and have the potential to create pollution problems with respect to the water table. Nevertheless using dyes, Flury, Fluhler, Jury and Leuenberger (1994) showed that preferential flow is the rule rather than the exception in well structured soils. Peters *et al.* (1995) confirm that slopes having shallow soils induce interflow to occur at the soil and bedrock interface with some water moving as preferential flow feeding the groundwater body.

* * *

In Chapter 2 different subsurface processes which can occur on hillslopes have been emphasised, together with factors which control them. The hillslopes discussed are typified as having shallow soils underlain either by semi-permeable layers or semi-permeable bedrock. These conditions are conducive to the formation of subsurface flows in response to perched water table development. Various measurement procedures used in the literature to determine these processes and their interaction with one another, are highlighted. These include the interception of flow and the use of hydrological tracers. Chapter 3 continues with a discussion on models in general and procedures used in the selection of an appropriate model. Literature on modelling infiltration and redistribution is presented and then three models which simulate some of the processes outlined in Chapter 2, are reviewed.

3. REVIEW OF HILLSLOPE MODELS

Before modelling hillslope hydrological processes, detailed experiments need to be carried out to determine which processes occur and what their relationship is with each other. Soil physical and hydraulic characteristics also need to be determined, from which important parameters can be determined using the Brooks and Corey (1964) or van Genuchten (1980) functions of unsaturated flows. With these prerequisites in place the modelling of a hillslope hydrological system can take place.

A general objective of hydrological research and modelling is to give decision makers scientific information about the particular hydrological system, so that objective and informed decisions can be made. This allows the transfer of knowledge from a measured area, to an area where hydrological decisions and information are needed. Mathematical expressions of observations and predictions of the time variant interactions of various hydrological processes can be determined, for use in the planning design and management of hydrological related structures (Fleming, 1975; Schulze, 1987). In other words, models enable scientists to learn about hydrological processes and state them mathematically.

3.1 The Need for Modelling

Models allow for "what if" questions to be posed and different scenarios to be simulated. Before the advent of computers and computer simulated models, these "what if" questions could have been answered by physical experiments, which could require years to run to completion (Smith, 1992). With the manifestation of computers and computing technology, the trend in hydrological modelling, according to Maaren (1991), is towards physically based models. These physically based models solve hydrological problems and consider physical realities to evaluate certain catchment scenarios and land use changes (Hillel, 1977). Hutson (1984) has cautioned against the indiscriminate and blind use of simulation models: " It must be remembered that simulation *per se* cannot solve a real problem. It can only simulate a solution. Its results are predetermined by the input, although the full consequences of this determinism are often unforseen for complex systems. A simulation can indeed provide new perspectives on the problem, but its predictions are sometimes doubtful, even when the model is hydrologically sound. When a model is not sound, i.e.

when its premises or data are wrong, there is a great danger that it will gain a false aura of respectability merely because it was processed on a computer, which still conveys a sense of magic to many laymen. Simulation is not a panacea. It is not a substitute for experimentation, but a possibly more rational basis for experimentation. Detailed, sound and comprehensive experimentation is required as a basis for devising models and for supplying the necessary parameters and for validating their results. Reciprocally, such results can help economise experimentation by guiding it to where it is needed most." This argument gives a sound basis upon which hydrological simulation models should be based and reinstates the importance of field work and experimentation.

Many different types of hydrological simulation models are available, each appropriate for certain hydrological problems. Types of models are highlighted in Section 3.2 below.

3.2 Types of Models

A model is a quantitative mathematical expression of analysis, observation and prediction, which contains physical laws and experimental observations all of which are combined to produce outputs based on a set of known or boundary conditions. Hydrological models can either be predictive, achieving a specific answer for a specific question, or investigative, where a further understanding of the hydrological processes is attained (Grayson, Moore and McMahon, 1992). Investigative models require more data, are sophisticated and provide more insight into the specific processes than predictive models (Grayson *et al.*, 1992). These models can be classified as either theoretical or empirical models. A theoretical model includes a set of general laws or theoretical principles and is physically based if the physical laws are describable by mathematical physics. However, all existing theoretical models simplify the physical system and often include empirical components and are thus conceptual models. If the modelled results are free from random variation, the model is deterministic. Other models include calibrated parameter models, where one or more parameters can only be determined by fitting computed values to the observed values. A measured parameter model has parameters that can be easily determined satisfactorily from known catchment characteristics, either by measurement or by estimation, so that it can be applied to totally ungauged catchments. Lumped models do not explicitly take into account the spatial variability of inputs, outputs, or parameters. They are usually structured

to use average values of the catchment characteristics affecting runoff volume. Averaging a certain parameter also implicitly averages the process being represented. Because of non-linearity and threshold values, this can lead to significant error. Distributed models include spatial variation in inputs, outputs, and parameters.

In this study, physically based investigative and predictive models are required. The purpose for using an investigative model is to understand the basic hillslope subsurface processes and their relationship with each other. An example of such a model is a simple hillslope water budget (*cf.* Section 6.2), where subsurface processes and soil water fluxes are investigated. With a knowledge of these processes, their interactions can be established. Once an accurate hillslope water budget has been achieved, predictive models (*cf.* Section 3.5) can be used to simulate these subsurface processes under different scenarios.

In order to simulate subsurface processes, the hydrological problem needs to be defined, followed by the use of the simplest model with appropriate complexity and adequate accuracy. Section 3.3 below, reviews the question of model selection.

3.3 Model Selection

A model that is appropriate to simulate the problem needs to be sought, rather than adapting the hydrological processes to the model. Physically based, continuous soil moisture accounting models are the most accurate models currently available with the SHE (Systeme Hydrolique International) catchment model being the most comprehensive model of this type. The SHE model (Bathurst, 1986) links surface runoff and subsurface processes and is a very good model at the catchment scale. Nevertheless, at a smaller scale, such as the hillslope scale, it is not satisfactory, as more detail is needed. Such detailed models include the physically based models such as SWIM (Soil Water Infiltration Model), (Ross, 1990) and LEACHM (Soil water Leaching and Chemistry Model), (Hutson and Wagenet, 1992) which are detailed in soil moisture budgeting. However, these models do not consider interflow nor perched water table movement down hillslopes. Therefore a specific model is required which considers the processes that occur at Weatherly.

Three models are described in Section 3.5 The sections that follow summarise some infiltration and redistribution models, which use Darcy and Richards (1931) type equations. This is followed by the review of three hillslope models that were recognized as appropriate models that can be used at the hillslope scale. Each of these models has merits for the simulation of hydrological processes at Weatherly but for reasons given , one appropriate hillslope model is selected. The models are the *ACRU* / TOP*ACRU* (Schulze, 1995; Howe, 1997) modelling system, HILL5D (Hebbert and Smith, 1996) and HILLFLOW-3D (Bronstert, 1995).

3.4 Approaches to Modelling Infiltration and Redistribution

The modelling of infiltration and redistribution can be carried out using simple or complex models. Complex models for this purpose require numerical solutions to solve Richards equation. Many equations and models have been developed for estimating infiltration rates. These models are outlined and special attention is paid to the Green and Ampt (1911) infiltration model, because this relatively simple model has parameters which are easily determined and the approach is widely used in many simulation models.

3.4.1 Infiltration

The prediction of infiltration is a key step in modelling runoff, soil water recharge and redistribution within the soil profile (Buitendag, 1990). Therefore, a need for accurate and easily applicable models is necessary. Most methods use simplified concepts that predict the infiltration rate or cumulative infiltration volume assuming that surface ponding begins when the rainfall intensity exceeds the infiltration rate at the soil surface (Rawls, Ahuja, Brakensiek and Shirmohammadi, 1992). These methods require highly site specific data that are difficult to obtain.

Complex models do exist. For example, Mein and Larson (1973; cited by Aron, 1992) used a procedure that combined the Green and Ampt (1911) and Richards (1931) equations where conductivity and retention characteristics of the soils are required. Using physically based models that solve the Richards (1931) equation, boundary conditions and detailed

data input are needed. The Richards (1931) equation is very difficult to solve, requiring much computing power and time (Rawls *et al.*, 1992).

The Horton (1933) equation, as used by Aron (1992), is a simpler method of calculating infiltration. In this equation the infiltration rate depends *inter alia* on the cumulative antecedent infiltration. Other simple models include rainfall excess models where all losses such as infiltration, depression storage and interception are lumped, or alternatively empirical and approximate models which consider the soil as a semi-infinite medium with a wetting front moving downwards in response to gravity. Examples of these simple, empirical and approximate models can be found in Rawls *et al.* (1992). For the sake of brevity the Green and Ampt (1911) model will be described, as it is a commonly used method in the hillslope models reviewed in this chapter.

The Green and Ampt model (1911) is an approximate model that uses Darcy's law, and was originally developed for ponded infiltration into a homogeneous soil with a uniform initial water content (Rawls *et al.*, 1992). The model considers infiltration to be represented by a vertical piston flow. This assumes that the entire pore space between the soil surface and a well-defined wetting front takes part in the flow process where old water is replaced by new water (Germann, 1990). The model assumes that:

a. the water diffusivity, water content, K and matric potential head in the wetted region all remain constant and
b. the matric potential head at the wetting front is constant (Jury, Gardner and Gardner, 1991).

Figure 7 shows how the Green and Ampt (1911) model is conceptualized in the soil profile. The soil surface is ponded with a head of water (H_o), below which extends a saturated zone (L_f) interfaced with an unsaturated zone having an initial water content (θ_i). Omitting the head of water at the soil surface and assuming that the soil is single layered, having an infiltration rate equal to the rate at which infiltrated water enters the soil or the infiltration capacity, the basic Green and Ampt (1911) rate equation is:

$$f=K[1+\frac{(\Phi-\theta_i)S_f}{F}] \qquad (1)$$

where K = effective hydraulic conductivity ($mm.h^{-1}$)

S_f = effective suction at wetting front (mm),

ϕ = soil porosity ($m.m^{-3}$),

θ_i = initial water content ($m.m^{-3}$),

F = accumulated infiltration (mm) and

f = infiltration rate ($mm.h^{-1}$).

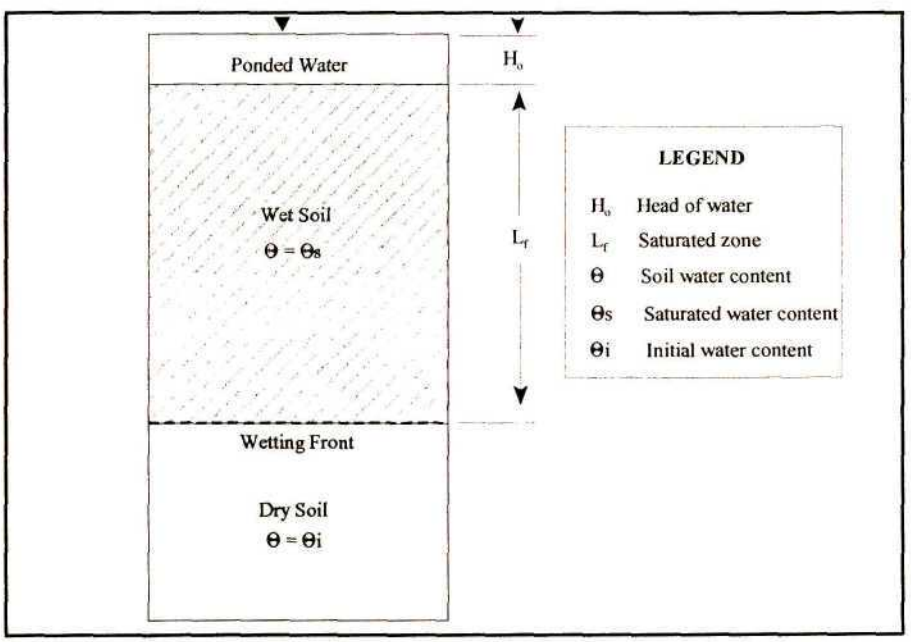

Figure 7. Representation of the Green and Ampt (1911) model, after Rawls *et al.* (1992).

However, homogeneous single layered soils are rarely found. Most soils are composed of three soil layers, a situation which does not satisfy the conditions and assumptions of Equation 1. Buitendag (1990) outlines the development from a one layered Green and Ampt (1911) model to that for a three layered soil.

The parameters that need to be specified in the Green and Ampt (1911) model are K and S_f, which is calculated as a function of the K and WRC of the soil as well as, ϕ and Θ_i, all of which can be measured or estimated. The wetting front suction parameter can be estimated from Brooks and Corey (1964) parameters as

$$S_f = \frac{2+3\lambda}{1+3\lambda}\frac{h_b}{2} \qquad (2)$$

where λ = Brooks and Corey (1964) pore size distribution index

h_b = Brooks and Corey (1964) bubbling matric pressure head (m).

The Brooks and Corey (1964) parameters can be determined by fitting functions to actual WRC measured data (*cf.* Section 5.2.2).

3.4.2 Redistribution

Soil water redistribution models vary in complexity from simple water budgeting models to more complex ones, solvable by either analytical or numerical methods. Water budgeting models calculate a water budget within the soil profile, keeping a record of the inputs and outputs to the system. Complex models concentrate on the soil water dynamics in the unsaturated zone. The soil water dynamics are considered in terms of the flux density distributions, changing water contents and matric potentials.

Modelling soil water movement in the unsaturated zone involves the computation of complex equations, which cannot usually be solved by analytical methods (Reece, 1986). Numerical methods are thus sought and can be of two types. These methods are finite difference and finite element solutions, each to be used depending on the problem to be solved. Finite element methods are superior to finite difference methods, as complex boundary conditions can be more easily defined and the non-linearity of the soil water characteristic is recognised (Binley and Bevan, 1992). To use these methods, a grid is placed over the area of consideration. These grid sizes can vary from a coarse grid size, which is spatially inaccurate, to a fine grid which enables the simulation of localised hydrological processes, but requires much computer time due to the number of computations to be performed. These methods solve for the dependant variable at each grid node. The governing Richards (1931) equation, is approximated by a set of algebraic equations which are solved usually by iteration.

These methods are used to solve the Richards (1931) equation. This equation is widely used in solving unsaturated flow problems and is derived from Darcy's law and the continuity equation. Darcy's law refers to flow through saturated soils, where the flow is proportional directly to head loss and inversely to the length of the flow path, with a proportionality constant called the hydraulic conductivity. For steady state flow the equation can be written as follows, where this applies to a homogeneous and isotropic soil in which soil water properties do not vary with direction or location:

$$q = -K\frac{dH}{dZ} \qquad \textbf{(3)}$$

where q = flow rate per unit cross-sectional area ($mm.h^{-1}$)

K = hydraulic conductivity ($mm.h^{-1}$)

Z = distance in direction of flow (mm)

H = hydraulic head (m), which can be further expressed as

$$H = h + z \qquad \textbf{(4)}$$

where h = soil water pressure head (m)

z = elevation above a reference (m).

The water conservation equation relates water fluxes, storage changes and sources and sinks of water. When combined with Equations 3 and 4, the Richards equation can be written to predict water content in a soil during transient flow as follows:

$$\frac{\partial\theta(z,t)}{\partial t} = \frac{\partial}{\partial z}[K(\theta,z)\frac{\partial h(\theta,z)}{\partial z} - 1] \qquad \textbf{(5)}$$

where t = time (h), and

$K(\theta, z)$ and $h(\theta, z)$ allow for variation of $K(\theta)$ and $h(\theta)$ with depth z.

Many hillslope models use Equation 5 to model redistribution. Each model is usually modified to include source or sink terms that relate to the type of catchment in terms of seepage areas and possible lateral flows outside the set boundary conditions.

Section 3.5 below reviews actual hillslope models and the methods by which the various subsurface processes are modelled.

3.5 Hillslope Models

Hillslope models can be 1-dimensional, simulating soil water movement vertically through the profile, 2-dimensional, where the horizontal component is considered and 3-dimensional, which are usually grid-based, simulating flows vertically, laterally and horizontally. Each of the models varies in complexity and input requirements. Hillslope models can be further subdivided into event based or continuous models. An event based model represents a single runoff event occurring over a time period, ranging from several hours to several days. The initial conditions in the catchment for each event must be assumed, or determined, and used as input information. The accuracy of the model output will depend on the reliability of these initial conditions. Continuous models operate over an extended time period, determining flow rates and conditions during both runoff periods and periods of no surface runoff. Thus the model keeps a continuous account of the hillslope soil moisture status and allows for the determination of initial conditions needed for different runoff events. However, the effect of the selection of those initial conditions decreases rapidly as the simulation advances.

3.5.1 *ACRU* and TOP*ACRU*

The *ACRU* agrohydrological modelling system is a physical conceptual, multipurpose, multilevel and multilayer model which uses a daily time step with daily rainfall input and combines the various water budgeting and runoff producing components of the hydrological cycle (Schulze, Angus, Lynch, and Smithers, 1995). *ACRU* uses a daily multilayer water budgeting approach where the soil profile is partitioned into two layers, each with a set of predetermined soil characteristics pertaining to the drained upper limit (DUL), permanent wilting point (PWP) and ϕ. Each layer acts as a reservoir, which responds once the DUL

is reached, with water draining to the next layer. Any water exiting the subsoil contributes to the groundwater recharge. This water budget technique is adequate only for daily studies and does not account for processes shorter than one day, as they do not consider the transitory phenomena occurring in most heterogeneous soil profiles. Infiltration is calculated using equations developed by Buitendag (1990). Soil water flux equations based on Darcy's law, have been extended to represent flow in unsaturated porous media. *ACRU* does not account for macropore flow nor for lateral flow.

Because of the aforementioned shortcomings of a daily model, TOP*ACRU* (Howe, 1997) is currently under construction. Although it is a stand-alone model, it is embedded within *ACRU* using all the *ACRU* inputs, but using different intra-day equations, simulating subsurface processes such as interflow and macropore flow. TOP*ACRU* is a quasi 3-dimensional grid based model which requires a Digital Elevation Model (DEM) and can model the spatial variation in runoff generation, especially in seepage areas. TOP*ACRU* operates on an hourly time step and in distributed mode during a rainfall event, but in lumped mode during "no-rainfall" time intervals, as indicated in Figure 8.

Two mechanisms operate during a rainfall event to control the infiltration and runoff rates. The first comprises a Green and Ampt (1911) wetting front in the soil and the second a

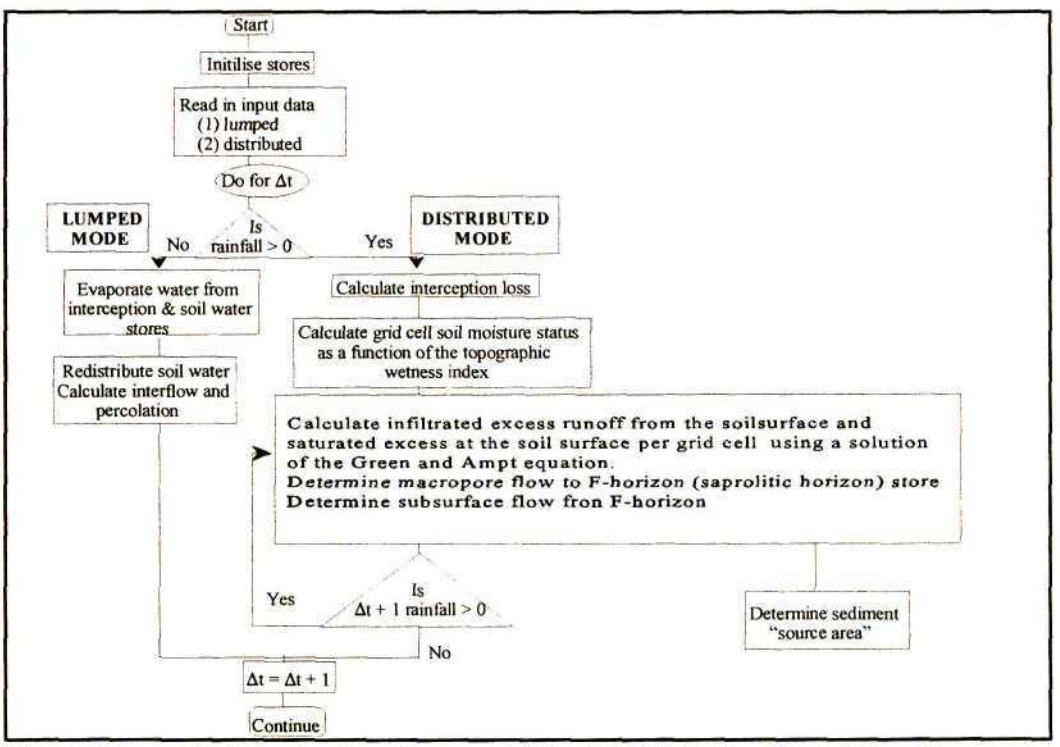

Figure 8. Schematic flow diagram of the TOP*ACRU* module (after Howe, 1997).

macropore flow routine where water rapidly bypasses the soil matrix to the F-horizon, which in TOP*ACRU* is the deepest soil horizon, usually saprolite, from where interflow is generated. The infiltration depth of the Green and Ampt (1911) wetting front can be determined for any time step.

Concurrently, interflow is determined via lateral fluxes from the F-horizon. During non rainfall periods, the distributed wetting fronts are lumped to give average moisture contents for each horizon. Using these water contents, hydraulic gradients are calculated and water is redistributed either upwards or downwards using Darcy's law. The F-horizon is the layer directly above the impermeable layer or bedrock and it is here that infiltrated water and interflow accumulates with the subsequent development of a water table. The volume of soil water in the F-horizon and the matric potential at the interface of the B-and F- horizons is determined by assuming an equilibrium steady state pressure distribution in the F-horizon. When this water ponds, interflow and percolation emanate due to saturated pressure flow.

TOP*ACRU* requires gridded point elevations derived from a DEM as an input, which at the catchment scale is acceptable, but at the hillslope scale is impractical. DEMs have a coarse grid size compared with a hillslope 200 m long for example. DEMs can be created for this hillslope scale which means that the hillslope needs to be surveyed at a very small scale which is time consuming. During the writing of this document TOP*ACRU* was still undergoing calibration. Therefore, TOP*ACRU* was not used in this research to simulate subsurface processes. The next model reviewed is the HILLFLOW-3D (Bronstert, 1995) hillslope modelling system.

3.5.2 HILLFLOW 3-D Model

HILLFLOW-3D is a physical conceptual model which simulates the water dynamics in three dimensions at the micro catchment scale. It uses a variable time step, enabling subsurface simulations during storm events with small time steps, to simulations over a few days with longer time steps. These time steps are controlled by the rainfall intensity. HILLFLOW-3D simulates the relevant hydrological processes such as interception, ET, infiltration, water dynamics within the soil matrix, surface runoff, non-Darcian subsurface storm flow, exfiltration (or return flow) and channel discharge. These subsurface processes are coupled in HILLFLOW-3D. This model cannot be used successfully in every situation. Urban

hydrological effects are not accounted for, pure groundwater flow is not well represented and the required CPU time is too large for catchments having a high resolution in space and time. Figure 9 gives a schematic representation of the structure of HILLFLOW-3D, listing the processes considered.

HILLFLOW-3D conceptualizes the decrease of K with depth and the accumulation of macropores towards the soil surface.

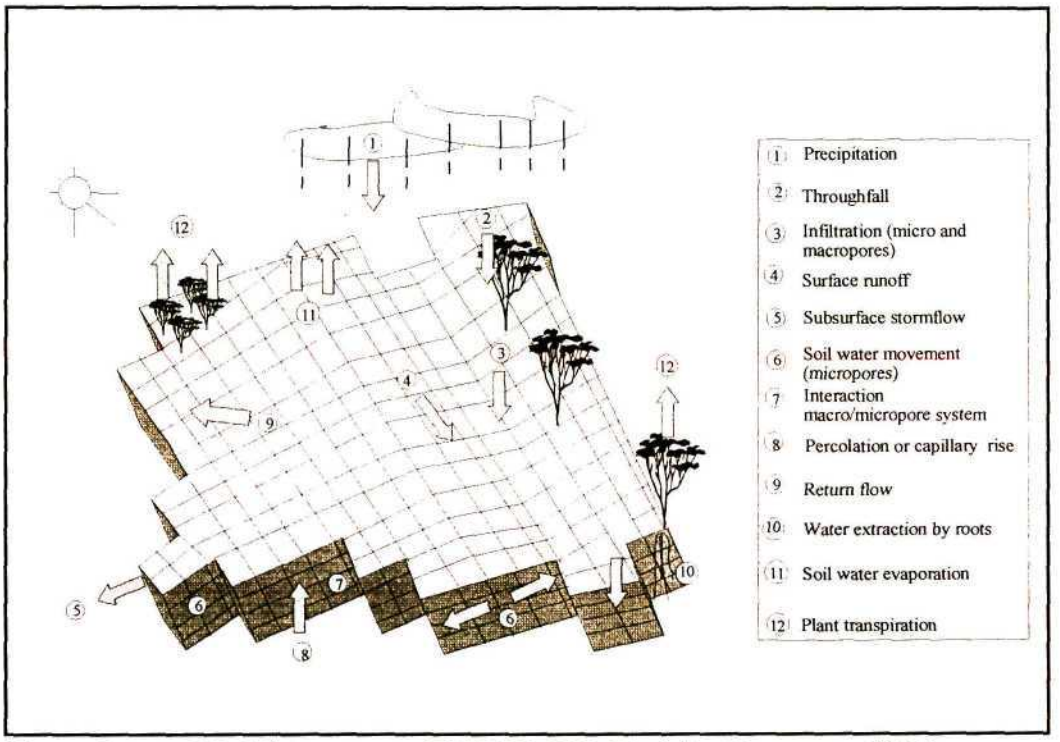

Figure 9. Model structure of HILLFLOW-3D (after Bronstert, 1995).

Apart from the soil matrix, the soil may contain a macropore network which is considered to exist only close to the soil surface, as shown in Figure 10. The surface layer is defined as the interflow layer having the parameters of depth (H_z) and effective macroporosity (V_{mak}), which are defined as the portion of soil which has hydraulically active macropores, which are parallel to the soil surface. The macropores are considered to be equally distributed over the interflow depth and influence the total infiltration capacity of the soil and interflow, which flows parallel to the surface within the interflow layer. The soil matrix extends from the soil surface down to the lower boundary of the modelled soil, thus interacting with the macropore system.

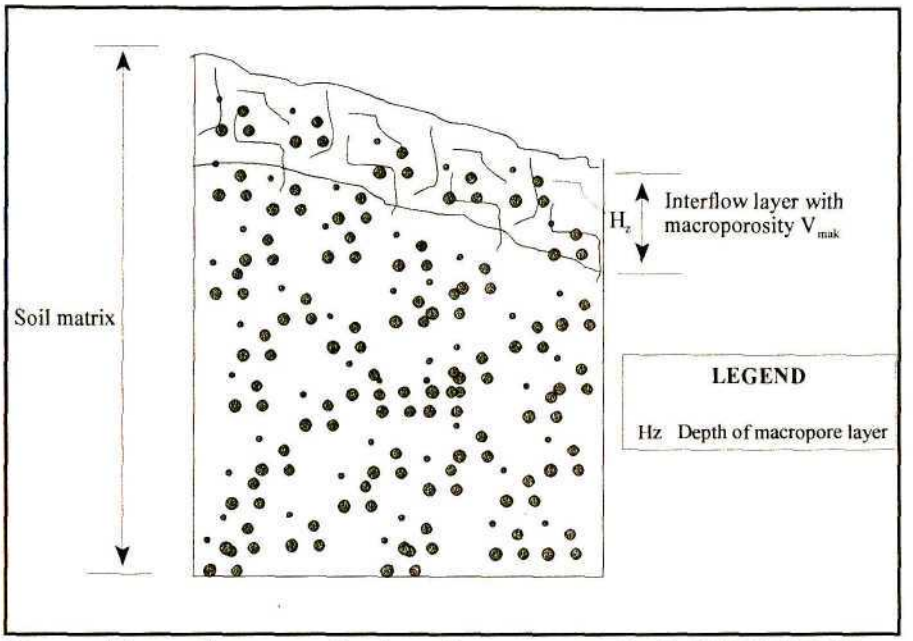

Figure 10. Conceptualization of macro-porosity in HILLFLOW-3D (after Bronstert, 1995).

The infiltration component within the interflow layer includes the calculation of infiltration rates for both the macropores and the soil matrix and is partitioned into the actual rate into the macropore system ($I_{mac\ act}$) and the micropore system ($I_{mic\ act}$) depicted in Figure 11.

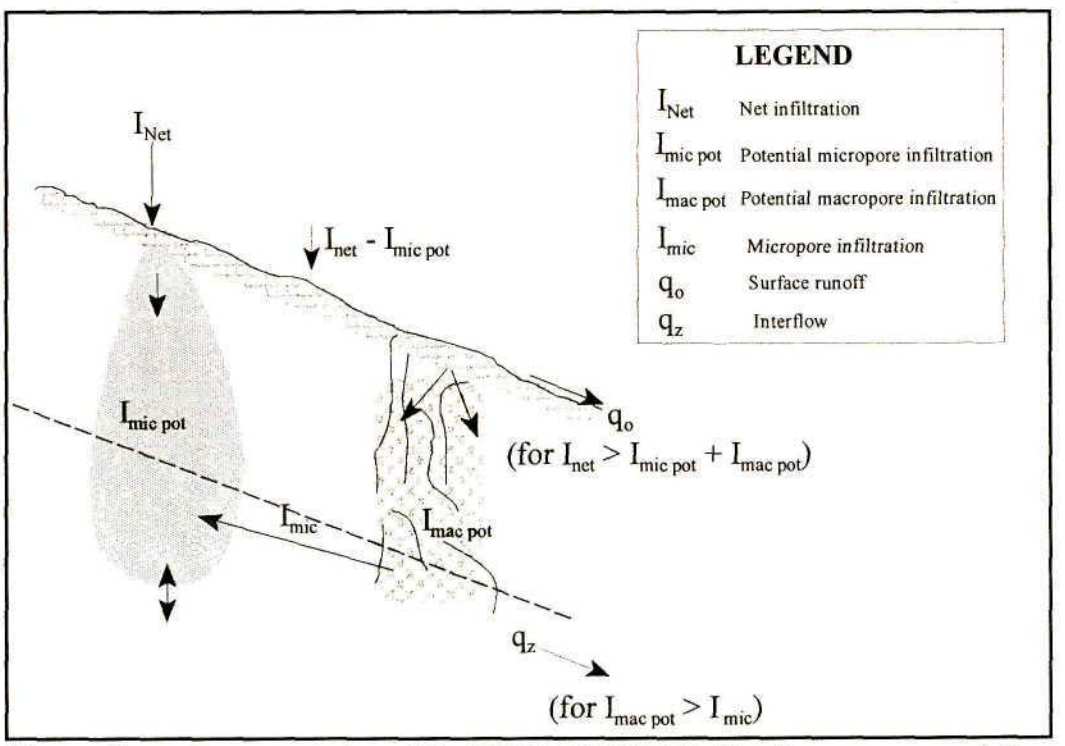

Figure 11. Representation of the HILLFLOW-3D infiltration component (after Bronstert, 1995).

The total infiltration is thus the sum of $I_{mic\ act}$, and $I_{mac\ act}$. Under the correct conditions (*cf.* Section 2.1.4) water can move out of the macropores into the surrounding soil matrix, which is controlled by the matrix moisture content.

The potential infiltration rate into the micropores , $I_{mic\ pot}$, is calculated as follows, according to Feddes, Kowalik and Zaradny (1978; cited by Bronstert, 1995):

$$I_{mic\ pot} = K[(\frac{\partial \psi}{\partial z}) - 1] \qquad (6)$$

where K = hydraulic conductivity of the 1st layer ($mm.h^{-1}$)

$\partial \psi / \partial z$ = hydraulic gradient in the 1st layer.

To obtain the actual infiltration rate into the micropore system, the available water and the net rainfall intensity at the surface needs to be calculated with respect to the water content of the soil. When the net precipitation exceeds the matrix infiltration rate, macropore infiltration, $I_{mac\ pot}$ occurs assuming no significant time delay as follows:

$$I_{mac\ pot} = \frac{V_{mac\ empty}.H_Z}{\Delta t} \qquad (7)$$

where $V_{mac\ empty}$ = free space of macropores (m^2)

H_z = depth of macropore layer (m)

Δt = duration of time step (h).

The flow processes within the macropore system respond mainly due to gravity and are modelled separately from the soil matrix. Owing to the complexity of the Richards (1931) equation, HILLFLOW-3D uses fuzzy, rule-based modelling to simulate unsaturated flow (Bronstert, 1995).

For both surface runoff and subsurface flow computations, gravity, friction and pressure forces are considered in a simplified form of the St. Venant equation, which consists of the continuity and the momentum equations. The equation of continuity is as follows:

$$\frac{\partial q}{\partial x}+\frac{\partial h}{\partial t}-i(x, t) = 0 \qquad \textbf{(8)}$$

where:

	q	=	specific runoff = runoff per unit width ($mm.h^{-1}$) (on the surface or within the interflow layer)
	x	=	co-ordinates of the flow direction
	h	=	corresponding flow depth (mm)
	t	=	time (h)
	i	=	effective lateral inflow ($mm.h^{-1}$) (Infiltration or matrix excess).

and the momentum equation:

$$S_f+\frac{\partial h}{\partial x} = S_0 \qquad \textbf{(9)}$$

where

	S_o	=	surface slope
	S_f	=	friction slope.

The expression "kinematic cascade" is used to characterize flow between grids of different elevations. Subsurface flow occurs within the interflow layer parallel to the soil surface. Since this cascade is the same as the surface cascade, the hydraulic computation of runoff and subsurface flow is analogous. The lateral inflow to the surface cascade is produced if the net rainfall intensity is greater than the infiltration rate, and to the subsurface cascade if the infiltration rate into the macropores less the flux from the macropore system to the micropore system.

HILLFLOW-3D documentation shows the model to simulate the most important subsurface processes. It may be a sound model to use on the Weatherly catchment. However, the code

was unobtainable and for this reason this model was not used. The third model reviewed, HILL5D, is outlined below in Section 3.5.3.

3.5.3 The HILL5D Model

HILL5D is a multi component, numerical simulation model which links surface, unsaturated and saturated subsurface flow in a two-layer, two-dimensional hillslope. Some three-dimensionality has been introduced by allowing for a small amount of convergence and divergence of the hillslope section (Hebbert and Smith, 1996). The model can be applied on hillslopes where a relatively shallow soil is underlain by a subsoil of lower permeability. It is in these areas that saturated zones form, with the subsequent development of perched water tables. The major objective of the model is the tracking of the soil water in this saturated zone. HILL5D can also simulate the response to recharge through the soil mantle, or conversely simulate the lateral water movement through the surface soil (Hebbert and Smith, 1996).

The most general use of the model, however, is in simulating the conditions in which these mechanisms are active and interact with each other, as in the formation of seepage areas. HILL5D considers the soil profile to be made up of an upper layer, i.e. the topsoil and a lower layer, i.e. the subsoil.

The topsoil is considered to be shallow and permeable with water movement taking place either as saturated or unsaturated flow. Unsaturated flow is in the vertical direction and is calculated using the Richards (1931) equation, plus a combination of the mass conservation and vertical Darcian velocity, as follows:

$$\frac{\partial \theta}{\partial t} = \frac{\partial}{\partial z}[D(\theta).\frac{\partial \theta}{\partial z} - K(\theta)] - e(z,t) \qquad \textbf{(10)}$$

where θ = is the volumetric soil moisture content ($m.m^{-3}$)

t = the time (h)

z = the distance below the soil surface (mm)

$K(\theta)$ = the unsaturated vertical hydraulic conductivity ($mm.h^{-1}$)

$D(\theta)$ = the soil water diffusivity ($mm.h^{-1}$), and

e = is a source or sink term ($m^3.m^{-3}$).

The hydraulic characteristics of the soil, $K(\theta)$ and $D(\theta)$, depend on the WRC calculated using the Brooks and Corey (1964) equation. The sequencing in the model operation is shown as a flow chart in Figure 12.

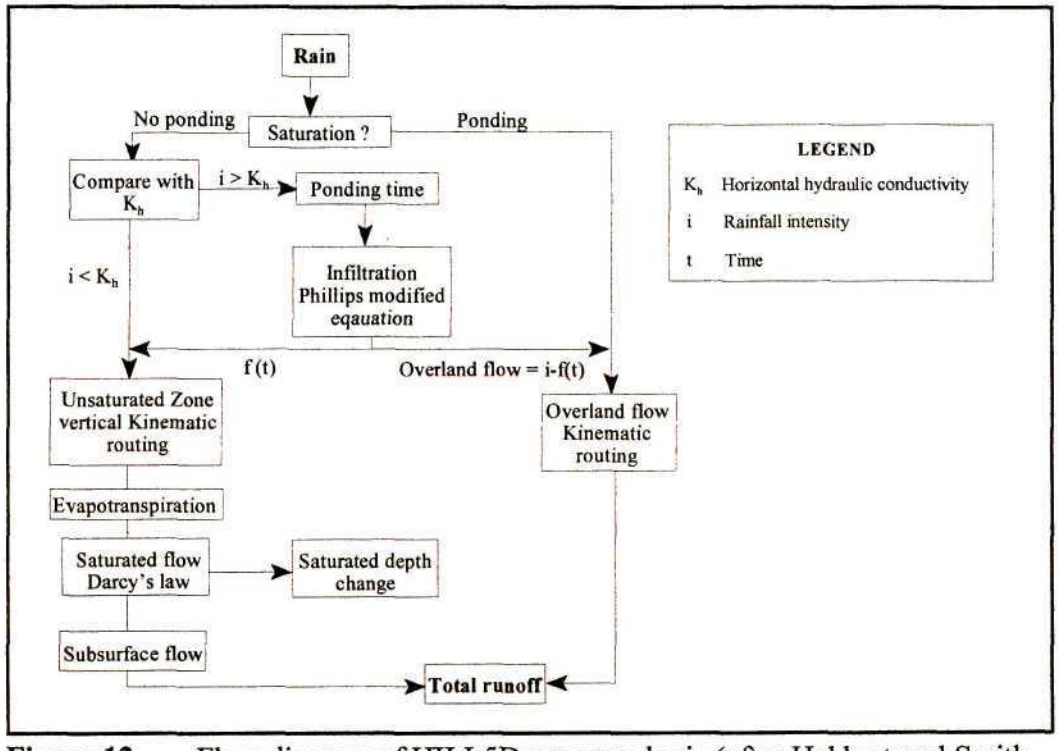

Figure 12. Flow diagram of HILL5D program logic (after Hebbert and Smith, 1996).

The soil water flux may be different according to different rainfall intensities (i). If $i > K_s$, then diffusive properties dominate. In this instance analytical infiltration approximations are used to describe the division between surface flow and infiltration. Conversely, if $i < K_s$ most of the water will infiltrate the soil and the unsaturated water movement calculated accordingly.

Saturated flow occurs when the vertical unsaturated flux arrives at the interface between the surface and subsurface soil layers at a flux greater than conductivity out of that layer, resulting in the development of a perched water table.

Lateral flow is assumed to be parallel to the interface and the soil surface and the Dupuit approximation of Darcy's law is applied to calculate the saturated flow within the soil, solvable by finite difference methods as follows:

$$Q(x,t)=K_h[(H(x,t)+c_f)[\sin\gamma-\cos\gamma.\frac{\partial H(x,t)}{\partial x}]] \qquad (11)$$

where :

	$Q(x,t)$	=	is the horizontal flux per unit width ($mm.h^{-1}$)
	K_h	=	is the horizontal hydraulic conductivity ($mm.h^{-1}$)
	γ	=	is the local soil interface slope (%)
	$H(x,t)$	=	is the depth of the saturated flow normal to the interface (mm), and
	c_f	=	is the capillary fringe height (mm).

The term in the inner square brackets is the net slope of the phreatic surface, where $\sin\gamma$ is the slope of the subsoil interface and $\partial H/\partial x$ is the slope of the phreatic surface relative to the interface. The subsoil is assumed to be relatively impermeable where the vertical flux does not change compared with the dynamic behaviour of the perched water table above it. A continuous water budget is kept, calculating the amount of water in the unsaturated portion of the profile above the perched water table and the amount of water in the perched aquifer. These amounts are added to the accumulated, return, lateral and overland flow routines.

According to Hebbert and Smith (1996) the model weaknesses are that the soil variables such as ϕ and K are site specific and not applicable to the catchment as a whole and in complex situations the problem with any model is how to transfer parameters between storms.

The HILL5D model considers most of the subsurface processes which occur in Weatherly and consequently HILL5D has been selected to simulate these processes.

* * *

In Chapter 3 the need for hydrological simulation models has been addressed. Differences between theoretical and empirical models are outlined, including factors that need to be taken into account before a model can be selected. Infiltration and redistribution models are reviewed with techniques used to model subsurface processes, such as interflow and macropore flow. Three hillslope models are reviewed and from those one model is selected. This model, HILL5D will be used as both an investigative and predictive model to simulate the subsurface processes that occur at Weatherly. On a hillslope transect at Weatherly a comprehensive hillslope experiment has been established. The methodology of this experiment is discussed next, in Chapter 4.

4. METHODOLOGY

4.1 Objectives

Field work forms an integral part of the development of modelling systems since it enables:

a. the development of information and understanding of complex natural processes, so that researchers may develop general trends based on these processes,
b. predict future events with the highest possible degree of certainty and
c. provide a data set, with which modelled results can be compared, to calibrate and validate the model.

The objectives of the fieldwork component of this research are threefold:

a. first, to carry out initial fieldwork to determine the physical and hydraulic characteristics of the soils, to provide bedrock descriptions and to conduct a geological survey;
b. secondly, to set up a well-instrumented hillslope transect and thirdly,
c. to monitor the main subsurface processes that occur at this hillslope scale.

Owing to the detailed scale of this study and since subsurface processes, especially the redistribution of water, continue even after the rainfall event has subsided, instrument automation was necessary. This implied that data should be recorded on an event by event basis and continue between the events.

This initial fieldwork component was followed by the establishment of instrumentation at one experimental site, Weatherly, owned by Mondi Forests (North East Cape Forests) in the NEC. A locational map is given in Figure 13, which shows the location of the Weatherly catchment in relation to the towns found in the area.

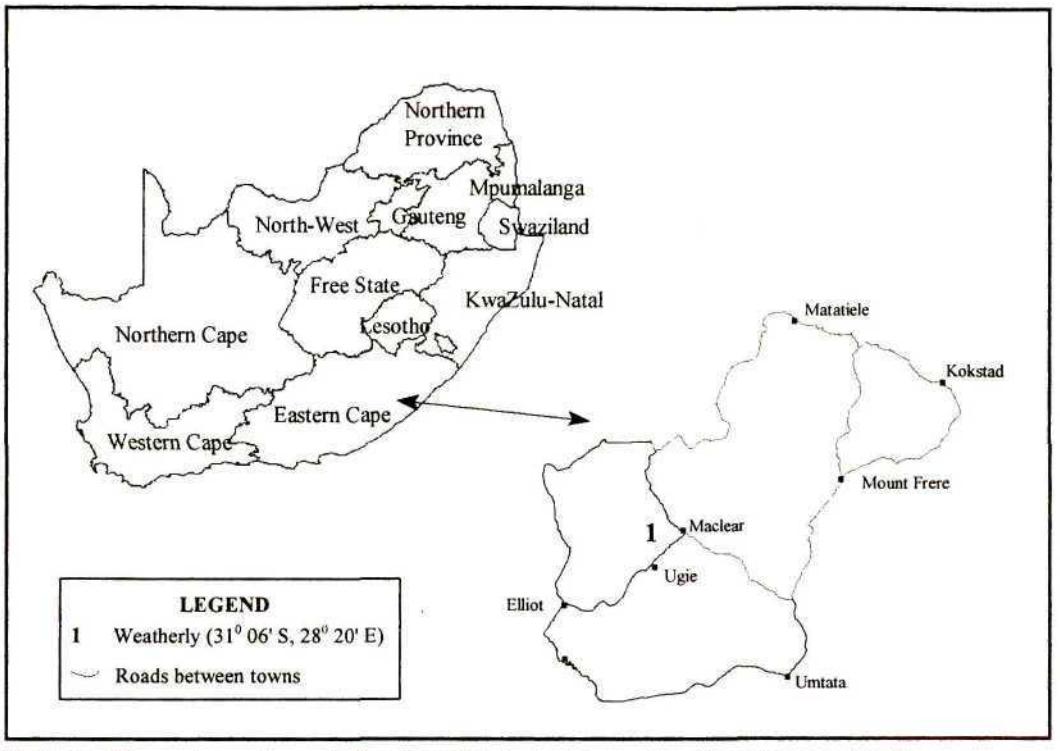

Figure 13. Location of the Weatherly catchment in the Eastern Cape.

4.2 Catchment Description

The Weatherly catchment is located approximately 5 km south of Maclear at a latitude of 31 ° 06' South and longitude 28 ° 20' East. The catchment covers an area of 1.5 km^2 and is at an average altitude of 1300 m above mean sea level. The vegetation, described as Highland Sourveld (Acocks, 1975), is dominated by grassland in moderate hydrological condition i.e. with a basal cover of 50-75% on the hillslopes. The soils show a large spatial distribution ranging from Avalons, Kroonstad and Pinedene soil forms on the crests to Oakleafs, Tukulus and Vilafontes in the valley (*cf.* Section 4.3.1.1). These soils display varying degrees of wetness and include red and yellow apedal mesotrophic soils plus neocutanic and hydromorphic soils. These soils are permeable, ranging in depth from a few millimetres to 3.5 m, and are underlain by semi-impermeable sandstones of the Molteno Formation (*cf.* Section 4.3.1.2). The bedrock within Weatherly is highly undulating, this having been determined by Ground Penetrating Radar (GPR), which has also been used to identify depth to bedrock and phreatic surfaces (*cf.* Section 4.3.1.3).

The NEC is considered a marginal rainfall region for the support of silviculture and Weatherly has a mean annual precipitation (MAP) of 750 mm. A summary of available climate data for Maclear is shown in Table 1. These data were obtained from the climate station, AM # 0151/604, situated at latitude 31^0 04 'S and longitude 28^0 21'E, some 5 km from Weatherly. The evaporation and temperature statistics have been calculated for 10 years from 1988, with the rainfall having a longer record, beginning in 1891. The comparison between rainfall and pan evaporation in Table 1 shows the potential evaporation exceeding the rainfall for every month of the year. This fact needs to be considered especially since the NEC region is undergoing afforestation, leading to a possible increase in potential ET.

Table 1. Monthly climatic information for Maclear (after Roberts, Hensley, Smith-Ballie and Paterson, 1996).

Month	Rainfall (mm)	A-Pan (mm)	Monthly means of daily		
			Maximum (°C)	Minimum (°C)	Average (°C)
January	122.5	142.6	25.2	13.9	19.6
February	119.6	128.8	25.2	14.0	19.6
March	107.5	130.2	23.7	12.1	17.9
April	42.8	102.0	24.1	10.7	17.5
May	18.2	102.3	21.2	7.2	14.2
June	10.9	90.0	17.9	3.8	10.9
July	11.2	96.1	18.6	3.8	11.2
August	18.2	117.8	18.7	5.6	11.2
September	34.5	132.0	20.9	7.7	14.3
October	61.5	139.5	20.7	9.8	15.3
November	83.3	165.0	24.4	11.6	18.1
December	109.4	142.6	24.3	13.2	18.8
Yearly Average	739.7	1488.9	22.1	9.5	15.7

The Weatherly catchment, showing four hillslope transects, with a more detailed map of Transect 1, is presented in Figure 14. At the catchment scale, 28 soil pits have been established along these transects, each with a neutron probe access tube. This study focuses on Transect 1 (shown as stations 1 to 4), which has a slope angle of 11%.

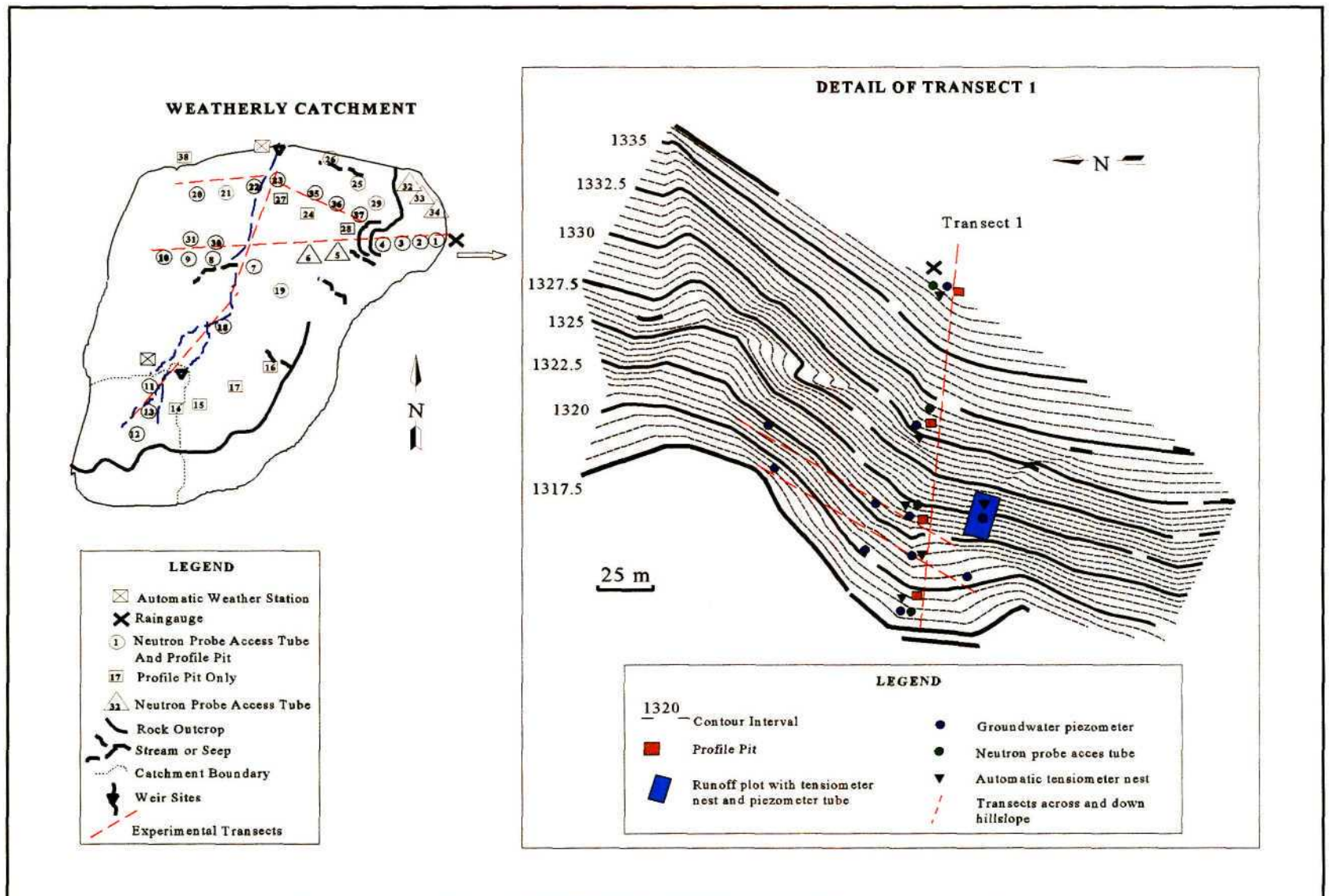

Figure 14. Weatherly catchment showing a hillslope section (Transect 1), where measurements and experimentation are currently taking place.

Shown also in Figure 14 are the locations of a standard rainguage, installed in October 1995 by the Department of Agricultural Engineering (DAE), the two AWSs and the two weir sites. Figure 15 gives a view of the Weatherly catchment taken from Pit 2 looking east down Transect 1.

Figure 15. Weatherly catchment, showing a view down Transect 1. Shown in the foreground is Pit 3.

This chapter is divided into an initial fieldwork component in which various surveys have been performed, along with specific tests to determine the hydraulic characteristics of the soils, followed by the actual experimental layout of various instrumentation. The initial fieldwork component is discussed in Section 4.3 below.

4.3 Field and Laboratory Measurements

Conducting fieldwork and ground truthing with great care and accuracy is imperative before the establishment of field instrumentation. This initial fieldwork component provided invaluable data and information pertaining to the soils and their physical properties, as well as the geology and topography along Transect 1. Information acquired and data collected serve as building blocks upon which hillslope models are based and built. Furthermore, knowledge of the physical properties of the soils allows the calculation of model input and

Brooks and Corey (1964) type parameters (*cf.* Section 5.2.2). Detailed soil, geological, bedrock and topographic surveys were completed during this study and are discussed in Section 4.3.1 below.

4.3.1 Descriptions of Soils, Geology, Topography and Bedrock

A detailed soil survey (*cf.* Section 4.3.1.1) was completed by Roberts *et al.* (1996) of the Institute for Soil, Climate and Water (ISCW). This survey was carried out on a 90 m x 90 m grid over the entire catchment and a more detailed 30 m x 30 m grid along Transect 1. Using a 2 m contour interval map supplied by Mondi Forests and a 1:50 000 topographic map, a comprehensive geological survey (*cf.* Section 4.3.1.2) was conducted on the eastern slope of the catchment by Hughes (1997). The survey helped isolate the geological sequencing of the various lithologies found in Weatherly, and insight into the various subsurface processes. Two topographical surveys were carried out in Weatherly: the first by Mondi Forests where a 2 m contour interval map was produced, and the second by the DAE, where Transect 1 was surveyed in more detail to identify source / seep regions and rock outcrops. A second objective of the latter survey was to geographically 'fix' the locations of neutron probe access tubes, tensiometers and piezometer tubes. The bedrock topography was determined using a GPR carried out by the ISCW (Paterson, 1996) to determine the depth to bedrock and depth and lateral extent of the water table. Both the topographical and GPR surveys are outlined in Section 4.3.1.3 below. Each survey discussion is limited to the hillslope Transect 1, with the remainder of the catchment descriptions outlined in the relevant references given.

4.3.1.1. Soil Survey

Soil profile descriptions were completed at each auger point, on the 30 m x 30 m grid. A large spatial distribution in soil forms was found and a further feature of the soils is the varying degree of hydromorphology present as expressed in the soil colour (Roberts *et al.*, 1996). This ranges from mottling, thin horizons with bleached sand grains to well developed E-and-G-horizons. The pit profiles on Transect 1 are given in Figure 16, determined from profile observations from each pit.

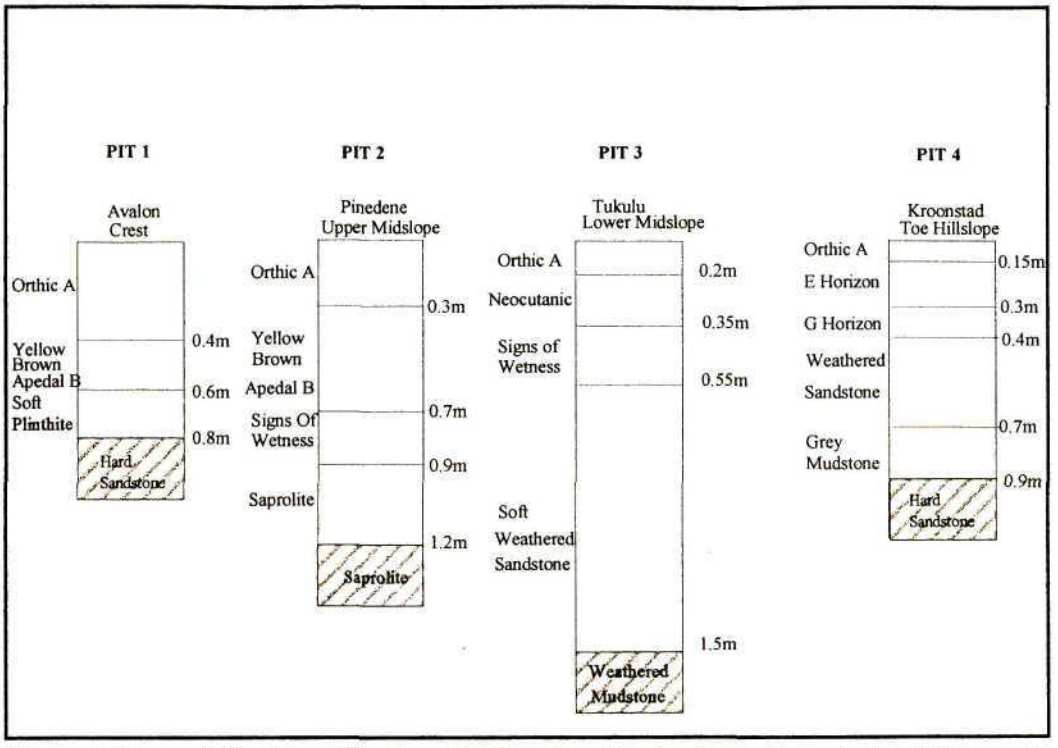

Figure 16. Soil pit profiles for pits 1-4 showing horizonation, derived from soil survey.

Soils along Transect 1 are dominated by Avalon, Pinedene, Tukulu and Kroonstad soil forms, each having medium to fine sandy loam topsoils and sandy clay loam subsoils. Soils with unconsolidated material show signs of wetness due to the accumulation of water on the bedrock forming Pinedene and Avalon soil forms.

4.3.1.2 Geological Survey

The portion of the catchment mapped comprises rocks of the Elliot and Molteno Formations of the Karoo Supergroup. The geology found along Transect 1 is depicted in Figure 17 where the stratigraphic column of the units mapped is provided. Owing to the lack of outcrop, detail with respect to the thicknesses of the units may be inaccurate, compounded by the fact that the 2 m contour map was found to be incorrect in parts (Hughes, 1997).

Three rock types predominate, namely, sandstone, mudstone and conglomerate. The sandstones are coarse grained lenticular units which exhibit cross troughed bedding. These are generally undeformed and show few signs of metamorphism.

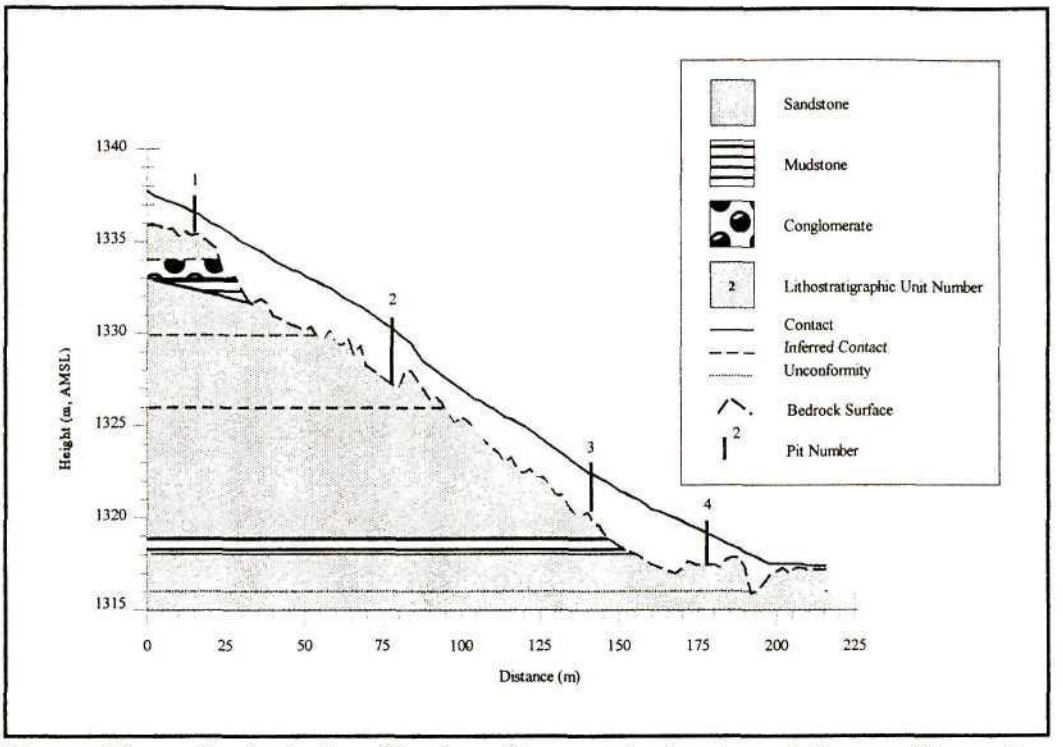

Figure 17. Geological profile along Transect 1, showing relative positions of soil pits. The sandstone profiles were established by ground penetrating radar.

The conglomerates typically occur above the mudstone units. These layers of mudstone within the sandstone are likely to act as semi-impermeable layers, having a lower K than the sandstones. The deeper soil profiles appear to be developed in the region of the shales and softer sandstones. The undulating nature of the bedrock is likely to be a result of weathering along joints and fractures combined with the lenticular nature of the sandstone, where lenses of different hardness weather differently.

4.3.1.3. Hillslope and Bedrock Topography

A common view among many hydrologists is that downslope water movement can be described accurately using the surface topography of a catchment, because the gravitational potential dominates the hydraulic gradients. Many researchers use Digital Terrain Models (DTM) for this very purpose, especially in 3-D grid based models. McDonnell, Freer, Hooper, Kendall, Burns, Bevan and Peters (1996) believe that this may be true at the catchment scale, but at smaller scales such as hillslopes with shallow soils underlain by impermeable bedrock subsurface, flow is affected by the actual bedrock surface. Using a detailed hillslope experiment McDonnell *et al.* (1996) have shown this hypothesis to be true

at the Panola Catchment, New Zealand. Thus the need to map the bedrock surface is vitally important in calculating groundwater fluxes, perched water table movement and interflow. Similarly a DTM is important in determining potential seepage and exfiltration areas. GPRs are therefore commonly used in determining the bedrock topography of hillslopes.

A GPR is a radar system consisting of transmitting and receiving antennae linked by cable, where the transmitter radiates a short pulse of electromagnetic energy into the ground, which changes in response to the soil's electrical properties. This usually occurs at the interface of different horizons, due to contrasting conductivities which cause part of the transmitted signal to be reflected and detected by the receiver. A few factors may cause the radar to perform less well. These include high conductivity values caused by either a high clay content, salt content or water content of the soil, especially during the rainfall season. A compromise needs to be made between the range and resolution of the GPR. The lower the frequency of the transmitted signal the deeper the penetration into the soil, but then the resolution is less and vice versa. The radar is site specific due to the variability of soils from one place to the next, which does not allow for the extrapolation of results.

This relatively new concept has many widespread applications such as evaluating soil properties and estimating the variability and composition of soils (Birkhead, Heritage, White and von Niekerk.,1996). Collins, Doolittle and Rourke (1989) have used GPR studies successfully to determine the depth to the phreatic surface and bedrock and have shown there to be a high correlation between GPR data and augured depths at a granite site, with an error of approximately 7.9% when compared with piezometer tube data.

A GPR investigation was conducted along Transect 1, with depths to both the bedrock and water table being recorded every 2 m, thus giving a detailed and comprehensive data set, but not without error. The 1995/96 rainfall season was an exceptionally wet one and in the lower regions of the hillslope, water tables levels were very high. These high water tables restricted the overall depth of radar penetration due to the increased attenuation of the signal. In spite of this, both water table and bedrock depths were determined in Transect 1 from the investigation, as shown in Figure 18.

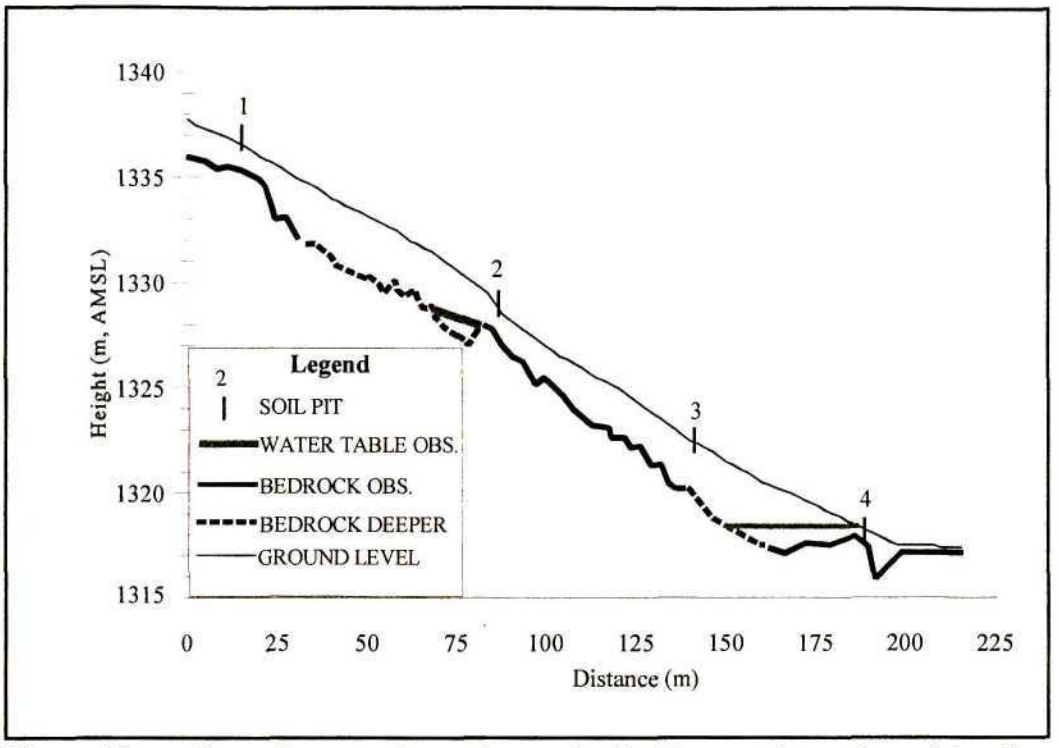

Figure 18. Ground penetrating radar results for Transect 1 together with soil pits, showing the delineation of the bedrock and phreatic surfaces.

Dotted lines indicating deeper bedrock, represent cases where water in the soil obscured data and the depth to bedrock was inferred using pit and piezometer depths. Furthermore, only the depth to phreatic surface was observed as its presence had a shadowing effect, blocking the underlying rock. Figure 18 shows how undulating the bedrock topography is. This has important implications in the modelling of subsurface processes on this hillslope. This, together with fracturing determined in the geological survey, is conducive to the formation of localised water bodies and deep percolation through the rock into the layers below. Results of the GPR investigation can be regarded as satisfactory, but a drier season would have yielded clearer results (Paterson, 1996).

Actual soil depths were determined from the soil pits, piezometer tubes which were installed to the bedrock and from random measurements of depth to bedrock made in a more recent study. Using these soil depths, data collected from the GPR and the topographical survey, allowed the calculation of relative bedrock elevations. These bedrock elevations are useful, especially when used with groundwater data, since hydraulic gradients and soil water fluxes which are important in the water budget studies discussed in Chapter 6 can be calculated. The relative bedrock and soil surface elevations are given in Appendix A for each location where data are available.

Knowledge of the soil physical and hydraulic properties are also essential in determining soil water fluxes. These fluxes are a function of the soil water tension and K. The determination of the soils' physical and hydraulic characteristics are discussed below in Sections 4.3.2 and 4.3.3 respectively.

4.3.2 Measurement of Soil Physical Properties

Many methods are available to measure soil physical properties. Commonly used methods are shown in Table 2 and methods shown in bold have been used in this study.

Table 2. Some more common methods available to determine soil physical properties.

Soil Property	Method	Result	Infer/calculate	Reference
Particle size distribution	Pipette	Texture, and % sand, silt and clay	Calculate estimates of water retention characteristics and soil texture, eg. sandy loam	Sheldrick and Wang (1993)
	Hydrometer			
	Sieve			
Bulk density (ρ_b)	**Core**	$Mg.m^{-3}$	Porosity, instrument calibration	Culley (1993) Rawls *et al.* (1992) Blake and Hartage (1986)
	Excavation			
	Clod			
	Nuclear Radiation			

Undisturbed soil samples were collected from Transect 1 next to each of the four soil pits (*cf.* Figure 14). These samples were taken from each soil profile (Pits 1 to 4) at increments of approximately 0.2 m, starting at the soil surface and concluding at the bedrock or saprolite layers. Methodologies used in the measurement of the physical properties follow. These are outlined in Klute (1986). In general, deviations from the standard procedures are discussed in detail.

4.3.2.1 Particle Size Distribution

The PSD of a soil refers to the size distribution of the individual soil particles. The PSD influences the soil's unsaturated ($K(\theta)$) and saturated conductivity (K_s), water holding

capacity, ability to aggregate and the propensity for crusting after successive periods of wetting and drying.

For each of the 30 samples collected, a hydrometer test was performed (for a period of 36 hours) using approximately 0.1kg of subsample. Following the hydrometer test, the soil subsample was mixed with water and poured through a series of seven sieves, with opening sizes ranging from 0.053 to 2 mm. Finally the subsample was dried. These data were entered into a spreadsheet to calculate the PSD. Separate textural analyses were performed by the ISCW, using soil samples taken from each of the four pits. These samples were analysed using the pipette method. Results show small insignificant differences compared with the hydrometer method. These results and differences are given in Section 5.1.1.

4.3.2.2. Bulk Density and Porosity

Bulk density, as defined by Rawls *et al.* (1992), is the ratio of the mass of dry solids to the bulk volume of the soil, which includes the volume of the solids and the pore space. This parameter can be used to calculate the soil's ϕ. and mass-based determinations to a volume basis (Sheldrick and Wang 1993).

Three methods (*cf.* Table 2) were used to determine the ρ_b of the soil at each of the four soil pits. Each method gave different results. The extraction method was used. However, according to Hensley (1996) this method can lead to inaccuracies since refilling the excavation with calibrated sand can lead to inaccuracies. Subsequently, the core and radiation methods (*cf.* Table 2) were used together, giving similar bulk densities. The ϕ was calculated using the ρ_b and the particle density, ρ_s (assuming a value of 2.65Mg.m^{-3}) as:

$$\phi = 1 - \frac{\rho_b}{\rho_s} \qquad \textbf{(12)}$$

Results are presented in Section 5.1.2.

These lengthy methodologies used to determine the ρ_b were necessary to calibrate the neutron moisture meter (NMM). Using these results and soil samples extracted from the field, a comprehensive calibration of the NMM was performed by the ISCW. These

calibrations yielded equations which have been used to calculate the volumetric water content expressed in per cent ($\theta_{\%}$) for different soils and soil horizons on Transect 1. The sets of equations derived from each method are shown in Table 3, together with the coefficients of determination (r^2) which give an indication of the strength of the relationship between the dependent and independent variables, or the relationship between the water content and count ratio (CR). These r^2 values show the radiation method to produce a more accurate calibration equation.

Table 3. Calibration equations for neutron moisture meter No. 8550, where $\theta_{\%}$ is the volumetric soil moisture content in per cent and CR is the neutron moisture meter Count Ratio.

Horizon	Equation (Corer)	r^2	Equation (Radiation)	r^2
A				
CR<1.45	$\theta_{\%}$=16.60*CR-1.68	0.75	$\theta_{\%}$=15.87*CR-0.94	0.96
CR>1.45-1.90	$\theta_{\%}$=38.40*CR-33.60			
B				
CR<1.45	$\theta_{\%}$=13.38*CR-2.99	0.59	$\theta_{\%}$=17.16*CR-5.9	0.92
CR>1.45	$\theta_{\%}$=37.80*CR-38.3			
C				
1.45<CR<1.95	$\theta_{\%}$=26.50*CR-21.9	0.59	$\theta_{\%}$=21.27*CR-12.67	0.79

Also shown also in Table 3 are the criteria used to determine which calibration equation to use for each of the horizons. These criteria imply that the equation given for each horizon applies only if the CR is between the predetermined values for that particular horizon. In other words, this criterion is in the form of CR ranges, where 1.45 is the lower limit and 1.95 the upper limit.

4.3.3 Measurement of Hydraulic Characteristics

Again several methods are available to determine soil hydraulic characteristics. These are outlined in Klute (1986). In general only deviations from the standard procedures are discussed in detail. Some of these are shown in Table 4, with methods used in this study shown in bold.

Table 4. Methods commonly used in the determination of soil hydraulic characteristics.

Soil Property	Method	Result	Infer/ Calculate	Reference
Saturated Conductivity	Constant Head Permeater Single Ring Infiltrometer **Double Ring Infiltrometer** Piezometer Guelph Permeater Auger Hole Method	K_s		Reynolds (1993) Rawls *et al.* (1992)
Unsaturated Conductivity	**Tension Infiltrometer** Unit Drainage Gradient	$K(\theta)$		Reynolds (1993)
Water Retention Characteristic	Soil Core Sampling Tension Tables Pressure Plates Gypsum Blocks **Outflow Cell**	Matric potential water content	Pore size distribution	Rawls *et al.* (1992) Topp *et al.* (1993) Lorentz (1993)

Of the many input parameters needed for physically based hillslope models, accurate estimates of K and retention characteristics are necessary. Both are used in solving mass balance equations in models. Methodologies for each parameter are outlined below in Sections 4.3.3.1 and 4.3.3.2 respectively.

4.3.3.1 Measurement of Hydraulic Conductivity

The K of the soil is divided into the saturated (K_s) and unsaturated ($K(\theta)$) conductivity. The K is the soil's ability to transmit water, which depends on the soil's properties (Rawls *et al.*, 1992), texture and structure (Reynolds, 1993). K_s is greater than $K(\theta)$ as water moves

through all the soil pores. Since K is a non-linear function of volumetric water content, it decreases as the water content decreases.

The K_s and the K (θ) of the soil at four locations along Transect 1 were determined by *in-situ* Double Ring (DR) and Tension Infiltrometer (TI) tests respectively. Figure 19 shows a double ring and a tension infiltrometer in operation at Pit 2.

Figure 19. An example of two double rings (left) and a tension infiltrometer (right) at Pit 2. These tests are being performed at a depth of 0.20 m.

At each soil pit along Transect 1, beginning at the soil surface and down the profile at increments of approximately 0.20 m, two replications of each test were completed. After the completion of each test, a soil core was extracted so that the WRC could be determined (*cf.* Section 4.3.3.2).

Where water table levels intersected the soil surface, these tests could not be carried out. In such instances the auger hole method was used to determine the saturated conductivity. According to Amoozegar and Warrick (1986) the auger hole method is widely used to determine the conductivity below the water table. In order to calculate K , drawdown tests were performed in which the depth to water table is recorded followed by the removal of water out of a piezometer tube several times to clear any blocked pores. Following this procedure water is removed to a predetermined level and the rate of change of water table

height is recorded. The equation given by Amoozegar and Warrick (1986) to determine K is as follows:

$$K = \frac{4.63r^2}{y(He+20r)(2-\frac{y}{He})} \frac{\Delta y}{\Delta t} \qquad (13)$$

where K = hydraulic conductivity ($mm.h^{-1}$)

r = radius of the hole (mm)

He = depth of groundwater hole (mm)

y = the difference between the depth of the groundwater and the depth of the hole (mm), and

$\Delta y/\Delta t$ = the rate of change of y ($mm.h^{-1}$).

Results from the auger hole method are presented in Section 5.2.

4.3.3.2 Water Retention Characteristic

The WRC gives an indication of the soil's ability to store and release water. It is the functional relationship between the soil water content and the soil matric potential of the soil (Rawls *et al.*, 1992). The WRC is commonly used also to indicate the pore size distribution of the soil, but is more often used in the prediction of the flow of water in the soil (Topp, Galganov, Ball and Carter, 1993). Water contents can also be determined from the matric potentials.

Using soil samples collected from each soil profile, a method developed at Colorado State University (Lorentz, Durnford and Corey, 1991), was used to characterise the water retention properties of the soil. This new method called the "controlled outflow" method is used to determine each point on the retention curve by equilibration of the capillary pressure at a fixed saturation. Detailed explanations can be found in Lorentz (1993). These water retention data are presented together with the curve fitting procedure (*cf.* Section 5.2.2), where Brooks and Corey (1964) functions are fitted to actual data.

With the initial fieldwork and laboratory measurements complete, instrumentation was established on Transect 1. Descriptions of the experiment layout and monitoring approach follow in Section 4.4 below.

4.4 Layout of the Experiment and Monitoring Approach

Upon completion of the initial fieldwork, a detailed hillslope experiment was established, along Transect 1. At the catchment scale the instrumentation installed comprised of two AWS, a standard rainguage, two fog interceptors and 28 neutron probe access tubes. Along Transect 1 four neutron probe access tubes are present, with a further 11 piezometer tubes, one runoff plot and six nests of automated tensiometers (*cf.* Figure 14). All these instruments were made up by the DAE. The sections which follow discuss the preparation and installation of these instruments and the monitoring approach used.

4.4.1 Hydrometeorological Instrumentation

One standard tipping bucket rainguage and two fog interceptors (*cf.* Figure 14) were installed by the DAE in October 1995 and November 1996 respectively. The rainguage records the rainfall total for each minute, with the data being written to a memory module. These data are downloaded monthly. The rainfall data comprise an excellent data set with no missing data for the period July 1996 to May 1997. The two fog interceptors are located next to the downstream weir and the rainguage on the hillslope crest. These data are not recorded automatically, but weekly totals are taken.

Two AWSs were established at Weatherly by the ISCW in July 1997. Their locations are adjacent to the location of the two weirs shown in Figure 14. These AWS's record maximum and minimum dry bulb temperatures, solar radiation, wind speed and wind direction and rainfall. Data from the weather stations are downloaded weekly by an operations team based at Mondi, NEC.

4.4.2 Runoff Plot

The NEC is characterised by high intensity storms that produce rapid responses and large amounts of overland flow, especially when the AMC is high. In order to collect runoff data, a 8 m x 22 m runoff plot was erected on the steepest section of Transect 1, between Pits 2 and 3 (Figure 20). The 8 m length was parallel to the slope.

Figure 20. Runoff plot on steepest section of Transect 1, with one piezometer tube and tensiometer nest included.

Sheet steel was firmly embedded into the ground and at the outlet a gutter was inserted and cemented flush with the soil surface, feeding into a collection container sunk below the soil surface. To prevent direct precipitation falling into the gutter and collection container, a wooden covering was placed over these openings. Included in the runoff plot is a piezometer tube and a tensiometer nest (*cf.* Sections 4.4.4 and 4.4.5).

4.4.3 Neutron Probes

The determination of soil water content according to Topp (1993) is the most commonly performed analysis and can be determined using either direct methods which are destructive, or indirect methods. Indirect methods such as the NMM are accurate, but require an instrument calibration so that volumetric water contents can be calculated from data

collected in the field. The usefulness of the NMM data is important in calculating the change in water volumes within different soil horizons and fluxes, both of which are very important for water budget calculations.

The neutron probe access tubes were installed in the last quarter of 1995 on each of the four transects. The locations of these neutron probe tubes were established in areas where different soil types are found, based on the soils information collected by the ISCW. Along Transect 1 there are four such probes, each extending to the bedrock. Using NMM No. 8550, readings were taken weekly during summer and twice a month during the dry season. Using the calibration equations from Table 3 these data were converted to a corresponding water content. These results are presented in Section 5.3.

4.4.4 Piezometer Tubes

On completion of the GPR investigation it was evident that the bedrock topography along Transect 1, is complex, irregular and undulating and this is conducive to the development of perched and discontinuous water tables. Following an on-site inspection, in conjunction with the topographical survey and GPR data, eleven locations were thus chosen to install piezometer tubes. These locations were chosen so that the direction and magnitude of saturated subsurface fluxes down and transverse to the slope could be calculated. These data could thus yield predictions of the movement of perched water tables and thus interflow. Figure 21 shows the overall layout of the hillslope experiment along Transect 1. This layout shows the positions of the piezometer tubes, neutron probe access tubes and tensiometer nests (*cf.* Section 4.4.5).

Holes were augured to the bedrock using a 0.10 m diameter bucket auger. Each of these depths was recorded, with its relative elevation calculated from the topographical survey. Machine slotted, 0.05 m diameter, PVC pipes were manufactured. These had 1.5 m of slotting from the base upwards and a total length of 3m. These slots allow the groundwater to enter the piezometer tube from the surrounding soil. Each tube has a sealed base to prevent soil and sediments moving into the tube. Upon installation, coarse Umgeni sand was used to pack the area surrounding the tube and a clay plug was inserted at the surface to prevent water from moving down the sides of the tube.

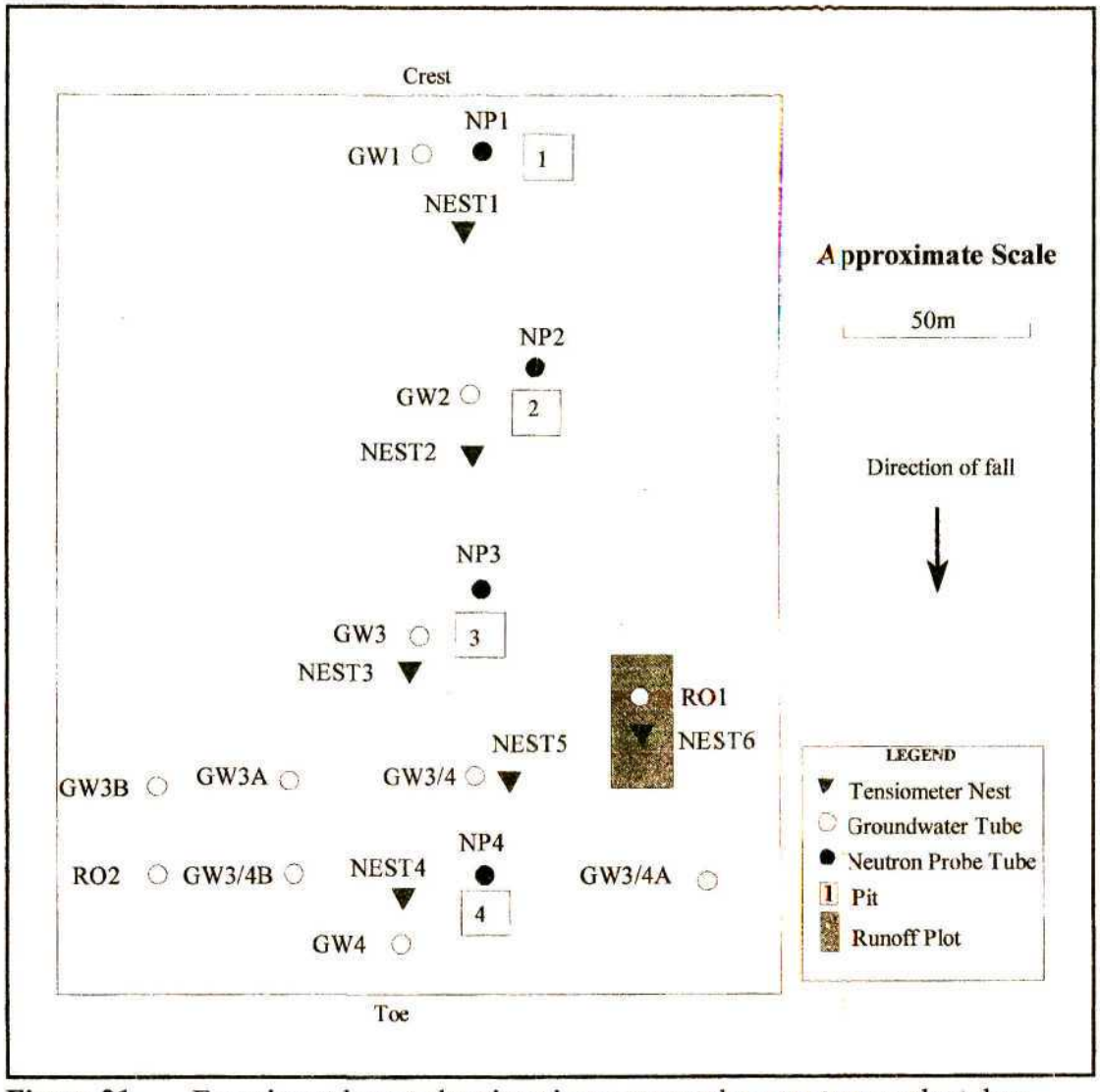

Figure 21. Experiment layout showing piezometers tubes, neutron probe tubes, tensiometer nests and excavation pits.

Figure 22 shows a typical piezometer tube with a hand held beeper used to determine the depth to the water table. The beeper consists of a battery, cable sensor and a sounding device. In contact with water, the sensor closes a circuit and the beeper sounds. After the installation of the piezometer tubes, depth to water table readings were taken manually. Several drawdown tests were also performed in order to calculate the K_s of the soil (*cf.* Section 4.3.3.1).

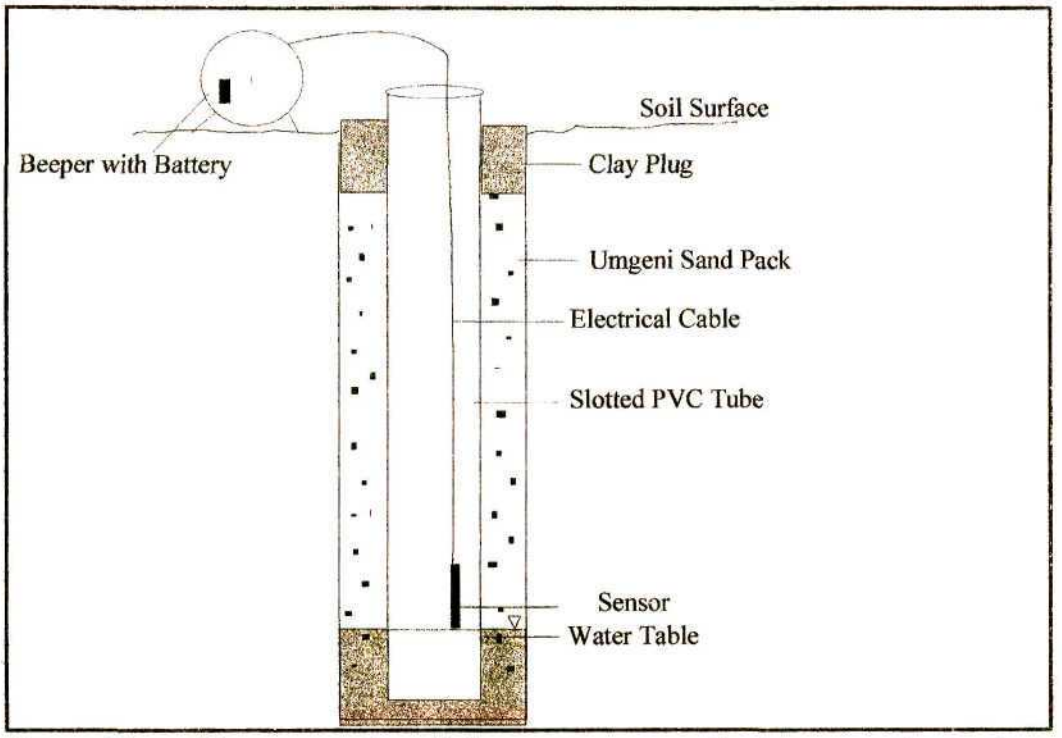

Figure 22. Piezometer tube with beeper to measure depth to groundwater (not drawn to scale).

Using the knowledge of the soil depth at each of the piezometer locations and the depth to the water table, actual water table heights were calculated. Results from these data are shown in Section 5.3.

4.4.5 Tensiometer Nests

Using the NMM to measure water contents alone is not adequate because the soil moisture is not an independent variable, from a physical perspective. A knowledge of the water content in the soil does not give a direct indication of soil water fluxes, which can be calculated when the matric potential of the soil is known. Therefore, automated tensiometers were installed to measure the matric potential of the soils at six locations along Transect 1.

A total of six tensiometer nests has been established along Transect 1, as shown in Figure 21. Each nest comprises four tensiometers, each installed at different depths. Pressure transducers are connected to each tensiometer and to a four channel logger, which is powered by a 6V battery. Each logger and battery is housed in tubing as shown in Figure

23. The components of each tensiometer nest are discussed in detail in the following subsections.

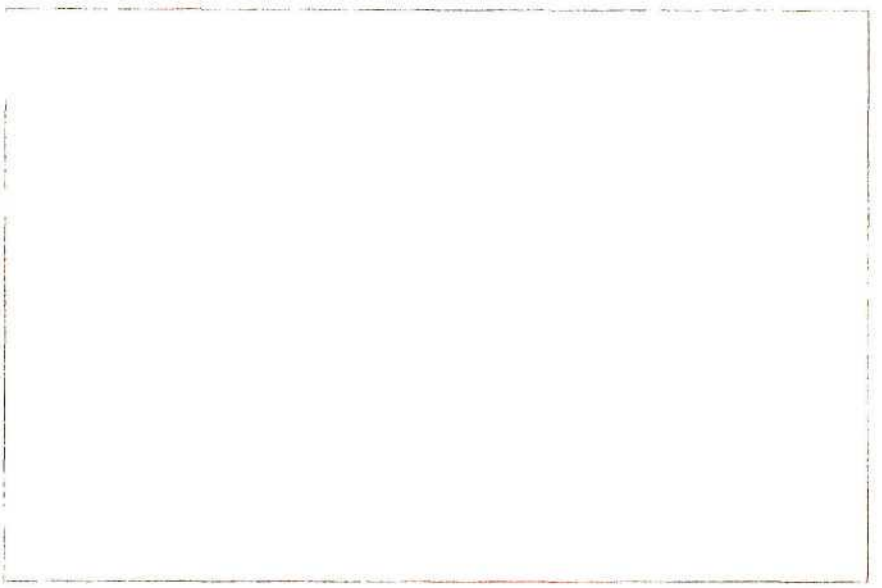

Figure 23. Logger housed in a sealed tube together with a six volt battery.

4.4.5.1 Tensiometers

In total, 23 tensiometers were installed. These can be divided into four groups with respect to their lengths, which range from 0.11 m to 1.20 m. Each tensiometer was modified so that pressure transducers could be easily connected and maintenance could be carried out *in situ*. Figure 24 shows an example of one such modified tensiometer.

Perspex squares were machined to the diameter of the connecting tube and glued to the top of the tensiometers. Threads were turned into this perspex tube into which bolts were screwed. On the side of the connecting tube a small hole was drilled and an U-shaped piece of perspex tubing was glued in place with Tensol, a special glue. At the open end of the U-shaped tubing, a pressure transducer's negative port was connected, with the positive port open to the atmosphere. These pressure transducers and methods used in their calibration are outlined in Section 4.4.5.2.

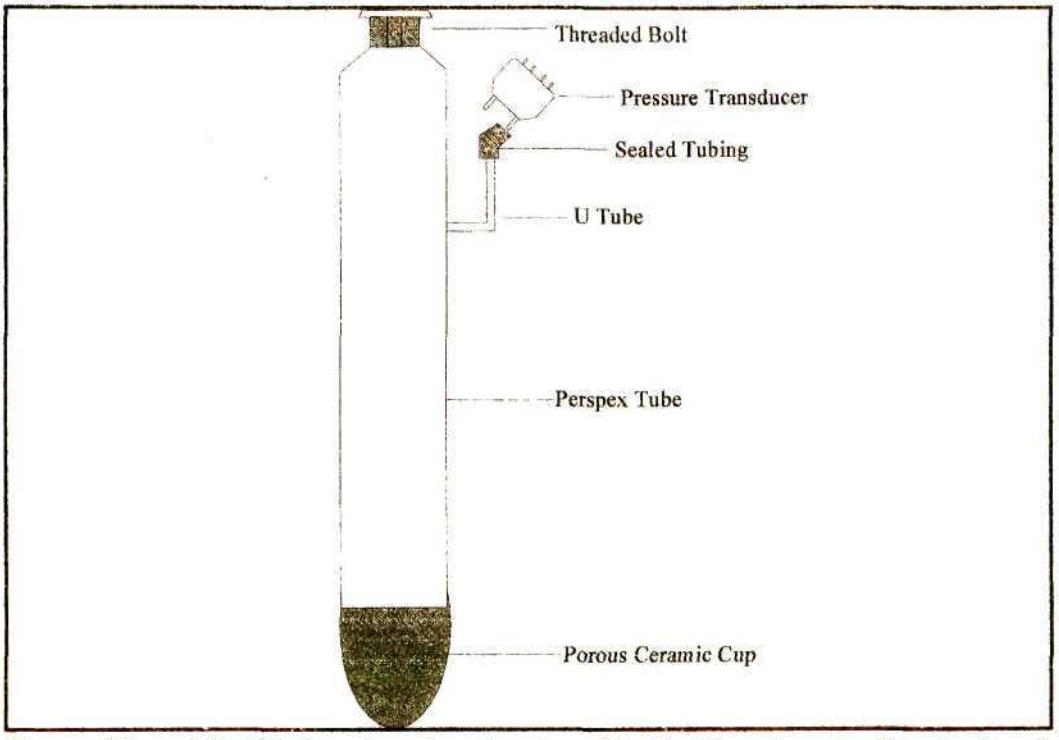

Figure 24. Modified tensiometer, developed by the Department of Agricultural Engineering.

4.4.5.2 Pressure Transducers

Connected to each tensiometer are Motorola MPX5100 piezoresistive pressure transducers. These are state of the art transducers and can be described as a "one chip signalled conditional temperature compensated monolithic silicon pressure sensor". This basically means that no error arises due to changes in temperature during operation. These sensors have a pressure range of 100 kPa and are powered by a voltage supply of 5.25 V. Each transducer has a positive port open to the atmosphere and the negative port connected to the tensiometer and hence the water. Between these ports, inside the transducer casing, is a silicon diaphragm that vibrates in response to a change in pressure within the tensiometer. Within pre-programmed time intervals, an electronic signal is sent to a monitoring device and is recorded. These transducers have been calibrated so that this electronic signal (voltage) can be converted to a corresponding potential, or suction head, of the soil.

To calibrate the pressure transducers a volt meter, a 5 Volt power source, a vacuum pump and a mercury U-tube were used. Each of the 23 transducers was calibrated by connecting

them to the voltage supply and vacuum pump (with a valve that allows the user to change the negative pressure), which in turn was connected to the mercury U-Tube. Using the valve, a suction was created changing the head in the mercury U-tube. A vacuum was created ranging from 0 mm Hg to 700 mm Hg and the corresponding voltages were recorded. Between this range five points were selected. Once the maximum suction head was reached the same procedure was repeated by decreasing the pressure to check whether the transducer gave the same readings as when the pressure was increased to the same points. These data are illustrated in Table 5, which shows the voltages to be very similar at the identical points.

Table 5. An example of voltages recorded by pressure transducer No. 1 for corresponding suction heads of Mercury with a regressed equation.

Increase (mmHg)	**Voltage (V)**	**Decrease (mm Hg)**	**Voltage (V)**
0	0.21	700	4.39
200	1.38	600	3.77
400	2.60	400	2.60
600	3.76	200	1.38
700	4.39	0	0.21
EQUATIONS	[illegible]		

Data given in Table 5 shows the accuracy of these transducers under hysteresis conditions. This procedure was repeated for all the transducers. Using regression analysis, curves were fitted to the data and equations developed. An example is shown in Table 5 for transducer No 1. The remainder of the calibration equations are given in Appendix B.

Each logger has an inherent calibration equation converting the voltage to a digital signal for storage. Using this calibration, the transducer equation and the depth of the tensiometer below the soil surface, corresponding matric potentials have been calculated for all tensiometers and their data.

Equation 14 is an example of one such equation for transducer 1 connected to tensiometer 1 at Pit 1, used to calculate the matric potential head (ψ) of the soil.

$$\psi = ([-33.84 + 167.63 * (V * 0.001219 + 0.00366)] * 1.36) + D \quad \textbf{(14)}$$

where			
	ψ	=	Matric potential head (m)
	V	=	voltage (V)
	0.001219	=	slope of logger calibration equation
	0.00366	=	intercept of logger calibration equation
	D	=	depth of tensiometer below soil surface (m).

4.4.5.3 Robust Loggers

To record data automatically and continuously a recording device was required. Loggers are expensive and for a detailed experiment such as this one, many recording devices were needed. The DAE therefore set about to develop their own loggers which have proved to be inexpensive, robust and successful in recording tensiometer data. These loggers interface directly to four pressure sensors which have an amplified and temperature compensated output in the range 0 to +5 Volts. A 6V battery powers both the logger and the transducers. Figure 25 illustrates one such logger with the various connecting ports.

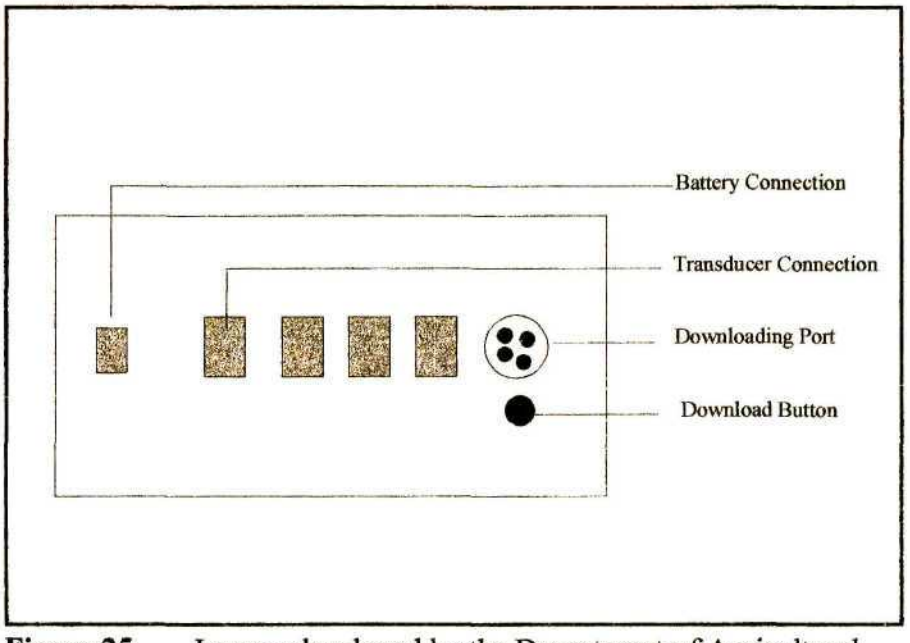

Figure 25. Logger developed by the Department of Agricultural Engineering to record electronic signals from attached pressure transducers.

Four transducers linked to 4 tensiometers are attached to each logger. A change in pressure inside the tensiometer is digitized and saved to non-volatile memory for a predetermined time interval. This time interval can be changed, depending on how frequently data are required. For example, during summer when there is significant soil moisture variation within the unsaturated zone, a smaller sampling time is important. Conversely in winter, when the soil is relatively dry, data may only be needed every hour. Before readings are recorded, the logger preforms an internal check on the battery. If the voltage of the battery is below a predetermined threshold, a low battery symbol is recorded in the data file.

For this research the data sampling time was set at 12 minutes with the signal from each sensor being sampled 256 times, averaged and stored. Special functions built into the logger software automatically switch off the logger between readings. This power saving technique enables the battery to remain charged for up to 68 days when sampling at this 12 minute interval. Data can then be downloaded on site to a PC (Figure 26) by depressing the button shown in the Figure 25. The data can then be imported into a spreadsheet program where it is converted to matric potentials using Equation 14, which is valid for transducer number one. For the remainder of the transducers the correct equation must be used. The specifications and limitations of these loggers can be found in Appendix C.

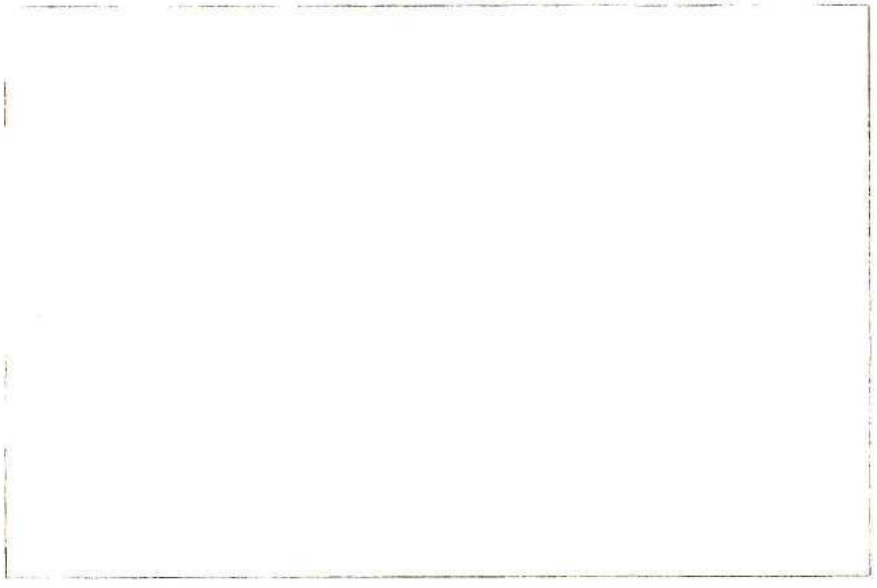

Figure 26. Tensiometer nest showing a laptop computer used in the downloading process.

4.4.5.4 Installation of a Tensiometer Nest

The location of each tensiometer nest is shown in Figure 21, shown as Nest 1 to Nest 6. Appendix D shows how the tensiometers are numbered for each nest, with corresponding depths below the soil surface.

Using a muddy slurry to ensure a good contact between the tensiometers and the soil, the tensiometers were inserted into augered holes. Each tensiometer was filled with deaired water. Using a syringe, water was injected into each transducer ensuring no air bubbles remained. Air bubbles cause incorrect results. Transducers were connected to each tensiometer with tubing connected to the negative port of the transducer and tensiometer U-tube. Each transducer was connected to 3-core cable linked to the logger and battery. Each logger and battery at each nest were housed in tubing cemented into the ground (Figure 26). To protect the cable, conduit tubing was used through which the cable was passed. Holes have been drilled into the tubing which houses the logger to prevent condensation taking place. Figure 27 shows the setup of such a nest.

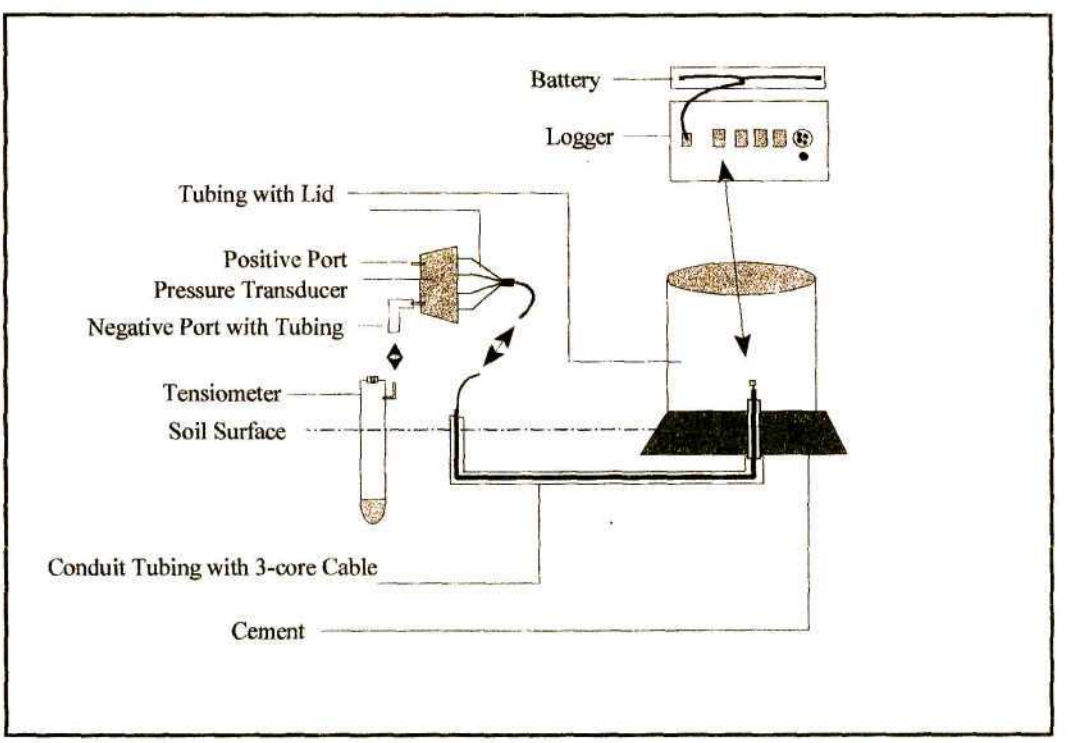

Figure 27. Tensiometer nest showing all components (Not drawn to scale).

Once installed the tensiometers do not require much maintenance. The battery needs to be replaced, with a recharged unit, every 60 days and the tensiometer itself needs to be maintained every two weeks. Often, when the soil is exceptionally dry, the air entry pressure into the ceramic is exceeded and air enters the system. Air in the system leads to inaccuracies in the data and the air needs to be removed. In this event the threaded bolt is simply removed and the water replenished. This procedure was carried out after the data had been downloaded so as not to affect the recorded data.

4.4.6 Specific Experiments

In conjunction with the detailed hillslope experiment described, various specific experiments were carried out. These "once-off " ventures were considered "look and see" type experiments. The first experiment was to establish the extent and proliferation of macropores and their flow and the second to measure infiltration and redistribution from a controlled ponded test. Results for each of these specific experiments are presented in Section 5.4.

4.4.6.1 Macropore Flow

Using a steel ring, water mixed with Fluorescein Sodium salt (C20 H10 O5 Na2 : 376.27) was ponded at both Pit 3 and Pit 4. This salt is a dye which illuminates with a maximum absorption pH 8 buffer, absorbing in the wavelength region of 490 - 492 nm. The latter experiment was abandoned due to a proliferation of macropores which became evident when the ponded water disappeared in a matter of minutes. However, at Pit 3 the test was successful.

4.4.6.2 Three-Dimensional Infiltration and Redistribution Experiment

On the hillslope above RO2 (*cf.* Figure 21), an area was selected where water was ponded, periodically over a 2 month period. Two nests of 3 tensiometers were installed downslope of the ponded area and readings were taken manually. This experiment gave some interesting results which are presented in Section 5.4.

* * *

In Chapter 4 the Weatherly catchment has been described, with more detail given to the soils, geology, topography and bedrock of Transect 1. The methodology used to determine the physical and hydraulic characteristics was highlighted, followed by a discussion on the instrumentation installed. This instrumentation included automated tensiometers, piezometer and neutron probe access tubes.

Chapter 5 follows with results from data collected from each of the measurements of the hydraulic characteristics of the soils found along Transect 1 and monitored data collected from the instruments.

5. RESULTS FROM FIELDWORK

5.1 Soil Physical Properties

Descriptions of PSD, ρ_b and ϕ, with methodologies used in their measurement were outlined in Section 4.3.2. Section 5.1.1 below, gives results pertaining to these soil physical characteristics along Transect 1.

5.1.1 Particle Size Distribution

The hydrometer and pipette methods (*cf.* Section 4.3.2.1) were used to determine the percentages of sand, silt and clay at four locations (Pit 1-4) along Transect 1. These percentages are referred to as per cent finer throughout the remainder of this document. Soil samples used in the hydrometer method were taken throughout the soil profile, with samples taken within each of the three horizons, identified by the ISCW (*cf.* Figure 16), at each of the four pits. To attain results representative of each soil horizon, two or three samples from each horizon were extracted and analysed. These results within each horizon were then averaged. A comparison of results is shown as a bar chart in Figure 28 with actual figures given in Table 6.

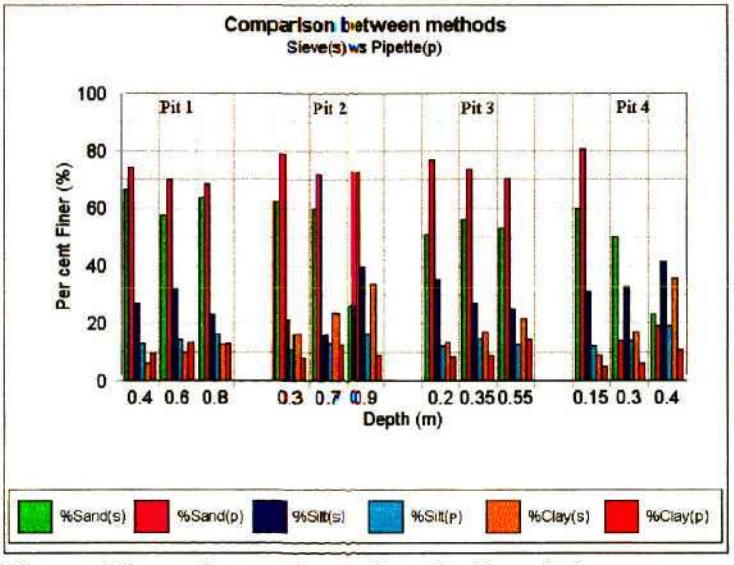

Figure 28. Comparison of sand, silt and clay percentages determined by sieve and pipette methods along Transect 1.

These results, show that the per cent finer determined from each of the two methods do not have large differences, except that the silt fractions are under estimated and the per cent clays over estimated to a lessor extent when using the pipette method. Furthermore, the sum of the per cent finer attained from the pipette method does not add up to 100%. A reason for these differences is that the entire soil sample is used in the analysis with the hydrometer method, whereas, the pipette method, uses a 'representative' sub-sample of the initial soil sample, with the subsequent loss of soil.

Most of the soils within Transect 1 comprise more than 50% sand. Deeper soils close to the bedrock at Pit 2 and Pit 3 have sand fractions ranging from approximately 15% to 35%, with clay fractions in excess of 35% (*cf.* Appendix F, Tables F1 to F11).

Table 6. Textural analysis. A comparison of results between the pipette and sieve/hydrometer methods at each pit along Transect 1.

Pit	**Depth (m)**	**Sieve / Hydrometer Method**			**Pipette Method (ISCW)**			**Error Term**
		Sand (%)	**Silt (%)**	**Clay (%)**	**Sand (%)**	**Silt (%)**	**Clay (%)**	**(%)**
Pit 1	0-0.4	66.5	27.3	6.2	74.2	13.3	9.6	2.9
	0.4-0.6	57.7	32.3	10.0	70.2	14.3	13.5	2.0
	0.6-0.8	63.8	23.4	12.8	68.5	16.4	13.2	1.9
Pit 2	0-0.3	62.5	21.3	16.2	78 9	10.9	8.0	2.2
	0.3-0.7	60.0	16.2	23.8	71.9	13.1	12.6	2.4
	0.7-0.9	26.3	40.0	33.7	72.5	16.2	9.1	2.2
Pit 3	0-0.2	51.0	35.5	13.5	76.6	12.3	8.5	2.6
	0.2-0.35	56.0	27.0	17.0	73.7	14.6	9.2	2.5
	0.35-0.55	53.3	24.9	21.8	70.4	13	14.5	2.1
Pit 4	0-0.15	60.0	31.0	9.0	80.7	12.3	5.2	1.8
	0.15-0.3	50.0	33.0	17.0	14.2	14.2	6.3	2.2
	0.3-0.4	23.2	41.4	35.6	19.2	19.2	10.9	2.1

The per cent sand decreases both down the soil profile and down the hillslope transect, as shown in Figures 29 and 30. Table 6 shows the per cent sand at Pit 1 to vary from 66.5%

to 57.7% down the profile. Within the A-horizon at Pit 2 the sand is 62%, Pit 3, 51% and Pit 4, 60%, with the same trend occurring within the deeper horizons. Clay fractions at Pit 1, increase from 6% near the soil surface to 13% at the base of the soil profile, with the same trend occurring within each of the other soil profiles. These clay percentages increase down the hillslope, except at Pit 4, where the percentages clay are similar to those of Pit 1, but have the highest silt fractions in comparison to the other soil profiles.

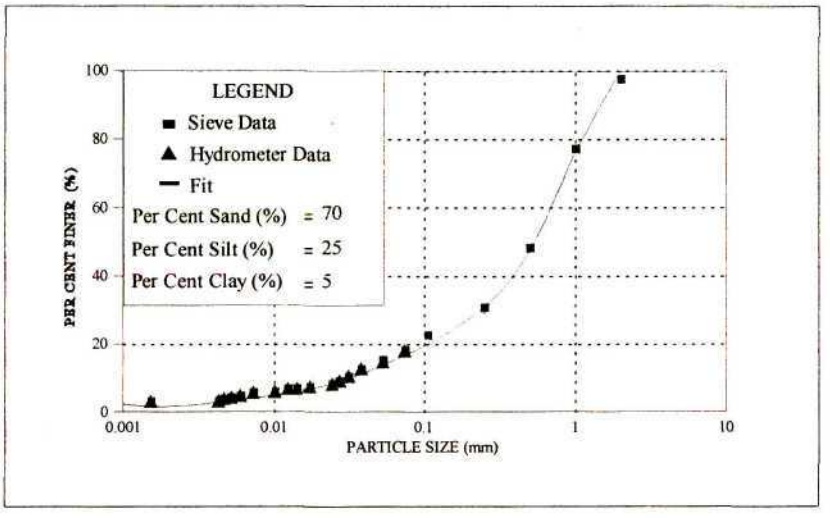

Figure 29. Cumulative particle size distribution: Pit1, 0.10m depth.

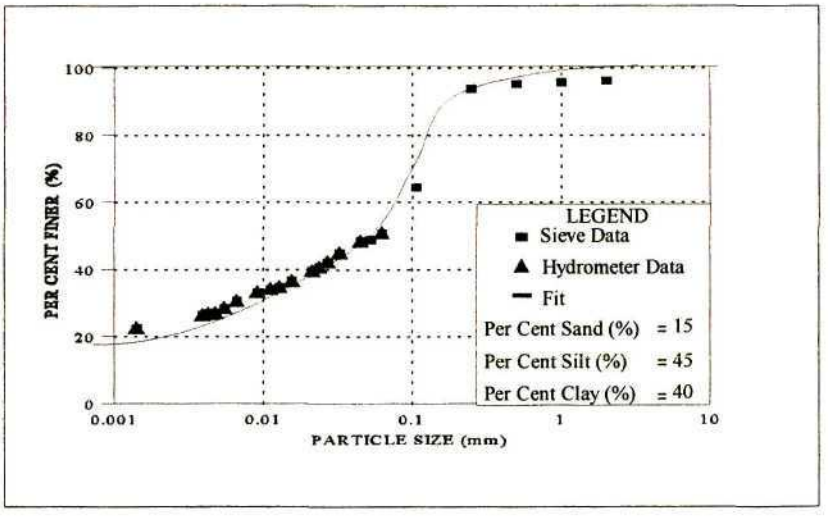

Figure 30. Cumulative particle size distribution: Pit 2, 1.80m depth.

The PSD for Pit 1 at 0.1 m (Figure 29) shows that the soil has a high sand percentage, with a lessor amount of clay compared with the deeper soils (Figure 30). These PSD extremes are hypothesised to be due the different positions on the hillslope and because the PSD curves represent the topsoil (Figure 29) and the subsoil (Figure 30). These differences between the topsoil and subsoil are presented in Figure 31, which shows clearly that within deeper soils the percentage of clay is large compared to soils closer to the surface. The remainder of the PSD curves at each location on Transect 1 are presented as Figures 1F to 9F in Appendix F.

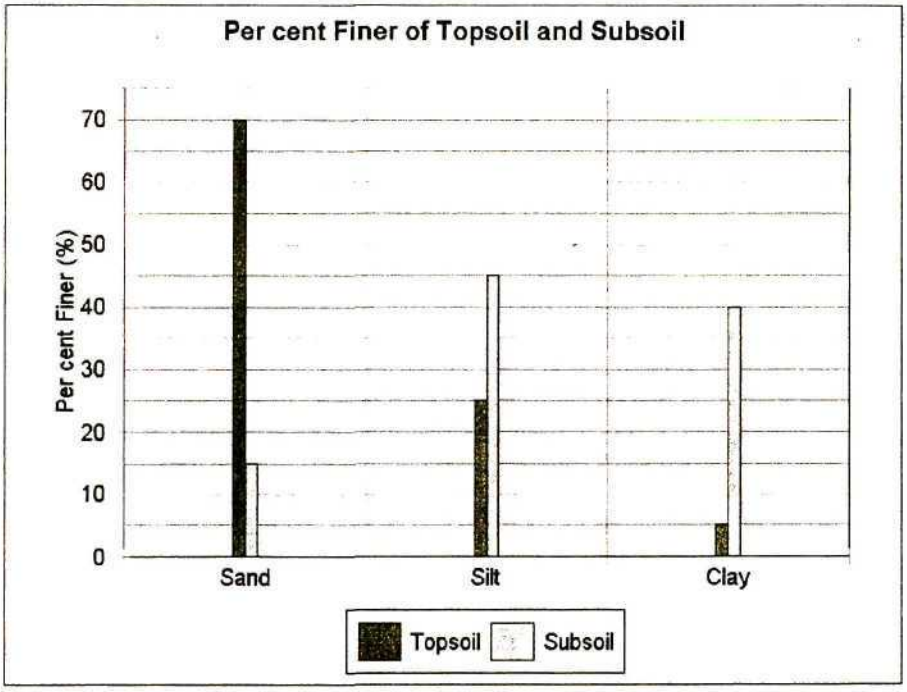

Figure 31. Comparison of per cent finer between the topsoil (Pit 1) and the subsoil (Pit 2).

5.1.2 Bulk Density and Porosity

The ρ_b and porosities of the soils were determined using the corer and excavation methods (*cf.* Section 4.3.2.2) at each of the 4 pits, from the soil surface down to the bedrock. For each depth down the soil profile (Table 7), a number of samples were taken and analysed. Results shown are the average ρ_b and ϕ for each depth. As a data check, Table 7 shows

also the porosities and bulk densities calculated during the outflow cell analysis. Missing data are a result of lost samples or from problems which arose during analysis.

Table 7. Comparison of bulk density and porosity determined using the Corer, Replacement and controlled outflow cell sample, with the soil type at each pit along Transect 1.

	Soil Type	Depth (m)	Corer Method		Excavation Method		Outflow Method	
			Bulk Density (ρ_b) ($Mg.m^{-3}$)	Porosity (ϕ) (%)	Bulk Density (ρ_b) ($Mg.m^{-3}$)	Porosity (ϕ) (%)	Bulk Density (ρ_b) ($Mg.m^{-3}$)	Porosity (ϕ) (%)
PIT 1	Avalon	0 - 0.40	1.63	38.41	1.62	38.86	1.83	41.00
		0.4 - 0.60	1.58	40.39	1.50	43.40	-	-
		0.6 - 1.10	1.78	32.83	1.64	38.11	-	-
PIT 2	Pinedene	0 - 0.30	1.62	38.94	1.43	46.04	1.71	35.50
		0.3 - 0.70	1.74	34.25	1.55	41.51	1.81	32.00
		0.7 - 1.80	1.79	32.15	1.71	35.47	1.89	28.70
PIT 3	Tukulu	0 - 0.20	1.67	37.02	1.51	43.01	-	-
		0.2 - 0.35	1.71	35.57	1.47	44.52	1.79	32.00
		0.35 - 2.10	1.84	30.72	1.93	27.12	1.83	36.00
PIT 4	Kroonstad	0 - 0.15	1.49	43.92	1.55	41.51	1.89	13.00
		0.15 - 0.3	1.74	34.33	1.81	31.69	1.72	15.00

Results from the corer method at Pit 1 and Pit 2 are higher than those determined from the excavation method. These differences are negligible in comparison to other errors of measurement. A reason for these differences could be that the soils within this midslope region along Transect 1 are very compact, making excavations difficult, thus resulting in error. Samples were only taken up to a depth 0.3 m at Pit 4 due to the presence of very high water tables at the time of sampling. The bulk densities for each soil profile increase down the profile, except for the Avalon soil between 0.40 m and 0.60 m. No large differences are noted between the soils along Transect 1, except that the bulk densities increase slightly with depth due to the compact nature of these soils. In the Avalons at 0.4 m, Pinedenes at the surface and the Kroonstads at the toe of the hillslope, the ρ_b is lower at depth than nearer the surface. This is possibly due to the proliferation of macropores observed in the field.

A discrepancy exists between these measured ρ_b and ϕ and those measured in the controlled outflow method. This could be attributable to the fact that the locations from where the soil samples were extracted for physical measurements, were different to the location of samples taken for WRC analysis. A reason for these differing locations are because the soil samples were taken at different times throughout 1996 and the identical locations could not always be found. These different results therefore show the large spatial variability of soil properties which occur along Transect 1.

5.2. Soil Hydraulic Characteristics

An outline of the soil hydraulic characteristics and methodologies used in their measurement is presented in Section 4.3.3. Theoretical curves defining the WRC have been fitted to the data using Brooks and Corey (1964) functions. These are presented in Section 5.2.2. Where water tables intersected the soil surface at Pits 3 and 4 the auger hole method was used to calculate the K_s of the soil (*cf.* Section 4.3.3.1). Results from the auger hole method were totally different to those measured in the field, showing a common error that occurs when using such an empirical equation, derived under different conditions. Double ring and tension infiltrometer results are presented in Section 5.2.1. below.

5.2.1 Hydraulic Conductivity

A total of 40 DR and 42 TI tests were successfully completed. Table 8 shows a comparison between the conductivities at the soil surface at Pit 1 and Pit 4. The remainder of the conductivities determined for each of the soil profiles are given in Appendix G (Tables G1 to G20).These results show a large variation in conductivities. The high $K(\theta)$ at Pit 4 suggest that the soils have a larger clay content than at Pit 1. The K_s , at Pit 1 on the other hand, is an order of magnitude larger than that at Pit 4, suggesting either the presence of preferential flow pathways or very sandy soils, with relatively large pore sizes. From field observations preferential flow pathways have been observed in the region of Pit 4, substantiating these findings.

Table 8. Comparison of unsaturated and saturated conductivities for Pit 1 and Pit 4 at the soil surface.

Pit	Tension (mm)	Final Hydraulic Conductivity ($mm.h^{-1}$)	Saturated Conductivity ($mm.h^{-1}$)
1	5	1.24	
	50	0.41	
	100	0.20	
	165	0.22	
	0		1054.8
4	5	16.58	
	50	7.39	
	100	3.89	
	165	3.94	
	0		292.41

An in-depth analysis of these results is presented together with the WRC of the soils in Section 5.2.3. First, however, the procedure used to fit Brooks and Corey (1964) parameters to the measured WRC data is outlined below in Section 5.2.2.

5.2.2 Water Retention Characteristics

Using the controlled outflow cell method the WRC for each soil sample taken from Transect 1 were determined. Brooks and Corey (1964) parameters were fitted to these data. This procedure was carried out by plotting the matric potential head (h) against the effective water content (Se) on a logarithmic scale, as shown in Figure 32.

Se can be expressed in two ways depending on the input parameters. In terms of water contents Se is expressed as (*cf.* Appendix E):

$$Se=\left(\frac{\theta-\theta_r}{\theta_s-\theta_r}\right) \qquad \textbf{(15)}$$

where θ = water content of the soil ($m^3.m^{-3}$)

θ_r = Brooks and Corey (1964) residual water content ($m^3.m^{-3}$)

θ_s = soil water content at saturation ($m^3.m^{-3}$).

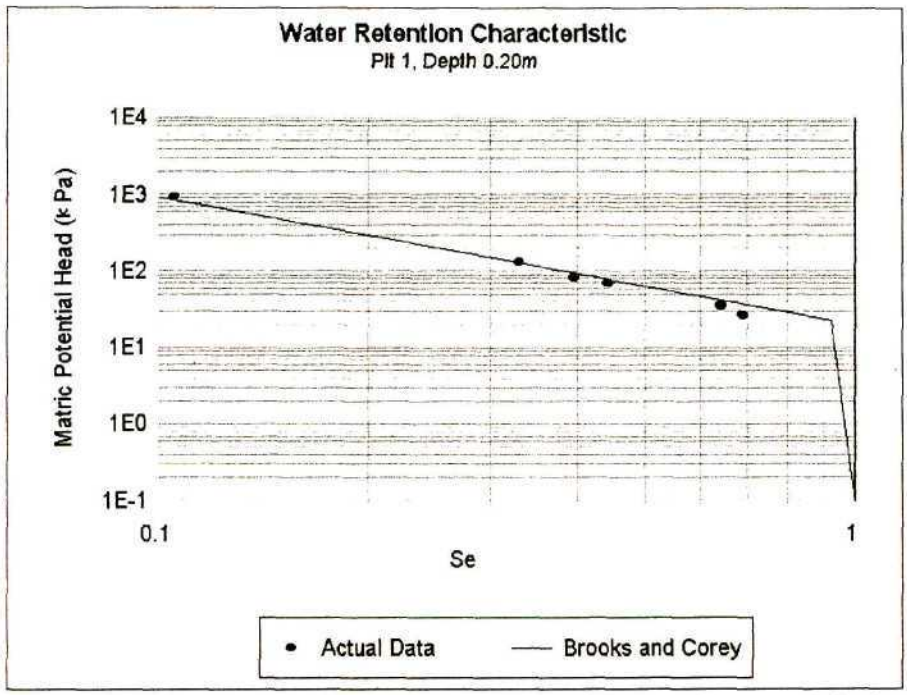

Figure 32. An example of a log/log plot of the matric potential of the soil against the effective water content, where a straight line is fitted to the data.

The residual water content of a soil is the air dry water content. A clayey soil therefore has a larger residual water content compared to a sandy soil. Using Brooks and Corey (1964) parameters Se can also be expressed as follows, with each of the two equations satisfying different conditions:

$$Se = 1 \qquad \text{when } h \leq h_d$$

$$Se = \left(\frac{h_d}{h}\right)^{\lambda} \qquad \text{when } h > h_d$$

where h_d = Brooks and Corey (1964) air entry pressure (m) and

h = matric pressure head (m)

λ = Brooks and Corey (1964) pore size distribution index.

By adjusting θ_r, λ and h_d, curves were fitted to the data according to the method of Brooks and Corey (1964). Changing the log/log plot to a standard plot then yields an exponential curve through the data as shown in Figure 33, which depicts the fitted WRC and shows the calculated parameters of air entry and residual water content.

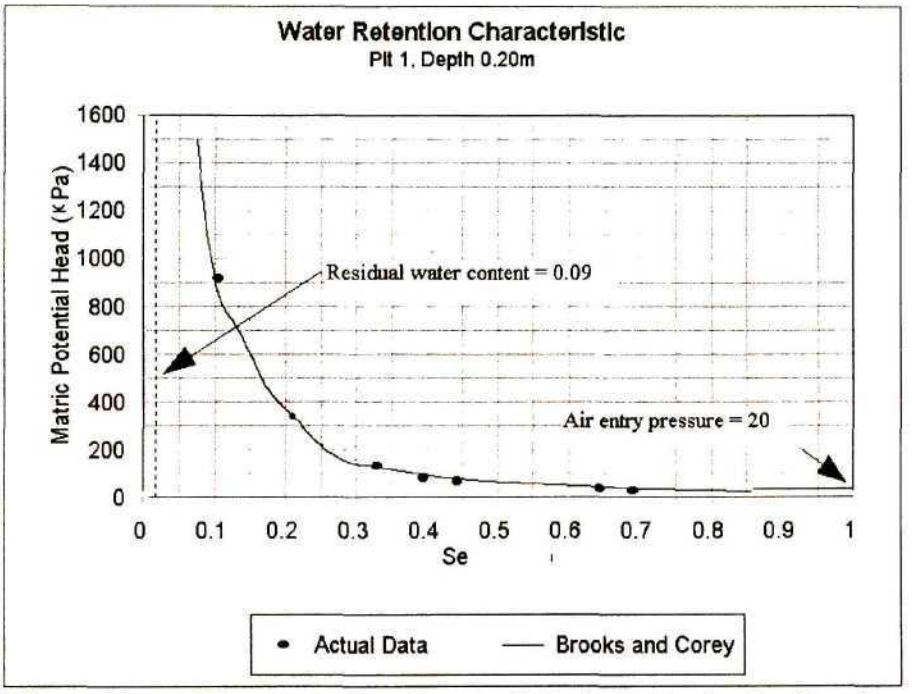

Figure 33. Water retention characteristic determined using Brooks and Corey (1964) parameters

This procedure was carried out on each of the WRC's from the soil samples taken from Transect 1. The Brooks and Corey (1964) parameters obtained for each WRC are presented in Table 9. Highlighted values show errors in measurement. Such incorrect results can occur if the soil sample taken from the field is not stored correctly. Such samples break up and WRC analyses cannot be performed. Other errors occurred during the operation of the outflow instrumentation.

Table 9. Brooks and Corey (1964) parameters, with porosities and bulk densities calculated from the controlled outflow method.

Pit Number	Depth (m)	Pore Size Distribution Index (λ)	Residual Water Content ($m^3.m^{-3}$) (θ_r)	Air Entry (m) (h_d)
1	Surface	0.185	0.160	0.02
	0.20	0.600	0.090	0.20
	0.40	**0.052**	0.100	0.08
2	Surface	0.500	0.050	0.40
	0.20	0.230	0.088	0.26
	0.40	0.500	0.230	0.70
	0.90	**0.025**	0.060	0.62
	1.40	0.130	0.220	0.50
3	0.50	**0.060**	0.030	**0.000284**
	0.70	0.250	0.020	0.35
	1.40	0.800	0.095	0.34
4	0.40	0.334	0.13	0.10

These WRC, Brooks and Corey (1964) parameters and the hydraulic characteristics are discussed in Section 5.2.3 below.

5.2.3 Comment on Physical Hydraulic Characteristics

The water retention and hydraulic conductivity characteristic curves are given in Appendix G (Figures G1 to G20). WRC curves paired with conductivities represent data collected from identical locations. Where WRC data are not available, only K characteristics are presented.

Table 10 gives a summary of the percentages of pore water drained at 1000 mm tension for each of the soil profiles. Included are the saturated and unsaturated conductivities at both the upper and lower limits of tensions, 5 mm to 165 mm, used in determining the unsaturated conductivity characteristics.

Table 10. Percentage of water drained at 1000 mm together with K_s and $K(\theta)$ at two different tensions, with θ_r, ϕ and ρ_b.

Pit Number	Depth (m)	θ_r ($m^3.m^{-3}$)	$\theta_{\%}$ (%)	K_s 0 mm ($mm.h^{-1}$)	$K(\theta)$ 5 mm ($mm.h^{-1}$)	$K(\theta)$ 165 mm ($mm.h^{-1}$)	ϕ (%)	ρ_b ($Mg.m^3$)
	Surface	0.160	68	1054	1.240	0.220	0.458	1.437
1	0.20	0.090	90	262	0.660	* 0.110	0.381	1.640
	0.40	0.100	92	353	36.060	*1.380	0.402	1.584
	0.70	**	**	345	42.260	*1.630	**	**
	0.90	**	**	151	12.030	0.610	**	**
	1.40	**	**	3	1.710	0.160	**	**
	Surface	0.050	80	492	2.200	0.370	0.341	1.746
2	0.20	0.088	75	162	0.720	0.260	0.369	1.672
	0.40	0.230	75	552	61.190	5.590	0.337	1.758
	0.60	**	**	117	7.490	0.560	**	**
	0.90	0.060	55	151	12.030	0.610	0.302	1.977
	1.40	0.130	30	3	1.710	0.160	0.305	1.843
	Surface	**	**	329	6.480	0.630	**	**
3	0.20	**	**	97	6.630	*0.490	**	**
	0.50	0.030	55	52	0.720	0.180	0.336	1.759
	0.70	0.020	45	73	33.610	2.200	0.324	1.791
	1.40	0.095	90	8	1.530	0.160	0.294	1.872
4	Surface	**	**	292	16.580	3.940	**	**
	0.20	**	**	25	10.680	1.640	**	**
	0.40	0.130	80	54	5.920	0.710	0.286	1.891
	0.60	**	**	22	12.920	*2.080	**	**

* No value for K_s available at 165 mm, instead value taken at 100 mm.

** No WRC data available.

The percentage of pore water drained, at a matric pressure head of 1000 mm, increases with increasing depth for the Avalon and Tukulu soils. Those percentages of pore water drained decreased with an increase in depth on the midslope at Pit 3 (*cf.* Appendix G, Figures G14 to G21). Approximately 92% of the pore water has drained at 0.40 m in the Avalons at a matric pressure head of 1000 mm compared with 75% at Pit 2 at the same depth (*cf.* Appendix G, Figures G5 and G13). A large amount of water drained from a soil

at a low matric pressure head suggests a presence of macropores. This is supported by the very high K_s at the same location. Pit 2, at a depth of 1.40 m, shows that 30% of the pore water has drained at a matric pressure head of 1000 mm, followed by a slow desorption of water, as shown in Figure 34.

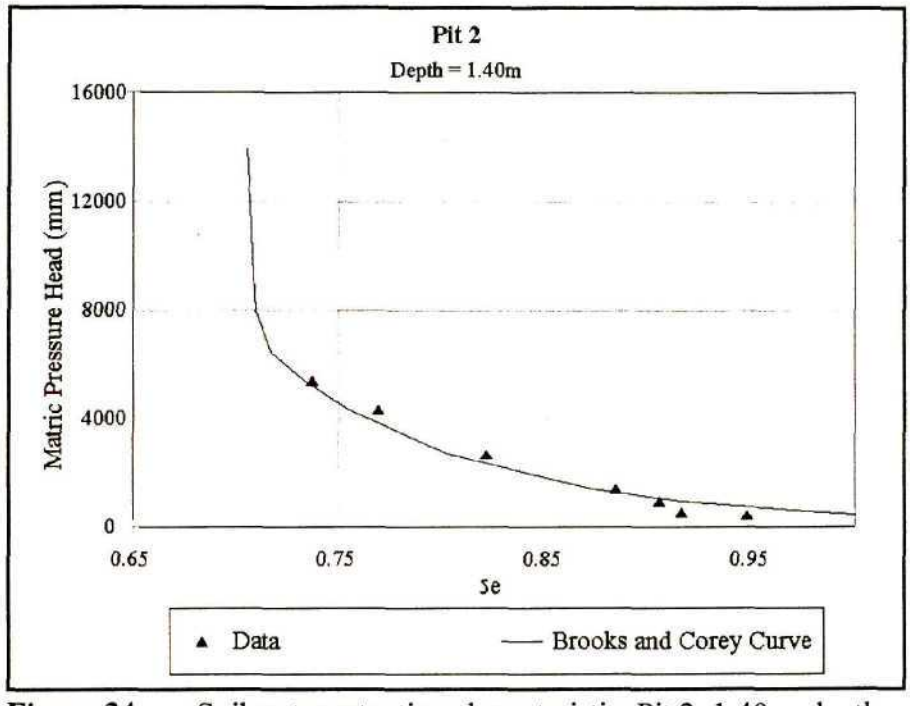

Figure 34. Soil water retention characteristic: Pit 2, 1.40 m depth.

This slow desorption shows that the soil has a large water holding capacity since it has a larger residual water content compared with those of the other soils. The conductivities at this depth reflect the high clay content since these K_s values are relatively lower (Figure 35) than those of the soil in the toe region of the hillslope (Figure 36).

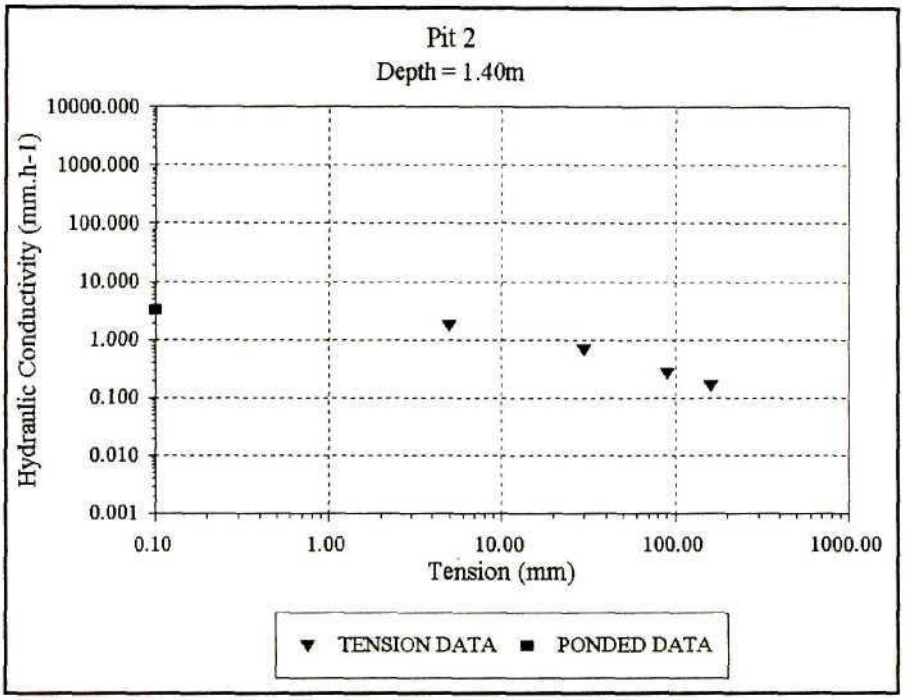

Figure 35. Hydraulic conductivity: Pit 2, 1.40 m depth.

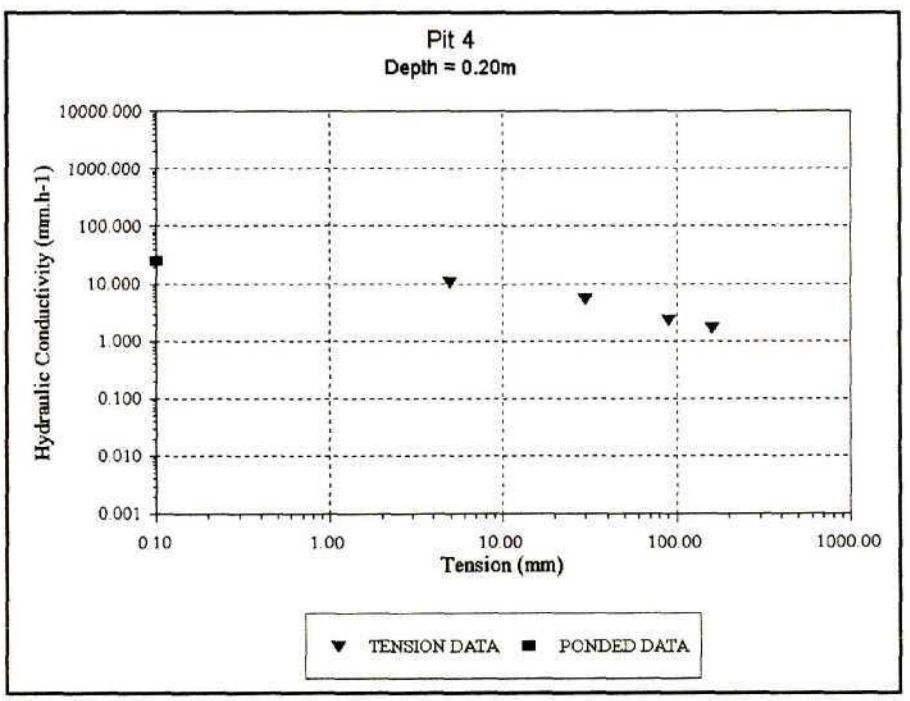

Figure 36. Hydraulic conductivity: Pit 4, 0.20 m depth.

In comparison to Pit 1 at the soil surface, 68% of the pore water has drained at a matric pressure head of 1000 mm, and has a very high conductivity illustrated in Figures 37 and 38 respectively.

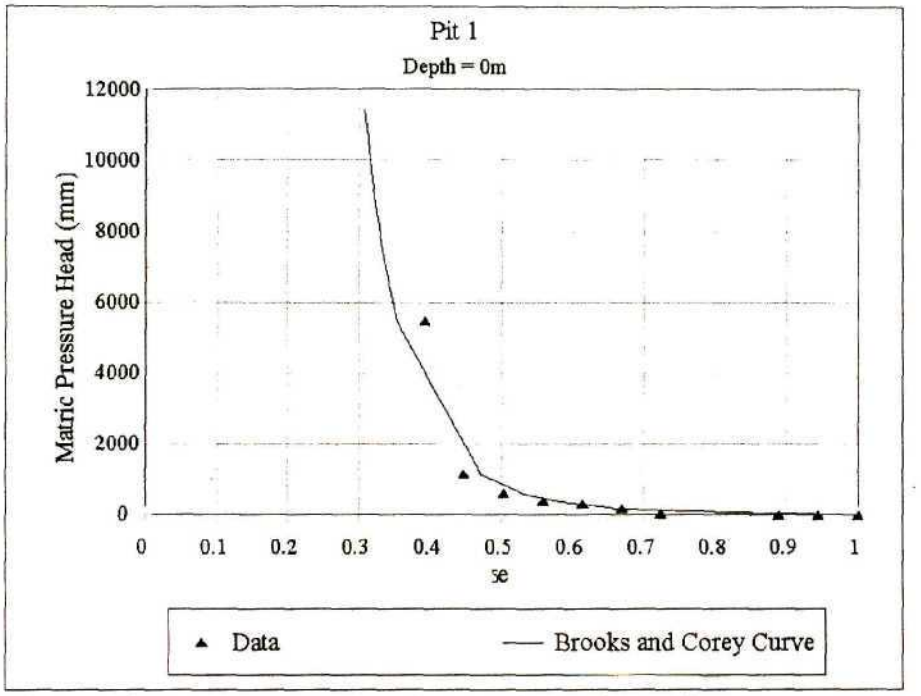

Figure 37. Water retention characteristic: Pit1, soil surface.

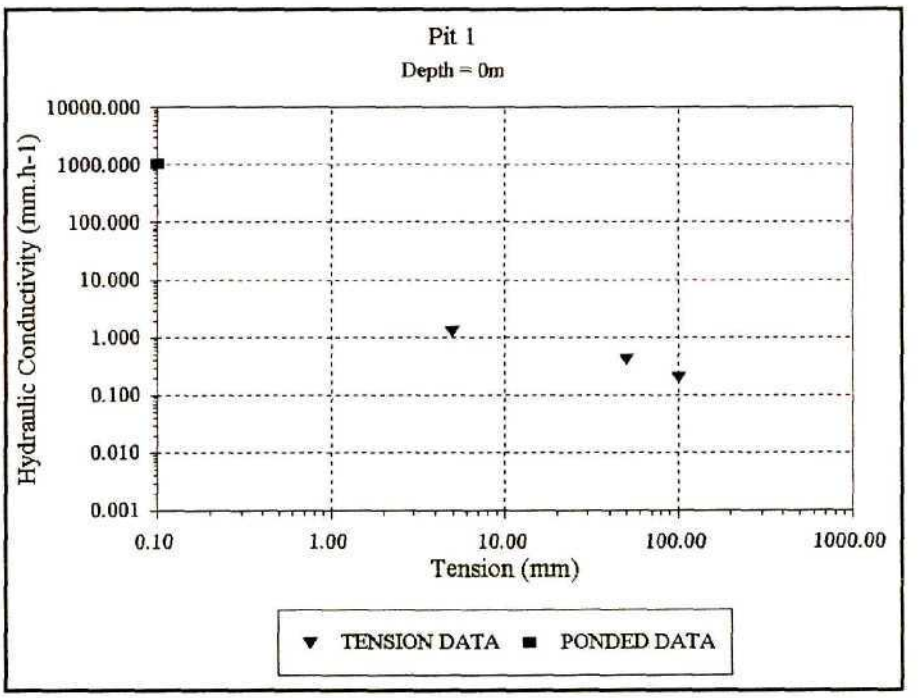

Figure 38. Hydraulic conductivity: Pit 1, soil surface.

In general K_s decreases with depth following an increasing clay content. No clear cut trend can be seen with the $K(\theta)$ as shown in Table 10, except that they are much lower than the

K_s . Occasionally the $K(\theta)$ are relatively high as often happens for Pit 2 and 3 at 0.40 m and 0.70 m respectively (*cf.* Appendix G). This is most likely due to more sandy layers present within the profiles.

Simple and multiple regression analyses were performed to identify whether trends are evident between the K_s , soil depth and clay content. A multiple regression analysis gave an r^2 of 0.37, showing no significant relationship. For each profile, except at Pit 1, a simple linear regression was performed between K_s and soil depth and the clay content. These results are presented in Table 11.

Table 11. Coefficients of determination for K_s regressed against soil depth and clay content for each soil profile along Transect 1.

Pit	Soil Depth	Clay Content
2	0.67	0.77
3	0.78	0.80
4	0.58	0.55

From the information presented in Table 11 there is clearly a reasonably good relationship between K_s and clay content down the soil profile. These results can be expected since K_s is related to the PSD of the soil, in that a higher sand content causes larger K_s . There is a good relationship between the K_s and soil depth, as one would expect, since along Transect 1 the clay content increases with depth (*cf.* Section 5.1.1).

5.3 Monitored Results

Details of the methodology of the monitoring of soil moisture, groundwater and tensiometers is outlined in Section 4.4. This section considers the soil moisture, tensiometer and groundwater results and their interaction, since each is related as a result of the various process interactions (*cf.* Section 2.1).

Transect 1 was visited during many of the rainfall events, where some informative general observations were made:

a. Storms of a high intensity produce mainly surface runoff (Figure 39) with little evidence of infiltration. This response to the high input flux is compounded by the grassland that is in a poor hydrological condition. Analysis of the soil moisture and tensiometer data after such events shows little or no change to the soil moisture status, indicating an absence of an infiltration wetting front.

Figure 39. Surface runoff production after a storm having a high rainfall intensity.

b. Low intensity, long duration events result in significant infiltration especially if the AMC is low.

In response to b. above, rapid water table rises have been observed with an increase in the soil water contents and a decrease in tensions in the upper layers. Exfiltration was observed in the toe region of the hillslope, shown in Figure 40, taken just below Pit 4. Also observed was macropore and pipe flow (Figure 41), where flow from these conduits continued for up to 3 days after a rainfall event of 26 mm on the 29 December 1996. A large pipe, approximately half a metre in diameter was observed. Here water gushed continuously for two days after the same rainfall event.

Figure 40. Exfiltration occurring in the toe region of the hillslope

Figure 41. Macropore flow occurring at the toe of the hillslope.

These frequent field visits enabled important general observations to be made, enabling a clearer understanding of data collected from the field.

To interpret these detailed observations, it is expedient to begin with an understanding of the variation in the soil profiles along Transect 1. Table 12 shows the soil types found at each pit with their horizons, depth ranges and positions on the hillslope. Depths shown in bold make up the total depth of the soil profile to bedrock. The depths at which readings take place with the NMM are also shown.

Table 12. Information regarding the soil horizons found at each pit location with their respective soil depths and position on the hillslope.

Pit Number	Horizon	Depth Range (m)	Neutron Probe Depth (m)	Position on Hillslope
1	A	0-0.40	0.150	
	B	0.40-0.60	0.450	Crest
	F	0.60-**1.12**	0.750	
2	A	0-0.30	0.150	
	B	0.30-0.70	0.450	Midslope
	F	0.70-**2.30**	0.750-2.250	
3	A	0-0.20	0.150	
	B	0.20-0.55	0.450	Midslope
	F	0.55-**3.10**	0.750-1.950	
4	A	0-0.15	0.150	
	E	0.15-0.30	0.450	Toe
	G	0.30-0.40	0.450	
	F	0.40-**1.19**	0.750-1.050	

Pit 1 near the crest of the hillslope has shallow soils overlying an undulating and fractured bedrock (*cf.* Figure 18). Water appears to feed this region from further upslope and from field observations it has been observed that this section of Transect 1 becomes very wet after prolonged rainfall. There are two possible explanations for this. First, immediately upslope of Pit 1, there is a large area covered by rock outcrop, providing a direct runoff surface. Secondly from field observations there is a rock outcrop downslope of Pit 1, immediately

upslope of Pit 2. This area behaves in the same way as the toe region of the hillslope with water building up at this interface, inducing saturated conditions. For these reasons the groundwater observations at this location are higher than would be expected of a location near the crest of a hillslope. In the midslope, Pits 2 and 3 have very deep soils and low water tables compared to Pits 1 and 4. These soils are well drained, with water being able to redistribute quickly within the soil profile. In the toe region at Pit 4, the soils are shallow and a high water table is supported and was present since the beginning of the monitoring in April 1996 until April 1997. It is in this region that exfiltration and return flows occur with significant preferential water flow, because of the large abundance of macropores found here. A more detailed explanation of these observations, with results, is discussed in Section 5.3.1.

Rainfall data for 1996 and 1997 is presented in Figure 42, showing the daily rainfall totals, with the periods when measurements and monitoring occurred.

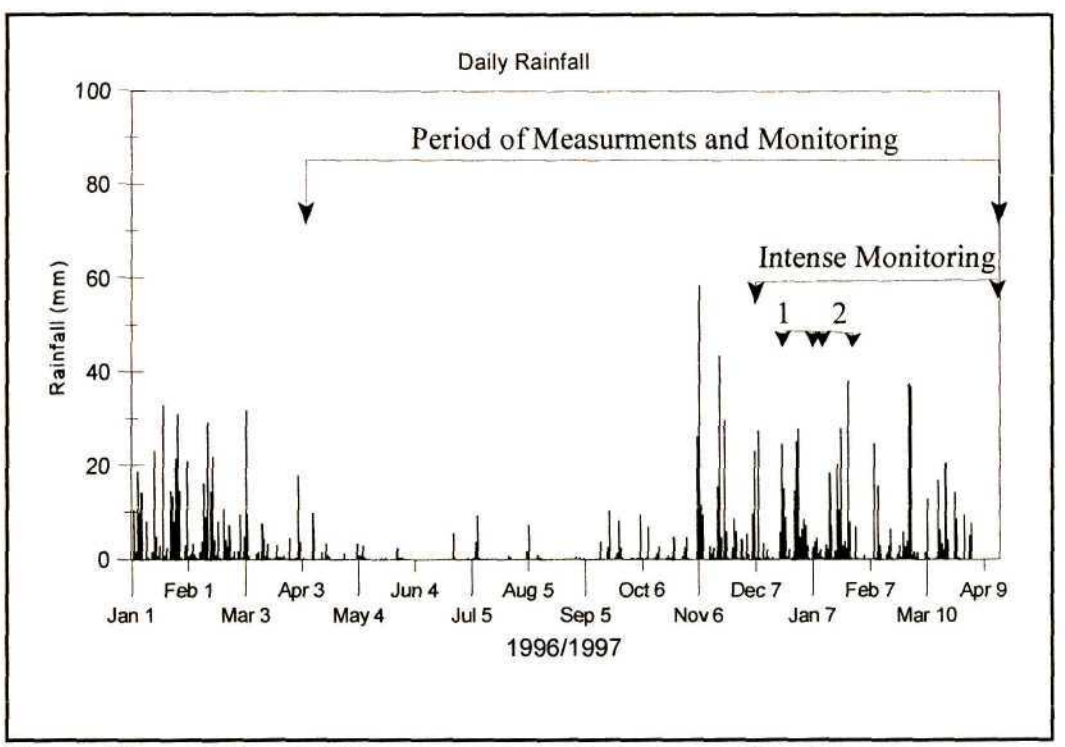

Figure 42. Daily rainfall totals and the periods when soil moisture measurements and monitoring occurred.

Detailed data were collected during an intensive monitoring period between December 1996 and April 1997. These data are divided into:

a. manual monitoring of soil moisture, groundwater and tensiometer data (December 1996 to January 1997), and

b. continuous automated tensiometer monitoring with manual monitoring of soil moisture and groundwater data (February 1997 to April 1997). This period has been further subdivided into smaller time periods, as shown in Figure 43. These periods are 7 February 1997 to 15 February 1997 and 19 February 1997 to 7 March 1997. These periods have been selected to show the soils' response to individual rainfall events.

5.3.1 Manually Monitored Results (December 1996 - January 1997)

5.3.1.1 Runoff

Two major runoff events were observed and runoff data were collected. These rainfall events occurred on 22 and 28 December 1996 having total rainfalls of 15 mm and 14 mm respectively. Runoff volumes on both events exceeded 0.21 m^3 over an area of 176 m^2, which equates to only 1.193 mm over the area. Exact volumes were therefore unable to be determined since the container into which the runoff was routed, proved to be too small, attributable to poor planning. During both rainfall events the container overflowed, with the subsequent loss of water.

5.3.1.2 Soil and Groundwater

Figure 43 presents data collected manually for the period 15 December 1996 to 18 January 1997. These data include matric head potentials (MHP) of the soil at varying depths, soil moisture status for each soil horizon (*cf.* Section 4.3.1.1) and the water table heights. As a reminder, the abbreviations GW1 to GW4 refer to the water table heights at the piezometer tubes near Pits 1 to 4. Similarly, Nest1 to Nest4 refers to the tensiometer nests and NP1 to NP4 to the neutron probe access tubes near Pits 1 to 4 (*cf.* Figure 21).

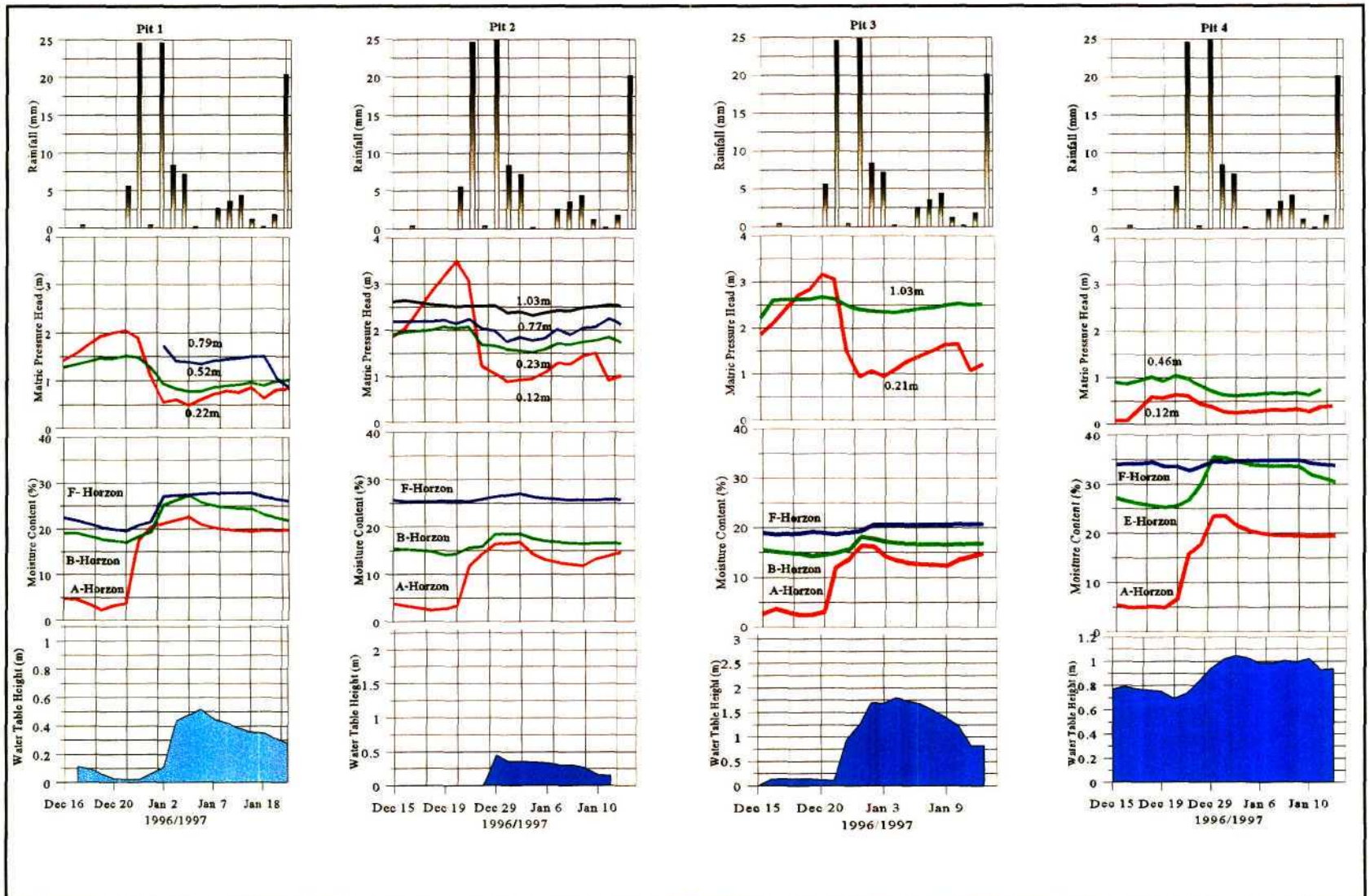

Figure 43. Results from data collected manually from each of the 4 pits along Transect 1. Results include, (from the top) daily rainfall totals, matric head potential of the soil with depths from which readings have been taken, neutron moisture meter data for each horizon and water table heights.

The MHP of the soil refers to the tensions within the soil. A larger value compared with a smaller value indicate higher tensions within the soil, implying a drier soil in comparison to a soil with a lower matric potential. In this instance water will tend to move in the direction of the higher matric potential (drier soil) and in response to gravity. On the other hand, the moisture content data shows the water content (per cent by volume) to have a low value, representing a dry soil. The response of soil moisture and hydraulic head data should therefore be a mirror image of one another at any point within a soil profile.

Furthermore the observed soil moisture data obtained at a depth close to the water table may follow the same trend as the phreatic surface of the groundwater volume due to the capillary fringe. These trends are clearly demonstrated for Nests 1 and 3, where the MHP at a depth of 0.22 m and 0.21 m, respectively, correspond with the soil moisture within the A-horizon. These soil moisture contents increase rapidly in response to two rainfall events on the 21 and 22 December (when 24.6 mm and 15 mm fell). The soil moisture content continues to increase with a further rainfall amount of 8.8 mm on 23 December. Within deeper horizons, the redistribution response to rainfall is not as pronounced as within the A-horizon, as shown by the MHP and moisture content data. An anomaly is evident at Nest 4. Data recorded at 0.46m shows the soil to be drier than the soil above at 0.12 m. This is unusual since the water table is present at this depth and saturated conditions should be reflected. A reason for this anomaly could be explained by the localised differences in the soils and the fact that Nest 4 is 2 m away from the piezometer tube (NP4).

Three observations with respect to the water tables are immediately apparent:

a. first, disregarding GW 1, water table heights increase downslope, reaching a maximum in the toe region (Pit 4);
b. secondly, GW 4 shows a water table throughout the six-week period (in fact, the water table has been present since the beginning of 1996) compared with the water tables at GW 2 and 3, which have been predominantly very low. These water tables at GW 2 and 3 responded only to rainfall on the 15 December 1996 at GW 3 and later in the same month at GW 2 and,

c. thirdly, GW 1 and GW 4 seem to behave in a similar fashion regarding soil water tensions, which are generally lower than in the midslope. This suggests predominantly wetter soils at GW 1 and GW 4. A reason for this is that there is possibly a high capillary fringe because of high groundwater tables. Both water tables respond in a similar way due to a water build up in the toe region at each location. On the hillslope crest, bedrock outcrops just downslope of Pit 1, with the soil depth decreasing as the outcrop is approached. Water moving downslope causes a water build up, behaving in a similar fashion to the toe of the hillslope.

The water table responses are different at each of the four locations. Pit 4 responds immediately to rainfall since the water table is very close to the soil surface and push through (interflow) from upslope probably occurs. Rainwater thus does not have far to travel to replenish the groundwater store compared with the other piezometer tubes, where the soils are deeper and the water table heights are not as high as that in GW 4. Water table responses within the midslope occur between one and 10 days after large rainfall events. These response times increase down the slope, indicating possible subsurface flow, with water moving along the bedrock and soil interface downslope. During periods of no rainfall, GW1, 2 and 3 show a water table drop while GW4's water table height increases. This can be explained by possible preferential flow and subsurface flow that continues after the rainfall event, with water replenishing this water store from upslope. Towards the end of December 1996 exfiltration was observed in the toe region where the water table intersected the soil surface, producing waterlogged and saturated conditions with subsequent exfiltration of water (*cf.* Figure 40).

5.3.2 Automatically and Manually Monitored Results

The automatic monitoring of six tensiometer nests commenced in February 1997. Data from each of the six nests have been error checked. The predominant breakdown in tensiometry measurements was related to cracked ceramics or air entry into the tensiometer in the connections of the pressure transducer. These incorrect data have been disregarded and are reflected as discontinuous gaps in the data sets. Tensiometer data from each nest next to Pits 1 to 4 are demonstrated for the period February 1997 to April 1997, when intensive

monitoring took place. During the same time period soil moisture and water table measurements were continued. These data sets are analysed and interpreted together to gain a better understanding of the hillslope subsurface processes which occur at Weatherly. These data records are discussed below in Section 5.3.2.1.

5.3.2.1 Tensiometer and Groundwater Monitoring

Tensiometer data sets with daily rainfall totals are presented as Figures 44 to 47 for Pits 1 through 4 respectively. At each tensiometer nest, data are recorded from four tensiometers which reside at various depths within the soil (*cf.* Appendix D). At Nest 3 there are data only for one soil depth because the other tensiometers gave problems and no usable data were collected.

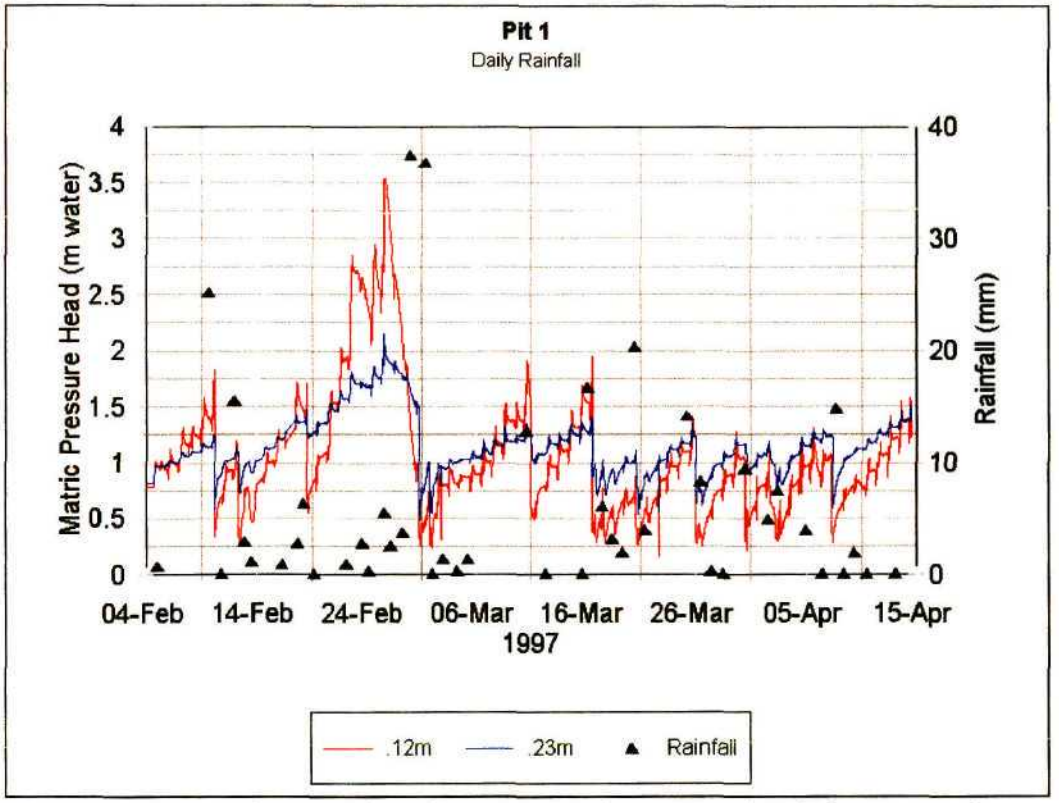

Figure 44. Tensiometer data shown as matric pressure heads for Nest 1, from 4 April 1997 to 15 April 1997.

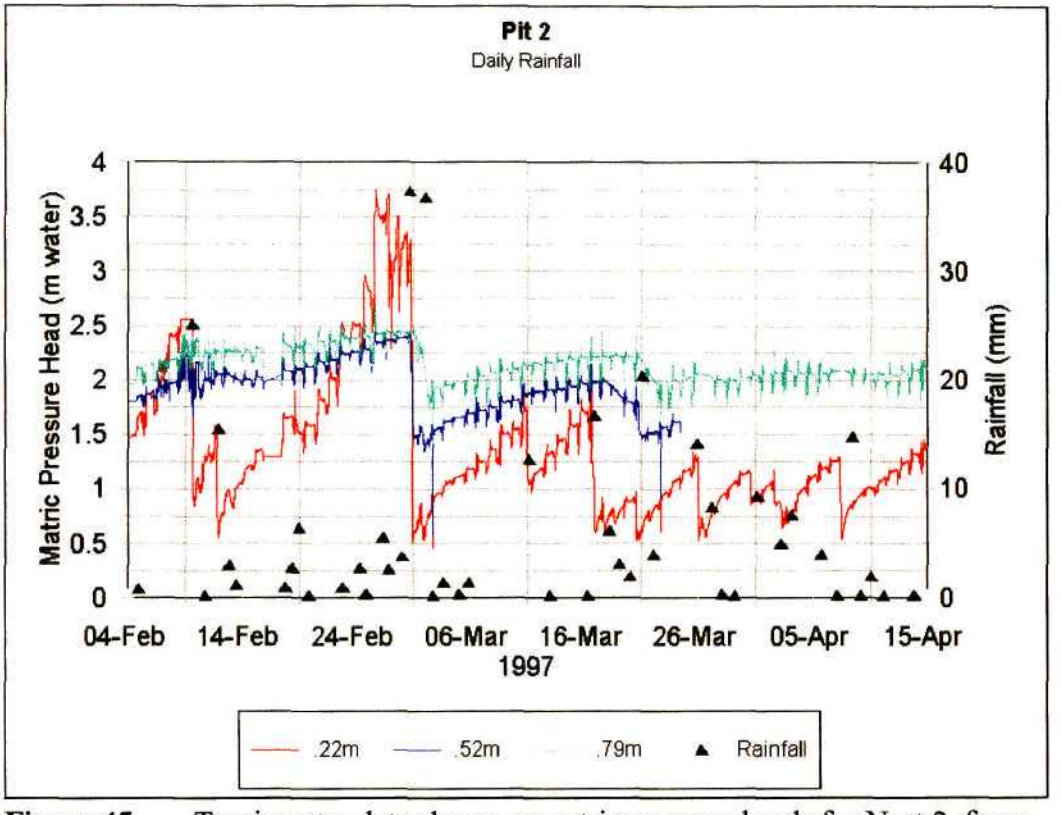

Figure 45. Tensiometer data shown as matric pressure heads for Nest 2, from 4 April 1997 to 15 April 1997.

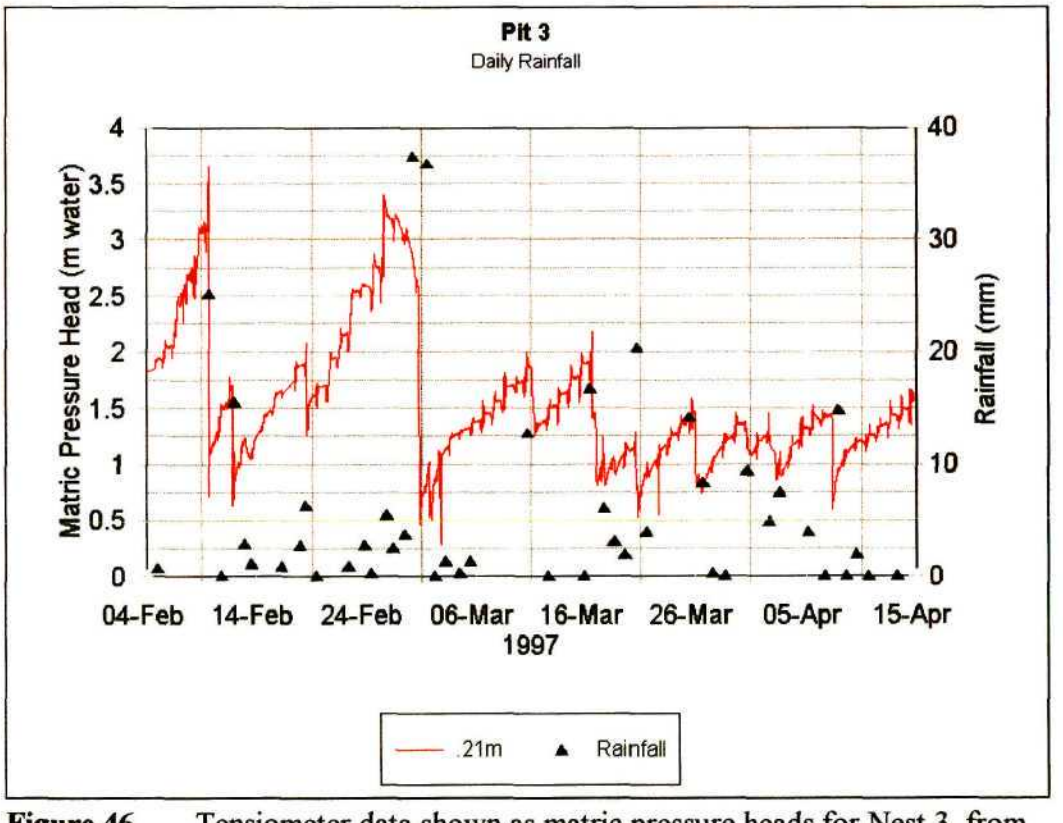

Figure 46. Tensiometer data shown as matric pressure heads for Nest 3, from 4 April 1997 to 15 April 1997.

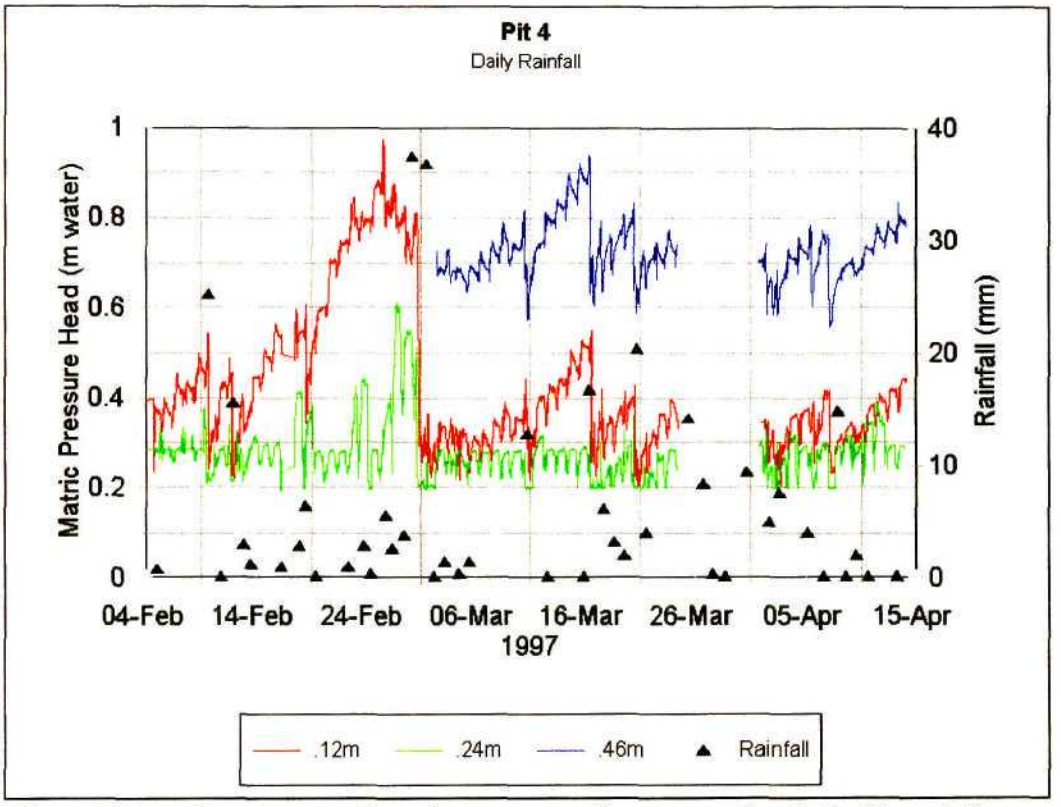

Figure 47. Tensiometer data shown as matric pressure heads for Nest 4, from 4 April 1997 to 15 April 1997.

Distinct differences are evident between tensiometer data sets as shown in Figures 44 to 47. These are the MHP ranges of the soil within the first 0.2 m of the soil profile. Prior to 26 February 1997, there was little rainfall. During this time the MHP of the soil exceeds 3 m at Nests 1 to 3 and at Nest 4 the MHP of the soil is less than 1 m. Between 3 of March 1997 and 15 of April 1997 rainfall exceeded 130 mm, resulting in a very wet hillslope transect, as reflected in the data. During this time the MHP of the soil decreases as the soil becomes wetter. In explaining these MHP ranges, the water table heights at each location along Transect 1 need to be considered.

The total groundwater records for GW 1 to GW 4 are shown in Figures 48 to 51 respectively.

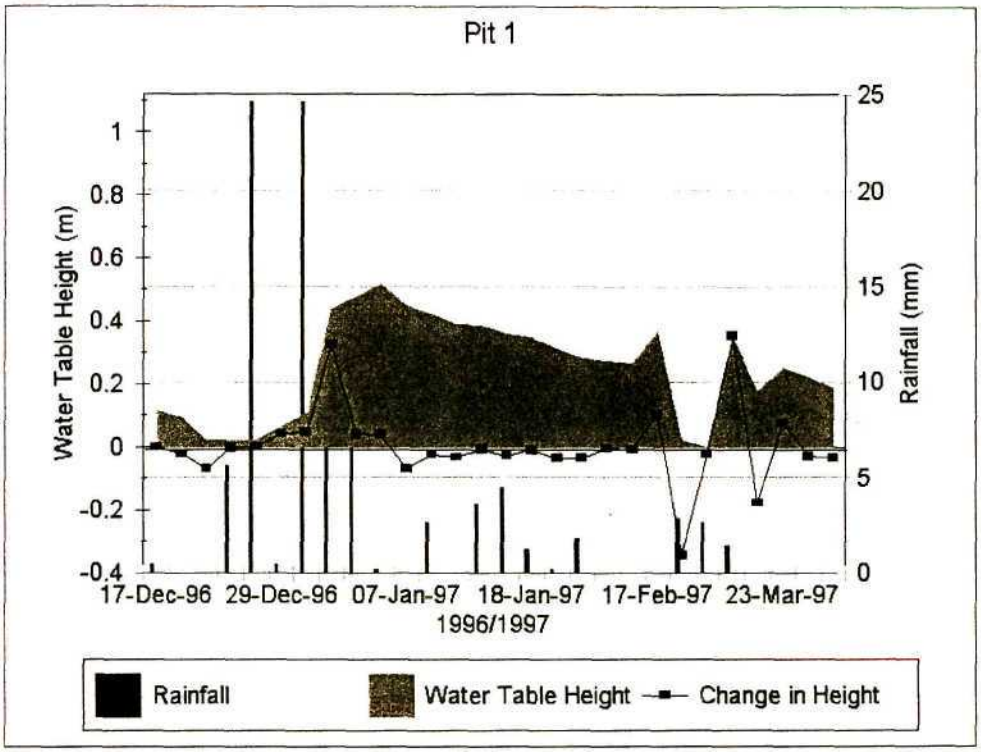

Figure 48. Groundwater heights at GW 1, from 16 December 1996 to 23 March 1997.

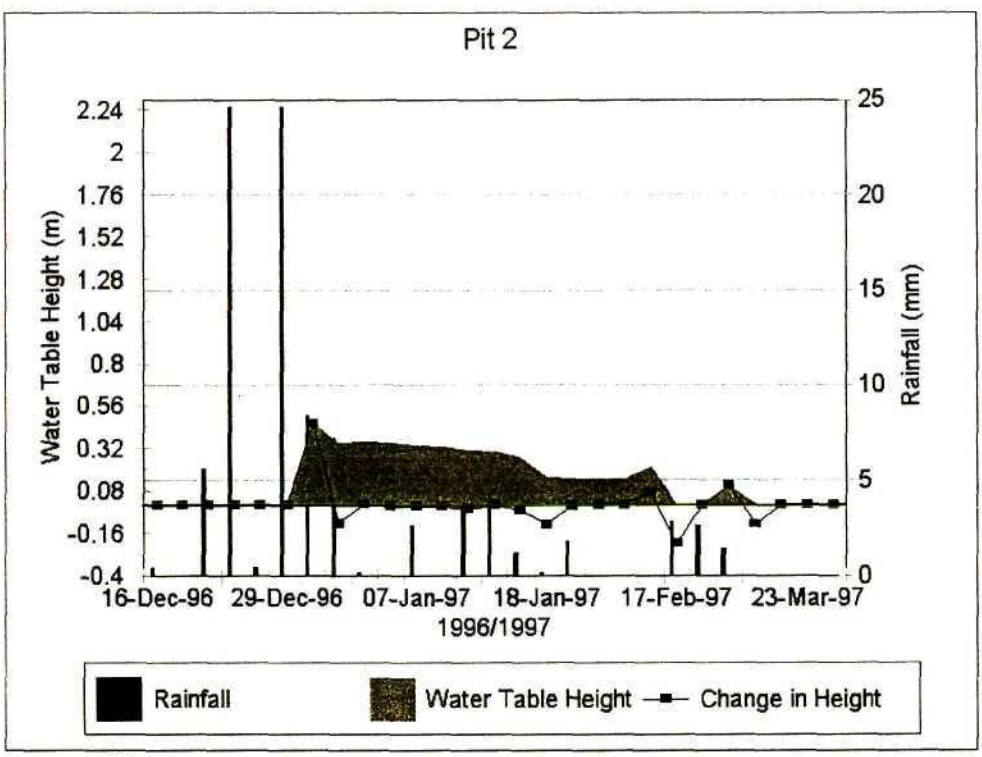

Figure 49. Groundwater heights at GW 2, from 16 December 1996 to 23 March 1997.

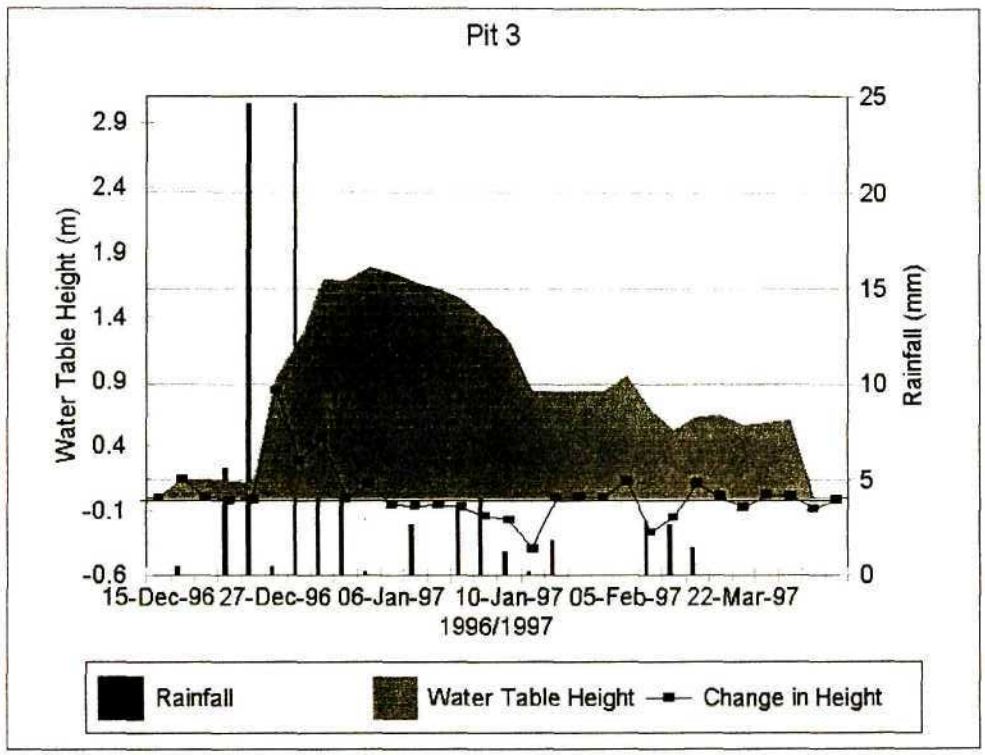

Figure 50. Groundwater heights at GW 3, from 16 December 1996 to 23 March 1997.

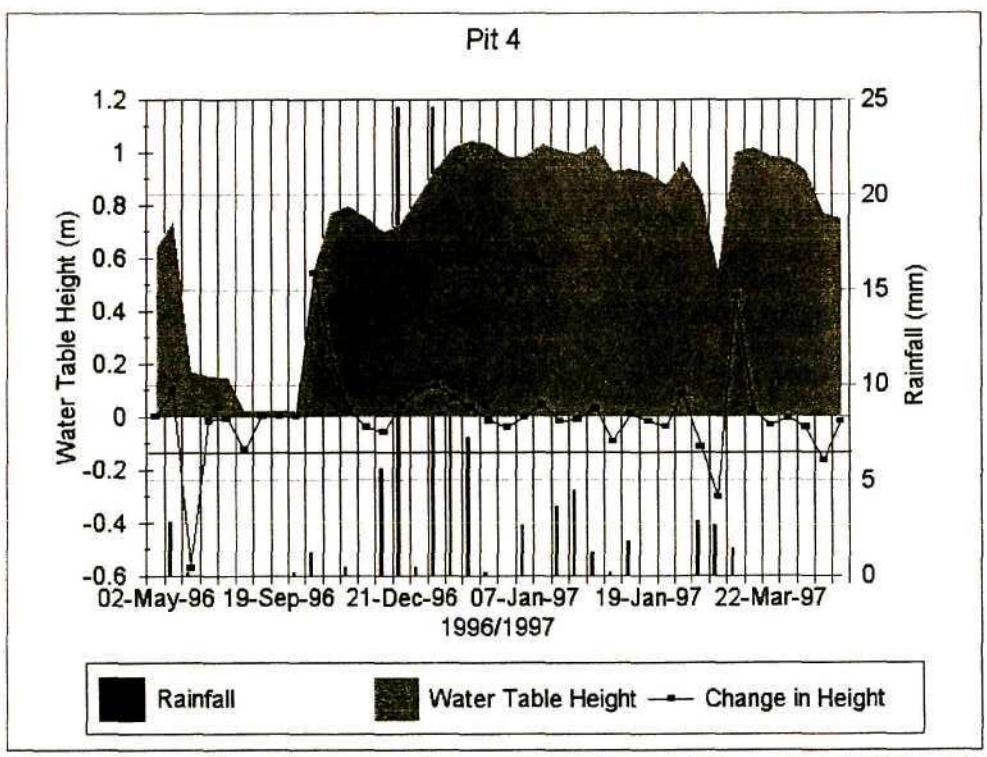

Figure 51. Groundwater heights at GW 4, from 16 December 1996 to 23 March 1997.

These data show the groundwater heights above the bedrock, rainfall totals and the change in water table heights between measurements. Values which are negative show that the water table has decreased since the previous measurement was taken. On each figure the actual soil depth is reflected by the maximum value on the Y axis. Plotting the data in this way allows direct comparison of data from the four piezometer tubes at transect locations along Transect 1.

A water table has been present since the beginning of monitoring at GW 4 (Figure 51). During the latter part of December 1996, water tables developed at the other locations on Transect 1, as shown in Figures 48, 49 and 50. Disregarding GW 1 (Figure 48), water table heights tend to increase down Transect 1. For example, on 5 January 1997 the water table heights are 0.36m, 1.791m and 1.030m at GW 2, 3 and 4 shown in Figures 49, 50 and 51 respectively. At GW 4 the depth is 1.30 m, which is less than the water table height at GW 3, but then the soil at Pit 4 is so much shallower (*cf.* Appendix A).

During periods of low rainfall each water table along Transect 1 deceases at different rates. The water table at GW 2 (Figure 49) decreases to zero at a rate that is greater than that at Pit 3 (Figure 50). At GW4 the water table (Figure 51) does not drop substantially in comparison to the other locations on the hillslope and varies between 1.02 m and 0.70 m throughout the measured period. These data indicate possible subsurface flows where water from upslope feeds the water body at GW 4, increasing the water table height here, with the subsequent decreases in water table heights upslope.

In terms of rainfall, Figures 48 to 51 show that the water tables at each location along Transect 1 respond differently. The water table response to rainfall increases down the hillslope transect. This can be explained not only by interflow downslope, but also by the depths to the water tables. Furthermore, these increased water table heights are related to the MHP of the soils as shown in Figures 44 to 47. These MHP differences, approximate water table depths below the soil surface and water table heights above the bedrock are tabulated in Table 13 for a dry and wet period, *viz* 26 February and 3 March 1997 respectively. Using MHP and depth to water table data, it is assumed that the wetter the soil, the quicker the water table response is to rainfall.

Table 13. Monitored differences in MHP of the soil at different soil depths at each tensiometer nest over a dry and wet period, depths to water table (DW) and water table height (WTH).

		Dry period (26 February 1997)			Wet period (3 March 1997)		
Pit/Nest	**Depth (m)**	**MHP (m)**	**DW (m)**	**WH (m)**	**MHP (m)**	**DW (m)**	**WH (m)**
1	0.12 0.23	3.50 2.20	-	0	0.25 0.50	0.76	0.36
2	0.22 0.52 0.79	3.75 2.40 2.55	-	0	0.50 1.50 2.50	2.19	0.11
3	0.21	3.40	2.57	0.53	0.50	2.47	0.63
4	0.12 0.24 0.46	0.98 0.35 -	0.64	0.55	0.19 0.19 0.27	0.19	1.02

The surface soils close to Pit 2 have a lower MHP than these soils at deeper depths. This is attributable to the fact that these soils near the soil surface are sandy, wetting up relatively quickly in comparison to the deeper soils which have a higher clay content. The lowest the MHP reaches is 0.5 m and 0.25 m at Nests 2 and 3 respectively and 0.19 m for Nests 1 and 4. It should be noted that a MHP value of 0.19 represents saturated conditions. These MHPs of the soil tend to decrease down the soil profile at all Nests, showing a wetter soil on average.

For a dry period around 26 February 1997 little rain fell, which is reflected in the data shown in Table 12. There is no evidence of a water table at GW 2 and 3 and the soils at these locations have MHPs ranging between 2.4 m and 3.75 m respectively. At GW 3 a water table is present 2.57 m below the soil surface. Unfortunately no usable tensiometer data were available at soil depths greater than 0.12 m. MHP data at Nest 4 differ in comparison with those at the other Nests on Transect 1. These values at Nest 4 range from 0.98 m to 0.35 m at a depth of 0.24 m. A water table is present just 0.64 m below the soils surface at GW4. Under these circumstances the soil is very wet, as shown by the low MHP

data (Figure 47) compared to the MPHs at the other pits. Between 26 February and 3 March 1997, a period of seven days, rainfall totalled 86 mm. During this period water tables were seen to develop at GW 1 and 2 reaching heights of 0.36 m and 0.11 m respectively. At GW 3 and 4 the water table heights increased by 0.105 m and 0.475 m respectively. The MHP data for the same period decreased in response to infiltrating water, as shown in Table 13.

These data support two arguments:

a. first, the closer the water table to the soil surface, the wetter the soil will be, as indicated by low MHP and

b. secondly, water tables respond quicker when close to the soil surface as a result of infiltration and push through (interflow) from upslope.

Another factor which influences the rate at which the soil increases in wetness followed by a subsequent change in water table height, is the intensity of the rainfall. This is shown in Figures 52 and 53.

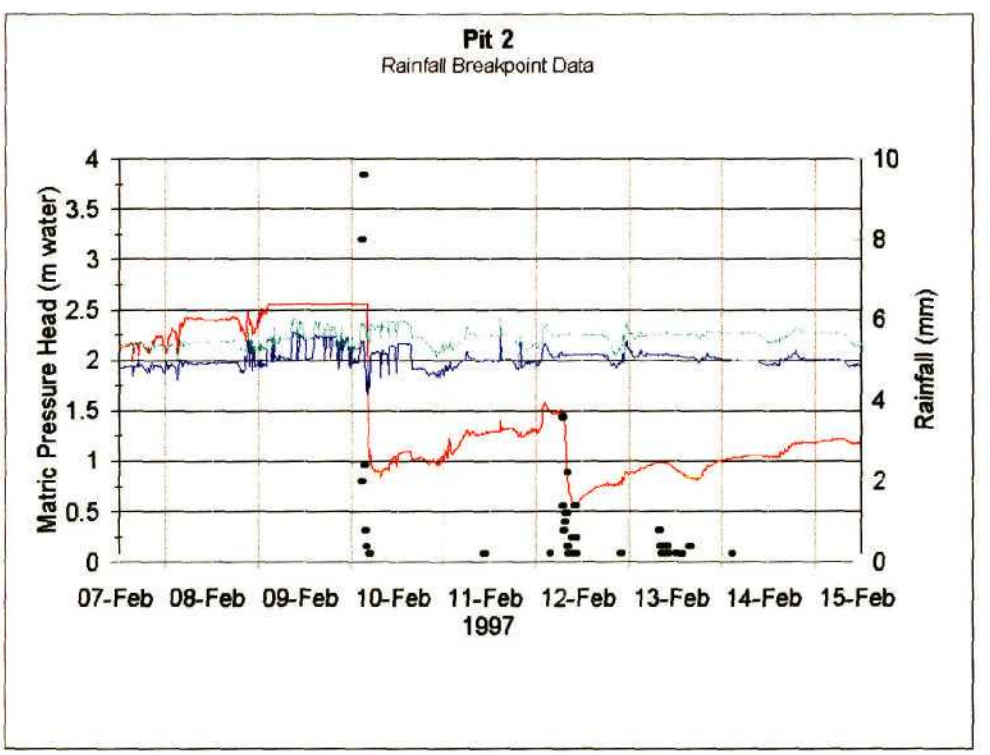

Figure 52. Tensiometer data taken during a high rainfall intensity event at Nest 2.

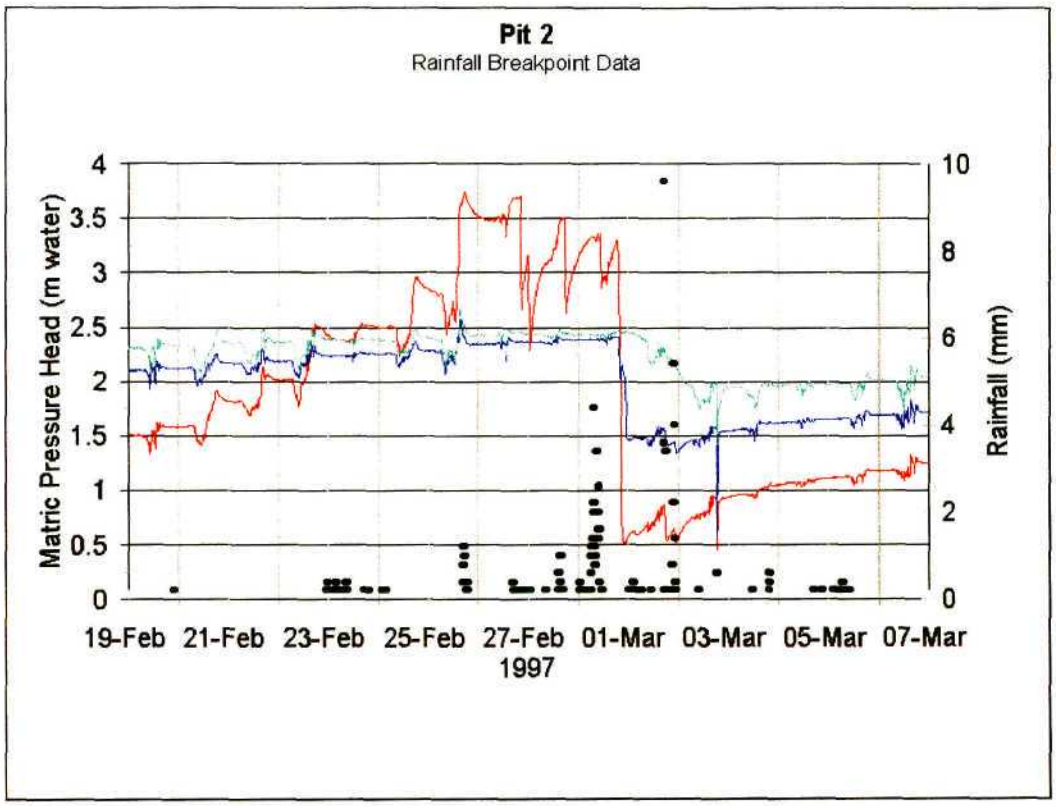

Figure 53. Tensiometer data taken during a low rainfall intensity event at Nest 2.

These figures show tensiometer data for Nest 2, during a high and low intensity rainfall event respectively. These figures are subsets of Figure 45, which are taken at a smaller time scale and show rainfall breakpoint data. The remainder of these data for the other nests are presented in Appendix H.

A high intensity rainfall event occurred on 10 February 1997 when 30 mm fell over a period of one hour (Figure 52). A large amount of runoff was observed from the runoff plot. At Nest 2 (Figure 52) the response to infiltrating water at a depth of 0.22 m was relatively rapid, with a decrease in MHP from 2.5m to less than 1m. The deeper soil horizons show a very small change in the MHP. These trends are consistent with those of the other data sets along Transect 1. These data therefore show that for a high intensity rainfall event little water infiltrates as shown by small changes in the MHP and water table heights.

By contrast, a low intensity long duration rainfall event occurred on 28 February 1997 when 38 mm fell over a period of 24 hours. No runoff was observed. Changes in MHP show

a slow response initially, with the soil wetting up approximately 10 hours later (Figure 53). At a soil depth of 0.22 m the MHP decreases from 3.25 m to 0.4 m. After a couple more hours at a soil depth of 0.52 m these MHPs decrease from 2.45 m to 1.25 m with the soil wetting up, but remaining relatively drier than the soil horizons above. Furthermore, at a soil depth of 0.79 m the MHP response to infiltrating water is lagged by a few days to 1.75 m. These tensiometer data show that the soil horizons before rainfall are relatively dry. As the soil horizons approach saturation, a wetting front moves down the profile, increasing the soil water content. During this low intensity event the water table heights at GW 2 and 3 increased in height by a small amount, possibly because of very deep soils on the midslope. Infiltrating water therefore needs to travel further to replenish the groundwater. At GW 1 and 4 the water tables increased significantly from 0-0.36 m and 0.45-1.0 m respectively. These large increases are attributable to the shallow soil depths and the initially high water tables (GW 4) before the commencement of the rainfall.

From these interpretations it is clear that a continuous record of tensiometer and water table data together, provide invaluable information pertaining to infiltration, redistribution and soil water fluxes on a hillslope. Using these data sets a great deal of insight into processes occurring at this hillslope scale can be gained. Other data can be used to infer these processes, but without the same degree of accuracy. The soil moisture contents have been monitored at four locations along Transect 1. These data are analysed in Section 5.3.2.2 below.

5.3.2.2 Soil Moisture Data

Other commonly used data to infer the soil moisture status of the soil is NMM data. The problem associated with such data is that they do not provide a continuous data record, nor do they give an indication of hydraulic gradients. These hydraulic gradients are very useful for the calculation of soil water fluxes, which can be calculated from the tensiometer data. Figures 54 to 57 show the total soil moisture and rainfall records for NP 1 through 4. These data are shown for the A, B and F-horizons for Pits 1 to 3 and the A, E and F-horizons for Pit 4 as described by the ISCW (*cf.* Section 4.3.1.1). Using the NMM , data are taken at 0.1

m intervals to a depth of 0.6 m and thereafter every 0.2 m to the base of the soil profile. These data were then averaged accordingly for the A, B, E and F-horizons.

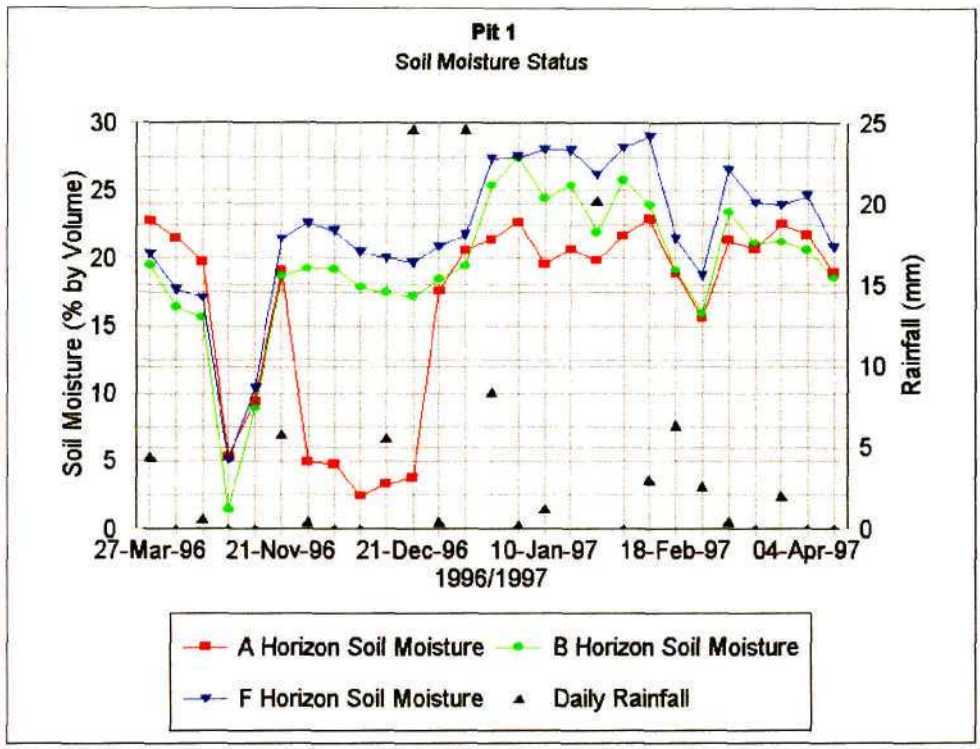

Figure 54. Soil moisture record for NP 1 from 27 March 1996 to 4 April 1997.

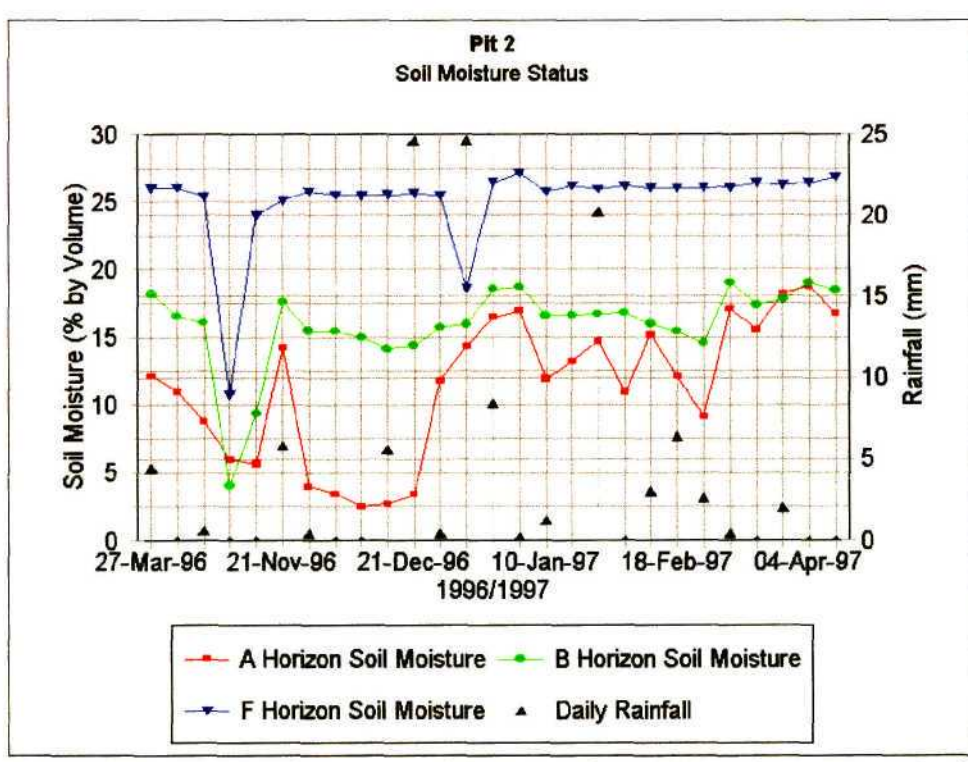

Figure 55. Soil moisture record for NP 2 from 27 March 1996 to 4 April 1997.

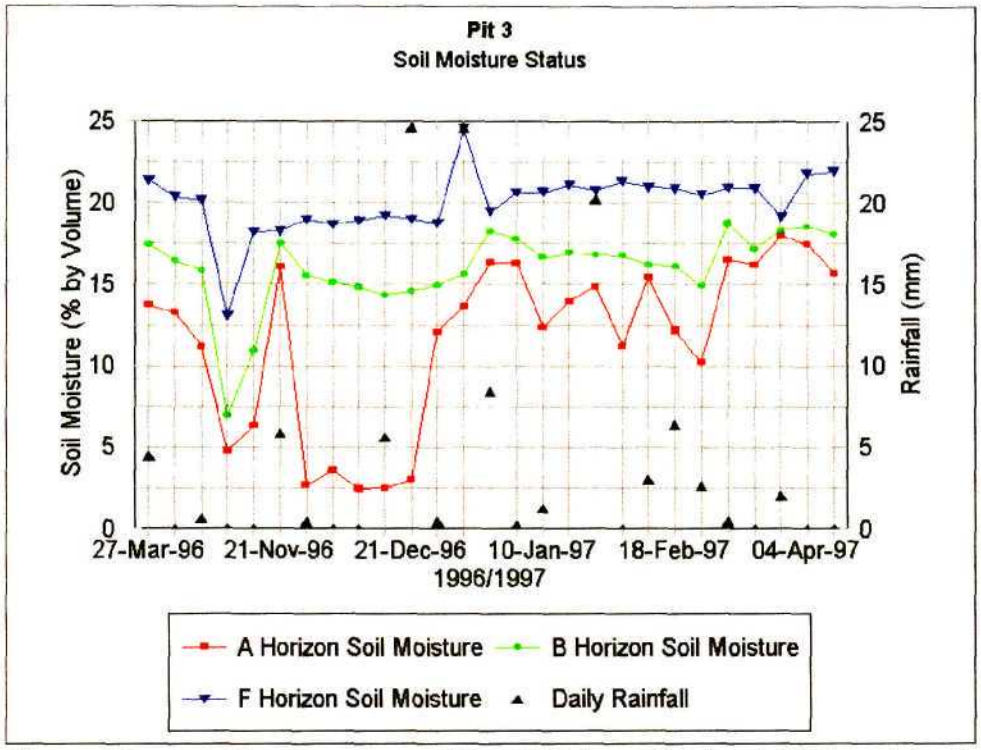

Figure 56. Soil moisture record for NP 3 from 27 March 1996 to 4 April 1997.

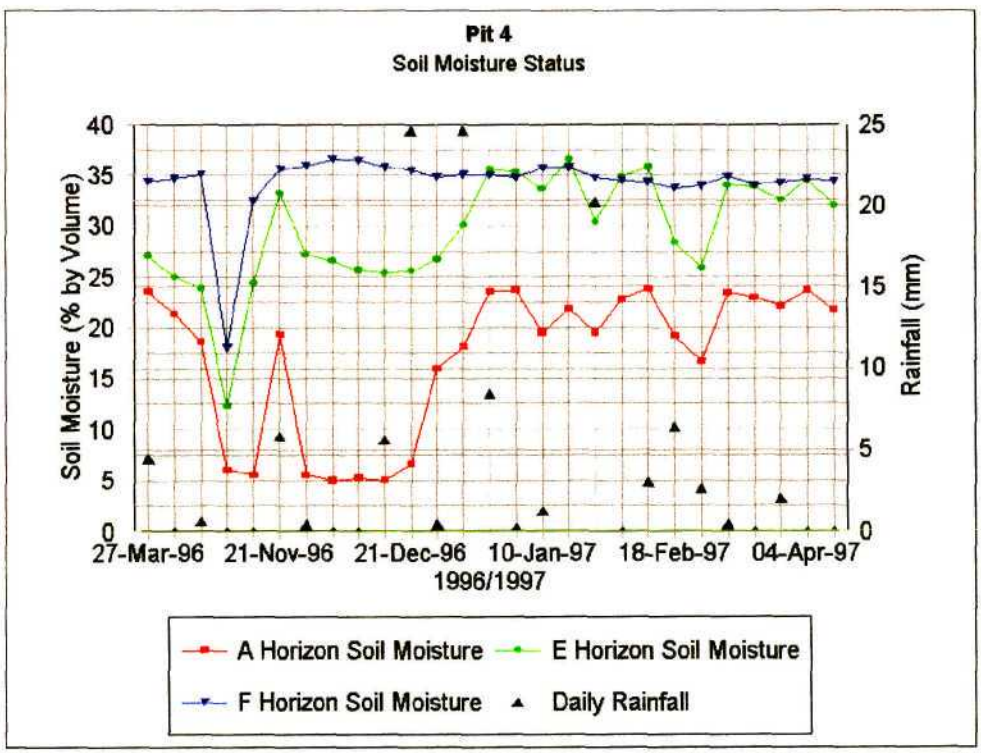

Figure 57. Soil moisture record for NP 4 from 27 March 1996 to 4 April 1997.

These soil moisture data show an opposite trend or mirror image of the tensiometer data, as shown in Figure 44 to 47 (*cf.* Section 5.3.1.2). For example, a high soil moisture content will be reflected by a lower MHP, indicating a wet soil and vice versa.

Four days, *viz.* 28 June 1996, 19 December 1996, 26 February 1997 and 3 March 1997 have been selected where the measured soil moisture is either very high or low (Figures 54 to 57). For each of these selected days, the soil moisture at each horizon is tabulated in Table 14. These data are compared and interpreted in conjunction with Figures 54 to 57.

Table 14. Comparison of soil moisture data (percentage by volume) for selected days at each soil horizon along Transect 1.

Pit	Horizon	28 June 1996	19 December 1996	26 February 1997	3 March 1997
		Soil Moisture Content (% by volume)			
1	A	5.3	2.4	17.6	21.3
	B	1.4	17.9	18.4	23.4
	F	5.1	20.4	20.8	26.6
2	A	5.9	2.5	9.1	17.1
	B	4.0	14.9	14.5	19.0
	F	12.2	24.7	25.6	24.9
3	A	4.8	2.4	10.2	16.5
	B	6.9	14.8	14.9	17.2
	F	14	19.5	21.0	21.2
4	A	6.0	5.2	16.6	23.6
	E	12.3	25.6	25.8	34.5
	F	18.0	36.4	33.9	35.0

At each of the four pits the soil moisture content is seen to increase down the soil profile except at NP 4, where in January 1997 the E-horizon is wetter than the F-horizon (Figure 57). There is a definite transition within horizons at each pit throughout the year, with soil moisture contents increasing in the period between the winter and summer months. On 21 December 1996 a rainfall event of 24.6 mm caused the water contents to increase radically at all locations of Transect 1, especially in the A-horizon and to a lesser extent in the B-horizons. The moisture contents in the E and F-horizons remain relatively constant

throughout the year. Soil moisture data from 26 February and 3 March 1997 (Table 14) corresponds with the tensiometer data on the same days (Table 13), with lower soil moisture contents and higher MHP for the drier period and the reverse being true for the wetter period.

To attaint a greater understanding of how the soil moisture content varies within each horizon within Transect 1 it is important to compare soil moisture data for each horizon at each location on the hillslope. These comparisons are shown in Figures 58 to 60 for the A, B and F-horizons for each of the four pits.

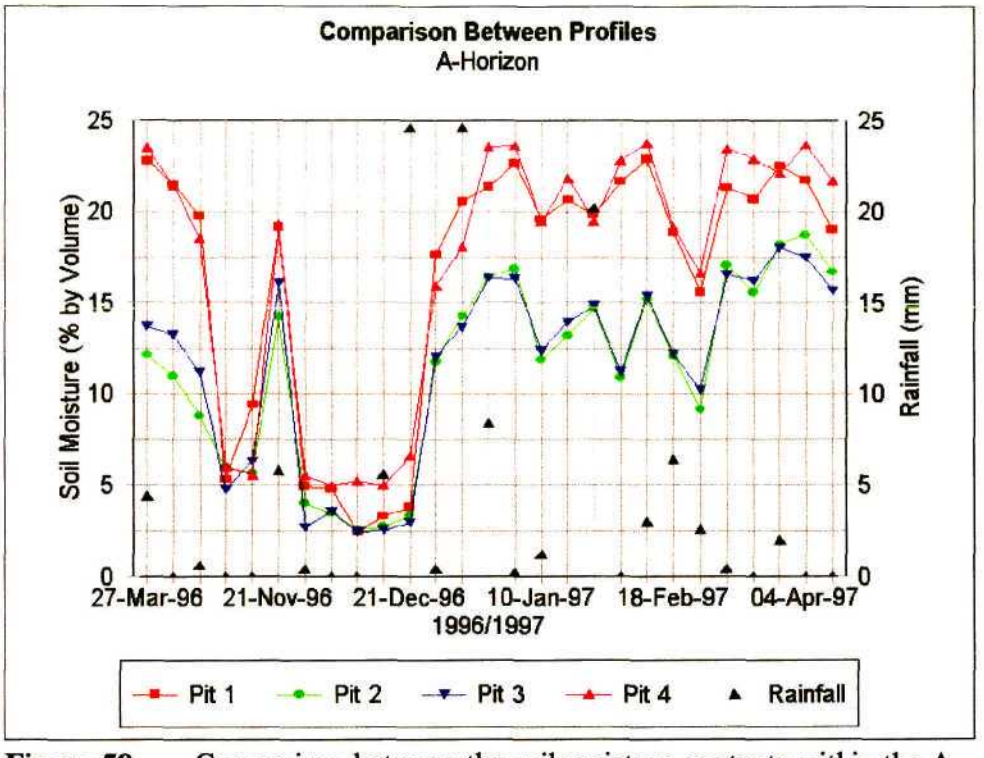

Figure 58. Comparison between the soil moisture contents within the A-horizon at each pit.

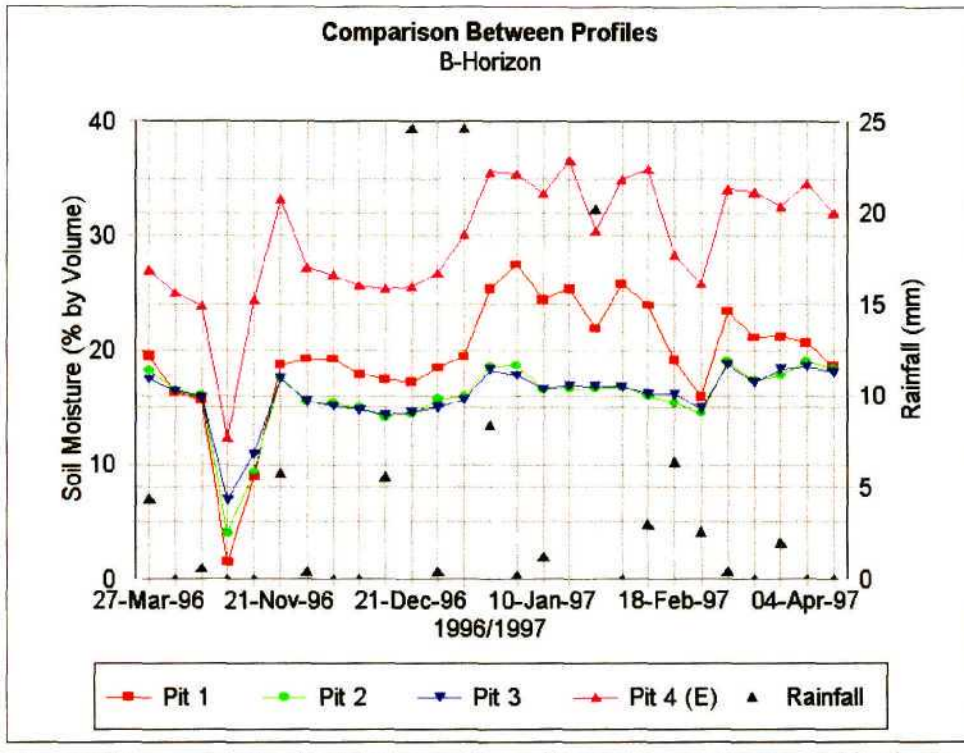

Figure 59. Comparison between the soil moisture contents within the B-horizon at each pit.

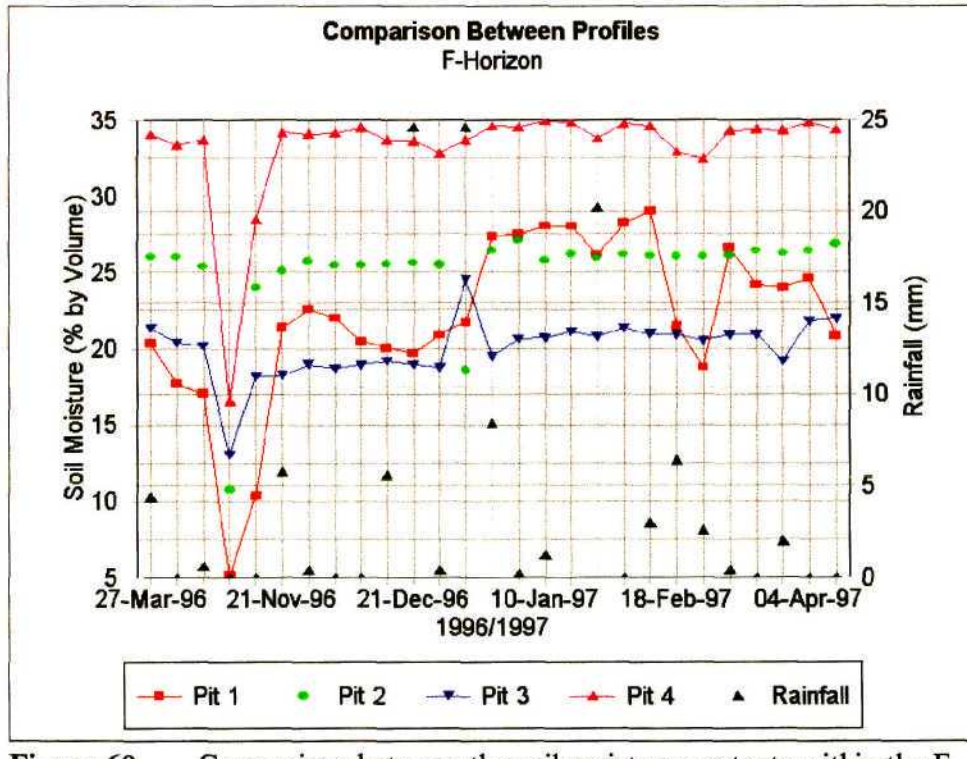

Figure 60. Comparison between the soil moisture contents within the F-horizon at each pit.

During the winter months (*cf.* Table 14, June 1996) the soil moisture within each horizon at each pit is not significantly different, except for the F-horizon at Pit 4, which has a soil moisture content that is greater than that at the other pits.

Between February and March 1997 the soil moisture contents of the A-horizon (Figure 58) at NP 1 and 4 are very similar and differ from those at NP 2 and 3, which have lower soil moisture contents due to the well drained soils at these locations. Within the B-horizons (Figure 59) the moisture contents at NP 2 and 3 are very similar. NP 4 has relatively higher soil moisture contents which also exceed the soil moisture content at NP 1 at the same depth. This is possibly because of the higher water tables found here. This trend is evident in the F-horizon, as shown in Figure 60, except that the soil moisture contents at NP 2 and 3 differ. These soil moisture data therefore show that on average the moisture content increases down the profile and transect. An important point to consider is that, since these soil moisture data are collected weekly, diurnal wetting and drying cycles within the soil are often missed.

5.4 An Overview of Physical and Hydraulic Properties and Monitored Results

The PSD data show that the percentage sand decreases both down the soil profiles and down the transect, with the inverse being true for the percentage clay. The ρ_b indicate the presence of macropores both on the crest and toe of the hillslope. This is verified by field observations. The K of the soils decrease with depth within the soil horizons. There are, however, conductivity variations within certain soil profiles also reflected in the PSD data. This may be a result of either sandy or clayey lenses that are present within the soil profiles. Using linear regression techniques it was found that a reasonably strong relationship exists between the K_s and the soil depth and clay content within each profile. The WRC data verify conclusions drawn from the PSD data and K of the soil, especially when considering the proliferation of macropores in this region.

With respect to actual monitored data, the soil moisture within the soil profiles show a large variation between NP 1 and 4 in comparison to the soil moisture in the Pits on the midslope.

Reasons for this are that the midslope locations have deep and well-drained soils in comparison to the soils found at the crest and toe of the hillslope. Pits 1 and 4 may be hydrologically similar with much water accumulating in the summer months. Groundwater data show a similar trend in terms of water accumulation, with the crest (Pit 1) and toe regions (Pit 4) exhibiting large water tables. The remainder of the data show the water tables to be localised. The tensiometer data help determine the water fluxes within the soil profile giving also an indication of the redistribution of water during and after a rainfall event. These MHP and groundwater data show that water infiltrates vertically down the soil profile, which upon reaching the bedrock, forms perched water tables. These perched water tables induce soil water fluxes in response to hydraulic gradients with water moving laterally along the bedrock downslope as interflow.

Results from the infiltration and redistribution test (*cf.* Section 4.4.6.2) confirm these observations. Data showed that at the onset of ponding, water infiltrates moving vertically until the bedrock below is reached. From there it appears to move laterally downslope as subsurface flow. Once the test was abandoned, the tensiometer data showed the soil profile to dry considerably with a receding of the wetting front.

Although no direct measurements were performed to study macropore flow, a fluorecent dye was used to isolate preferential flow pathways (*cf.* Section 4.4.6.1). After water had been ponded for 20 hours the soil adjacent to the ponded area was cut carefully and illuminated with UV light at night and photographed (Figure 61). The result was not as expected as the dye did not show up all that well, probably because it was adsorbed by the significant clay fraction. Figure 61 shows an illuminated soil section at Pit 3, from which the various flow paths through the soil capillaries and macropores can be seen.

From all data sets discussed in Chapter 5 a clearer understanding and insight into hillslope hydrological processes has been achieved. Using MHP and NP data, infiltration and redistribution within the soils on Transect 1 were inferred. These data showed that the soil moisture contents increase both down the profile and the Transect. The rainfall intensity also plays a role, with low intensity rainfall allowing more effective infiltration, which in turn feeds the water tables.

Figure 61. Preferential flow pathways illuminated with a fluorescent dye at Pit 3.

Interpretation of these data sets, show that the dominant process which occurs along Transect 1 is the movement of soil water vertically with the subsequent formation of perched water bodies. Once these water bodies reach a critical height, interflow occurs, which feeds the water bodies downslope. An interpretation of the soils' data also seems to indicate possible macropore flow in the toe. These fluxes certainly contribute to the overall hillslope water budget.

* * *

In Chapter 5 results from the hillslope experiment along Transect 1 at Weatherly were analysed and interpreted. These data included tensiometer, groundwater and NMM data sets. These data allowed an in depth study of hillslope hydrological processes and results

showed that with much rainfall water infiltrates the soil feeding water tables. Upon reaching a critical height these water tables move downslope forming interflow. Each water table responds at different rates depending on the position on the hillslope.

Chapter 6 presents a simple water budget of the hillslope. This is an attempt at isolating the dominant surface and subsurface processes. Once these dominant processes have been identified in this way, a decision is made as to how to set up a numerical model. The HILL5D model has been selected to simulate these subsurface processes, especially interflow, at the hillslope scale. These simulated results are then compared with actual data collected in the field.

6. HILLSLOPE WATER BUDGET AND MODELLING

Hillslope hydrological models usually include:

a. input parameters which represent the physical characteristics of the hillslope;
b. inputs of rainfall and other meteorological data which, together with hydrological process algorithms allow calculation of,
c. surface and subsurface water fluxes, changes in storage within the vadose zone / water table and water losses from the system (Larson, Onstad, Richardson and Brooks 1982).

The third of the above points is the 'heart' of most catchment and hillslope models, which consist of a series of sub-models, each representing separate hydrological processes. Sub-model selection is an important criterion in model building, dependent on the modelling objective. The modelling objective of this research is to simulate the water fluxes within the saturated and unsaturated zones and the changes in storages within these zones, *viz.* the vadose and groundwater zones. HILL5D (*cf.* Section 3.5.3) satisfies these sub-model criteria, as this model includes the simulation of the perched water table within the saturated zone.

Before using such a model, a manual hillslope water budget needs to be performed to identify the dominant subsurface processes that occur within the given "system", which in this case is Transect 1. Such a water budget will allow the assessment of whether or not the mathematical model is suited to the system. Using input data from Transect 1 (*cf.* Section 4.4), water fluxes and storage changes within the vadose and saturated zones have been calculated for a short period consisting of a four days, *viz.* 20, 29 December 1996 and 2, 3 January 1997. First bedrock information was collected, a necessity for the calculation of hydraulic gradients.

6.1. Bedrock and Water Table Descriptions

Holes to bedrock depth were augured at selected locations along Transect 1, with the majority of holes being concentrated in the toe region around Pit 1. These depths to bedrock with the hillslope survey (*cf.* Section 4.3.1.3) allowed the calculation of the relative bedrock elevations above mean sea level. From these data, bedrock contours were delineated, as shown in Figure 62.

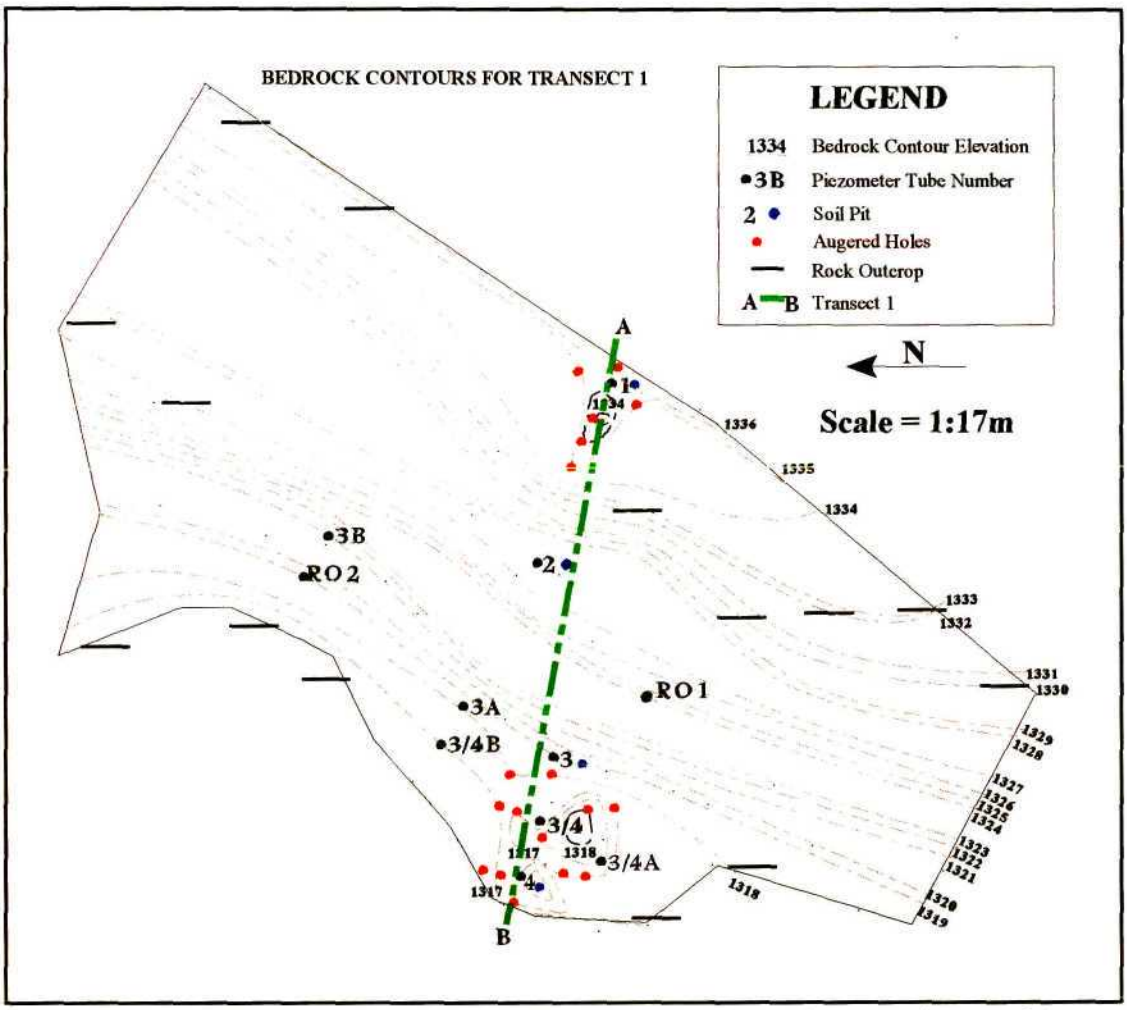

Figure 62. Bedrock contours (m) for Transect 1 showing relative positions of the pits, piezometer tubes and auger holes used in their determination.

Soils at the crest of the hillslope become shallower towards the rock outcrop at an elevation of 1332 m. This region behaves in a similar way to the toe region of Transect 1, which explains the high water tables found here in comparison to the water levels at the midslope,

around Pit 2. Therefore, the area from Pit 1 to Pit 2 has been excluded from the water budget calculations.

Bedrock elevations in the midslope vary considerably when compared with those at the toe region, where the bedrock is flatter. The bedrock elevations change by 18 m between the crest and toe of the hillslope over a horizontal distance of 200 m. A cross-section along Transect 1 (denoted by AB in Figure 62) is shown in Figure 63.

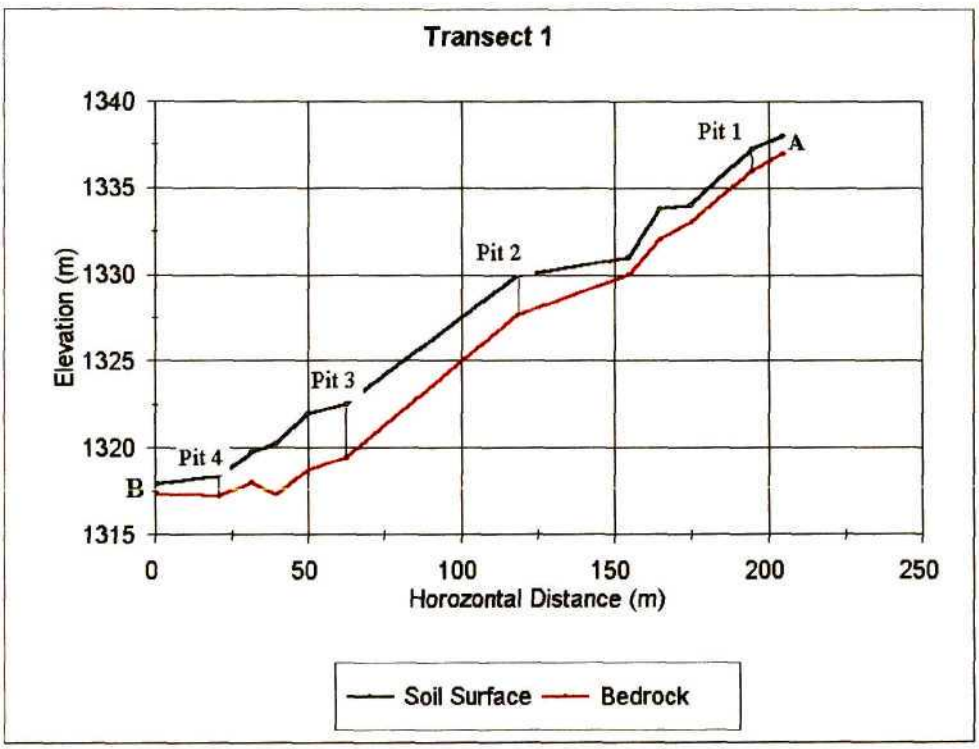

Figure 63. Cross section along Transect 1, showing the relative positions of Pit 1 to Pit 4.

Using the contoured map of the bedrock (Figure 62), water table elevations above bedrock were plotted and these were used to interpret soil water flow pathways, water fluxes and hydraulic gradients. Table 15 shows the bedrock elevations from which the contoured map was derived with water table heights measured for each of four selected days.

Table 15. Bedrock elevations (BR), WTH elevations above mean sea level and actual WTH at each piezometer tube for four different days.

Tube	Dates								
		20 Dec. 1996		29 Dec. 1996		2 Jan. 1997		3 Jan. 1997	
	BR Elevation (m)	W/TH (m)	WTH Elevation (m)	WTH (m)	WTH Elevation (m)	WTH (m)	WTH Elevation (m)	WTH (m)	WTH Elevation (m)
GW1	1336.00	0.02	1336.17	0.11	1336.26	0.44	1336.59	0.48	1336.63
GW2	1327.71	0.00	1327.71	0.00	1327.71	0.46	1328.17	0.36	1328.17
GW3	1319.40	0.13	1319.53	1.23	1320.63	1.70	1321.10	1.69	1321.09
GW3A	1318.81	0.09	1318.89	0.18	1318.99	1.20	1320.00	1.22	1320.02
GW3B	1321.63	0.00	1321.60	0.09	1321.69	0.16	1321.76	0.22	1321.82
GW3/4	1317.30	1.79	1319.09	2.00	1319.30	2.60	1319.90	2.62	1319.90
GW3/4A	1318.00	0.19	1318.19	0.45	1318.45	0.65	1318.65	0.71	1318.71
GW3/4B	1317.36	1.09	1318.69	1.10	1318.70	1.70	1319.30	1.74	1319.34
GW4	1317.20	0.70	1317.90	0.94	1318.14	1.02	1318.22	1.05	1318.25
RO1	1324.80	0.00	1324.80	0.00	1324.80	0.00	1324.80	0.00	1324.80
RO2	1319.20	0.19	1319.39	0.23	1319.43	0.79	1320.00	0.82	1320.02
Rainfall (mm)		5.6		24.6		8.4		7.0	

December 20, 1996 was selected as the starting point of the water budget as the catchment was relatively dry and water table heights were used as a standard from which to compare the rest of the data sets. Data from the remaining three days, *viz.* 29 December 1996, 2 and 3 January 1997, were used in water budget calculations. Table 15 shows also the water table elevation, which is the sum of the water table height and bedrock elevation at that point, and the amount of rainfall that fell for each day.

Using information from Figure 62, water table heights (WTH) for each day were plotted. Using visual interpolation based on the bedrock elevations and source and seep regions identified on Transect 1, WTH contours were inferred, as shown in Figures 64 to 67.

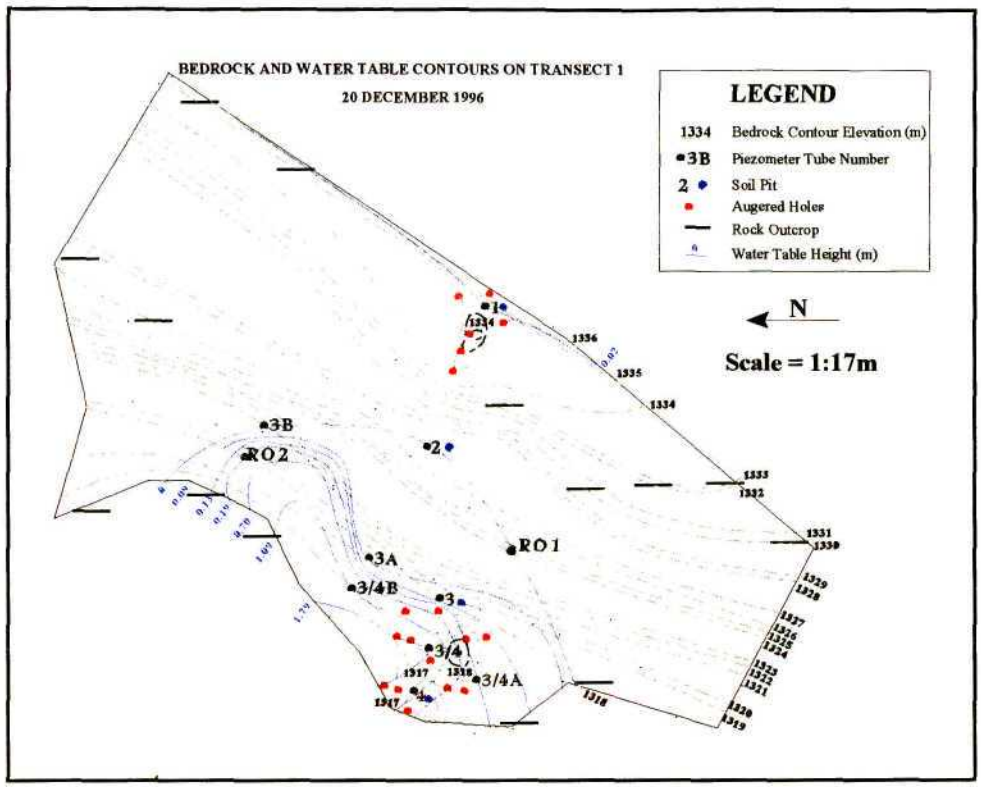

Figure 64. Bedrock elevations and water table heights for 20 December 1996.

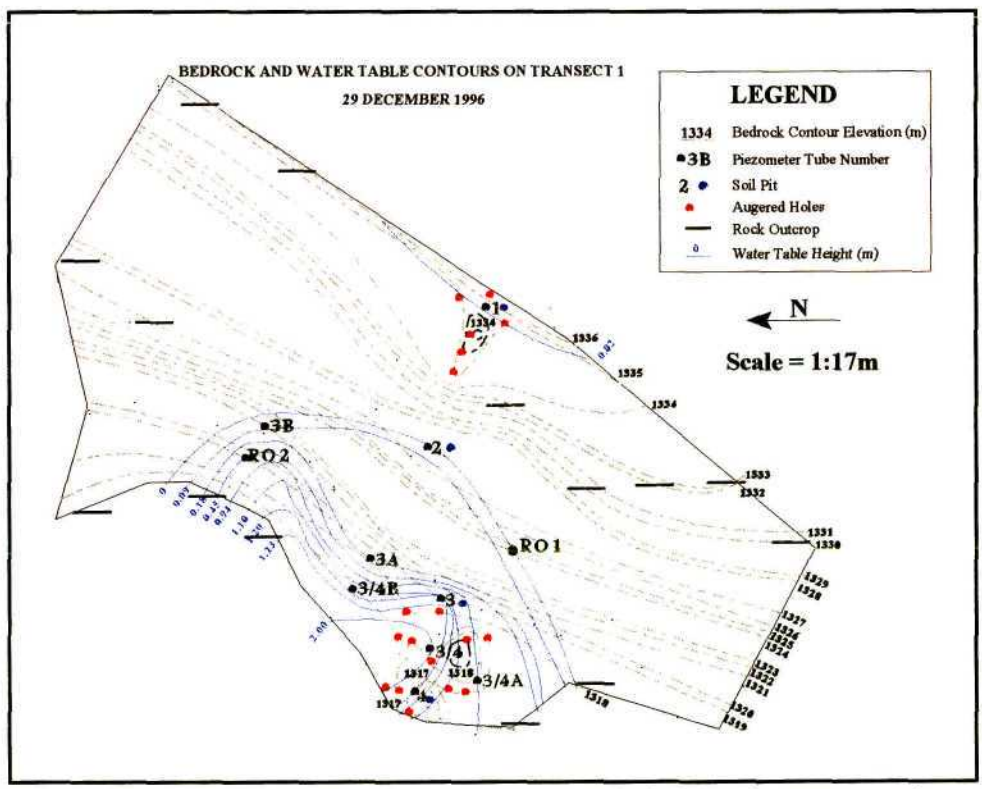

Figure 65. Bedrock elevations and water table heights for 29 December 1996.

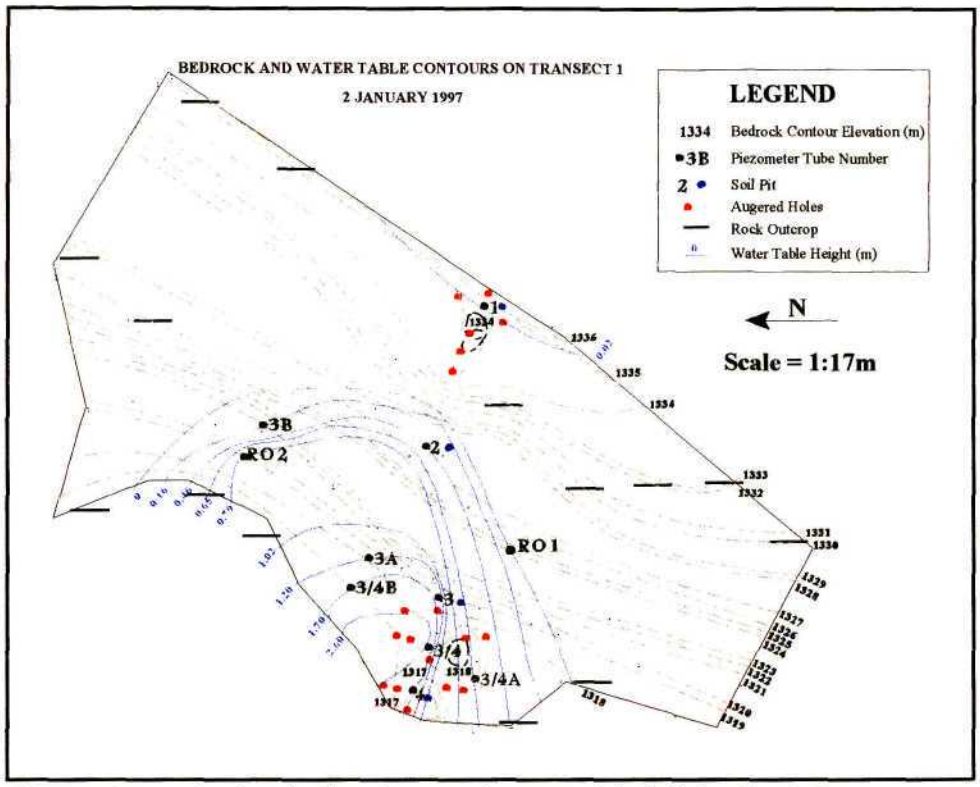

Figure 66. Bedrock elevations and water table heights for 2 January 1997.

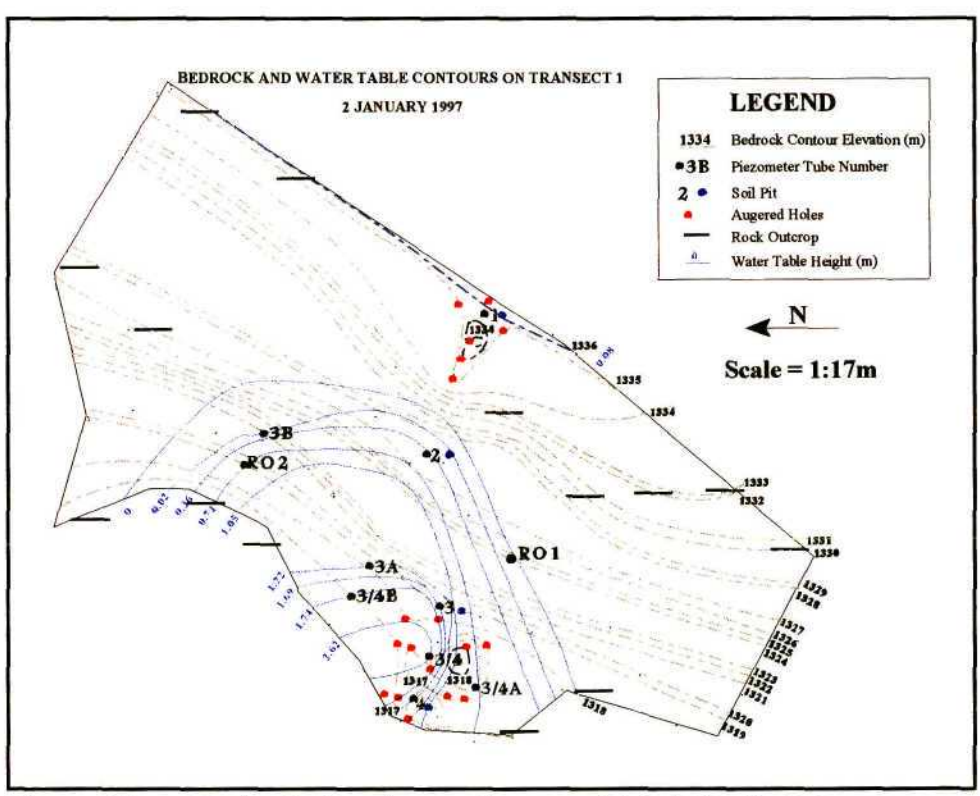

Figure 67. Bedrock elevations and water table heights for 3 January 1997.

Figures 64 through 67 clearly show how an initially dry hillslope (Figure 64) becomes wetter with prolonged rainfall, shown by the WTH contours. Initially, below Pit 2, there is no water table, with most of the groundwater residing in the toe region of the hillslope. Following a rainfall event of 25mm on the 29 December 1996, water tables developed in the midslope region with the water body at the toe growing in size. WTH contours for each day show that the toe region of the hillslope is in fact on the left-hand side of the hillslope base, since the contours converge in this region. Using these water table height contours, hydraulic gradients and soil water fluxes can be calculated. These show gradients to exist between Pit 4 and 3/4 B, a factor which is important when considering left and right lateral flow (*cf.* Equation 18).

6.2 Water Budget of Transect 1

A simple water budget equation, which represents a simplified form of the continuity equation, is as follows:

$$\text{Inflow} - \text{Outflow} = \Delta\text{Storage} \qquad \textbf{(17)}$$

According to Ward (1975), Equation 17 can be applied at both the hillslope and catchment scale at any time scale. In contrast, Singh (1989) reports that for reasonable water budget estimates to be achieved, long time periods, greater than one month, are needed. It was felt by the author that since the area on which the water budget was to be performed is relatively small, a short time period of a few days was adequate.

Using the principles of the continuity equation and knowledge of processes occurring at the hillslope scale (*cf.* Section 2.1), equation 18 has been developed. A schematic representation of a soil block is presented in Figure 68, which shows the components of the water budget.

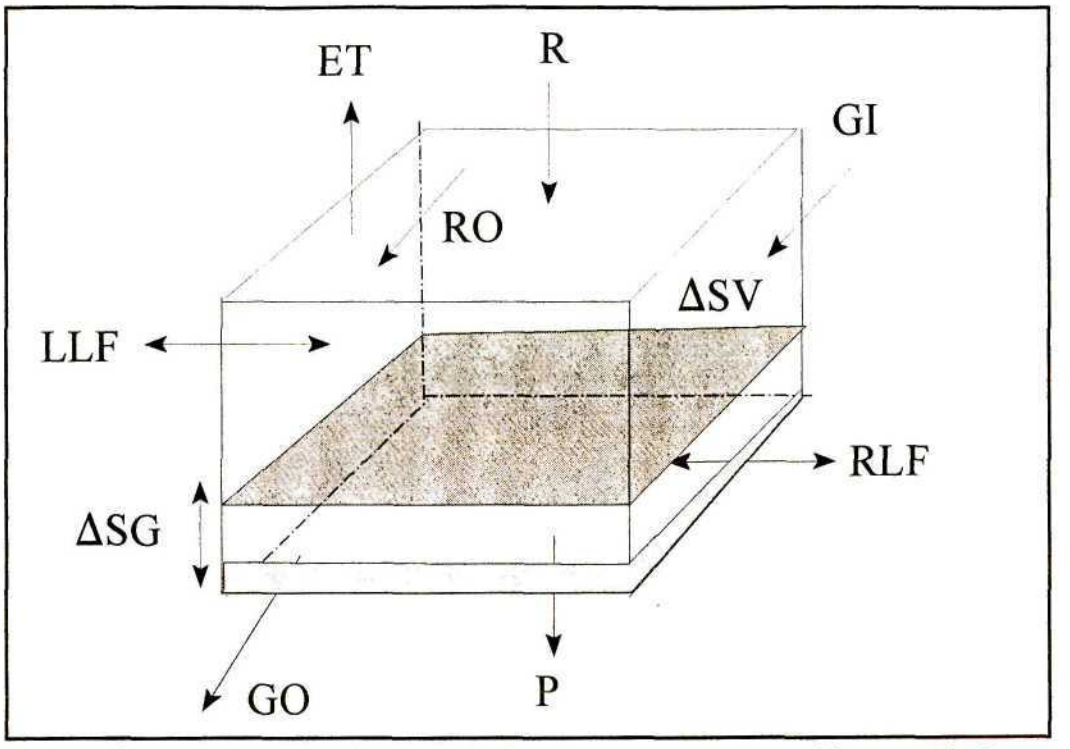

Figure 68. Schematic of soil block showing components used in water budget equation.

The water budget equation is therefore

$$RLF+LLF+GI+R-(RO+ET+P+GO) = \Delta SV+\Delta SG \qquad \textbf{(18)}$$

where

	RLF	=	right lateral flow into the block under consideration (m^3)
	LLF	=	left lateral flow into the block under consideration (m^3)
	GI	=	groundwater in (m^3)
	R	=	rainfall (m^3)
	RO	=	runoff (m^3)
	ET	=	evapotranspiration (m^3)
	P	=	percolation (m^3)
	GO	=	groundwater out (m^3)
	ΔSV	=	change in storage in the vadose zone (m^3)
	ΔSG	=	change in storage in the saturated zone (m^3).

Section 6.2.1 below outlines each component used in Equation 18.

6.2.1 Components of the Water Budget Equation

The components of the water budget equation have been calculated for four blocks, as shown in Figure 69.

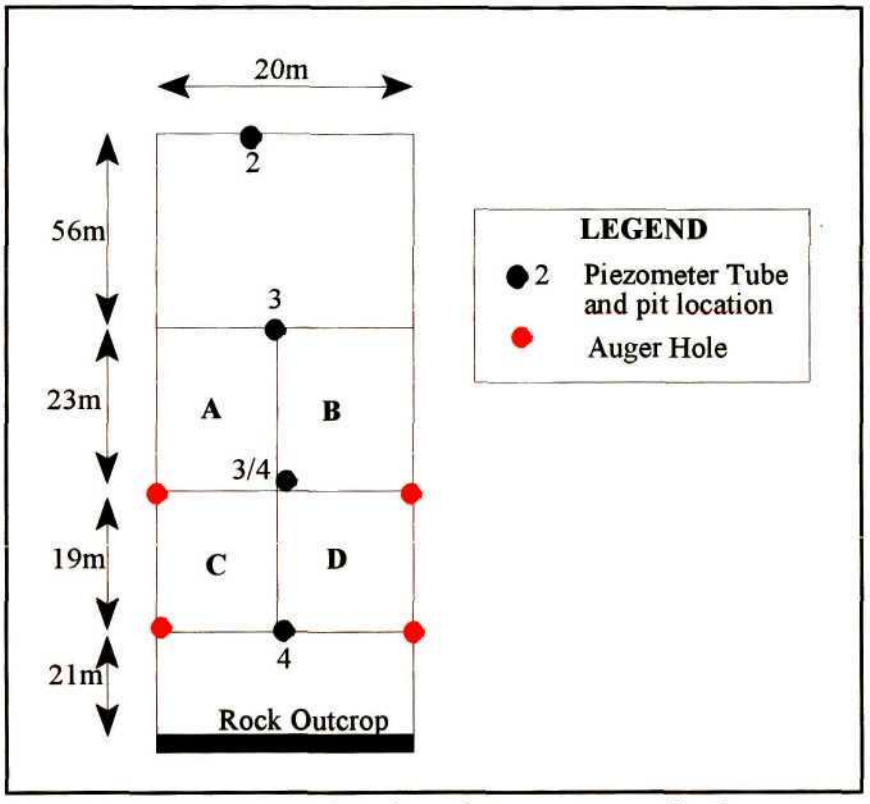

Figure 69. Segmented portion of Transect 1 used in the water budget studies

Inflow, outflow and storage components from Equation 18 are grouped together, and their calculation discussed in Sections 6.2.1.1, 6.2.1.2 and 6.2.1.3 respectively, with results given in Section 6.2.2.

6.2.1.1 Inflow Components (LLF, RLF, GI, R)

The dominant inflow components are left and right lateral flow as well as groundwater flow from the area above the block under consideration. To calculate these flows, a form of Darcy's equation was used, as follows:

$$Q = A.K_s \frac{\Delta H}{L} \qquad (19)$$

where Q = inflow ($mm^3.h^{-1}$)

A = area under consideration (m^2)

K_s = saturated hydraulic conductivity of the soil ($mm.h^{-1}$)

ΔH = change in elevation between water tables (mm)

L = distance between observation points (mm).

Using water table elevations measured from each piezometer tube, ΔH is calculated. Using measured K (*cf.* Section 4.3.3.1), a value for the K of the soil at the point under consideration was determined (*cf.* Appendix G). Inflow into Blocks A and B have been calculated as the contribution of the area from surrounding piezometer 2 to piezometer 3/4, as this entire area has water moving downslope in response to the various gradients calculated from Figures 64 to 67. The rainfall amounts which fell on the preceding day were used in the calculations for the following days to calculate infiltration and the storage changes within the vadose and groundwater zones.

6.2.1.2 Outflow Components (ET,P,RO,GO)

ET for each day was set to 2 mm (Schulze, 1997). Due to the fractured nature of the bedrock found on Transect 1 percolation was not measured directly. Percolation was therefore assumed to be 0.001 m. day^{-1}, which according to Rawles *et al.* (1992) is the water flux which occurs through fractured sandstone. Runoff which was observed on 22 and 28 December 1996 was assumed to be representative of the hillslope transect. These runoff data were converted into runoff volumes for Blocks C and D (Figure 69). GI was calculated in the same manner as GO using Equation 19.

6.2.1.3 Changes in Storages (ΔSV, ΔSG)

Using recorded tensiometer data for the dates under review soil water contents for the soil profiles were calculated as follows (given that $\theta_r = 0$):

$$\theta = \theta_s \left(\frac{h_d}{h}\right)^{\lambda} \qquad (20)$$

where θ = water content of the soil ($m^3.m^{-3}$)

θ_s = soil water content at saturation ($m^3.m^{-3}$)

h_d = air entry pressure (m)

h = hydraulic head (m)

λ = pore size distribution index.

These calculated water contents were verified against measured moisture contents (*cf.* Section 4.4.3). The results showed the NMM data to overestimate the soil moisture contents when compared to water contents derived from the tensiometer data. A plausible explanation for these discrepancies could be attributable to the fact that the NMM measures the concentration of hydrogen in the soil. Hydrogen is not only present in water, but also in some clays. For this reason the soil water content could be overestimated. Nevertheless the NMM measurements provide a useful verification of the estimated water contents. However these estimated water contents were used since they are abundant (continuous data set) and can be calculated anywhere along Transect 1. Table 16 shows the water contents calculated at each location along Transect 1. The tensiometer nest at Pit 3 only had one tensiometer in operation at 0.21 m, as shown in Table 16.

Using these soil moisture contents (Table 16), changes in vadose zone storage were calculated for each day. Depths to the actual water table were taken into account to determine the depth of the unsaturated zone for each day. Using these depths and soil water contents, changes in storage within the vadose zone were calculated daily. A similar procedure was used to calculate the changes in groundwater storage. Water table depth

changes were converted into volumes. The product of these volumes and the ϕ of the soil yields the change in groundwater storage for any day.

Table 16. Water contents ($m^3.m^{-3}$) calculated from tensiometer data at different depths along Transect 1 (*cf.* Figure 69).

Location	Depths Below Soil Surface (m)			
3	0.21			
29 Dec 1996	0.206			
2 Jan 1997	0.205			
3 Jan 1997	0.206			
3/4	0.12	0.2	0.5	1.04
29 Dec 1996	0.207	0.205	0.201	0.070
2 Jan 1997	0.236	0.212	0.207	0.100
3 Jan 1997	0.236	0.214	0.208	0.100
4	0.12	0.24		
29 Dec 1996	0.182	0.147		
2 Jan 1997	0.204	0.154		
3 Jan 1997	0.210	0.156		

6.2.2 Water Budget Results

Using the calculations and equations discussed in the preceding sections the final water budget was calculated for each of the four soil blocks (A, B, C and D) shown in Figure 69. Each of the four soil blocks was treated separately. Soil water outflows from Blocks A and B formed additions to the blocks below, i.e. C and D. Results from these computations are shown in Table 17. Results are given for a two day period. The water balance on 29 December 1996 is not shown, as this date served as the starting point from which change in storages were calculated. Negative values indicate an outflow from the soil block in response to negative hydraulic gradients.

Table 17. Hillslope water budget results for each component for the entire area derived from Equation 18.

Date (1997)	LLF (m^3)	RLF (m^3)	R (m^3)	GI (m^3)	ET (m^3)	P (m^3)	RO (m^3)	GO (m^3)	ΔSV (m^3)	ΔSG (m^3)
2 Jan	-0.20	1.40	2.88	13.24	0.046	0.46	0	0.25	0.91	23.8
3 Jan	-1.60	1.90	0.92	13.21	0.046	0.46	0.50	9.01	0.87	2.07

Using Equation 18, each component was used to obtain an answer in a form similar to that in Equation 17. Results of total inflows, outflows and storage changes are presented in Table 18. The percentage error is calculated as the difference between the total of inflows less the outflows and the storage change.

Table 18. Results of inflows, outflows and changes in storage for a two day period.

Date (1997)	Inflows (m^3)	Outflows (m^3)	Total (m^3)	Change in Storage (m^3)	Error (%)
2 Jan	15.905	0.756	15.149	24.734	37.500
3 Jan	14.510	10.001	7.494	4.499	41.000

These results show that for 2 January 1997, during which large changes in storages occurred, the sum of the inflows and outflows is less than the changes in storage, with the opposite being true for 3 January 1997. Reasons for this could be that lateral inflows have not been taken into account fully on 2 January 1997. On 3 January 1997 the overestimation could be because too little water is exiting the system. This outflow is very difficult to determine and from field observations during this time it was observed that large amounts of exfiltration were occurring with macropore flow.

The results from this water budget show that subsurface processes are difficult to quantify since the processes occurring at this scale are very complex. These results do not give absolute answers to the many questions asked, but do provide a better understanding of the types of processes which are playing a dominant role in the hillslope. The dominant processes are seen to be interflow (GO, GI) cascading down the bedrock in response to hydraulic gradients. Lateral flow also moves to the left and the right of the main transect

because of the undulating nature of the bedrock. The changes in storage, especially in the groundwater zone are large (Table 18) indicating water movement down the hillslope. The storage change in the vadose zone is relatively less, but still plays a role in the overall water budget. An important question to now ask is whether the HILL5D model can account for these processes identified on Transect 1.

Since the main objective of the HILL5D model is to simulate perched water table movement downslope, the model should perform well on this hillslope transect. As an input the HILL5D requires the water table depth at the crest and toe of the hillslope. This may be the weak link in this model because results from the water budget show water movement to occur at all locations on the hillslope transect. These processes are simulated in Section 6.3 below using the HILL5D model.

6.3 HILL5D Simulations

Section 3.1 considers four hillslope models. It was surmised that the HILL5D model would be able to simulate some of the main subsurface processes that occur along Transect 1. Consequently HILL5D has been used in an attempt to simulate these processes, specifically the movement of a perched water table downslope (interflow). The sections that follow outline the main input parameters and present a qualitative parameter analysis. A simulation has been performed for the period 20 December 1996 to 3 January 1997 and results are compared with the water budget results.

6.3.1 Model Parameters

The main input parameters are outlined, and for the sake of brevity the parameters concerning runoff and ET are omitted because this study is concerned with hillslope subsurface processes. Descriptions of these parameters can be found in Smith and Hibbert (1996).

6.3.1.1 Hillslope Geometry and Topography

Figure 70 illustrates schematically the parameters used to describe the shape of the hillslope segment. Each parameter shown is defined in this section. First, the distance between the hillslope crest and toe (DS) is specified with the average hillslope angle (SURF). With respect to soil depths, a program default can be used, where soil depths at the hillslope crest (YU) and base of the hillslope (YB) are specified. Using these depth parameters HILL5D interpolates the soil depths between YU and YB down the hillslope.

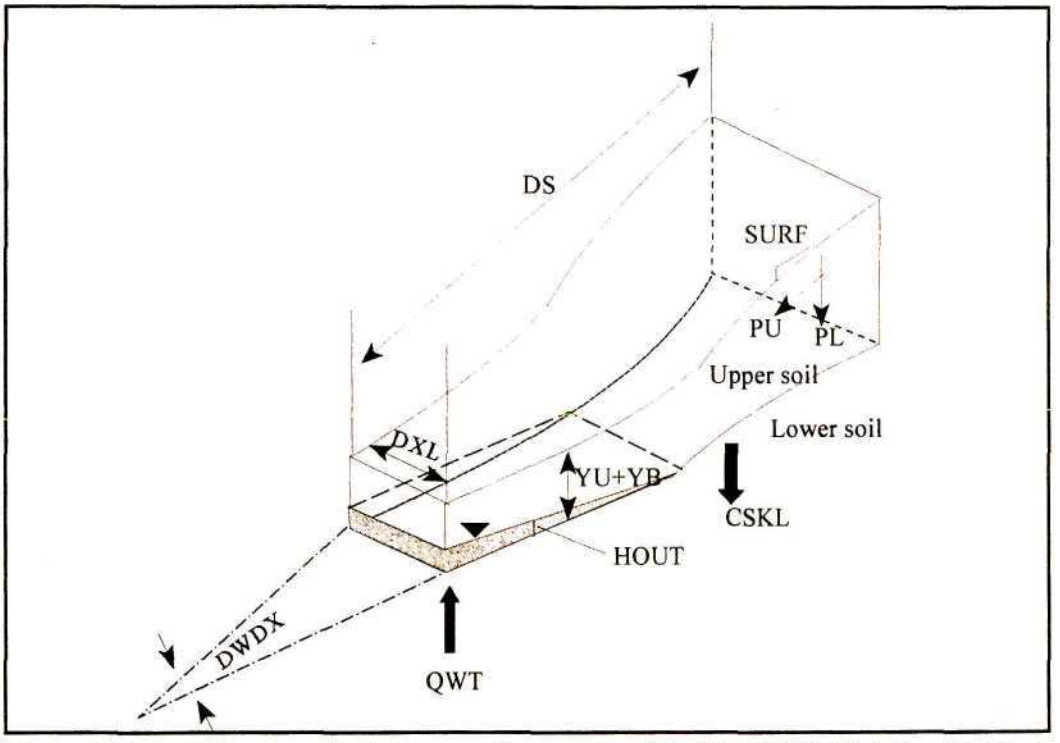

Figure 70. Diagram of hillslope section as simulated by HILL5D (after Hebbert and Smith, 1990; Hebbert and Smith, 1996).

For a more accurate representation of the hillslope surface, up to 10 soil depths and slope angles can be specified (NDX). The toe of the hillslope, having a width parameter (DXL), is assumed to be a streambank. In this region of the hillslope, HILL5D allows some three dimensionality by considering flow lines, which can be either convergent or divergent. According to Bevan (1977), convergent flow lines are important in generating direct runoff, as a result of increases in soil saturated depth. Thus, if flow lines are convergent the parameter DWDX can be specified, this being the angle created by the tangent to the flow lines.

Relative hillslope elevations are calculated internally using SURF and DS, from which information can be derived regarding soil water fluxes and perched water table movement. Since the main objective of HILL5D is to track the movement of the perched water table in soils of finite thickness, it is paramount that these surface elevations be accurate.

6.3.1.2 Soil Hydrological Parameters

The soil hydraulic properties are described by Brooks and Corey (1964) functions. The most important hydraulic parameters in HILL5D according to Smith and Hebbert (1990), are the saturated conductivity and the soil's capillarity. The saturated conductivity is specified for the topsoil (PU) and the subsoil (PL) at the toe of the hillslope.

The saturated and residual water contents, which are standardised, take account of the relative saturation and represent the maximum (SWMX) and minimum (SWMN) levels to which water contents can reach respectively.

The soil's porosity (PHI), pore size distribution index (ALAM) and the air entry pressure, or capillary suction (CF), are also required. ALAM varies between 0.01 and 2. Large values imply a small CF and vice versa. The soil's anisotropy (FISOT) can be determined by estimating the ratio of the downslope conductivity to the vertical conductivity.

The soil's physical and hydraulic characteristics, together with these soil parameters, are vitally important in simulating soil water fluxes down a hillslope. A main downfall of the HILL5D model is that one set of these parameters is used for the entire hillslope. This is not adequate, since the soils on Transect 1 vary spatially and therefore one set of soil parameters is not representative of the hillslope. This inadequacy becomes clearer in Section 6.3.3 in which large discrepancies become apparent when comparing simulated results to actual data.

6.3.1.3 Subsurface Process Parameters

For subsurface and groundwater flow, the upper boundary of the hillslope is always assumed to be a no-flow condition, having a local water surface gradient of zero. If a perched water table is present on the first day of the simulation, the outflow flux (QINI) needs to be specified. The lower boundary (toe region around Pit 4) of the hillslope is a fixed head boundary that can be fixed or be allowed to vary as the saturated zone changes in depth. In this region the initial water table height (HOUT) needs to be specified, corresponding to the initial water table height at the toe. Where fractured bedrock exists, leakage (CSKL) will occur. This leakage flux can be specified as having a value of either zero, which is the simplest case, or a value greater than zero. A value greater than zero induces a maximum loss rate at the hillslope crest and a corresponding upward flux in the toe region (QWT), in response to water flow down the hillslope. In such cases, uniform seepage rates are specified using CSKL and QGW, by setting their values equal but with opposite signs.

6.3.2 Qualitative Parameter Analysis

After each input parameter was determined or calculated from field measurements and observations, numerous simulations were performed. For each model simulation, the soil's hydraulic parameters, QINI, HOUT, CSKL and QWT, and topographical parameters, YU, YB, PU and PL were found to be the most sensitive parameters.

In total seven simulations were performed. For each, one parameter was changed and results analysed. Table 19 shows the values used for each parameter in each of these simulations. Explanations for each simulation follow.

Table 19. Qualitative parameter analysis for the HILL5D modelling system. Bold values show which parameters have been changed.

Parameter	Initial Values	Run 1	Run 2	Run 3	Run 4	Run 5	Run 6	Run 7	Final Values
YU (m)	1.8	1.8	1.8	1.8	1.8	1.8	**1.2**	1.8	1.8
YB (m)	0.6	0.6	0.6	0.6	0.6	0.6	0.6	**1.0**	0.6
PU ($m.h^{-1}$)	0.025	0.025	0.025	0.025	0.025	**0.030**	0.030	0.030	0.030
PL ($m.h^{-1}$)	0.022	0.022	0.022	0.022	0.022	**0.028**	0.028	0.028	0.028
QINI ($m^3/h/m$)	0.0007	0.0007	0.0007	**0.007**	0.0007	0.0007	0.0007	0.0007	0.0007
HOUT (m)	0.50	0.50	0.50	0.50	**0.10**	0.50	0.50	0.50	0.50
CSKL ($m.h^{-1}$)	1	**-1**	**-0.001**	-0.003	-0.003	-0.003	-0.003	-0.003	-0.003
QWT ($m.h^{-1}$)	-1	**1**	**0.001**	0.003	0.003	0.003	0.003	0.003	0.003

RUN 1: Initial values of unity were used for CSKL and QWT. It was suspected that the signs of these parameters determined the status of the water in the profile. Reversing the signs showed marked changes in terms of the simulated subsurface fluxes. Seepage areas developed from which exfiltration occurred, resulting in overland flow. Water table heights were at a maximum throughout the hillslope. For these reasons these values were obviously too high, therefore, these parameter values were decreased accordingly.

RUN 2: As CSKL and QWT decrease and increase respectively, the seepage face decreases, with a subsequent drop in water table heights. Final values used were approximately 0.003.

RUN 3: An increase in QINI results in larger water fluxes and thus the original calculated value used in Run 1 was retained.

RUN 4: As the water table depth (HOUT) at the base of the hillslope decreases, so to does the entire water table on the transect. As the initial HOUT is a measured value, it was kept as 0.50 m.

RUN 5: Increasing the saturated conductivities of the topsoil (PU) and subsoil (PL) changes the hillslope hydrology substantially. An increase in these conductivities, allows water to flow more rapidly through the soil, hence exiting more quickly, resulting in the rapid drying out of the profile. These new K values (Table 19) were kept, as they seemed representative of the area between GW 3/4 and GW 4 in the toe region of Transect 1.

RUN 6: A depth of 1.8 m (YU) is the shallowest depth that can be specified for the top of the hillslope, otherwise the program does not run. Using a value of 1.2m, which is the actual depth of the location, causes the model to give an error message.

RUN 7: As the soil depth in the toe (YB) of the hillslope is increased, water table heights decrease and more water is retained in the soil profile and overland flow or exfiltration decreases. Since 0.6 m had been measured in the field, it was kept as such.

The final parameter values, shown in Table 19 were used in the final HILL5D simulation, outlined in Section 6.3.3 below.

6.3.3 Simulation of Transect 1 using HILL5D

Using a detailed rainfall record for the simulation period (*cf.* Appendix I) and input parameters, shown in Table 20, the HILL5D model was run. The layout of the input parameter file is given in Appendix J.

Table 20. Parameters for the final HILL5D run.

Parameter Name	Parameter Description	User Specified Value
DWDX	Tangent of the angle of intersection of two flow lines at hillslope toe.	0
DXL	Length of smallest segment at bottom of hillslope (m).	10
NDX	Number of segments into which hillslope is divided.	18
SURF	The average slope of the hillslope (%).	0.11
YU	Soil depth at crest of hillslope (m).	1.80
YB	Soil depth at toe of hillslope (m).	0.60
DS	Hillslope length (m).	145
PU	Saturated conductivity of topsoil ($m.h^{-1}$).	0.03
PL	Saturated conductivity of subsoil ($m.h^{-1}$).	0.028
SWMX	Maximum level of soil water expressed as fraction of the porosity.	0.96
SWMN	Minimum level of soil water expressed as fraction of the porosity.	0.10
PHI	The soil porosity (%).	0.32
ALAM	Brooks and Corey (1964) pore size distribution parameter.	0.334
CPC	Capillary fringe height (m).	0.35
CF	Brooks and Corey (1964) capillary suction / air entry pressure (m)	0.52
FISOT	Anisotropy factor.	1
QINI	Initial value of outflow from the perched water table ($m^3.h^{-1}.m^{-1}$).	0.0007
HOUT	The depth of the perched water table at the bottom of the hillslope (m).	0.50
CSKL	Interface leakage enhancement coefficient ($m.h^{-1}$).	-0.003
QWT	Rate of groundwater upflow at the subsoil interface at hillslope base ($m.h^{-1}$).	0.003

6.3.4 Simulation Results

Groundwater data collected from Transect 1 for the period 20 December 1996 to 3 January 1997 were compared with the simulated groundwater results. An example of such an output is given in Appendix K. Figure 71 shows a comparison of observed and simulated groundwater table heights in the toe region of the hillslope. Results show the simulated groundwater tables to be less than the actual water tables and there is also a strong systematic error with the curves diverging, at a location corresponding to GW 3/4 on the hillslope. At GW4, observed water tables are initially lower than the simulated ones. These observed water tables increase with time, becoming similar towards the end of the simulation period.

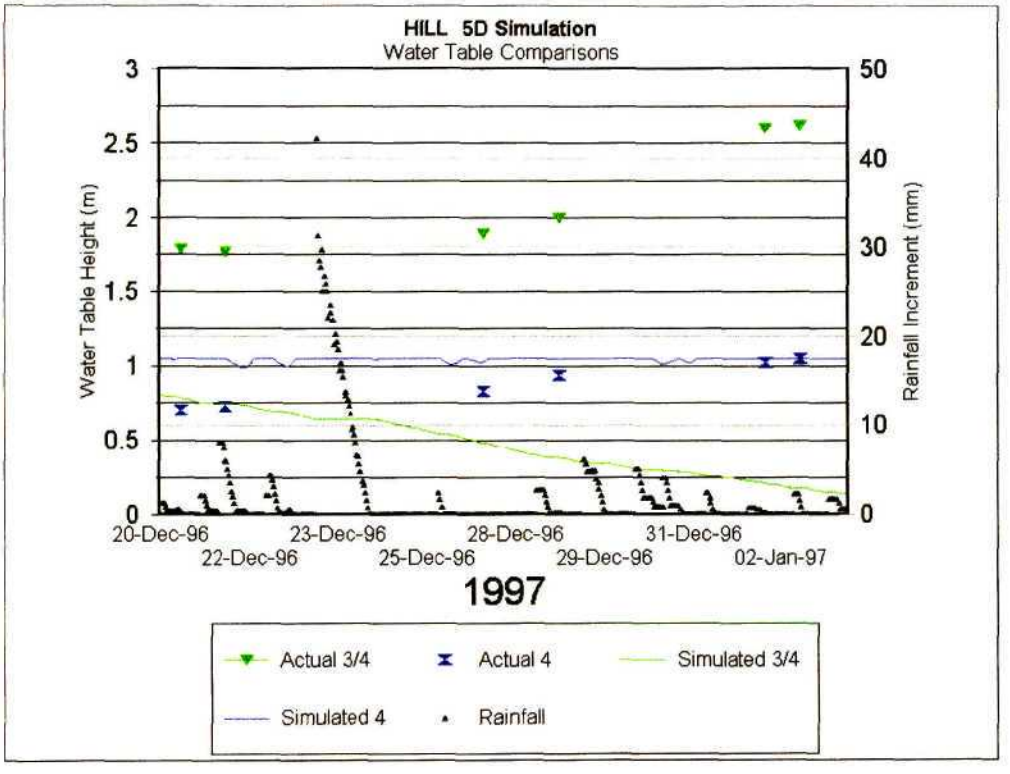

Figure 71. Simulated vs observed groundwater values with rainfall increments for the period 20 December 1996 to 2 January 1997.

Figure 72 shows simulated subsurface and overland flow and their sum. Since subsurface flow was not measured directly and no continuous runoff observations were made, no comparisons can be made. However, with observed results shown in Figure 71 conclusions can be drawn. Since, on average, water table heights were underestimated one can deduce that subsurface flow is underestimated, as the latter occurs in response to the movement of perched water tables.

Similarly, overland flow may be underestimated, although in comparison to the subsurface flow it is very high. In this respect the water budget shows the opposite to be true with subsurface flow being four times larger than the runoff.

These simulated results show therefore that the runoff fluxes are an order of magnitude higher than the subsurface fluxes. Both fluxes respond to large rainfall peaks, with subsurface flows having a larger response when compared with those associated with lesser rainfall amounts. This is a contradiction to results obtained from actual groundwater

measurements (*cf.* Section 5.3.1.2, Figure 43), which show groundwater heights to continue to rise after a rainfall event, in response to subsurface flow.

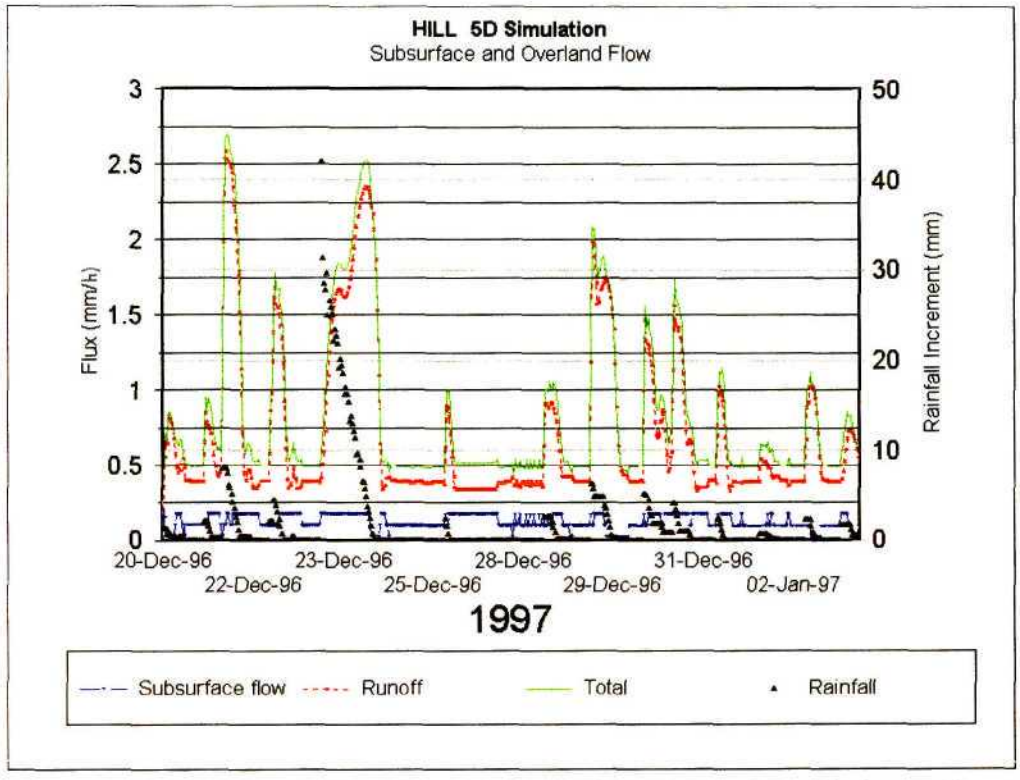

Figure 72. Simulated subsurface and overland flow together with the total water flux, for the simulation period.

These results show the importance of the soil parameters that are specific to the toe of the hillslope. In the simulations the soil in the region of GW3/4 dries out too quickly, with other locations on the hillslope being totally dry. ET may be the cause for the soil drying out too quickly. A broad conclusion can be drawn. The further from the toe, the larger the error, in terms of the water table heights.

A similar exercise, shown in Section 6.2, was carried out to calculate the water budget from these simulated results. Using simulated results from 1 January 1997 to 3 January 1997, parameters from Equation 18 were calculated. Owing to different simulated outputs, Equation 18 has been adapted slightly and is shown as Equation 22:

$$SFI+R-(RO+ET)=\Delta S \qquad \textbf{(21)}$$

where SFI = subsurface flow into system (m^3)

ΔS = storage change (m^3).

SFI is a combination of RLF, LLF (*cf.* Equation 18)and GI; RO includes GO and ΔS a combination of ΔSV and ΔSG. Table 21 and 22 show a comparison of simulated and observed results for each component and the total simulated and observed inflows and outflows. The error term shown in Table 22 is the difference between the total of the inflows less the outflows and the storage change.

Table 21. Simulated (Sim) and observed (Obs) results for each component in Equation 22.

Date (1997)	**SFI (m^3)**		**R (m^3)**		**RO (m^3)**		**ET (m^3)**		**ΔS (m^3)**	
	Sim	Obs	Sim	Obs	Sim	Obs	Sim	Obs	Sim	Obs
2 Jan	0.99	15.91	2.88	2.88	4.69	0.00	0.05	0.05	1.55	24.73
3 Jan	0.84	14.51	0.92	0.92	5.52	0.50	0.05	0.05	8.48	4.49

Table 22. Results of inflows, outflows and storage changes for the simulation period.

Date (1997)	**Inflows (m^3)**	**Outflows (m^3)**	**Total (m^3)**	**Storage Change**	**Error (%)**
2 Jan	3.87	4.74	8.61	1.55	81.90%
3 Jan	1.76	5.57	7.33	8.48	13.60%

These results show a large error for 2 January 1997 compared with the following day. This implies that HILL5D continues to simulate relatively high subsurface and overland flows although the water table heights are decreasing. These simulated results show, therefore, that the HILL5D model does not account adequately for the subsurface processes along Transect 1. A set of parameters could not be found to improve this conclusion.

The main shortcoming of the model is in the simulation of the water table heights. The same cannot be said for the subsurface and overland flows, since there are no observed measurements of these processes. The simulated subsurface flow results may be correct but this is doubtful because of erroneous water table heights.

6.4 An Overview of Water budget and Simulated Results

Results of the water budget showed that the GI component dominated, suggesting interflow processes. Groundwater outflow was not all that high for the first day of the water budget, but on the second day it was high. This was a result of large water fluxes exiting the hillslope in the toe region as exfiltration. Change in soil water storage in the soil (vadose zone) was not large, suggesting that all infiltrating water moved rapidly through the soil to the capillary fringe. This rapid movement shows up in the change in groundwater storage which was 23.8m^3 for this event. The following day the change in groundwater storage increased by 2.07 m^3 possibly due to redistribution within the soil, entering the groundwater zone after a few hours. GO was very large suggesting interflow and exfiltration as already mentioned.

In comparison, the HILL5D model undersimulates the interflow component and overestimates runoff. On 2 January 1997 simulated changes in storage are 20 times lower than measured changes. The following day these storage changes are double the actual changes. This does not seem correct since if these changes were true, the SFI component would surely have increased (Table 21).

The water budget results were considered acceptable as interpretation of the data conformed to some initial assumptions put forward regarding the dominant processes which occur along Transect 1. These processes include a dominance of water movement down the hillslope as interflow, followed by exfiltration in the toe region. Also shown was that water infiltrates vertically through the soil, replenishing the groundwater store. The HILL5D simulations were disappointing, as results did not support those from the water budget study. Reasons are many and include the fact that only one set of soil physical parameters

was used for the entire hillslope. This is too much of a simplification of a complex real system due to the spatial distribution of the soils found on this transect.

* * *

Procedures used to describe bedrock and WTH contours were presented in Chapter 6. These contours are very useful to calculate soil water fluxes at the hillslope scale. These data are very important in water budget studies. A simple water budget was presented, which took into account some dominant processes which occur on hillslopes having shallow soils underlain by semi-permeable fractured bedrock. Processes considered included runoff, interflow, percolation and changes in soil water storage within the soil. A section of Transect 1 was selected and water budget calculations were performed, using actual data to calculate the necessary input components. Using the HILL5D model, a qualitative parameter analysis was performed before simulating subsurface processes. Results showed the soil hydraulic parameters to be the most sensitive. Subsurface processes were then simulated. Results from both the water budget and simulations are presented.

Chapter 7 follows, in which a discussion is presented which aims to bring each chapter together. Conclusions are drawn pertaining to this first phase research.

7. DISCUSSION AND CONCLUSIONS

One of the predominant RDP objectives is to achieve the building of 300 000 new house per annum. In order to meet this objective a large supply of timber is required. Current timber production in South Africa does not meet these needs and therefore large scale afforestation needs to be set into action. Most of the prime forestry regions in South Africa already have commercial plantations, such as the Sabie and Zululand areas to name just two. New areas therefore need to be sought.

The NEC, although climatically and physiologically marginal for the support of silviculture, has been recognised as a potentially viable location for large scale expansion of commercial plantations. The sustainability of afforestation in the NEC is questionable. Not only is the NEC characterised by a hilly topography with shallow soils, but also has a range of complex hillslope hydrological processes. Interflow down a hillslope followed by exfiltration induces saturated conditions, which in turn replenish groundwater reserves from which rivers derive their water. These saturated conditions are detrimental to forests, especially in the lower regions of the hillslope.

Since this research is a pilot study, not all these questions can be answered, but a foundation can be developed upon which further research can be conducted. In this way many questions can be answered. This research therefore concentrates on a first phase which has three main objectives. They are to understand and identify the dominant subsurface processes occurring at the hillslope scale, secondly to set up a hillslope experiment to monitor these processes and thirdly, to simulate these processes with an appropriate hillslope model. The second phase objectives are to carry on the research once trees have been introduced. This phase is outlined in more detail in Chapter 8.

To understand the dominant hillslope subsurface processes an intensive literature review was undertaken (Chapter 2). Literature from a wide range of sources was perused and studied. Most research carried out was very site specific with the research objectives pertaining to specific processes. Results of such research all gave similar conclusions. These were that interflow dominates hillslopes with shallow soils underlain by semi-permeable bedrock. In

the presence of macropores water moves rapidly into the soil profile, bypassing the soil matrix and replenishing groundwater bodies. This in turn, speeds up lateral flow production. The achievement of these results was carried out by interception of flow, which is not only destructive, but for reasons discussed in Chapter 2, induces unnatural conditions.

With a knowledge and comprehensive understanding of these processes the next step was to identify the dominant processes which occur within a hillslope at Weatherly in the NEC. To achieve this objective, an initial fieldwork component was conducted during which the soil physical and hydraulic properties were determined. Thereafter, an intensive hillslope experiment was established on Transect 1 (Chapter 4). Instruments included automated tensiometers, piezometer tubes, neutron probe access tubes and a runoff plot. Monitoring of all these instruments commenced for a period of 5 months from December 1996 to April 1997. Data collected pertained to the MPH of the soil, water table fluctuations and soil moisture contents along Transect 1.

In comparison to the research reviewed in the literature, this study is different in that this research considers the interaction of all processes. Data collected not only give an indication of infiltration and redistribution, but also of processes which are occurring within the vadose and groundwater zones. From these data the processes of interflow can be inferred and estimates of subsurface fluxes can be made. Also, the use of these instruments does not disturb the very processes which are being measured, compared with experiments using excavations.

Having completed the three research objectives, overall results are presented (Chapter 5). Results from the physical and hydraulic characteristic measurements show that on average the percentage clay increases both down the soil profile and the hillslope transect. This finding is substantiated by the bulk densities increasing in a similar fashion. As one would expect, the saturated conductivity should conform accordingly, which it does, and decreases with depth. These conductivities are greater on the crest and midslope due to the sandy nature of the soils and are very low in the toe region which has a higher clay content. These clayey soils have high unsaturated conductivities, which are seen also to increase with soil depth. Using regression analysis a good relationship was determined between the

conductivity and soil depth and clay contents ($r^2 = 0.78$ and 0.80 respectively). The WRC data show these soils along Transect 1 to have a large water holding capacity, especially at deeper horizons. Within the topsoil horizons the WRCs show large desorption rates indicative of the presence of macropores. All these results show, therefore, that the soils are well drained and permeable which allows water to infiltrate rapidly, especially if macropores are present. Upon reaching the bedrock these soils become more compact, as demonstrated by high bulk densities forming a semi permeable barrier which induce perched water table development.

Manual and automated tensiometer data collected show similar results. Data collected from the automated tensiometers gave a more comprehensive data set which allowed the calculation of fluxes and gradients. These MPH, groundwater and soil moisture data have allowed some broad conclusions to be drawn. Interflow occurs within Transect 1 and is dependent on various factors. These include the position in the hillslope, the AMC and the initial depth of the water table. Low intensity rainfall events were seen to induce a maximum rise in existing water tables, these having a larger response close to the toe region. After rainfall has subsided, infiltration was seen to continue and water tables continued to rise for a number of days after the event. On the midslope the water tables initially increased in height, to a lesser extent, after which they dropped markedly. In contrast, water tables in the toe region continued to rise due to water moving down the bedrock as interflow from the water tables upslope. With large and high intensity rainfall events the dominant response processes is surface runoff with little water entering the soil. Water which does enter the soil profile was seen to wet up only the first 0.1m of the soil on average.

Using the data collected, a water budget of the hillslope was conducted in an attempt to isolate the dominant processes and mechanisms (Chapter 6). These observed results were then compared to simulated results using the HILL5D modelling system (Chapter 3), which had been identified as the 'best' of three models to use under these conditions.

After completion of the water budget study similar conclusions were drawn. These included that the dominant process is interflow, moving as a perched water table downslope, followed by the subsequent exfiltration in the toe region. These results showed no

comparison to simulated results from the HILL5D mode. In conclusion it must therefore be stated that the HILL5D model does not simulate these hillslope processes adequately. Methods to improve this model's performance are presented in Chapter 8.

This research allowed considerable experience to be gained in the planning and setting up of a hillslope hydrology experiment. Furthermore, experience was gained in to the various instruments used and methods available to measure various parameters. Doing research of this nature required many long hours to be spent in the field. On many occasions, Transect 1 was frequented during rainfall events during which many of the processes discussed, were witnessed. These visits not only gave an appreciation of the complexity of hillslope subsurface processes, but also made the data analysis task so much easier.

Mention therefore needs to be made pertaining to fieldwork. Many researches studying hydrological processes seldom or never leave their offices. It is believed, in many cases, that a computer simulation model will provide all the answers. An understanding of these processes is paramount, however, before modelling can be achieved successfully, especially if one is seeking a model to give the right answers for the right reasons.

8. RECOMMENDATIONS FOR FUTURE RESEARCH

The research work presented in this document is possibly one of the first studies of this kind and intensity to be carried out in South Africa. For this reason no local 'guidelines' could be adhered to in terms of the setup of the experiment. In retrospect, with regard to the setup of this hillslope experiment, some recommendations for the future and continued research on this hillslope are outlined. These include the following:

a. Readings from the piezometer tubes need to be automated. This can be achieved by using pressure transducers attached to the same logger that the tensiometers are attached to. Together, the tensiometer and groundwater data will enable the calculation of accurate water fluxes and the wetting up and drying times in the soil in response to rainfall. ET can also be calculated using data collected from the AWS, which is especially important in the toe region where the water tables are high under saturated conditions.

b. More piezometers need to be installed, especially in the toe region of Transect 1. They should all be installed to different depths within the soil, especially in locations where clayey lenses are present. Infiltrating water upon these clay lenses may form perched water tables before redistributing further into the soil. Currently the piezometers are all concluded on bedrock. The midslope which showed little water table activity suggests that maybe these perched water tables are forming higher up in the profile.

c. Automated runoff plots would be extremely useful, using a tipping bucket system so that real time runoff data can be collected. The data, together with rainfall intensity and MPH data, will be useful in future water balance calculations.

d. Another intense GPR study should be conducted when the catchment is drier, so that a definite bedrock topography can be defined.

e. Using this bedrock topography data, a DTM should be developed and compared to the existing DTM of the surface topography of the transects. This may yield some important information regarding soil water fluxes.

f. An interception of interflow and macropore study should be initiated at a natural seepage face. This seepage face exists in the toe region and should be used to collect volumes of interflow, macropore flow and water which has exfiltrated.

g. Tracers should possibly be used to help determine the rate at which soil water moves from one piezometer tube to the next down the hillslope.

h. More research work needs to be incorporated into the HILL5D model. A macropore routine needs to be added and the ET component needs to be refined, since the soil is drying out too quickly. The model inputs need to be changed so that soil physical and hydraulic parameters at different locations on the hillslope can be used. With these modifications the HILL5D model may simulate the processes on Transect 1 adequately.

The second phase of this research needs to have *inter alia* the following objectives:

a. Monitoring of subsurface processes using automated tensiometers and piezometers should be continued and macropore and interflow should be measured more directly.

b. DTM of the bedrock surface should be developed and used in simulation modelling.

c. Processes after the introduction of trees should be monitored.

d. These results should be compared with those from the first phase to answer questions pertaining to the tree water use and the viability of planting trees on hillslopes.

9. REFERENCES

Acocks, J.P.H. (1975). Veld types of South Africa. *Botanical Research Institute*, Pretoria, Department of Agricultural Technical Services, *Memoirs* 40 pp 83.

Ahuja, L.R., DeCoursey, D.G., Barnes, P.B. and Rojas, K.W. (1991). Characteristics and importance of preferential macropore transport studied with the ARS root zone water quality model. *In*: *Proceedings of the National Symposium*. pp 32-49.

Amoozegar, A. and Warrick, A.W. (1986). *Methods of Soil Analysis, Part 1: Physical and Mineralogical Methods,* 2nd edition. American Society of Agronomy, Madison Publishers, U.S.A.

Anderson, M.G. and Burt, T.P. (1990). Process studies in hillslope hydrology: an overview. *In*: Anderson, M.G. and Burt, T.P. (Editors). *Process Studies in Hillslope Hydrology*. John Wiley and Sons, Chichester, UK. pp 1-8.

Anderson, M.G. and Brooks, S.M. (1996). Hillslope Processes: Research prospects. *In*: Anderson, M.G. and Brooks, S.M. (Editors). Advances in hillslope processes. John Wiley and Sons, Chichester, UK. pp 10-11.

Aron, G. (1992). Adaptation of Horton and SCS infiltration equations to complex storms. *Journal of Irrigation and Drainage Engineering* 118: 275-283.

Atkinson, T.C. (1978). Techniques for measuring subsurface flow on hillslopes. *In* : Kirkby, M. J. (Editor.) *Hillslope Hydrology*. John Wiley & Sons. England.

Bathurst, J.J. (1986). Physically based distributed modelling of an upland catchment using the Systeme Hydrologique Europeen. *Journal of Hydrology* 87: 79-102.

Beckedahl, H. (1996). *Subsurface Soil Erosion Phenomena in Transkei and Southern Kwa-Zulu - Natal, South Africa.* Unpublished PhD Thesis. University of Natal, Pietermaritzburg, RSA.

Bevan, K. and Germann, P. (1982). Macropores and water flow through soils. *Water Resources Research* 18: 1311-1325.

Binley, A. and Bevan, K. (1992). Three-dimensional modelling of hillslope hydrology. *Hydrological Processes* 6: 347-359.

Birkhead, A.L., Heritage, G.L., White, H. and von Niekerk, A.W. (1996). Ground penetrating radar as a tool for mapping the phreatic surface, bedrock profile and alluvial stratigraphy in the Sabie River, Kruger National Park. *Journal of Soil and Conservation* 51(3): 234-241.

Blake, G.R. and Hartage, K.H. (1986). Bulk density. *In*: Klute, A. (Ed) Methods of soil analysis. Part 1. *Physical and Mineralogical Methods.* American Society of Agronomy. No. 9: 363- 375.

Bosch, J.M. and Hewlett, J.D. (1982). A review of catchment experiments to determine the effect of vegetation changes on water yield and evapotranspiration. *Journal Hydrology* 55(3): 3-23.

Bronstert, A. (1995). *User Manual for the Hillflow-3D Catchment Modelling System Physically Based and Distributed Modelling of Runoff Generation and Soil Moisture Dynamics for Micro-catchments.* Working Document 95/4. 1-30

Brooks, R.H. and Corey, A.T. (1964). Hydraulic properties of porous media. Hydrology Paper 3, Colorado State University, Fort Collins, Colorado, USA.

Buitendag, I. (1990). *Modelling Infiltration Under Different Tilled Conditions.* Unpublished Msc. Eng. Dissertation. Department of Agricultural Engineering, University of Natal, Pietermaritzburg, RSA.

Burt, T.P. (1985). Slopes and slope processes. *Progress in Physical Geography* 9: 582-599.

Chorley, R.J. (1978). The hillslope hydrological cycle. *In*: Kirkby, M.J. (Editor). *Hillslope Hydrology*. John Wiley and Sons. 1-42.

Clothier, B.E. and White, I. (1981). Measurement of sorptivity and soil water diffusivity in the field. *Soil Science Society of America Journal* 45: 241-245.

Collins, M.E., Doolittle, J.A. and Rourke, R.V. (1989). Measuring depth to bedrock on a glaciated landscape with ground penetrating radar. *Soil Science Society of America Journal* 53: 1806-1812.

Corbett, E.S. (1979). Hydrological evaluation of the storm flow generation process on a forested watershed. Ph. D. Thesis. Office of Water Research And Technology, Washington, D.C., NTIS: PB80-129133, pp125.

Culley, J.L.B. (1993). Density and compressibility. *In*: Carter, M.R. (Editor). *Soil Sampling and Methods of Analysis*. Canadian Society of Soil Science. pp 529-540.

Denning, J.L., Bouma, J., Falayi, O. and van Rooyen, D.J. (1974). Calculation of hydraulic conductivities of horizons in some major soils in Wisconsin. *Geoderma* 11: 1-16.

Dunne, T. and Black, R.D. (1970). An experimental investigation of runoff production in permeable soils. *Water Resources Research* 6: 478-490.

Department of Water Affairs and Forestry (1995). Towards a policy for sustainable forest management in South Africa: A discussion paper. Department of Water Affairs and Forestry, Pretoria, RSA.

Feddes, R.A., Kowalik, P.J. and Zaradny, H. (1978). Simulation of field water use and crop yeild. Simulation Monograph. PUDOC, Wageningen (NL). pp 189.

Fernandes, N.F., Netto, A.L.C. and Lacerda, W.A. (1994). Subsurface hydrology of layered colluvium mantles in unchannelled valleys, South-Eastern Brazil. *Earth Surface Processes and Landforms* 19: 609-626.

Fleming, G. (1975). *Computer Simulation Techniques in Hydrology*. Elsevier, New York, USA. pp 333.

Flury, M., Fluhler, H., Jury, WA and Leuenberger, J. (1994). Susceptibility of soils to preferential flow of water: A field study. *Water Resources Research* 30: 1945-1954.

Flury, M. and Fluhler, H. (1995). Tracer characteristics of Brilliant Blue FCF. *Soil Science Society of America Journal* 59: 22-27.

Gardner, P. (1997). Personal Communication. Mondi Forests, Pietermaritzburg, RSA.

Gerke, H.H. and van Genuchten, M.T. (1993). A dual-porosity model for simulating the preferential movement of water and solutes in structured porous media. *Water Resources Research* 29: 305-319.

Germann, P.F., (1990). Macropores and hydrologic hillslope processes. *In*: Anderson, M.G. and Burt, T.P. (Editors). *Process Studies in Hillslope Hydrology*. John Wiley and sons Ltd.

Germann, P.F. and DiPietro, L. (1996). When is porous-media flow preferential? A hydromechanical perspective. *Geoderma* 74: 1-21.

Grayson, R.B., Moore, I.D. and McMahon, T.A. (1992). Physically based hydrologic modelling. 1. A terrain based model for investigating purposes. *Water Resources Research* 28: 2639-2658

Green, W.H. and Ampt, G.A. (1911). Studies on soil physics, I. The flow of air and water through soils. *Journal of Agricultural Science* 4: 1-24.

Gupta, S.I., Moravcik, P.S. and Lau, S.L. (1994). Use of injected helium as a hydrological tracer. *Hydrological Science Journal* 39: 109-118.

Habib, A., Zartman, R.E. and Ramsey, R.H. (1988). Intrapedal macropore distribution and infiltration rate of three friona polypedons. *Soil Science* 145: 244-249.

Harr, R.D. (1977). Water flux in soil and subsoil on a steep forested slope. *Journal of Hydrology* 33: 37-58.

Hebbert, R.H.B. and Smith, R.E. (1990). Hillslope parameter estimation using the inverse procedure. *Journal of Hydrology* 119: 307-334.

Hebbert, R.H.B. and Smith, R.E., (1996). *User Manual for Hill5d Numerical Simulation Model.* Agricultural Research Service, Water Management Research Unit, Fort Collins, Colorado, AERC, Colorado State University, 80523.

Hensley, M. (1996). Personal Communication. Glen Agricultural Development Institute, Glen, RSA.

Hewlett, J.D., Fortson, J.C. and Cunningham, G.B. (1984). Additional tests on the effect of rainfall intensity on storm flow and peak flow from wild-land basins. *Water Resources Research* 20: 985-989.

Hillel, D. (1977). *Computer Simulation of Soil-water Dynamics: A Compendium of Recent Work.* International Development Research Centre, Ottawa, Canada.

Hillel, D. (1982). *Introduction to Soil Physics.* Academic Press. New York: USA.

Horton, R.E. (1933). The role of infiltration in the hydrological cycle. *Transactions of American Geophysical Union* 14: 446-460.

Howe, B.J. (1997). *Development of New Techniques for Variable Source Area Sediment Yeild Modelling*. Unpublished MSc. Eng. dissertation, Department of Agricultural Engineering, University of Natal, Pietermaritzburg, RSA.

Hutson, J.L. (1984). *Estimation of Hydrological Properties of South African Soils.* Unpublished Ph.D. Dissertation. Department of Soil Science and Agromet. University of Natal, Pietermaritzburg. RSA. pp 2-3.

Hutson, J.L. and Wagenet, R.L. (1992). LEACHM, A Process Based Model ofWater and Solute Movement, Transformations, Plant Uptake and Chemical Reactions in the Unsaturated Zone. New York State College of Agriculture and Life Sciences, Cornell University, Ithaca, New York, 14853.

Hughes, G.O. (1997). Geological investigation of the upper Weatherly Catchment. Unpublished Report, Department of Agricultural Engineering, University of Natal, Pietermaritzburg, RSA.

Jeje, L.K., Ogunkoya, O.O. and 'Uyi, E. (1986). Subsurface flow from a forested slope in the Ife area of southwestern Nigeria. *Hydrological Sciences Journal* 31: 489-499.

Jury, W.A., Gardner, W.R. and Gardner, W.H. (1991). *Soil Physics*. 5 Edition. John Wiley and Sons Inc, USA. pp 131-134.

Kirkby, M. (1988). Hillslope runoff processes and models. *Journal of Hydrology* 100: 315-339.

Knapp, B.J. (1973). A system for the field measurement of soil water movement. *Technical Bulletin British Geomorphological Research*. No 9: pp26.

Klute, A. (1986). Methods of soil analysis. Part 1. *Physical and Mineralogical Methods.* American Society of Agronomy. Soil Science Society of America, Madison, Wisconsin, USA.

Koide, S. and Wheater, H.S. (1992). Subsurface flow simulation of a small plot at Loch Chon, Scotland. *Hydrological Processes* 6: 299-326.

Kubota, J. and Sivapalan, M. (1995). Towards a catchment-scale model of subsurface runoff generation based on synthesis of small-scale process-based modelling and field studies. *Hydrological Processes* 9: 541-554.

Larson, C.L., Onstad, C.A., Richardson, H.H. and Brooks, K.N. (1982). Some particular watershed models. *In*: Haan, C.T., Johnson, H.P and Brakensiek, D.L (Editors). *Hydrologic Modelling of Small Watersheds*. ASAE Monograph, American Society of Agricultural Engineers. USA. pp 410-412.

Lehman, O.S. and Ahuja, L.R. (1985). Interflow of water and tracer chemical on sloping field plots with exposed seepage faces. *Journal of Hydrology* 76: 307-317.

Lorentz, S.A. (1993). The use of accurate retention characteristics of porous media in hydrology. *Proceedings of the 6 South African National Hydrological Symposium*, Pietermaritzburg, RSA.

Lorentz, S.A., Durnford, D.S. and Corey , A.T. (1991). Tests of hydraulic and leaching properties of the vadose zone and groundwater: laboratory manual. Department of Agricultural and Chemical Engineering, Colorado State University, Fort Collins, Colorado, U.S.A.

Lorentz, S.A. (1997). Personal Communication. Department of Agricultural Engineering, University of Natal, Pietermaritzburg, RSA.

McDonnell, J.J., Freer, J., Hooper, R., Kendall, C., Burns, D., Bevan, K. and Peters, J. (1996). New method developed for studying flow on hillslopes. *EOS, Transactions, American Geophysical Union* 77(47): 471-472.

McCarthy, E.J., Flewelling, J.W. and Skaggs, R.W. (1991). Hydrologic model for drained forest watershed. *Journal of Irrigation and Drainage Engineering* 118: 242-255.

McCarthy, E.J., Skaggs, R.W. and Farnum, P. (1991). Experimental determination of the hydrologic components of a drained forest watershed. American Society of Agricultural Engineering. USA.

Mein, R.G. and Larson, C.L. (1973). Modelling infiltration during a steady rain. *Water Resources Research* 9: 384-394.

Morel-Seytoux, H.J., (1983). Infiltration affected by air, seal, crust, ice and various sources of heterogeneity (Special problems). *Proceedings of the ASAE National conference on : Advances in Infiltration.* Chicago, Illionois.

Mulholland, P.J., Wilson, G.V. and Jardine, P.M. (1990). Hydrogeochemical response of a forested watershed to storms : Effects of preferential flow along shallow and deep pathways. *Water Resources Research* 26: 3021-3036.

Parlange, M.B., Steenhuis, T.S., Timlin, D.J., Stagnitti, F. and Bryant, R.B. (1989). Subsurface flow above a fragipan horizon. *Soil Science* 148: 77-86.

Paterson, D.G. (1996). Ground penetrating radar investigations at Wheatherly, Maclear. Report Number GW/A/96/13. Institute for Soil, Climate and Water. RSA.

Perroux, K.M. and White, I. (1988). Designs for disk permeaters. *Soil Science Society of America Journal* 52: 1205-1215.

Peters, D.L., Buttle, J.M., Taylor, C.H. and LaZerte, B.D. (1995). Runoff production in a forested, shallow soil, Canadian Shield basin. *Water Resources Research* 31: 1291-1304.

Pilgrim, D.H., Huff, D.D. and Doak Steele, T. (1978). A field evaluation of subsurface and surface runoff. II. Runoff processes. *Journal of Hydrology* 38: 319-341.

Rawls, W.J., Ahuja, L.R., Brakensiek, D.L. and Shirmohammadi, A. (1992). Infiltration and soil water movement. *In*: Maidement, D.R. (Editor). *Handbook of Hydrology.* McGraw-Hill, Inc. New York, USA.

Reece, G. (1986). *Microcomputer Modelling by Finite Differences.* John Wiley and Sons, New York. pp 1-21.

Reynolds, W.D. (1993). Saturated hydraulic conductivity: Field measurement. *In*: Carter, M.R. (Editor). *Soil Sampling and Methods of Analysis.* Canadian Society of Soil Science. pp 599-614.

Reynolds, W.D. (1993). Unsaturated hydraulic conductivity: Field measurement. *In*: Carter, M.R. (Editor). *Soil Sampling and Methods of Analysis.* Canadian Society of Soil Science. pp 633-644.

Richards, L.A., (1931). Laws of soil moisture. *Transactions American Geophysical Union* 31: 750-756.

Roberts, V.G., Hensley, M., Smith-Baillie, A.L., and Paterson, D.G. (1996). Detailed soil survey of the Weatherly catchment. Institute for Soil, Climate and Water. Report GW/A/93/36. RSA.

Ross, P.J. (1990). SWIM, A Simulation Model for Soil Water Infiltration and Movement. CSIRO, Division of Soils, Davis Laboratory, Townsville, Qld4814, Australia.

Schulze, R.E. (1987). Hydrological science and hydrological practice: Reflections as we approach the 1990s. *Proceedings, Hydrological Sciences Symposium*, Rhodes University, Grahamstown, Department of Geography. pp 1-19.

Schulze, R.E. (1996). Personal Communication. Department of Agricultural Engineering. University of Natal, Pietermaritzburg, RSA.

Schulze, R.E. (1995). *Hydrology and Agrohydrology*: : *A Text to Accompany the ACRU 3.00 Agrohydrological Modelling System.* Water Research Commission, Pretoria, Report TT69/95. Pp AT2-1 AT2-7.

Schulze, R.E., Angus, G.R., Lynch, S.D and Smithers, J.C. (1995). *ACRU*: Concepts and Structure. *In*: Schulze, R.E. *Hydrology and Agrohydrology*: : *A Text to Accompany the ACRU 3.00 Agrohydrological Modelling System.* Water Research Commission, Pretoria, Report TT69/95. Pp AT2-1 AT2-7.

Scotcher, J. (1995). Forestry and water use: A company perspective. *SA Forestry*, May/June: 27-28.

Shaffer, K.A., Fritton, D.D. and Baker, D.E. (1979). Drainage water sampling in a wet dual-pore system. *Journal of Environmental Water Quality* 8: 241-246.

Sheldrick, B.H. and Wang, C. (1993). Particle size distribution. *In*: Carter, M.R. (Editor). *Soil Sampling and Methods of Analysis.* Canadian Society of Soil Science. pp 499-512.

Singh, V.P. (1989). *Hydrologic Systems: Watershed Modelling.* Volume 2. Prentice Hall, Englewood Cliffs, New Jersey. pp 20.

Sklash, M.G. and Farvolden, R.N. (1979). The role of groundwater in storm runoff. *Journal of Hydrology* 43: 45-65.

Sklash, M.G., Stewart, M.K. and Pearce, A.J. (1986). Storm and runoff generation in humid headwater catchments 1. A case study of hillslope and low order stream response. *Water Resources Research* 22: 1273-1282.

Sloan, P.G., Moore, I.D., Coltharp, G.B. and Eigel, J.D. (1983). Modelling surface and subsurface storm flow on steeply sloping forested watersheds. Water Resources Research Inst. Univ. of Kentucky, Lexington. 142: 4-21.

Sloan, P.G. and Moore, I.D. (1984). Modelling subsurface storm flow on steeply sloping forested watersheds. *Water Resources Research* 20: 1815-1822.

Smith, R.E. (1992). OPUS. An integrated simulation model for transport of non point source pollutant at the field scale : Volume I, Documentation. U.S. Department of Agriculture, Agricultural Research Service, ARS-98.

Smith, R.E. and Hebbert, R.H.B. (1983). Mathematical simulation of interdependent surface and subsurface hydrologic processes. *Water Resources Research* 19: 987-1001.

Stagnitti, F. and Parlange, J.Y. (1987). Streamflow generation from variable width, inclined, shallow hillslopes. *Mechanical Engineering Transactions* 12: 2-9.

Summerton, M.J. (1995). *Process and Modelling Studies in Forest Hydrology*. Unpublished MSc. dissertation, Department of Agricultural Engineering, University of Natal, Pietermaritzburg, RSA.

Thompson, J.C. and Moore, R.D. (1996). Relations between topography and water table depth in a shallow forest soil. *Hydrological Processes* 10: 1513-1525.

Topp, G.C. (1993). Soil water content. *In*: Carter, M.R. (Editor). *Soil Sampling and Methods of Analysis*. Canadian Society of Soil Science. Canada. pp 541-558.

Topp, G.C., Galganov, B.C., Ball, B.C. and Carter, M.R. (1993). Soil water desorption curves. *In*: Carter, M.R. (Editor). *Soil Sampling and Methods of Analysis.* Canadian Society of Soil Science. Canada. pp 569-580.

Trudgill, S.T., Pickles, A.M., Smettem, K.R.J. and Crabtree, R.W. (1983). Soil-water residence time and solute uptake. *Journal of Hydrology* 60: 257-279.

Tsukamoto, Y. and Ohta, T. (1988). Runoff processes on a steep forested slope. *Journal of Hydrology* 102: 165-178.

Tsuboyama, Y., Sidle, R.C., Noguchi, S. and Hosoda, I. (1994). Flow and solute transport through the soil matrix and macropores of a hillslope segment. *Water Resources Research* 30: 879-890.

Turton, D.J., Barnes, D.R. and de Jesus Navar. J. (1995). Old and new water in subsurface flow from a forest soil block. *Journal of Environmental Quality* 24: 139-146.

Turton, D.J., Haan, C.T. and Miller, E.L. (1992). Subsurface flow responses of a small forested catchment in the Ouachita mountains. *Hydrological Processes* 16: 111-125.

van Genuchtin, M. Th. (1980). A closed form equation for predicting the hydraulic conductivity of unsaturated soils. *Soil Science Society of America Journal* 44: 892-898.

Ward, R.C., 1975. *Principles of Hydrology.* McGraw-Hill Book Company (UK) Limited. pp 7-9.

Wagenet, R.J. (1988). Modelling soil hydrology: Perspectives, perils and directions. Modelling Agricultural Forest and Rangeland Hydrology. Proceedings of International Symposium. Chicago, Illinois ASAE Publication 07-88.

Wallach, R. and Zaslavsky, D. (1991). Lateral flow in a layered profile of an infinite uniform slope. *Water Resources Research* 27: 1809-1818.

Wang, D., Norman, J.M. and McSweeney, K. (1994). Nondestructive determination of hydrogeometrical characteristics of soil macropores. *Soil Science Society of America Journal* 58: 294-303.

Weyman, D.R. (1973). Measurements of the downslope flow of water in a soil. *Journal of Hydrology* 20: 267-288.

Whipkey, R.J. and Kirkby, M.J. (1978). Flow within the soil. *In* : Kirkby, M. J. (Editor) *Hillslope Hydrology*. John Wiley & Sons. England.

Wilson, G.V., Jardine, P.M., Luxmoore, R.J. and Jones, J.R. (1990). Hydrology of a forested watershed during storm events. *Geoderma* 46: 119-138.

Wilson, G.V., Jardine, P.M., Luxmoore, R.J., Zelanzny, L.W., Lietzke, D.A. and Todd, D.E. (1991). Hydrogeochemical processes controlling subsurface transport from an upper catchment of Walker Branch watershed during storm events. 1. Hydrologic transport processes. *Journal of Hydrology* 123: 297-316.

Wilson, G.W., Jardine, P.M., O'Dell and Collineau, M. (1993). Field-scale transport from a buried line source in variably saturated soil. *Journal of Hydrology* 145: 83-109.

APPENDIX A

Data relating to soil surface and bedrock elevations above a reference point (1300 m), located just below GW4. Included is the actual soil depth. GW and RO refers to groundwater access tubes and there locations are shown in Figure 21.

Location	Soil Surface (m)	Bedrock Surface (m)	Soil Depth (m)	Position on Hillslope
GW 1	20.27	19.5	1.12	Crest
GW 2	12.9	10.63	2.3	Midslope
GW 3	5.49	2.39	3.1	Midslope
GW 4	1.36	0.17	1.19	Toe
GW 3/4	3.22	0.3	2.92	Toe
GW 3/4A	2.24	1.39	0.85	Toe
GW 3/4B	2.75	0.36	2.39	Toe
GW 3A	4.71	1.81	2.9	Midslope
GW 3B	6.67	4.64	1.84	Midslope
RO 1	9.35	7.83	1.52	Midslope
RO 2	3.64	2.2	1.44	Toe

APPENDIX B

Calibration equations for all pressure transducers to convert electronic signal to a corresponding matric potential of the soil.

Transducer Number	Regression Equation
1	-33.8358 + 167.6322 (V)
2	-32.4398 + 167.6632 (V)
3	-31.7327 + 167.6288 (V)
4	-33.3452 + 168.8932 (V)
5	-32.3604 + 168.089 (V)
6	-30.447 + 166.8813 (V)
7	-32.4645 + 167.858 (V)
8	-32.6861 + 168.4173 (V)
9	-34.0115 + 167.7089 (V)
10	-33.064 + 167.2951 (V)
11	-32.7096 + 168.5667 (V)
12	-33.1953 + 167.9024 (V)
13	-33.9398 + 168.1365 (V)
14	-39.3731 + 168.8522 (V)
15	-30.7445 + 168.8286 (V)
16	-33.1193 + 167.5022 (V)
17	-31.7402 + 168.001 (V)
18	-30.9472 + 167.9014 (V)
19	-32.1072 + 168.255 (V)
20	-31.4514 + 167.6894 (V)
21	-33.072 + 169.0521 (V)
24	-32.7788 + 169.2027 (V)

APPENDIX C

Specifications and limitations of the loggers.

Resolution	12 bits (4096 counts)
A/D Reference Voltage	5 Volts
Number of channels	4
Memory Capacity	64k bytes
Memory type	Non-volatile Serial EEPROM
Maximum number of samples	8191 (x 4 channels)
Averaging	Average of 256 samples per point per channel
Logging Interval	Pre-set to 12 minutes
Warm-up delay	16 seconds
Comm port	RS232 (9600bd, no parity, 1 stop bit, hardware flow control)
Data format	ASCII text file, tab delimited, one data set per row
ASCII File Size	172032 bytes
Download time	2 min 51 sec
Pressure Sensors	Motorola MPX5100DP
Power Supply	6 Volts dc
Battery	6 Volt 7Ah, Sealed Lead Acid

APPENDIX D

The following tables give information relating to the tensiometer and transducer number with tensiometer lengths and depths below the soil surface for each tensiometer nest shown in Figure 21. The transducer number is related to the equations shown in Appendix B.

NEST 1

Tensiometer Number	Transducer Number	Tensiometer Length (m)	Depth Below Soil (m)
1	1	0.235	0.115
2	2	0.34	0.23
3	3	0.67	0.50
4	4	0.94	0.77

NEST 2

Tensiometer Number	Transducer Number	Tensiometer Length (m)	Depth Below Soil (m)
1	5	0.34	0.22
2	6	0.64	0.51
3	7	0.94	0.79
4	8	1.275	1.02

NEST 3

Tensiometer Number	Transducer Number	Tensiometer Length (m)	Depth Below Soil (m)
1	9	0.34	0.206
2	10	0.64	0.5
3	11	0.94	0.82
4	12	1.25	1.03

NEST 3/4

Tensiometer Number	Transducer Number	Tensiometer Length (m)	Depth Below Soil (m)
1	16	0.235	0.12
2	17	0.34	0.20
3	18	0.64	0.488
4	19	1.25	1.03

NEST 4

Tensiometer Number	Transducer Number	Tensiometer Length (m)	Depth Below Soil (m)
1	13	0.235	0.12
2	14	0.37	0.24
3	15	0.64	0.46

APPENDIX E

Example of water retention characteristic curve fitting procedure using Brooks and Corey (1964) parameters. Shown is the water content and matric potential values derived from the controlled outflow cell with effective water contents (Se) values calculated using Brooks and Corey (1964) equations.

Matric Pressure Cell, Channel 1B, Pit 2A - Soil Surface

Burette	W.cont	Ch1	Matr.p		
ml	(m3/m3)	mV	(m)	Se	Se
44.0	0.341	-20.13	0.001	1	
43.0	0.341	-19.61	0.005	1	
42.0	0.341	-19.56	0.006	1	
41.0	0.341	0.15	0.203	1	
40.0	0.341	0.53	0.207	1	
39.0	0.341	7.15	0.273	1.000	
38.0	0.326	18.27	0.384	0.949	
37.0	0.311	25.27	0.454	0.899	
36.0	0.297	33.98	0.541	0.848	
35.0	0.282	41.18	0.613	0.797	
34.2	0.270	48.91	0.690	0.757	
32.3	0.242	77.17	0.973	0.661	
31.0	0.223	96.00	1.161	0.595	
30.3	0.213	110.67	1.308	0.560	
29.2	0.197	133.07	1.532	0.504	
28.2	0.182	164.89	1.850	0.454	
27.2	0.167	210.94	2.310	0.403	
26.7	0.160	241.86	2.620	0.378	
			30	1	0.10
lamda	0.5		50	1	0.52
residual	0.05		70	1	0.57
hd	40		90	1	20.28
			110	1	20.66
Wet mass	210.3		130	1	27.28
Dry mass	199.6		150	1	38.40
Tare	82.8		170	0.939	45.40
Extra	6.2		190	0.860	54.11
Ex tare	4.4		210	0.808	61.31
Bulk den	1.746		230	0.761	69.04
Porosity	0.341		250	0.678	86.96
Final W.C.	0.160		270	0.641	97.30
			350	0.511	153.20
			370	0.465	185.02
			390	0.416	231.07
			430	0.365	300

APPENDIX F

Particle Size Distribution Data Together with Resulting Particle Size Distribution Curves

Table F1.

Pit 1, 0.10m

Size (mm)	% finer
0.0742	18.19
0.0533	14.90
0.0381	12.82
0.0314	10.62
0.0274	9.28
0.0246	8.30
0.0174	7.57
0.0143	6.96
0.0124	6.96
0.0101	6.11
0.0073	5.86
0.0060	4.88
0.0052	4.27
0.0046	3.91
0.0042	3.30
0.0015	3.17
2	97.558
1	77.253
0.5	48.376
0.25	30.830
0.106	22.772
0.053	15.519

Table F2.

Pit 1, 0.50m

Size (mm)	% finer
0.0687	30.77
0.0493	28.33
0.0357	23.57
0.0295	21.86
0.0256	20.88
0.0230	20.02
0.0165	17.95
0.0135	16.48
0.0117	16.00
0.0096	15.14
0.0069	13.92
0.0056	13.55
0.0049	12.70
0.0044	12.58
0.0040	12.45
0.0014	10.13
2	96.899
1	90.647
0.5	71.685
0.25	43.248
0.106	33.272
0.053	27.509

Table F3.

Pit 1, 1.10m

Size (mm)	% finer
0.0704	26.13
0.0503	24.18
0.0359	22.34
0.0295	21.12
0.0256	20.76
0.0230	20.02
0.0163	19.54
0.0134	18.68
0.0116	18.44
0.0095	18.44
0.0067	17.58
0.0055	16.61
0.0048	15.63
0.0043	14.90
0.0040	13.92
0.0014	13.43
2	96.007
1	89.988
0.5	67.045
0.25	32.125
0.106	26.606
0.053	22.210

Table F4.

Pit 2, 0.26m

Size (mm)	% finer
0.0736	27.14
0.0525	25.71
0.0374	24.17
0.0310	21.43
0.0269	20.95
0.0243	19.40
0.0172	19.40
0.0141	17.86
0.0122	17.86
0.0100	17.38
0.0058	16.43
0.0050	15.48
0.0045	15.24
0.0042	14.05
0.0015	14.05
2	94.393
1	91.190
0.5	66.012
0.25	38.917
0.106	29.452
0.053	23.321

Table F5.

Pit 2, 0.60m

Size (mm)	% finer
0.0689	40.48
0.0495	38.10
0.0355	35.71
0.0293	34.29
0.0257	32.14
0.0230	31.90
0.0163	31.19
0.0134	30.36
0.0116	29.76
0.0095	29.17
0.0056	27.50
0.0048	26.79
0.0043	26.55
0.0040	26.43
0.0014	23.81
2	89.048
1	82.321
0.5	56.071
0.25	42.143
0.106	34.024
0.053	26.798

Table F6.

Pit 2, 1.80m

Size (mm)	% finer
0.0631	50.95
0.0454	48.57
0.0329	45.00
0.0274	42.38
0.0240	40.83
0.0216	39.76
0.0156	36.67
0.0128	34.88
0.0112	34.29
0.0092	33.33
0.0054	28.57
0.0048	27.14
0.0043	26.90
0.0039	26.55
0.0014	22.62
2	96.226
1	95.810
0.5	95.357
0.25	93.929
0.106	64.500
0.053	48.905

Table F7.

Pit 3, 0.20m

Size (mm)	% finer
0.0731	26.97
0.0524	24.60
0.0377	21.06
0.0312	18.93
0.0273	16.92
0.0244	16.92
0.0173	16.80
0.0141	16.68
0.0122	16.32
0.0100	15.38
0.0051	12.54
0.0046	12.18
0.0042	12.18
0.0015	11.59
2	73.693
1	70.960
0.5	54.045
0.25	39.378
0.106	24.308
0.053	15.661

Table F8.

Pit 3, 0.40m

Size (mm)	% finer
0.0686	37.62
0.0502	31.94
0.0361	29.34
0.0296	28.39
0.0258	26.97
0.0231	26.97
0.0166	24.60
0.0135	24.49
0.0117	24.49
0.0096	24.01
0.0048	22.47
0.0043	22.00
0.0040	22.00
0.0014	21.06
2	92.418
1	87.024
0.5	58.978
0.25	45.091
0.106	32.411
0.053	23.468

Table F9.

Pit 3, 2.10m

Size (mm)	% finer
0.0628	52.64
0.0450	50.86
0.0327	47.31
0.0268	46.37
0.0234	45.19
0.0210	44.71
0.0151	42.58
0.0124	41.28
0.0108	40.81
0.0089	39.27
0.0045	37.14
0.0040	36.67
0.0037	35.72
0.0013	33.12
2	106.518
1	93.305
0.5	73.728
0.25	66.087
0.106	57.949
0.053	50.887

Table F10.

Pit 4, Surface

Size (mm)	% finer
0.0719	25.35
0.0525	19.13
0.0380	14.59
0.0312	13.15
0.0271	12.56
0.0243	12.20
0.0173	10.76
0.0141	10.52
0.0122	10.52
0.0100	9.57
0.0072	9.57
0.0059	9.57
0.0046	8.37
0.0042	8.37
0.0015	8.37
2	97.285
1	82.576
0.5	66.790
0.25	41.916
0.106	24.265
0.053	17.376

Table F11.

Pit 4, 0.20m

Size (mm)	% finer
0.0687	33.48
0.0493	31.09
0.0357	26.91
0.0295	24.16
0.0257	22.96
0.0231	22.72
0.0164	21.29
0.0135	19.37
0.0117	19.73
0.0096	19.73
0.0069	19.73
0.0056	17.94
0.0044	17.34
0.0040	16.98
0.0014	16.98
2	104.592
1	101.327
0.5	70.557
0.25	54.042
0.106	36.307
0.053	28.067

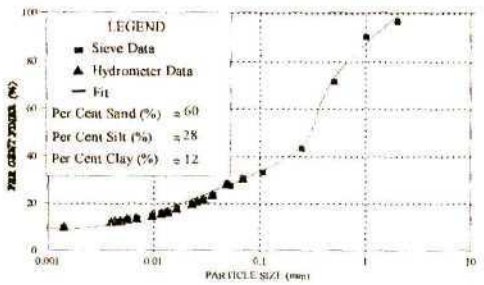

Figure1F. Pit 1, 0.50m

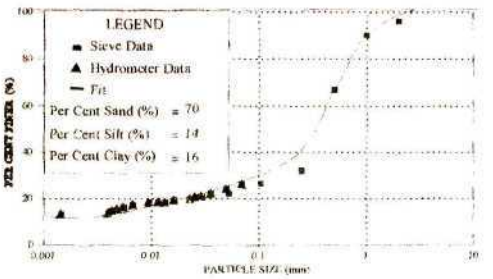

Figure 2F. Pit 1, 1.10m

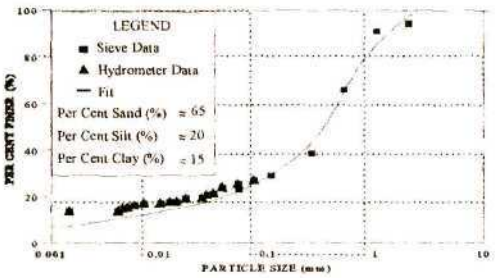

Figure 3F. Pit 2, 0.26m

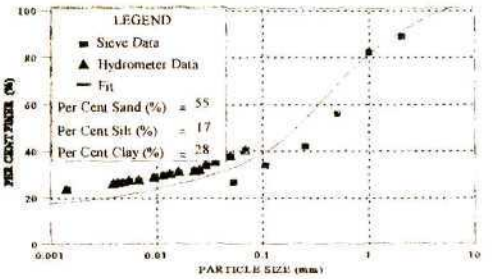

Figure 4F. Pit 2, 0.60m

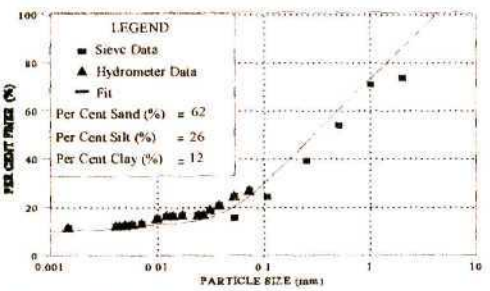

Figure 6F. Pit 3, 0.20m

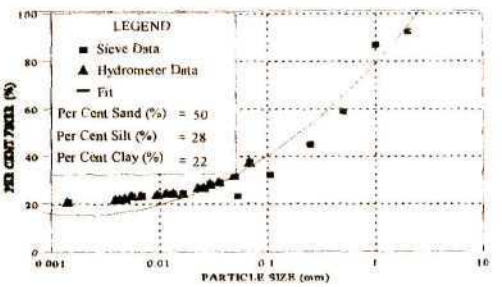

Figure 7F. Pit 3, 0.40m

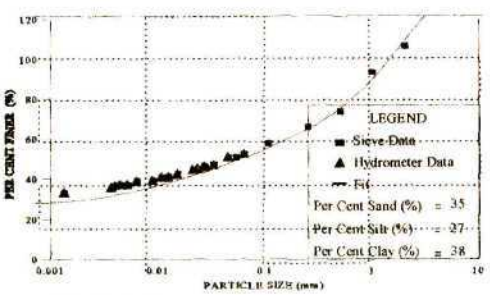

Figure 8F. Pit 3, 2.10m

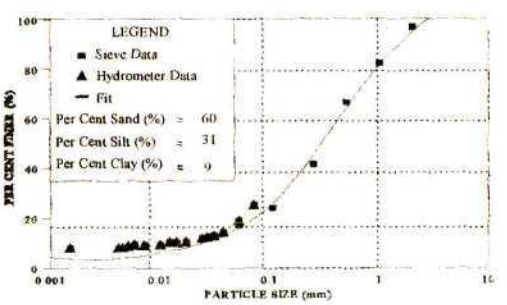

Figure 9F. Pit 4, surface

APPENDIX G

Hydraulic conductivity data, water retention and hydraulic conductivity characteristic curves

Table G1, Pit 1, 0.40m

Tension (mm)	Steady State Inflow ($mm.h^{-1}$)	Initial Hydraulic Conductivity ($mm.h^{-1}$)	Final Hydraulic Conductivity ($mm.h^{-1}$)	Saturated Hydraulic Conductivity ($mm.h^{-1}$)
5	3648.8400	36.0629	36.0629	
50	1353.3600	0.6961	7.0360	
100	320.2200	1.3784	1.3784	
0				353.8800

Table G2,Pit 1, 0.70m, Rep 1

Tension (mm)	Steady State Inflow ($mm.h^{-1}$)	Initial Hydraulic Conductivity ($mm.h^{-1}$)	Final Hydraulic Conductivity ($mm.h^{-1}$)	Saturated Hydraulic Conductivity ($mm.h^{-1}$)
5	6282.0000	42.2644	42.2644	
50	3972.0000	26.1317	26.4274	
100	1248.0000	1.6363	1.6363	
0				345.2400

Table G3, Pit 1, 0.70m, Rep 2

Tension (mm)	Steady State Inflow ($mm.h^{-1}$)	Initial Hydraulic Conductivity ($mm.h^{-1}$)	Final Hydraulic Conductivity ($mm.h^{-1}$)	Saturated Hydraulic Conductivity ($mm.h^{-1}$)
5	5790.0000	52.8224	52.8224	
50	2556.0000	1.3062	12.3123	
100	2424.0000	9.4401	9.4401	
0				225.0000

Table G4, Pit 2, Soil surface

Tension (mm)	Steady State Inflow ($mm.h^{-1}$)	Initial Hydraulic Conductivity ($mm.h^{-1}$)	Final Hydraulic Conductivity ($mm.h^{-1}$)	Saturated Hydraulic Conductivity ($mm.h^{-1}$)
5	501.7391	2.2027	2.2027	
50	321.2579	1.6587	1.5345	
100	171.5600	0.6171	0.7514	
165	103.9783	0.3740	0.3740	
0				492.8400

Table G5, Pit 2, 0.20m

Tension (mm)	Steady State Inflow ($mm.h^{-1}$)	Initial Hydraulic Conductivity ($mm.h^{-1}$)	Final Hydraulic Conductivity ($mm.h^{-1}$)	Saturated Hydraulic Conductivity ($mm.h^{-1}$)
5	228.7800	0.7163	0.7163	
50	195.0600	0.6353	0.6230	
100	129.9600	0.4157	0.4195	
165	81.6000	0.2610	0.2610	
0				162.3600

Table G6, Pit 2, 0.60m

Tension (mm)	Steady State Inflow ($mm.h^{-1}$)	Initial Hydraulic Conductivity ($mm.h^{-1}$)	Final Hydraulic Conductivity ($mm.h^{-1}$)	Saturated Hydraulic Conductivity ($mm.h^{-1}$)
5	8074.7400	61.1866	61.1866	
50	4598.2200	19.4736	27.1584	
100	2592.6600	11.3939	11.1870	
165	1272.3600	5.5916	5.5916	
0				552.2400

Table G7, Pit 2, 0.60m, Rep 1

Tension (mm)	Steady State Inflow (mm/hr)	Initial Hydraulic Conductivity (mm/hr)	Final Hydraulic Conductivity (mm/hr)	Saturated Hydraulic Conductivity (mm/hr)
5	1128.0000	7.4933	7.4933	
50	720.0000	4.4415	4.6122	
100	258.0000	1.1392	1.3654	
165	126.0000	0.5564	0.5564	
0				117.0000

Table G8, Pit 2, 0.60m, Rep 2

Tension (mm)	Steady State Inflow ($mm.h^{-1}$)	Initial Hydraulic Conductivity ($mm.h^{-1}$)	Final Hydraulic Conductivity ($mm.h^{-1}$)	Saturated Hydraulic Conductivity ($mm.h^{-1}$)
5	20136.0000	148.5711	148.5711	
50	11772.0000	53.8538	70.3561	
100	6216.0000	29.3386	28.8876	
165	2820.0000	13.3100	13.3100	
0				327.2400

Table G9 , Pit 2, 0.90 m

Tension (mm)	Steady State Inflow ($mm.h^{-1}$)	Initial Hydraulic Conductivity ($mm.h^{-1}$)	Final Hydraulic Conductivity ($mm.h^{-1}$)	Saturated Hydraulic Conductivity ($mm.h^{-1}$)
5	1301.7000	12.0280	12.0280	
50	560.9400	2.6874	3.9353	
100	283.3800	1.3405	1.3491	
165	128.2200	0.6065	0.6065	
0				151.9200

Table G10, Pit 2, 1.40m

Tension (mm)	Steady State Inflow ($mm.h^{-1}$)	Initial Hydraulic Conductivity ($mm.h^{-1}$)	Final Hydraulic Conductivity ($mm.h^{-1}$)	Saturated Hydraulic Conductivity ($mm.h^{-1}$)
5	219.7200	1.7067	1.7067	
50	121.8840	0.4199	0.6833	
100	78.8160	0.2430	0.2572	
165	50.5362	0.1558	0.1558	
0				3.2400

Table G11, Pit 3, Soil surface, Rep 1

Tension (mm)	Steady State Inflow ($mm.h^{-1}$)	Initial Hydraulic Conductivity ($mm.h^{-1}$)	Final Hydraulic Conductivity ($mm.h^{-1}$)	Saturated Hydraulic Conductivity ($mm.h^{-1}$)
5	858.1682	6.4818	6.4818	
50	490.3030	1.6947	2.6990	
100	316.4637	1.0014	1.0476	
165	199.9445	0.6327	0.6327	
0				329.4000

Table G12, Pit 3, Soil surface, Rep 2

Tension (mm)	Steady State Inflow ($mm.h^{-1}$)	Initial Hydraulic Conductivity ($mm.h^{-1}$)	Final Hydraulic Conductivity ($mm.h^{-1}$)	Saturated Hydraulic Conductivity ($mm.h^{-1}$)
5	347.9038	2.7196	2.7196	
50	191.6408	0.3881	0.9431	
100	152.1159	0.3397	0.3239	
165	112.4625	0.2512	0.2512	
0				289.8000

Table G13, Pit 3, 0.20m

Tension (mm)	Steady State Inflow ($mm.h^{-1}$)	Initial Hydraulic Conductivity ($mm.h^{-1}$)	Final Hydraulic Conductivity ($mm.h^{-1}$)	Saturated Hydraulic Conductivity ($mm.h^{-1}$)
5	935.4000	6.6255	6.6255	
50	567.4200	0.3595	2.1893	
100	397.0800	0.4868	0.4868	
0				97.5600

Table G14, Pit 3, 0.50m

Tension (mm)	Steady State Inflow ($mm.h^{-1}$)	Initial Hydraulic Conductivity ($mm.h^{-1}$)	Final Hydraulic Conductivity ($mm.h^{-1}$)	Saturated Hydraulic Conductivity ($mm.h^{-1}$)
5	165.4200	0.7223	0.7223	
50	129.7200	0.4412	0.5038	
100	84.4800	0.3010	0.2942	
165	49.5000	0.1764	0.1764	
0				52.2000

Table G15, Pit 3, 0.70m

Tension (mm)	Steady State Inflow ($mm.h^{-1}$)	Initial Hydraulic Conductivity ($mm.h^{-1}$)	Final Hydraulic Conductivity ($mm.h^{-1}$)	Saturated Hydraulic Conductivity ($mm.h^{-1}$)
5	4092.0000	33.6107	33.6107	
50	2124.0000	10.6761	14.0611	
100	1020.0000	4.2425	4.6847	
165	528.0000	2.1961	2.1961	
0				73.4400

Table G16, Pit 3, 1.40m

Tension (mm)	Steady State Inflow ($mm.h^{-1}$)	Initial Hydraulic Conductivity ($mm.h^{-1}$)	Final Hydraulic Conductivity ($mm.h^{-1}$)	Saturated Hydraulic Conductivity ($mm.h^{-1}$)
5	185.7000	1.5279	1.5279	
50	96.1800	0.1030	0.4472	
100	85.7400	0.2384	0.1651	
165	57.9600	0.1612	0.1612	
0				8.2800

Table G17, Pit 4, 0.20m, Rep 1

Tension (mm)	Steady State Inflow ($mm.h^{-1}$)	Initial Hydraulic Conductivity ($mm.h^{-1}$)	Final Hydraulic Conductivity ($mm.h^{-1}$)	Saturated Hydraulic Conductivity ($mm.h^{-1}$)
5	1922.2800	10.6767	10.6767	
50	1367.8800	3.1547	5.3761	
100	1046.1600	2.1619	2.2873	
165	793.6800	1.6402	1.6402	
0				25.2000

Table G18, Pit 4, 0.40m, Rep 1

Tension (mm)	Steady State Inflow ($mm.h^{-1}$)	Initial Hydraulic Conductivity ($mm.h^{-1}$)	Final Hydraulic Conductivity ($mm.h^{-1}$)	Saturated Hydraulic Conductivity ($mm.h^{-1}$)
5	853.5000	5.9212	5.9212	
50	526.8000	1.9385	2.7966	
100	327.7200	1.3780	1.2920	
165	167.9400	0.7062	0.7062	
0				54.0000

Table G19, Pit 4, 0.40m, Rep 2

TENSION (mm)	**Steady State Inflow ($mm.h^{-1}$)**	**Initial Hydraulic Conductivity ($mm.h^{-1}$)**	**Final Hydraulic Conductivity ($mm.h^{-1}$)**	**Saturated Hydraulic Conductivity ($mm.h^{-1}$)**
5	325.2000	3.6358	3.6358	
50	76.9800	0.8607	0.8607	
0				49.3200

Table G20, Pit 4, 0.60m

Tension (mm)	**Steady State Inflow ($mm.h^{-1}$)**	**Initial Hydraulic Conductivity ($mm.h^{-1}$)**	**Final Hydraulic Conductivity ($mm.h^{-1}$)**	**Saturated Hydraulic Conductivity ($mm.h^{-1}$)**
5	1609.3800	12.9230	12.9230	
50	859.3200	3.9576	5.4289	
100	450.9600	2.0769	2.0769	
0				22.3200

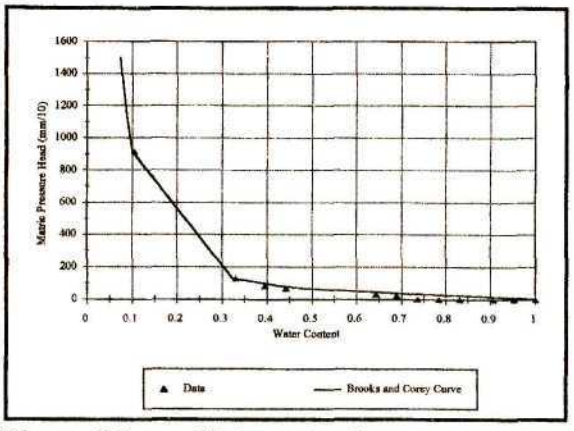

Figure G1. Water retention characteristic. Pit 1, 0.20m.

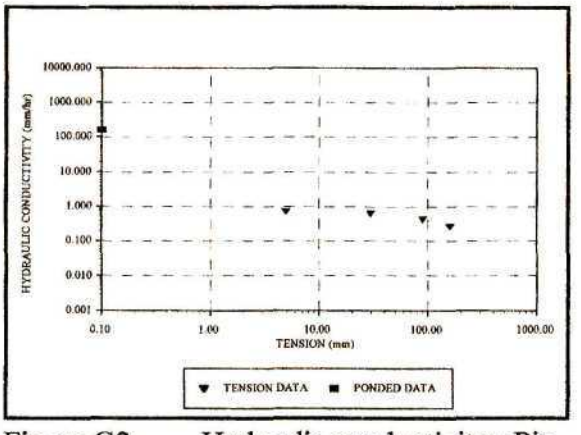

Figure G2. Hydraulic conductivity: Pit 1, 0.20m.

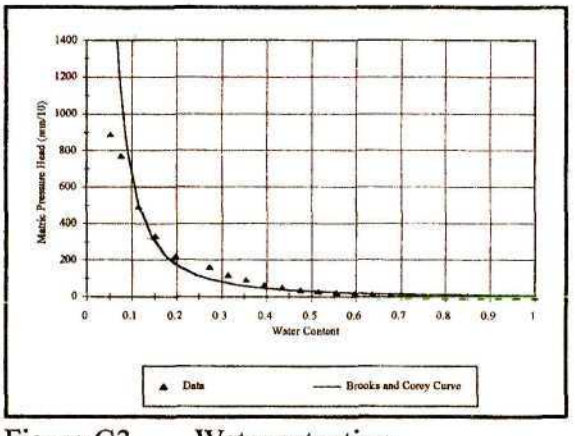

Figure G3. Water retention characteristic. Pit 1, 0.4m.

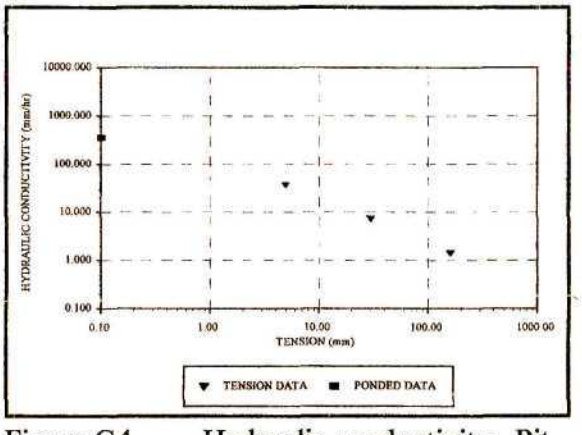

Figure G4. Hydraulic conductivity: Pit 1, 0.4m.

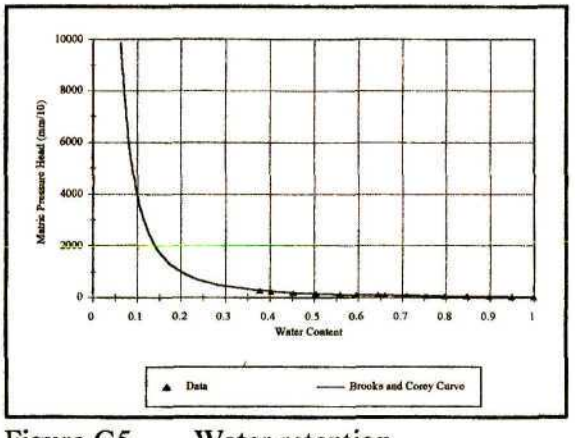

Figure G5. Water retention characteristic. Pit 2, soil surface.

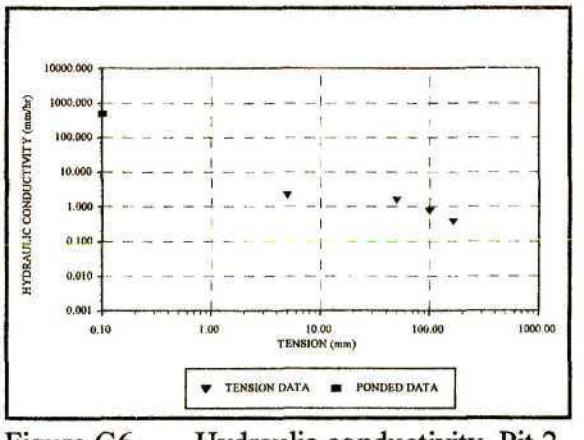

Figure G6. Hydraulic conductivity. Pit 2, soil surface.

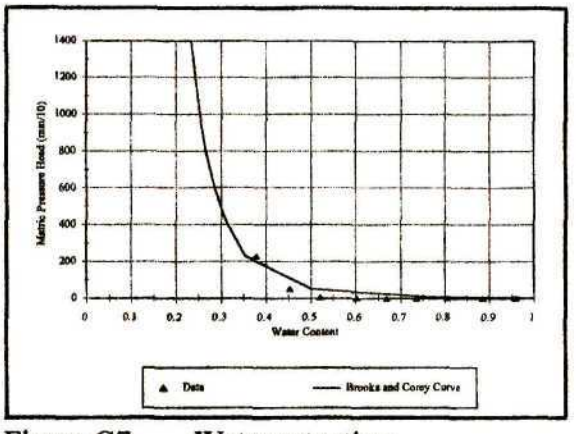

Figure G7. Water retention characteristic. Pit 2, 0.20m.

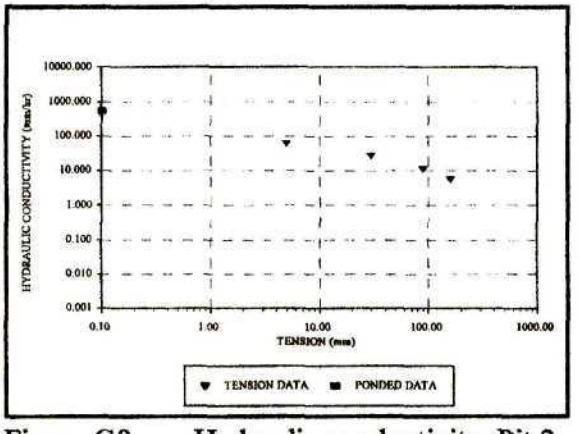

Figure G8. Hydraulic conductivity. Pit 2, 0.40m.

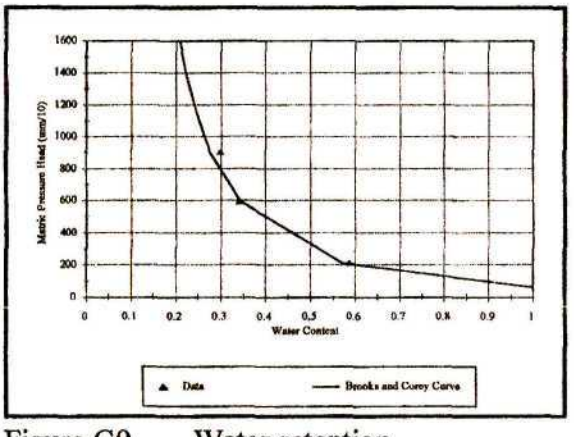

Figure G9. Water retention characteristic. Pit 2, 0.40m.

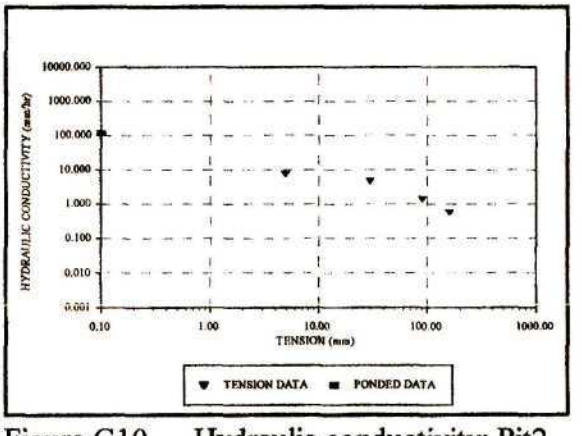

Figure G10. Hydraulic conductivity: Pit2, 0.60m.

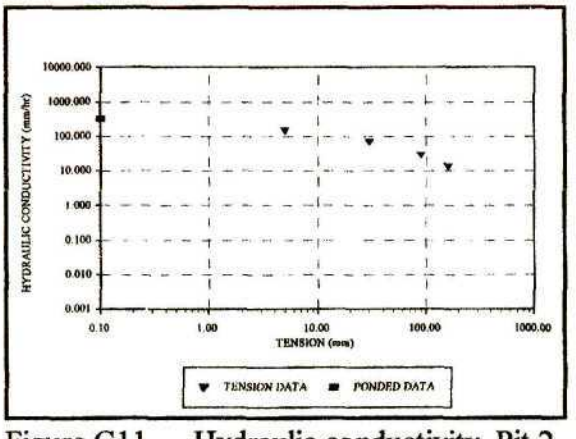

Figure G11. Hydraulic conductivity. Pit 2, 0.60m.

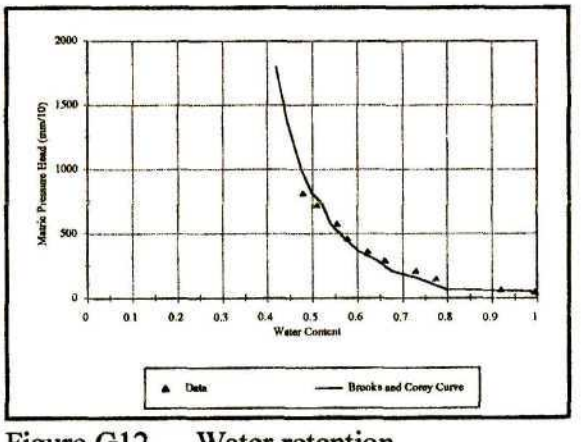

Figure G12. Water retention characteristic. Pit 2, 0.90m.

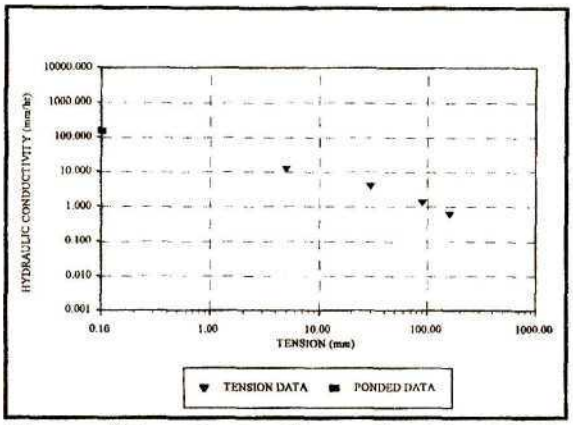

Figure G13. Hydraulic conductivity. Pit 2, 0.90m.

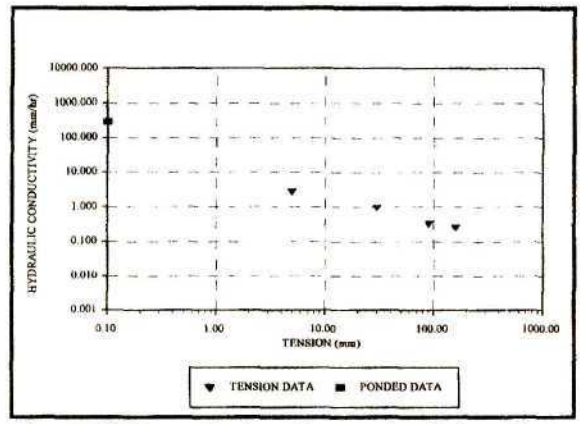

Figure G14. Hydraulic conductivity. Pit 3, soil surface.

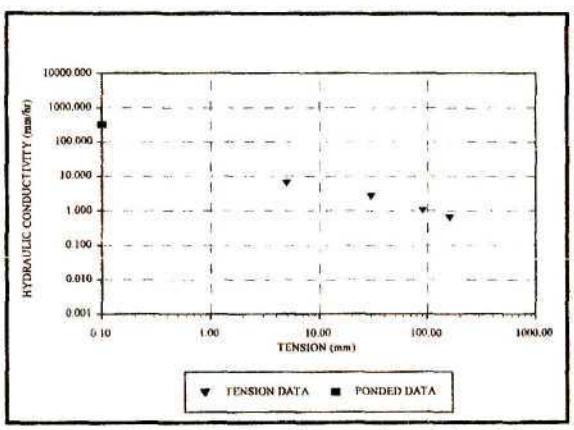

Figure G15. Hydraulic conductivity: Pit 3, soil surface.

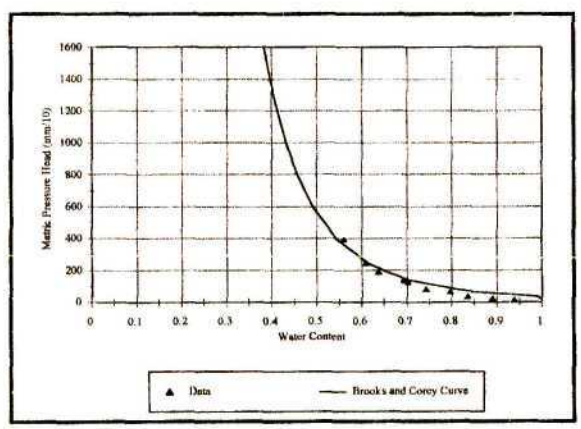

Figure G16 . Water retention characteristic. Pit 3, 0.50m.

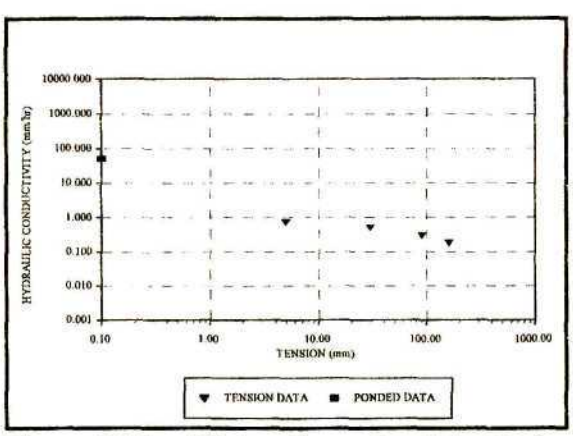

Figure G17. Hydraulic conductivity.Pit 3, 0.50m.

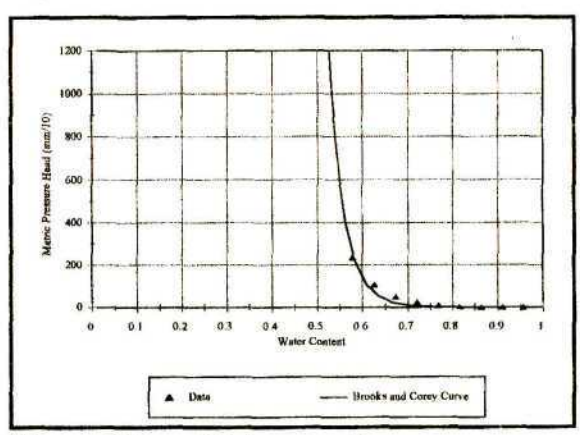

Figure G18. Water retention characteristic. Pit 3, 0.70m.

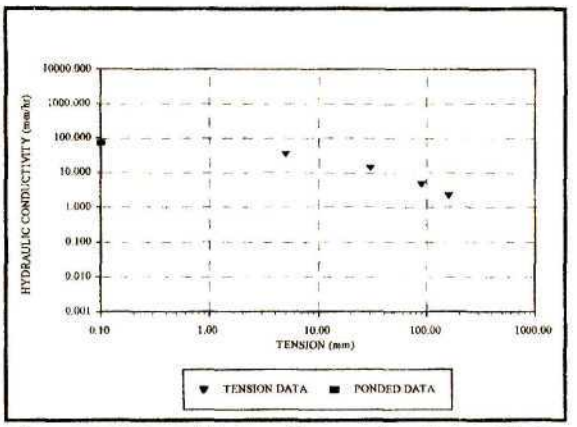

Figure G19. Hydraulic conductivity. Pit 3, 0.70m

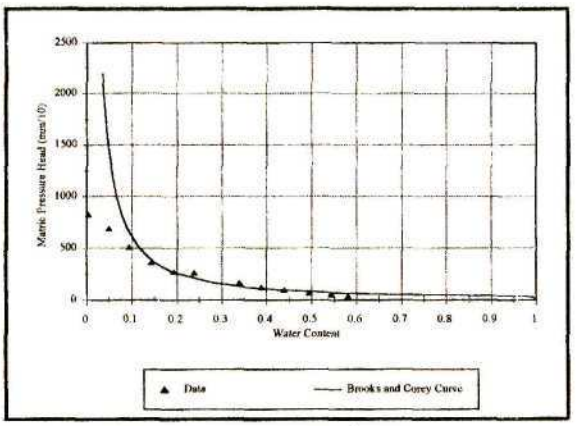

Figure G20. Water retention characteristic. Pit 3, 1.40m.

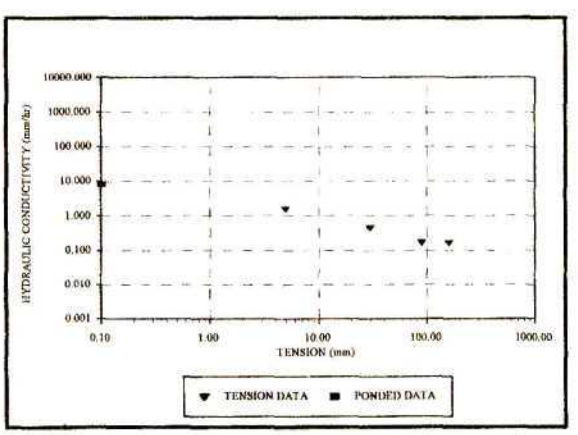

Figure G21. Hydraulic conductivity. Pit 3, 1.40m.

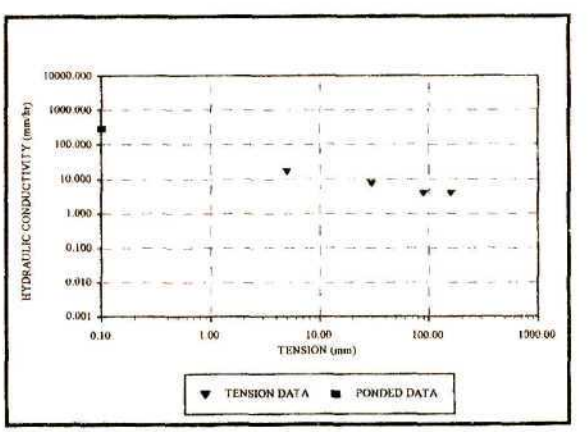

Figure G22. Hydraulic conductivity: Pit 4, soil surface.

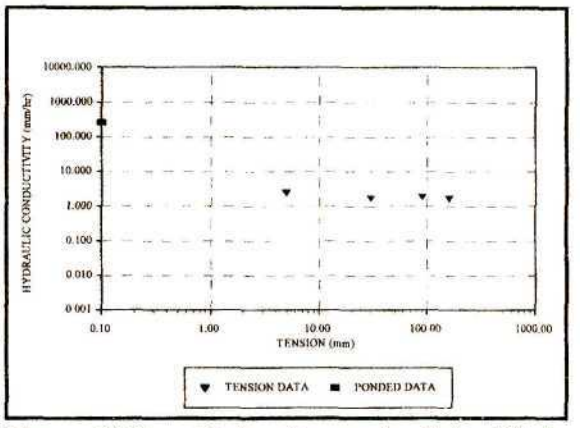

Figure G23. Hydraulic conductivity: Pit 4, 0.20m.

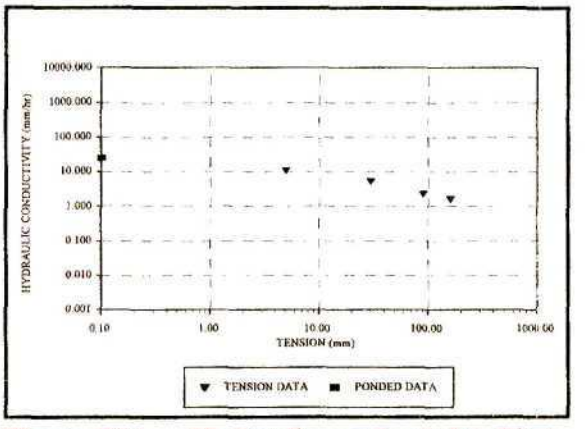

Figure G24. Hydraulic conductivity. Pit 4, 0.20m.

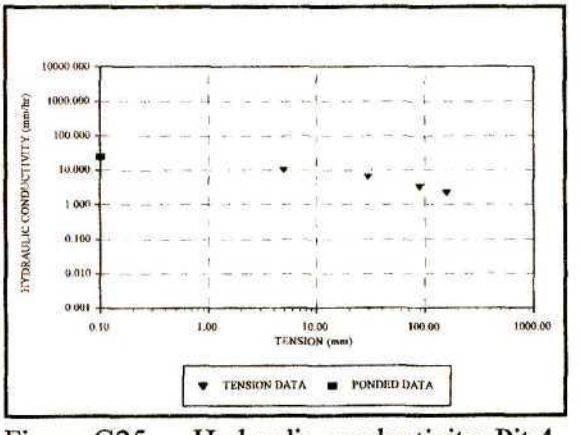

Figure G25. Hydraulic conductivity. Pit 4, 0.40m.

APPENDIX H

Tensiometer, soil moisture and groundwater data

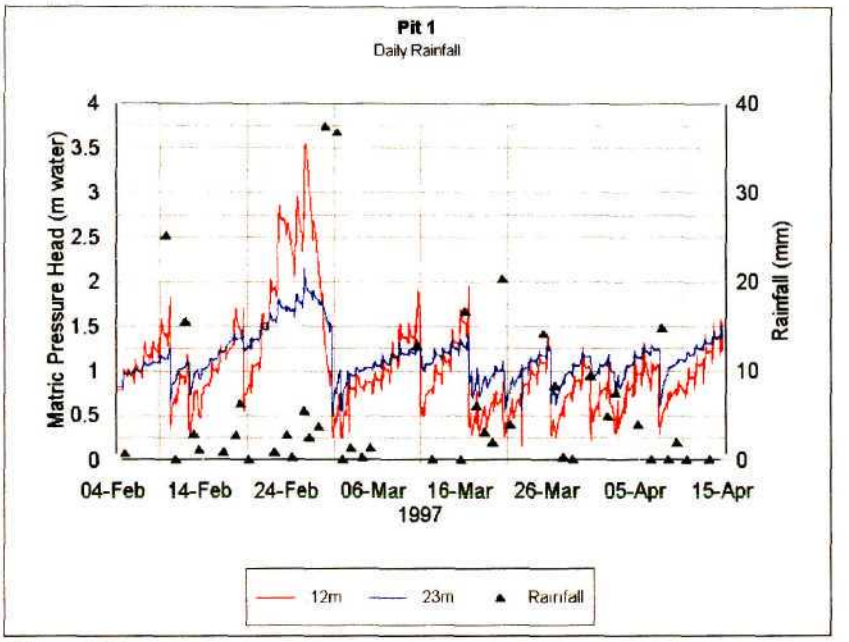

Figure H1

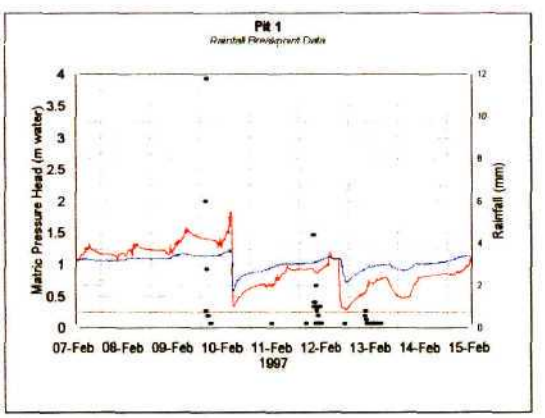

Figure H2

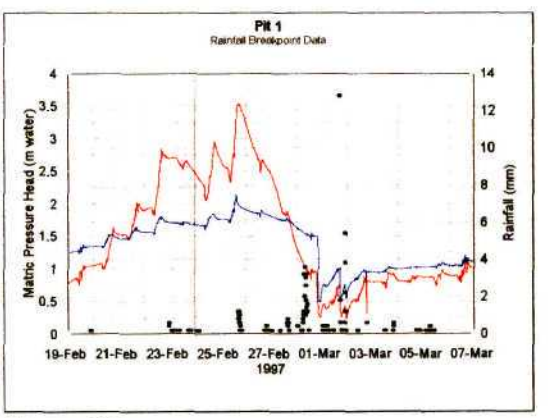

Figure H3

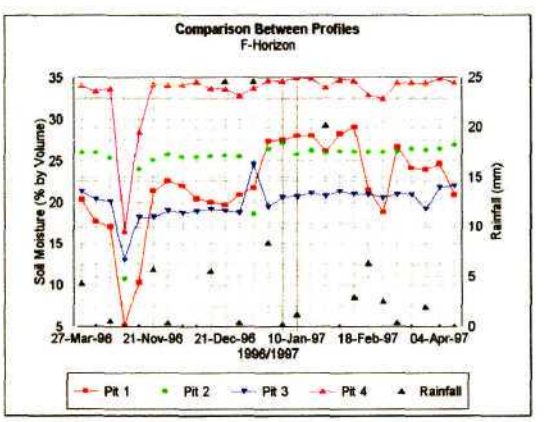

Figure H4

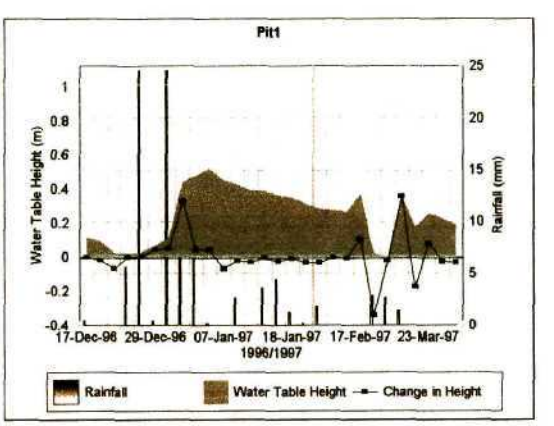

Figure H5

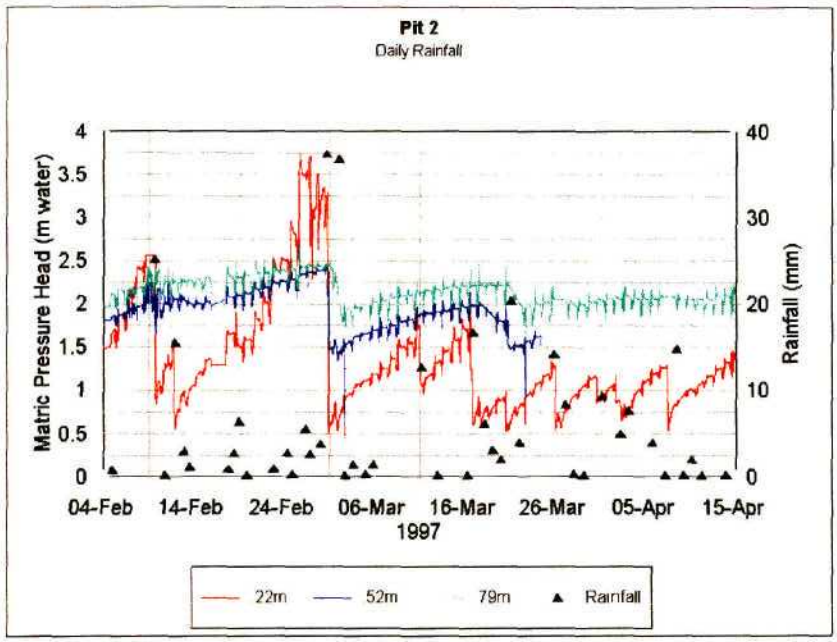

Figure H6

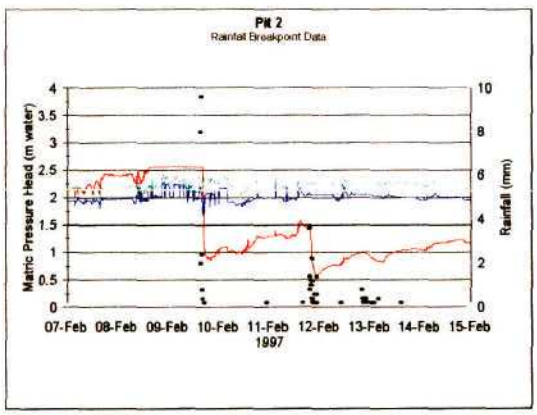

Figure H7

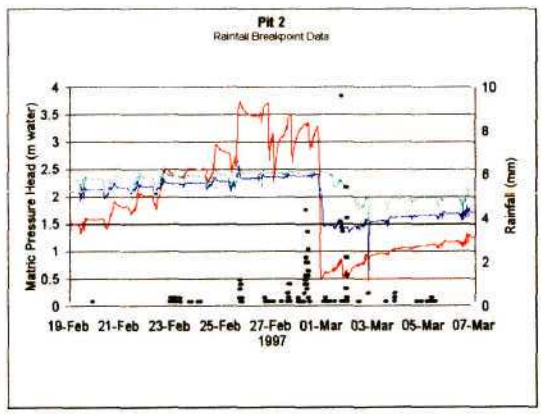

Figure H8

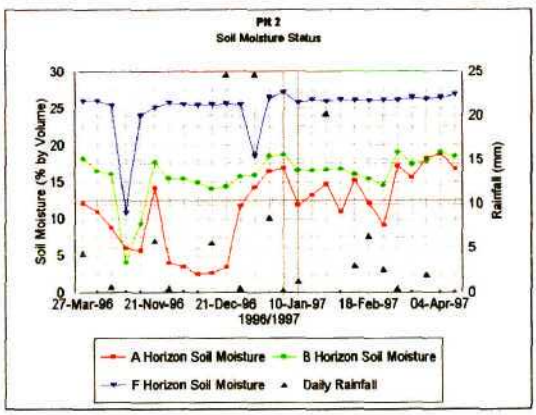

Figure H9

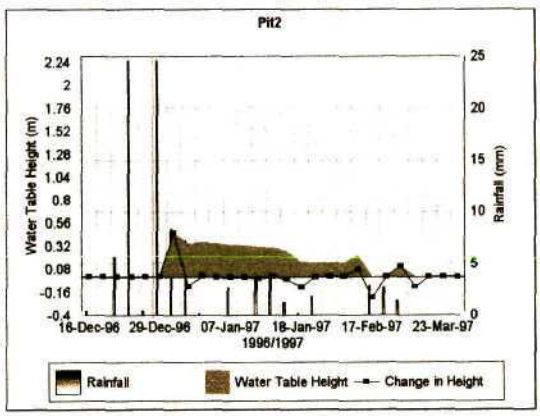

Figure H10

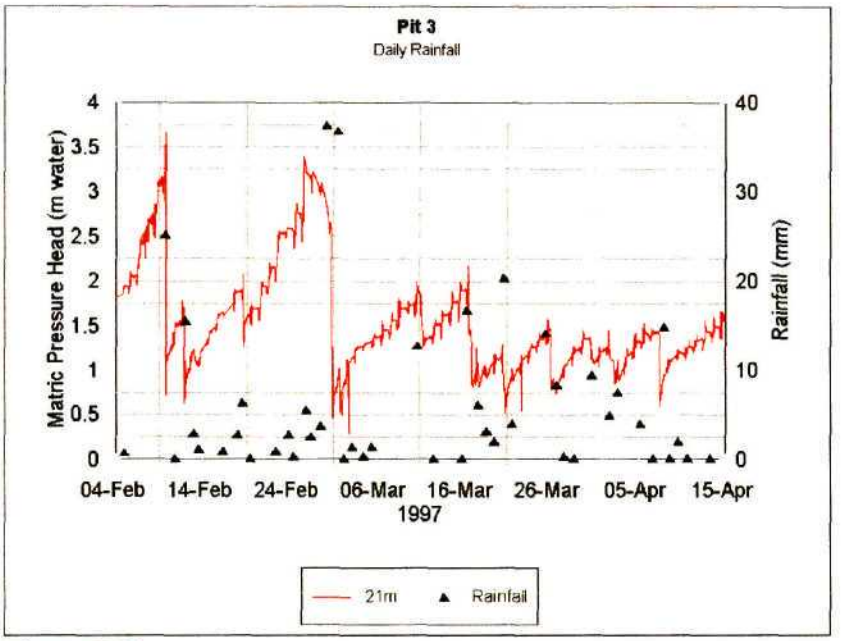

Figure H11

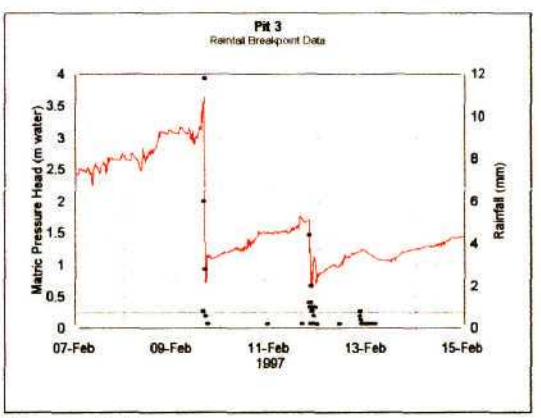

Figure H12

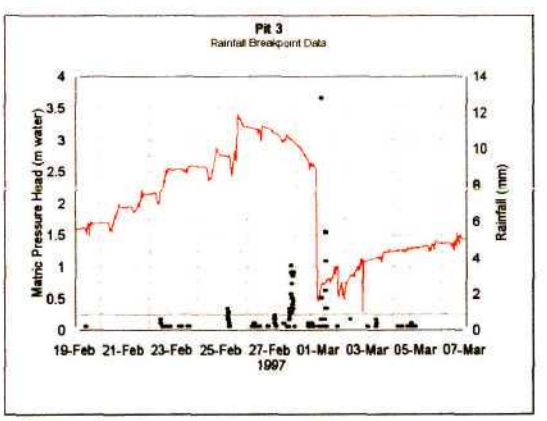

Figure H13

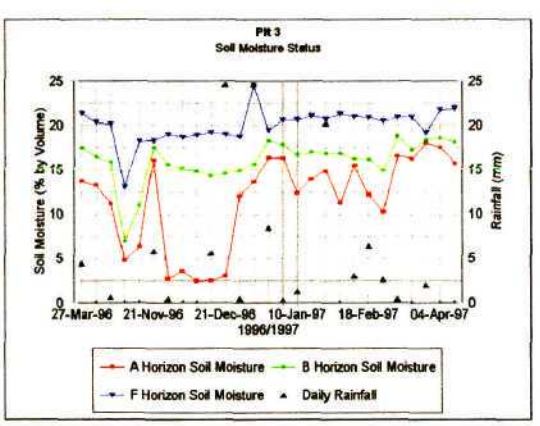

Figure H14

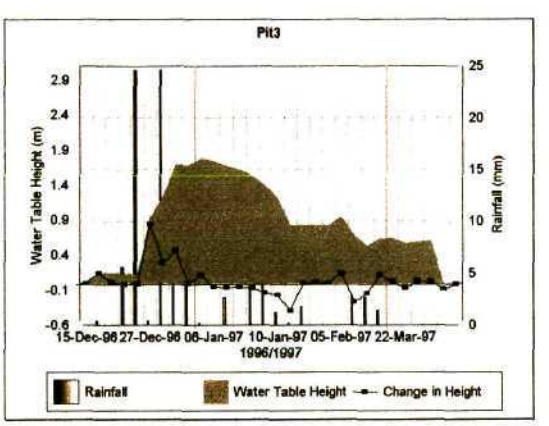

Figure H15

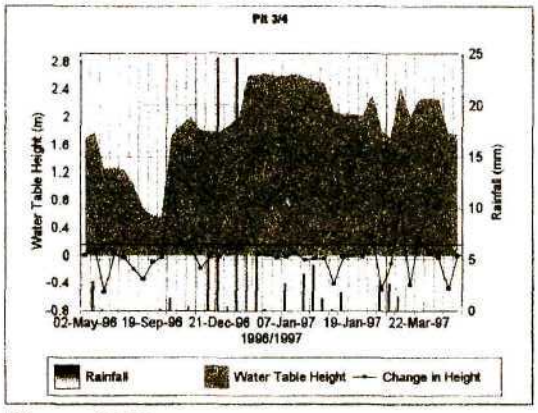

Figure H16

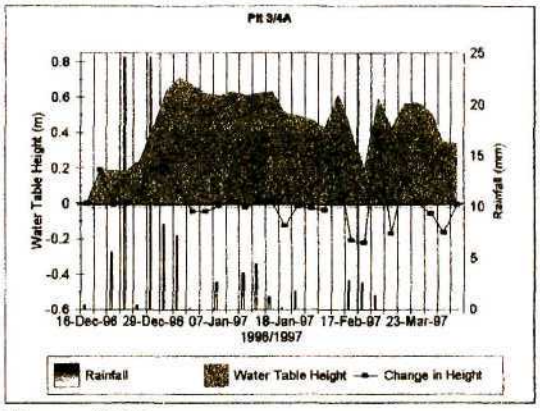

Figure H17

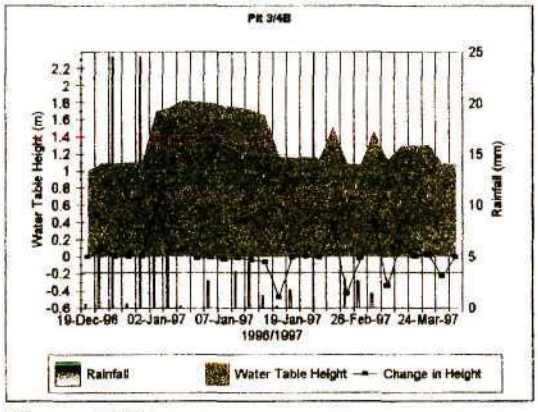

Figure H18

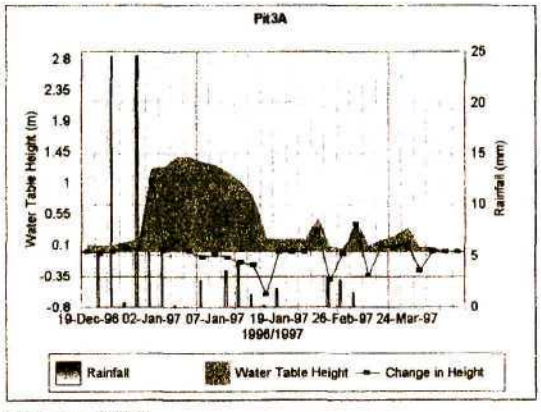

Figure H19

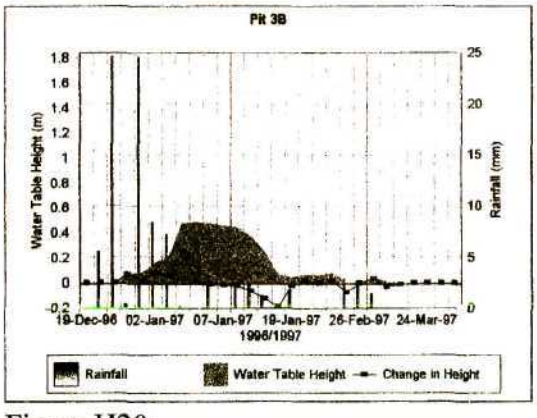

Figure H20

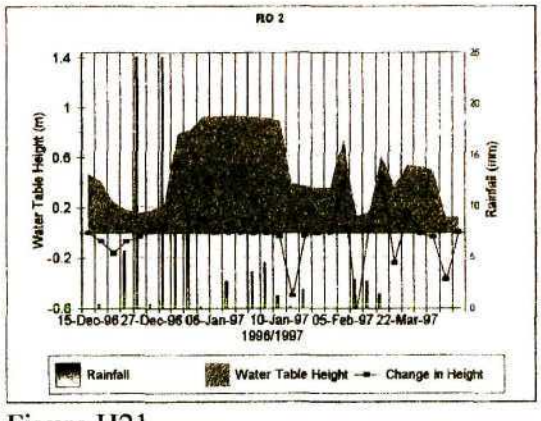

Figure H21

APPENDIX I

Example of a section of the HILL5D input rainfall file.

START DATE 20 DECEMBER 1996 END DATE 3 JANUARY 1997

Start	Year	Month	Day	Time	Rainfall
1	1996	12	20	1555	0.2
2	1996	12	20	1556	0.2
3	1996	12	20	1558	0.2
4	1996	12	20	1559	0.6
5	1996	12	20	1600	0.4
6	1996	12	20	1601	0.4
7	1996	12	20	1602	0.4
8	1996	12	20	1603	0.4
9	1996	12	20	1604	0.2
10	1996	12	20	1605	0.2
11	1996	12	20	1824	0.2
12	1996	12	20	1827	0.2
13	1996	12	20	1840	0.2
14	1996	12	20	1844	0.2
15	1996	12	20	2030	0.2
16	1996	12	20	2032	0.2
17	1996	12	20	2034	0.2
18	1996	12	20	2035	0.2
19	1996	12	20	2037	0.2
20	1996	12	20	2039	0.2
21	1996	12	20	2042	0.2
22	1996	12	20	2318	0.2
23	1996	12	20	2400	0.0
24	1996	12	21	253	0.2
25	1996	12	21	1421	0.2
26	1996	12	21	1422	0.2
27	1996	12	21	1423	0.2
28	1996	12	21	1427	0.2
29	1996	12	21	1428	0.2
30	1996	12	21	1429	0.2

APPENDIX J

Input Menu for the final HILL5D Simulation

```
**HILL5D Final Simulation
  20 December 1996 to 3 January 1997
  WEATHERLY TRANSECT 1
 KHOUT  KSUBF    UNITS    JPRNT   JIMIOS  JIDEP  HINIT[Option and Init. Data]
  1      0        1        1       0       0       0
  IQP    IPR    JPLO   JPROF  JCHAN   JBAL   JEVAP  JSALT  jlin
  1      1      2      1      0       1      1      0      0
   DS    NDX     DXL      DRAT   SURF    YU     YB   HOUT  DWDX[Geometry Data]
145.    18    10.0     2.0     0.11   1.80 0.60   0.30     0
   CPC     PHI     SWmx     SWmn   ALAM   CF  QINI      TINC [Soil Hydrology]
  .35      0.32     0.96   0.10   .324  0.52    0.0007   20.0
  NCK     PU       PL       QWT      FISOT    CFHD    CSKL
  1      .030    0.028       0.0030   1.0      1.      -0.0030
   DTR    ALPHA    TEMP      RFMAN    CVF   ITERMX  [Other Control Parameters]
  1.1      0.6      18.0      0.25    .005    50
  Nodes N1,N2 at which GW depths are followed in output:
  15   18
  NGP [no. locations at which profile slope and depth are given (below):]
    7
  XHL(I),YHL(I),SHL(I), on NGP cards following:
  27      2.30    .10
  83      3.10    .20
  96      3.26    .13
 106      2.92    .05
 115      1.73    .17
 124      1.19    .06
 145      0.60    .12
  TEV   ZROOT   PSIC    PSIM  [Profile Evap. control parameters]
  2.    0.15   .333     15.
 12 monthly mean pan Evap. values:
4.60  4.60  4.20  3.40  3.30  2.90  3.10  3.92  4.28  4.65  5.50  4.58
```

APPENDIX K

Output from final HILL5D simulation

Outputs showing initial fluxes and water table depths

Sub Node	Soil Dep.	Rel. Elev. (m)	Sub. Slope	Seep. Flux (mm.h^{-1})	Net Flux	Downsl Dist. (m)	Incr. Dist.	Lat Flow (mm.h^{-1})	Water Depth (m)
1	1.80	17.222	.100	.00	-28.00	.00	.00	-1.156	
2	2.30	16.416	.100	.00	-28.00	.00	8.06	.00	-.350
3	2.30	15.611	.100	.00	-26.48	8.06	8.06	9.85	-.350
4	2.30	14.805	.100	.00	-24.96	16.11	8.06	9.85	-.350
5	2.30	14.000	.100	.00	-23.44	24.17	8.06	9.85	-.350
6	2.37	13.046	.118	.00	-21.64	32.22	8.06	10.79	-.350
7	2.49	11.937	.138	.00	-19.54	40.28	8.06	12.34	-.350
8	2.60	10.714	.152	.00	-17.23	48.33	8.06	13.98	-.350
9	2.72	9.375	.166	.00	-14.70	56.39	8.06	15.72	-.350
10	2.83	7.919	.181	.00	-11.95	64.44	8.06	17.55	-.350
11	2.95	6.347	.195	.00	-8.99	72.50	8.06	19.47	-.350
12	3.07	4.657	.210	.00	-5.79	80.56	8.06	21.49	-.350
13	3.17	3.188	.182	.00	-3.02	88.61	8.06	19.91	-.350
14	3.24	2.116	.133	.00	-.99	96.67	8.06	16.18	.590
15	2.96	1.905	.026	.00	-.60	104.72	8.06	9.21	.801
16	2.02	1.718	.023	.00	-.24	112.78	8.06	11.13	.988
17	1.38	1.570	.018	-.04	.04	120.83	8.06	5.87	1.136
18	1.05	1.302	.033	-.54	.54	128.89	8.06	3.70	1.053
19	.78	.587	.074	-1.89	1.89	138.61	9.72	3.21	.780
20	.60	.000	.092	-3.00	3.00	145.00	6.39	3.13	.600

Time	Incr. Rain	Profile Depth at Node:		F L O W S: Subsurf.	OVRLND	TOTAL	Hillslope:	
(h:Min)	(mm.h^{-1})	15	18	(mm.h^{-1})	(mm.h^{-1})	(mm.h^{-1})	Evap	Error %
15:55	.00	.801	1.053	.28149	.00000	.28149	.000	.00
17: 1	1.29	.801	1.053	.15384	.55895	.71279	.000	.00
18: 7	1.29	.799	1.053	.02983	.65213	.68195	.000	-.50
18:24	1.29	.798	1.053	.03344	.64648	.67992	.000	-.92
18:25	.85	.798	1.053	.03340	.82378	.85718	.000	-1.06
18:26	.37	.798	1.053	.03337	.81113	.84450	.000	-1.05
18:28	.38	.798	1.053	.03337	.78506	.81843	.000	-1.05
18:33	.38	.798	1.053	.03337	.74231	.77568	.000	-1.06
18:43	.38	.797	1.048	.03337	.67444	.70781	.000	-1.08
19: 2	.38	.797	1.045	.10613	.57496	.68109	.000	-1.12
19:40	.38	.795	1.044	.17889	.48324	.66213	.000	-1.20
20:30	.38	.793	1.044	.17891	.44818	.62708	.000	-1.38
21:36	.50	.791	1.048	.17901	.46322	.64223	.000	-1.59
22:42	.50	.789	1.053	.17672	.50432	.68104	.000	-1.90
23:18	.50	.787	1.053	.10379	.54878	.65257	.000	-2.25